2 mil

TIS R74AEG153

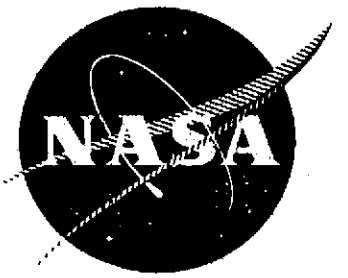

# HYDROGEN-METHANE FUEL CONTROL SYSTEMS FOR TURBOJET ENGINES

FINAL REPORT

by

J.S. Goldsmith and G.W. Bennett

GENERAL ELECTRIC COMPANY

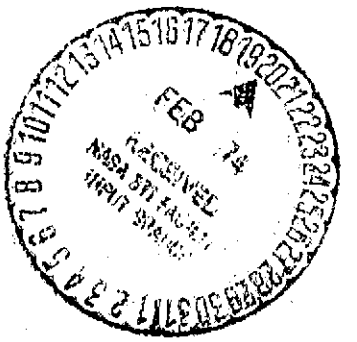


prepared for

NATIONAL AERONAUTICS AND SPACE ADMINISTRATION

(NASA-CR-121247) HYDROGEN-METHANE FUEL CONTROL SYSTEMS FOR TURBOJET ENGINES Final Report (General Electric Co.) ~~162~~ 169 p HC $10.25 CSCL 21E

N74-16493

G3/28 Unclas 28804

NASA Lewis Research Center

Contract NAS3-14319

Joseph M. Ladd, Project Manager

| 1. Report No. | 2. Government Accession No. | 3. Recipient's Catalog No. |
|---|---|---|
| | | |

| 4. Title and Subtitle | 5. Report Date |
|---|---|
| HYDROGEN-METHANE FUEL CONTROL SYSTEMS FOR TURBOJET ENGINES | October 1973 |
| | 6. Performing Organization Code |
| 7. Author(s) | 8. Performing Organization Report No. |
| J.S. Goldsmith and G.W. Bennett | GE TIS R74AEG153 |
| | 10. Work Unit No. |
| 9. Performing Organization Name and Address | 11. Contract or Grant No. |
| General Electric Company<br>Cincinnati, Ohio 45215 | NAS3-14319 |
| | 13. Type of Report and Period Covered |
| 12. Sponsoring Agency Name and Address | Contractor Report |
| National Aeronautics and Space Administration<br>Washington, D.C. 20546 | 14. Sponsoring Agency Code |

15. Supplementary Notes

Project Manager, Joseph M. Ladd, Airbreathing Engines Division
NASA Lewis Research Center
Cleveland, Ohio 44135

16. Abstract

Design, development, and test of a fuel conditioning and control system utilizing liquid methane (natural gas) and liquid hydrogen fuels for operation of a J85 jet engine were performed. The experimental program evaluated the stability and response of an engine fuel control employing liquid pumping of cryogenic fuels, gasification of the fuels at supercritical pressure, and gaseous metering and control. Acceptably stable and responsive control of the engine was demonstrated throughout the sea level power range for liquid gas fuel and up to 88 percent engine speed using liquid hydrogen fuel.

| 17. Key Words (Suggested by Author(s)) | 18. Distribution Statement |
|---|---|
| | UNCLASSIFIED - UNLIMITED |

| 19. Security Classif. (of this report) | 20. Security Classif. (of this page) | 21. No. of Pages | 22. Price* |
|---|---|---|---|
| UNCLASSIFIED | UNCLASSIFIED | 160 | |

* For sale by the National Technical Information Service, Springfield, Virginia 22151

## FOREWORD

The design, development, and test program described herein was conducted by the General Electric Flight Propulsion Division under NASA Contract NAS3-14319. The work was done under the direction of the NASA Project Manager, Mr. Joseph M. Ladd, and the NASA Technical Advisor, Mr. David G. Evans, Airbreathing Engines Division, NASA Lewis Research Center. This work has also been reported as General Electric Document TM73-489, January 1974.

TABLE OF CONTENTS

LIST OF ILLUSTRATIONS

LIST OF ILLUSTRATONS (Continued)

LIST OF ILLUSTRATIONS (Concluded)

LIST OF TABLES

## SUMMARY

Work performed in this contract program consisted of design, development, and test demonstration of fuel supply and control systems for operation of a J85 jet engine on both cryogenic hydrogen and methane fuels. Major objectives of the work were:

- Development of flight-type cryogenic fuel control systems for a jet engine which included liquid pumping to supercritical pressures, heat exchangers for gasification of the fuels, and gaseous metering and control.
- Test evaluation of the control system functional performance, stability, and response in controlling a J85 ground test engine on both liquid hydrogen and liquid methane fuels.
- Measurement of engine exhaust gas emissions resulting from combustion of the two fuels.

Study, analysis, and modeling of the intended systems indicated the functional feasibility of the control arrangement. Detail hardware design and fabrication were completed. One set of flexible hardware was designed to accommodate both fuels, except that heat exchangers were provided individually for each fuel.

NASA furnished a J85-13 engine and cryogenic storage trailers for the test demonstrations. Engine fuel injectors for the methane systems were provided by NASA based on comparative evaluation of candidate designs tested in a J85 combustor rig. The engine and system equipment were installed in the Contractor's outdoor ground test facility.

Testing of the methane system and engine were completed using a liquid natural gas supply fuel which was substituted for pure liquid methane because of availability and economy. System and component performance met objectives with the exception that an oil-to-methane heat exchanger at the fuel pump discharge froze the oil flowpath. Stable system and engine control was demonstrated from starting to maximum engine speed. An engine power setting transient from idle to 100% speed was accomplished in 3.5 seconds. Exhaust emissions were measured.

Planned testing of the hydrogen system was partially completed. Stable system and engine control from starting to 88% engine speed was demonstrated, and engine power transients from idle to 85% speed were accomplished. Heat exchanger performance was met without icing the air side. Deficient fuel pump delivery performance on liquid hydrogen limited the maximum flow and engine power available. After unsuccessful attempts to improve the pump delivery, a failure of the fuel pump hydraulic drive motor section necessitated termination of further testing. Limited engine exhaust emissions measurements were taken.

On the basis of design analysis and test results obtained, it was concluded that a suitably stable and responsive control of jet engines can be accomplished where gasification of the fuel delivery at supercritical pressure is employed as a heat sink for engine air with either liquid methane or liquid hydrogen

fuel. Further design development of the liquid hydrogen fuel pump for performance and life is required. Use of either cryogenic fuel to cool oil heat sources requires additional heat exchanger design development.

## INTRODUCTION

The Statement of Work for Contract NAS3-14319 set forth general requirements for the hydrogen-methane fuel systems arrangement and functional performance. Design of the fuel systems was guided by these requirements to the greatest extent practicable.

Generation of the requirements for the methane-fueled system configuration was stimulated by prior NASA studies of the potential use of liquid methane fuel as a source of energy for advanced supersonic transport propulsion. Studies reported in NASA TND-5928, "Turbine Aerodynamic and Cooling Requirements for a Turbojet Powered Mach 3 Transport Using Methane Fuel," by David G. Evans, Keith A. Furgalus, and Francis S. Stepka of the Lewis Research Center recognized the engine cycle performance advantages potentially available from use of a cryogenic fuel as a heat sink for engine cooling air. Use of the cryogenic fuel as a coolant for engine and aircraft systems implied the need to pump liquid fuel from the aircraft supply, to gasify the fuel through appropriate air and oil heat exchangers, and to control gaseous fuel delivery to the engine such that stable and responsive control over a wide range of flow conditions would be maintained. Experimental verification of the ability to insert the fuel gasification process into the engine fuel delivery system over the necessary range of operating conditions had not been obtained, and it became the purpose of the contract program reported herein to analyze, design and demonstrate engine operation of such a system. Thermal requirements for the methane system heat exchangers were sized by David G. Evans based on the engine studies reported in TND-5928 and on the anticipated aircraft system requirements of the NASA SCAT-15F aircraft studies.

At the same time NASA studies of the potential use of hydrogen-fueled air-breathing engines for Space Shuttle propulsion were being conducted. Requirements and potential problems involving gasification and engine control with liquid hydrogen fuel supply were similar to the methane-fueled system. A parallel purpose of the subject program was to design and demonstrate suitable operation of a turbojet engine employing gasification of liquid hydrogen fuel.

The J85 jet engine was chosen for an engine test demonstration vehicle because of its availability, proven work-horse capability, and relatively small fuel consumption required. Since the thermal requirements of interest were based on much larger propulsion engines, the air bleed and oil heat sources were simulated by facility supply equipment rather than taken from the J85 engine itself.

The work described herein was undertaken with the beginning of concept verification studies in August, 1970, and the final engine test attempt using liquid hydrogen fuel occurred in March, 1973.

## SYSTEM DESIGN AND ANALYSIS

### SYSTEM CONCEPTUAL DESIGN

The conceptual arrangement of the fuel supply, conditioning, and control system established for liquid hydrogen fuel is shown in Figure 1. A similar system for use with liquid methane fuel was established as shown in Figure 2. Liquid fuel was to be supplied to the system from tanker storage at 30 psia minimum ($2.07 \times 10^5$ N/m$^2$) and at temperatures ranging from saturated liquid to 6° F (3.33° K) subcooled for liquid hydrogen and 17° F (9.43° K) subcooled for liquid methane.

#### Inlet Fuel Conditioning

A fuel subcooler accepts cryogenic hydrogen at the fuel supply header conditions and provides adequate net positive suction pressure to the main pump element intake to ensure noncavitating main fuel pump operation. The subcooler was not a flight-type component but was intended to supply liquid hydrogen at the pump inlet at 12.5 psi ($8.62 \times 10^4$ N/m$^2$) or liquid methane at 13 psi ($8.97 \times 10^4$ N/m$^2$) net positive suction pressure, which was felt to be representative of a boost-pump-fed system.

#### Main Fuel Pump And Pressure Regulation Servo

Fuel with adequate suction pressure is supplied to the main fuel pump element which consists of a fixed-displacement, reciprocating-piston pumping element. Demand flow variation in the system is accommodated by varying the main pump piston element drive speed through the action of a hydraulically powered drive motor servo. The pump is operated as a pressure-regulated, variable-demand flow source. The variable speed piston pump was selected in preference to a centrifugal pump in order to satisfy the requirements for high discharge pressure, small maximum flow size, and 20/1 flow turndown capability. This type pump also yielded a compact unit representative of flight-type hardware, yet required minimum design development.

A feedback pressure transducer at the fuel pump discharge provides electrical feedback to a circuit in the central electronic control computer. Pressure feedback is compared to a fixed electrical reference set to hold 400 psia ($2.76 \times 10^6$ N/m$^2$) (LH2) or 900 psia ($6.21 \times 10^6$ N/m$^2$) (LCH4), and comparator error is amplified and integrated to provide driver-current to an electrohydraulic torque motor servo valve located on the pump drive motor. Torque motor current sets a proportional hydraulic flow into the fixed-displacement drive motor, thus varying pump speed and flow to null the discharge pressure error in the regulating loop.

Motor hydraulic power is taken from the engine-driven hydraulic power supply at 3000 psi ($2.07 \times 10^7$ N/m$^2$) and a maximum hydraulic flow rate of approximately 16 gpm ($1.01 \times 10^{-5}$ m$^3$/sec).

Pump speed and flow saturation limits are placed on the pressure-regulator electrical error signal in order to limit the mass flow rate at the pump discharge relative to the metered gas flow downstream during large transients in pump discharge pressure. Flow limit error is established by comparing pump

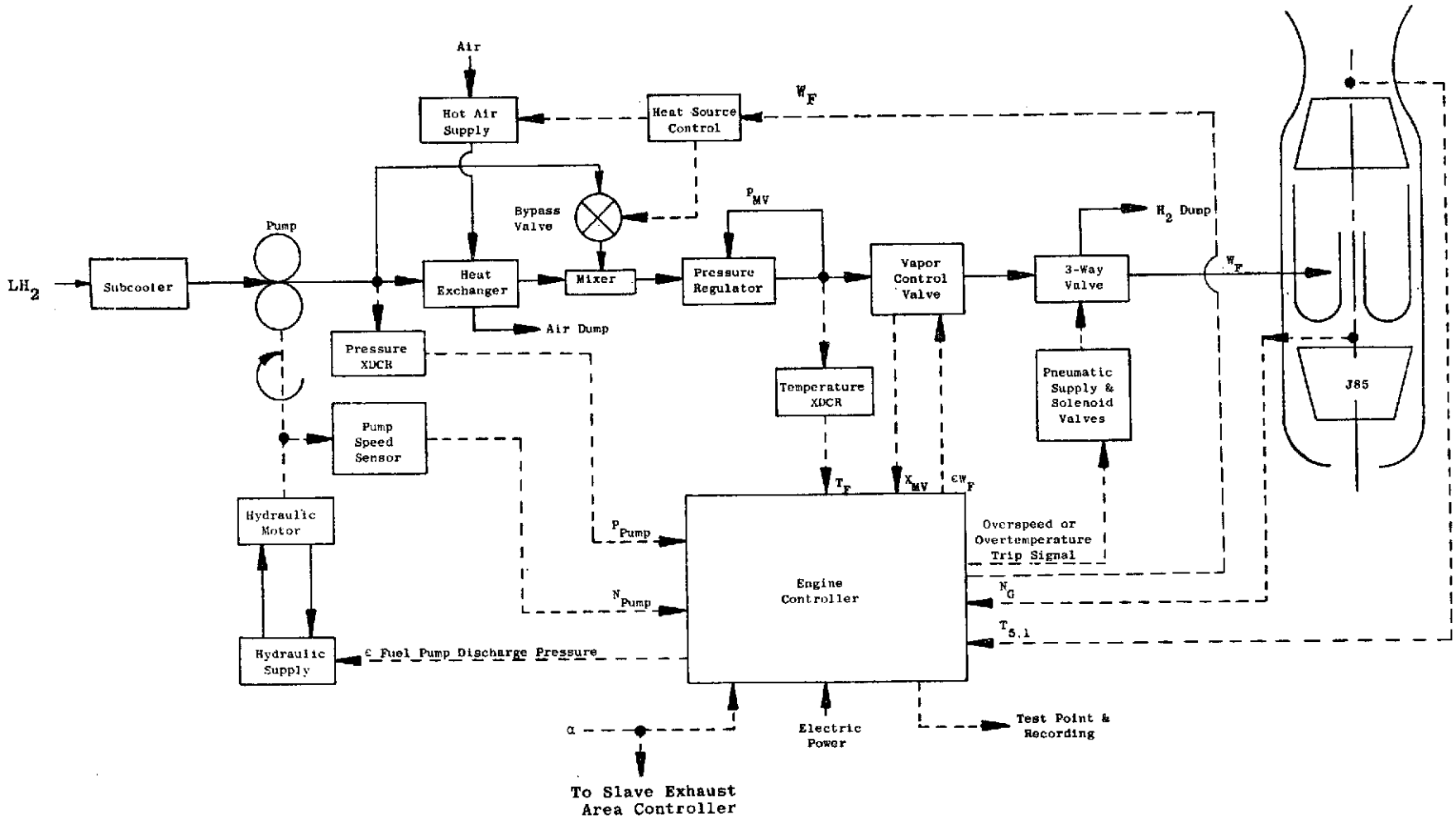


Figure 1. Schematic Diagram of Hydrogen Fuel System.

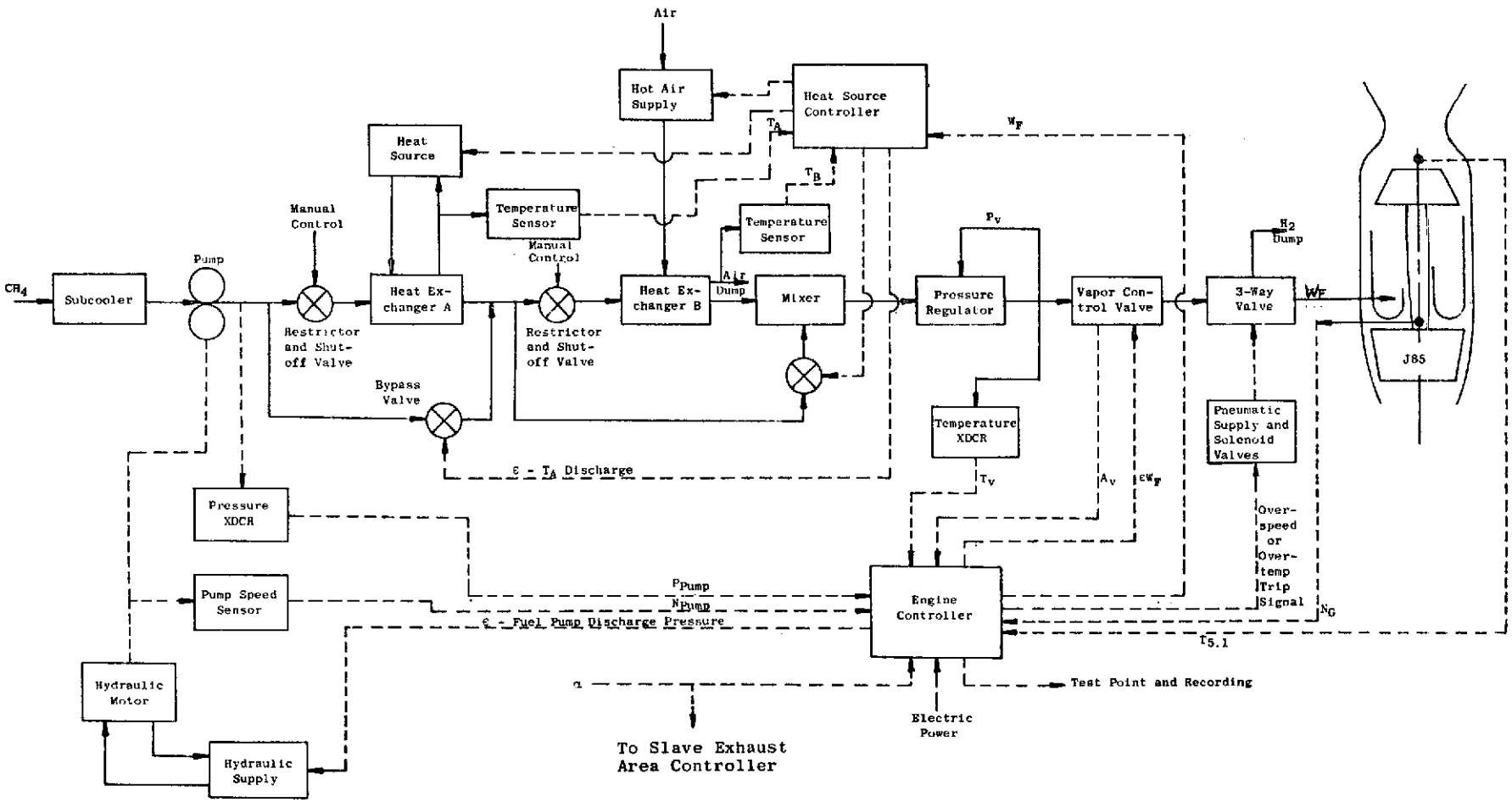


Figure 2. Schematic Interconnection Diagram of Methane Fuel System.

mass flow as a calibrated function of sensed pump speed against the metered mass flow computed within the metering control section of the electronic control computer.

Heat Exchangers and Bypass Valves

Pump discharge flow is supplied to a flight weight oil-to-fuel heat exchanger (methane system only) and then to flight weight air-to-fuel heat exchangers at rates required to sustain supercritical pressure in the exchangers or as limited by the pump flow limit computation. Flow is gasified in the heat exchanger and exits to a mixer in the discharge junction with bypass fuel.

Remotely operated bypass valves are provided to shunt total flow around the heat exchangers. To assure that total flow blockage in the exchanger path can be provided under total fuel bypass conditions, remotely operated valves are placed between the upstream bypass junction and the entrance port of each heat exchanger.

Bypassed flow joins with heat exchanger flow under partial bypass conditions at the downstream junctions of the heat exchangers which will contain mixer devices to assure thorough mixing and heat exchange between gaseous flow and any bypassed fuel in the liquid state. Baffled tees are provided to force mixing of the streams.

The oil-to-fuel heat exchanger is supplied a regulated, manually selected heat input rate by the oil-to-fuel heat source and control subsystem. The remotely operated bypass valve on the oil-to-fuel heat exchanger is used either at fixed settings manually selected or as an automatic bypass regulating oil exit temperature.

Variable heat input rate is supplied to the air-to-fuel heat exchangers by the air-to-fuel heat source and control subsystem as a function of engine fuel flow. The remotely operated fuel bypass valves on the air-to-fuel heat exchangers are capable of being automatically servoed by the heat source control system to regulate heat exchanger exit air temperature to a manually selected constant value. The air-to-hydrogen heat exchanger operates at steady-state fuel entrance conditions of 400 psia ($2.76 \times 10^6$ N/m$^2$) and -415° F (25° K). The air-to-methane exchanger operates at approximately 900 psia ($6.21 \times 10^6$ N/m$^2$) fuel conditions at temperatures as low as -235° F (125° K).

Pressure Regulating Throttle Valve Servo

Heat exchanger exit flow enters a throttling pressure-regulator servo which senses line pressure at its fuel discharge and is servoed to vary throttling area to fix the downstream pressure at a constant absolute pressure level. The regulator accommodates the system flow density ranges demanded by the metering system and heat exchanger conditions.

The regulating reference level set by this servo is chosen at 250 psia ($1.72 \times 10^6$ N/m$^2$) for H2 and 700 psia ($4.83 \times 10^6$ N/m$^2$) for $CH_4$ so that the downstream metering valve will have sufficient pressure-ratio available to operate as a choked nozzle and to assure supercritical fuel condition. Throttle valve maximum area is sized to accommodate maximum system flow rate at a supply pressure sufficiently low to accommodate transient excursions of heat exchanger

pressure during engine power setting changes. Regulation of the metering valve inlet pressure to ±1% of point permits use of a constant pressure representation to the fuel flow computation circuit.

Pressure feedback is sensed electrically and pressure error signals are amplified in the electronic control. An electrohydraulic servo valve converts the electrical error to proportional hydraulic flow controlling the actuation of the fuel throttling valve motion. Hydraulic power supply is obtained from the engine-driven hydraulic power supply subsystem.

Metering Valve and Flow Computation

Gaseous flow in the systems enters a convergent-nozzle metering valve which modulates system flow rate as a function of a variable-stroke valve position. Variation of valve stroke sets a variable throat area to the valve which is maintained choked at all system flow conditions. Downstream pressure at the plane of the throat exit is established by engine burner pressure level plus a small line pressure drop across the downstream impedances provided by the cutoff valve, manifold, and burner injection nozzles. Since the downstream pressure drops are small compared to the maximum engine burner pressure of approximately 92 psia ($6.34 \times 10^5$ N/m$^2$), the maximum metering valve exit pressure is on the order of 100 psia ($6.89 \times 10^5$ N/m$^2$) and sufficient pressure ratio to choke the metering area at all conditions is maintained by the throttling regulator upstream of the metering valve entrance. With the pressure conditions selected, the throttling process in the metering valve will maintain gaseous conditions from entrance to burner pressure at entrance fluid temperatures above -386° F (41.1° K) for $H_2$ and above -82° F (210° K) for $CH_4$.

Controlled modulation of the valve stroke is provided by an electrohydraulic torque-motor servo valve and a hydraulic actuator. Torque motor current is set by a fuel flow control loop error signal computed in the electronic control computer, and the hydraulic actuator integrates this error to set valve stroke. Actuator stroke is sensed by a linear-variable differential transformer whose output signal is sent to the electronic control computer to provide valve position feedback to the fuel flow computation loop.

A metering valve fluid entrance temperature sensor consisting of a resistance temperature detector is provided. The temperature signal is sent to the electronic control computer for use as density and throat velocity correction in the fuel flow computation.

Figure 3 diagrams the computational relationships which establish computed fuel flow rate within the electronic control computer using the metering valve stroke and entrance temperature intelligence. The computational principle used is based on the provision of choked gaseous flow in the metering throat such that:

$$W_8 = A_{x8} \cdot f(T_8) \qquad (1)$$

Since the metering valve supply pressure is regulated to a constant absolute value within ±1%, the supply density of the fluid can be represented as a unique function of the supply temperature, knowing the properties of the fluid. Similarly, the critical velocity characteristic at throat pressure can be defined as a unique function of temperature. These unique temperature functions are combined in a single function $f(T_8)$ as used in Equation (1).

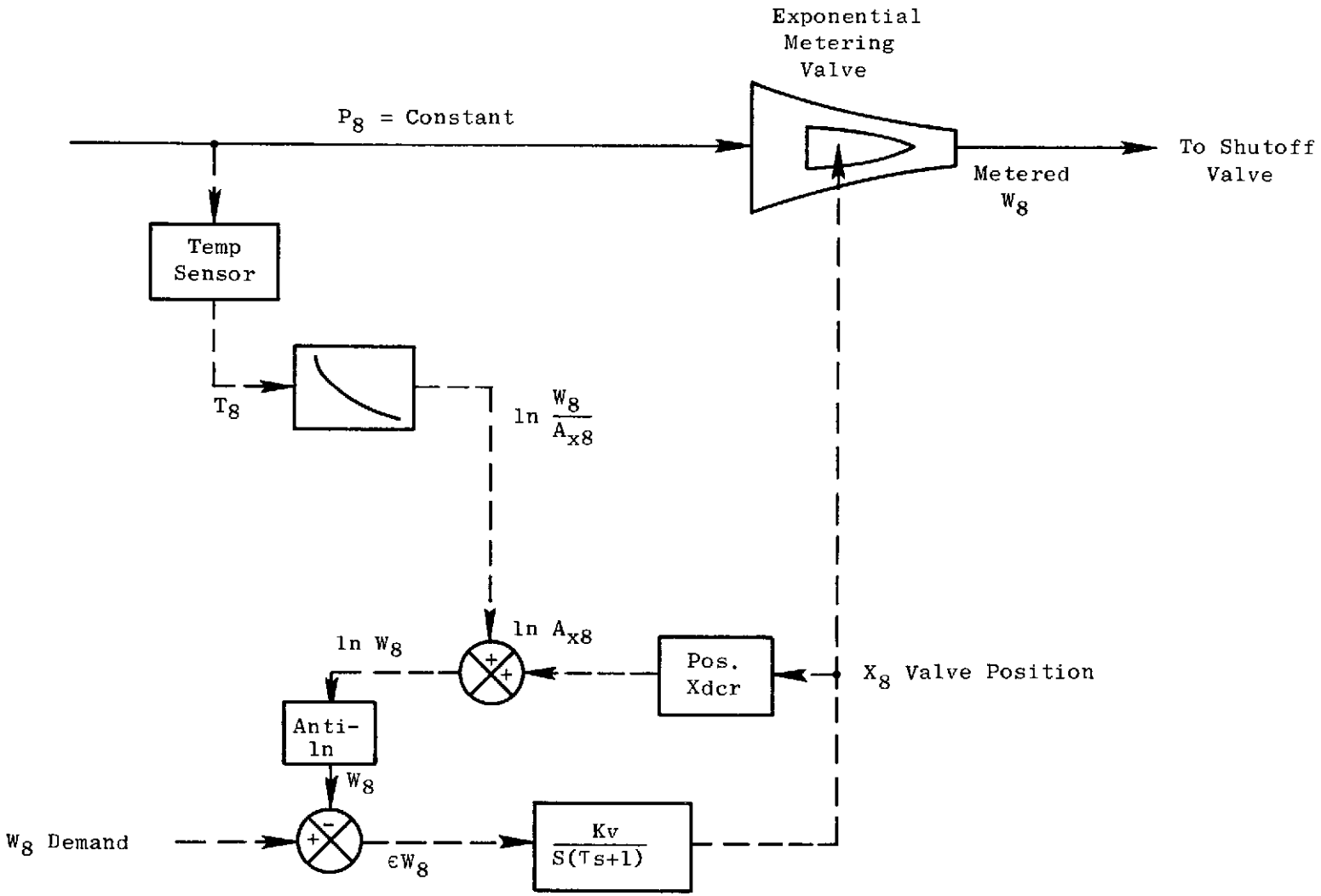


Figure 3. Schematic Diagram of Metering and Fuel Flow Computation.

The fuel mass flow rate computed in this fashion is used within the electronic control computer to provide feedback to the fuel valve area positioning servo and for readout indication.

Shutoff and Vent Valve

A pair of plug-type two-way valves act as a three-way cutoff and vent function which connects system flow to the engine manifold with the vent closed. The valves are pneumatically operated and electropneumatically controlled from the safety and mode control subsystem. If venting or cooldown are selected, the valve shuts off engine flow and vents system flow to a dump line. In the event of electrical or pneumatic failure, the valves shut off and vent to a dump line. Electrical overspeed and overtemperature signals are generated within the electronic control computer. In the event these limits are exceeded, the shutoff valve is closed and the vent valve is vented to protect the engine.

Electronic Control Computer

The central electronic control computer, which is control-room mounted, coordinates the fuel and control system signal intelligence and provides control functions for:

- Engine rotor speed governing in response to power lever input speed request
- Transient fuel flow limitation during engine power setting transients
- Fuel pump pressure regulation and speed limitation
- Metering valve flow computation for both control and readout
- Overspeed and overtemperature limit protection
- Fuel flow signal output for air-control scheduling
- Engine start fuel scheduling
- Exhaust nozzle reference scheduling and $T_{5e}$ error generation

A functional block diagram of the electronic control shown in relation to other system components is shown in Figure 4.

The electronic control, in conjunction with the fuel delivery and metering system, operates as a full-range isochronous governor for engine rotor speed. An electrical pick-off of the power lever setting signals a slave exhaust area control system to provide a coordinated speed and power-setting request. As the engine power setting is controlled by the electronic control and fuel metering system, the existing hydromechanical J85 controls operate to schedule compressor variable geometry and to position the exhaust nozzle. Rotor speed feedback to the electronic control is taken as a frequency signal from the existing J85 control alternator output, and signal conditioning is provided

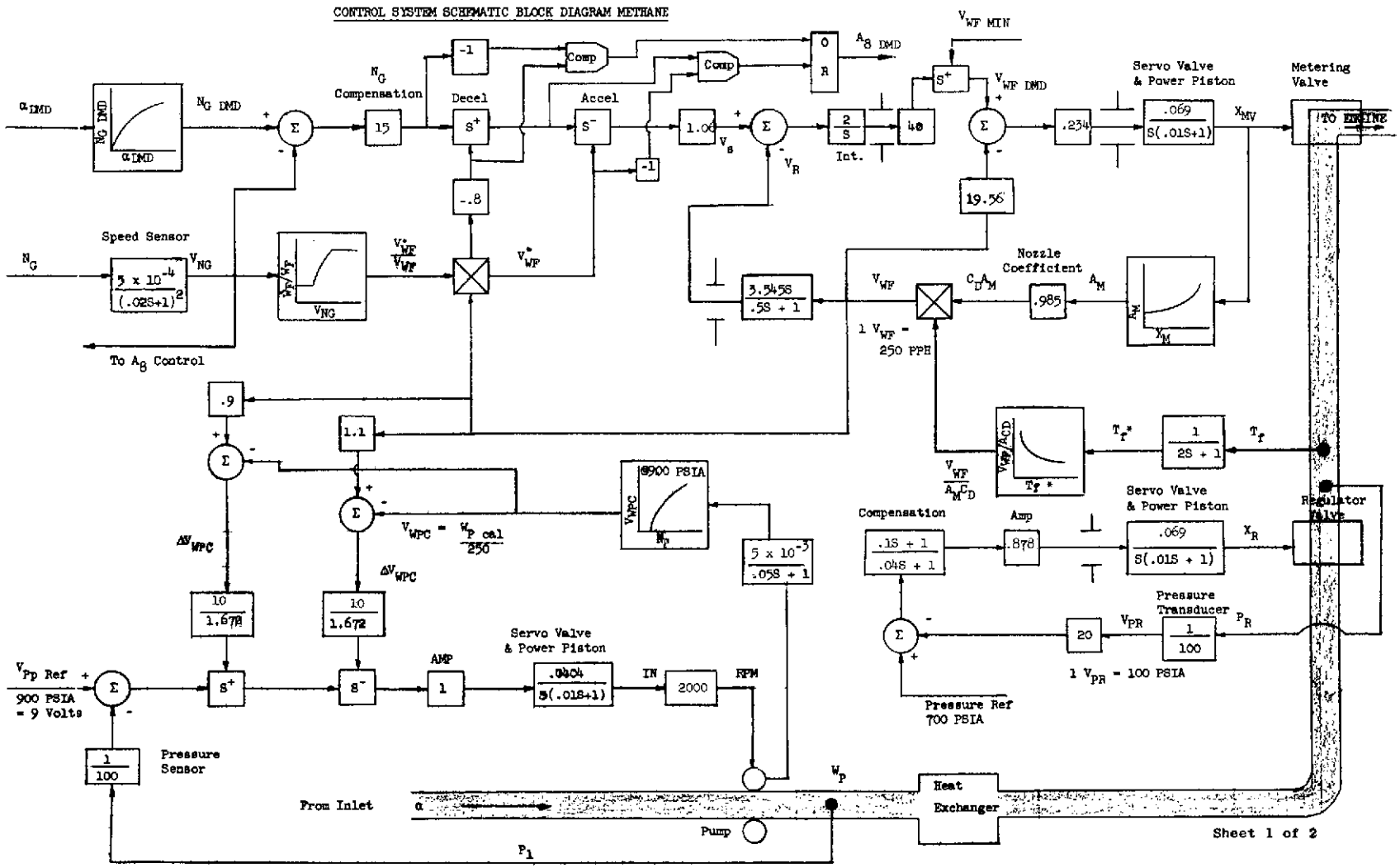


Figure 4. Control System Schematic Block Diagram for Methane and Hydrogen.

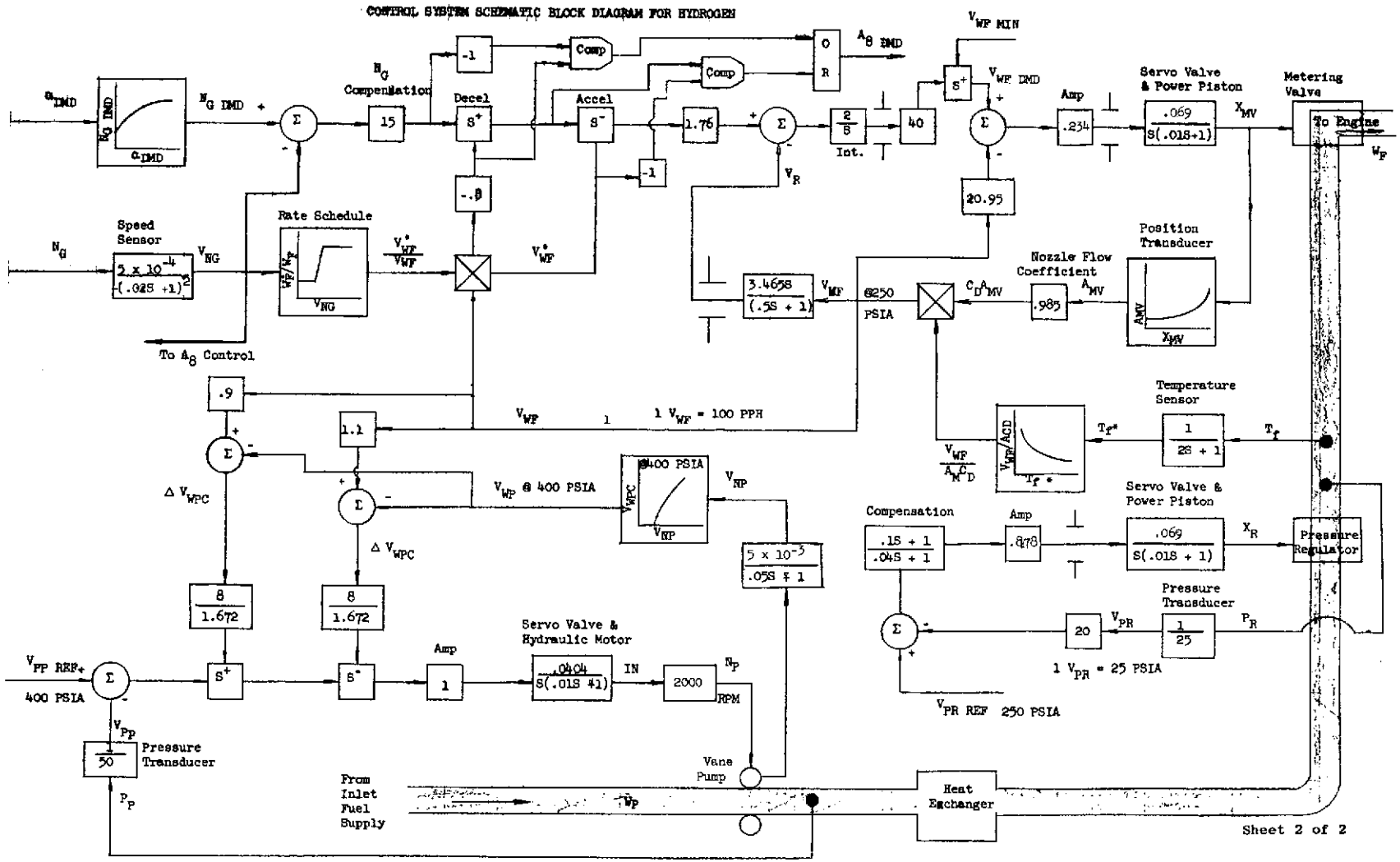


Figure 4. Control System Schematic Block Diagram for Methane and Hydrogen (Concluded).

within the electronic control. Test cell power is provided to the electronic control. A redundant engine speed sensor signal for overspeed protection is provided on the engine by NASA.

The acceleration and deceleration fuel control mode established by the system is such that $\dot{W}_{8Accel} = f\ (W_{8Actual}, N_g)$ (2)

and $\dot{W}_{8Decel} = -Kf(W_{8Actual}, N_g)$. (3)

Heat Sources and Controls

A source of heated air simulating engine compressor bleed extraction is provided for the air-to-hydrogen and air-to-methane heat exchanger by burning gaseous hydrogen in a coannular combustor supplied from a 150 psig ($1.034 \times 10^6$ $N/m^2$) facility air source. The vitiated burner exit air is supplied to the entrance of heat exchanger B at controlled temperature and pressure conditions, while burner airflow is set by a throttling valve downstream of the heat exchanger.

A source of heated oil simulating aircraft heat load is provided to heat exchanger A in the methane fuel system from a commercially procured oil heater cart powered electrically. Oil flow, pressure, and temperature are manually set by hand controls provided with the heater cart.

Electrical mode programming and control are provided for control of air and oil system parameters. The control functions performed by this system are as follows:

- Heat Exchanger A oil discharge temperature ($T_{19}$)
- Heat Exchanger B air discharge temperature ($T_{14}$)
- Heat Exchanger B air inlet temperature ($T_{13}$)
- Heat Exchanger B discharge pressure ($P_{14}$)
- Heat Exchanger B airflow ($W_{14}$)

Closed loop feedback controls are used to set and regulate all of the above parameters except airflow ($W_{14}$).

Hydraulic Supply

An engine-driven high pressure hydraulic supply source for operation of the system fuel pump drive motor and hydraulically powered servos is provided. The overspeed-governor drive pad of the J85 engine, which is an alternate starter pad, is used to drive the hydraulic pump. An aircraft-type piston pump operated as a pressure-regulated, variable delivery source is adapted for engine mounting.

A hydraulic supply reservoir and inlet booster pump for the engine-driven pump are provided in a remotely mounted boost-conditioning package of commercial design. Water cooling of the hydraulic system heat rejection is accommodated in the boost conditioning package. Electrical drive power is used for the booster package.

### Safety and Mode Control

An electrical control panel for system safety and mode control is provided. The panel controls, by means of electrical power distribution, the safety logic and valve and ignition control logic required for the orderly sequence of preparatory steps which must precede firing of the J85 engine. The control panel provides the following control functions for the system:

- Emergency shutoff
- Air heater ignition sequencing
- System purge and chilldown sequencing
- Engine start preparation sequencing
- Engine run and ignition sequencing
- Low oil level warning

Table I lists the system operating modes required with the resulting output conditions for system equipment.

## DYNAMIC ANALYSIS AND MODELING

### Engine Model Development

Analysis of the control system required development of an engine model. The engine selected for this study was a J85-13.

The model of an engine is a set of equations, the solutions of which represent the performance of an engine in response to some input. The determination of the necessary equations is presented here.

The engine model is separated into its various components: the compressor, combustor, turbine, fuel control, and nozzle. The equations describing each of these components involve the various temperatures, pressures, airflows, etc., throughout the engine. Figure 5 shows the relationship of these components and variables.

The equations relating most of the variables are independent of time and form an algebraic set. The time dependent variables enter the model in two places:

1) The rotor dynamics
2) Dynamics of the fuel system

Table I. System Mode Control Logic.

| System Mode \ Valve or Signal Condition | Air Pressure Control Valve (ROV-3) | Air Flow Control Valve (ROV-4) | Air Heater Ignition | HX Fuel Shutoff Valve (ROV-7 or ROV-5B) | HX Fuel Bypass Valve (ROV-8 or ROV-6B) | Engine S/O & Vent Valves (ROV-2A & 2B) | Engine Pump Servo Ref. | Engine Ignition | Air Heater Fuel Solenoid Valve (SV-1) | Air Heater Fuel Control Valves (ROV-10 & 11) |
|---|---|---|---|---|---|---|---|---|---|---|
| Emergency Purge (1) / Emergency Off (2) | Open | Open | Off | Closed | Closed | Vent | Off | Off | Closed | Closed |
| Engine Off | Normal (Local-Auto) | Normal (Local-Auto) | Off | (3) Closed | (3) Closed | Vent | Off | Off | (9) Closed | Normal (Local-Man) |
| Engine (4) Purge | Normal (Local-Auto) | Normal (Local-Auto) | Off | Normal (P/L) (7) | Normal (Local-Auto) | Vent | Off | Off | Closed | Normal (Local-Man) |
| Chilldown (5) | Normal (Local-Auto) | Normal (Local-Auto) | Off | Normal (P/L) | Normal (Local-Auto) | Vent | Off | Off | Closed | Normal (Local-Man) |
| Air Heater (6) Light-Off | Normal (Local-Auto) | Normal (Local-Auto) | On (Timed) | Normal (P/L) | Normal (Local-Auto) | Vent | Off | Off | Open | Normal (Local-Man) |
| Engine Start Prep. (8) | Normal (Local-Auto) | Normal (Local-Auto) | Off | Normal (P/L) | Normal (Local-Auto) | Vent | On | Off | Open | Normal (Local-Auto) |
| Air Heater Auto. | Normal (Rem.-Auto) | Normal (Rem.-Auto) | Off | Normal (P/L) | Normal (Local-Auto) | Vent | On | Off | Open | Normal (Rem.-Auto) |
| Engine Run | Normal (Rem.-Auto) | Normal (Rem.-Auto) | Off | Normal (P/L) | Normal (Local-Auto) | Open (To Engine) | On | On (Timed) | Open | Normal (Rem.-Auto) |

NOTES:
(1) Selected by NASA Interlocks T1-1 and T1-2.
(2) Selected by Emergency Off Button - Line 4.
(3) Normal if engine purge/chilldown previously selected.
(4) NASA control turns on purge gas.
(5) NASA control turns on fuel.
(6) NASA control turns on air.
(7) P/L = panel-loader
(8) Engine motoring required.
(9) Open if burner previously lit.

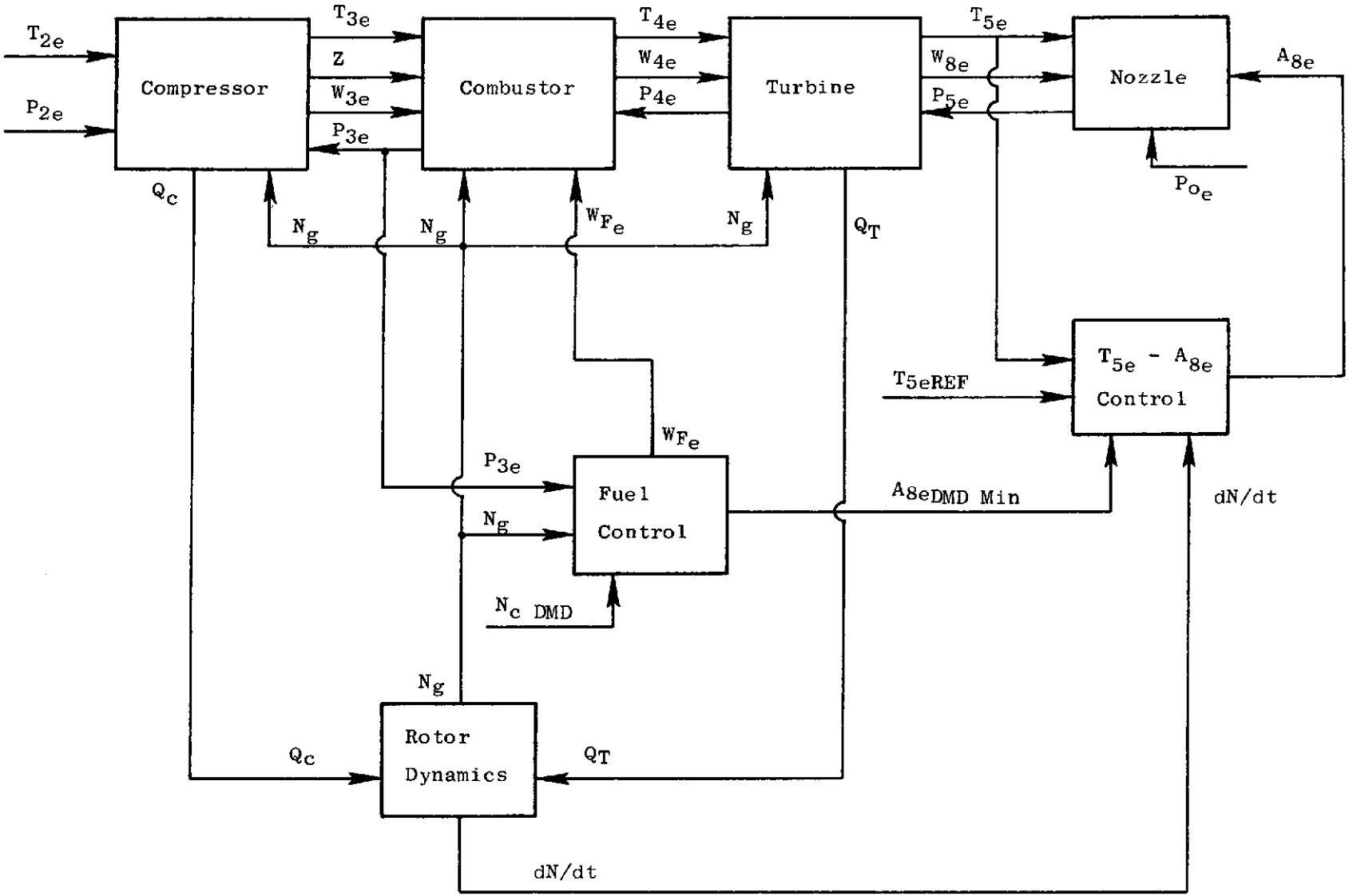


Figure 5. Schematic Diagram of Engine Model.

The cycle data used in designing the hybrid computer model was obtained from digital computer cycle analysis decks. Data were presented over a speed range from 57% to 100%.

Compressor Model

The compressor variables to be calculated are:

$$Z,\ Q_c,\ T_{3e},\ W_{3e}$$

and input variables are:

$$N_g,\ P_{3e}$$

The compressor stall parameter is defined by:

$$Z = \frac{P_{3e}/P_{2e} - P_{3e}/P_{2e})_{min}}{P_{3e}/P_{2e})_{stall} - P_{3e}/P_{2e})_{min}} \tag{4}$$

where the stall and minimum lines are functions of corrected speed.

The power required to drive the compressor is:

$$\Delta H_c = W_{3e} H_{3e} - W_{2e} H_{2e} \tag{5}$$

The nondimensional quantity $\Delta H_c/W_{2e}H_{2e}$ was calculated with the cycle deck and is used to calculate torque:

$$Q_c = \frac{60J}{2\pi}\left(\frac{\Delta H_c}{W_{2e} H_{2e}}\right)\left(\frac{W_{2e} H_{2e}}{N_g}\right) \tag{6}$$

To calculate the compressor temperature rise, the enthalpy change is required. It is assumed that bleed flow is either small or zero; therefore:

$$\frac{H_{3e} - H_{2e}}{H_{2e}} = \frac{\Delta H_c}{W_{2e} H_{2e}} \tag{7}$$

Thus, the approximation:

$$T_{3e} = T_{2e} + \left(H_{3e} - H_{2e}\right)\frac{1}{C_p} \doteq T_{2e} + \left(\frac{\Delta H_c}{W_{2e} H_{2e}}\right)\frac{H_{2e}}{C_p} \tag{8}$$

The value of Cp is a constant and can be used to help offset the approximation of enthalpy.

Inlet flow $W_{2e}$, was extracted from cycle data as a function of speed and stall parameter.

The J85 engine has a leakage flow which is bled from the compressor and returned aft of the turbine:

$$W_{3.0e} = W_{3e} - (0.01\ W_{3e}) = 0.99\ W_{3e} \tag{9}$$

Figure 6 shows the block diagram for the compressor model.

Combustor Model

The combustor variables to be calculated are:

$$W_{4e},\ T_{4e},\ P_{3e}$$

and the input variables are:

$$P_{4e},\ T_{3e},\ W_{3.1e},\ W_{Fe},\ N_g,\ Z$$

Turbine inlet flow is simply:

$$W_{4e} = W_{3.1e} + W_{Fe} \tag{10}$$

Combustor temperature rise is computed from:

$$T_{4e} - T_{3e} = \frac{W_{Fe}}{W_{3.1e}} \left(Q\eta_b - N_b\right) \frac{1}{C_p} \tag{11}$$

The data for efficiency $\eta_b$ were presented as a function of $W_{Fe}/W_{3.1e}$ and a variable $\beta_e$,

where:

$$\beta_e = \frac{103.1}{P_{3e}^{4/3} \cdot \left(\frac{T_{3e}}{1000}\right)^{1/10}} \tag{12}$$

This was rearranged to:

$$\beta_e = K\ \alpha_e\ \frac{W_{2e}\ \sqrt{\theta_{2e}}/\delta_{2e}}{\left(P_{3e}/P_{2e}\right)^{4/3}\ \left(T_{3e}/T_{2e}\right)^{1/10}} \tag{13}$$

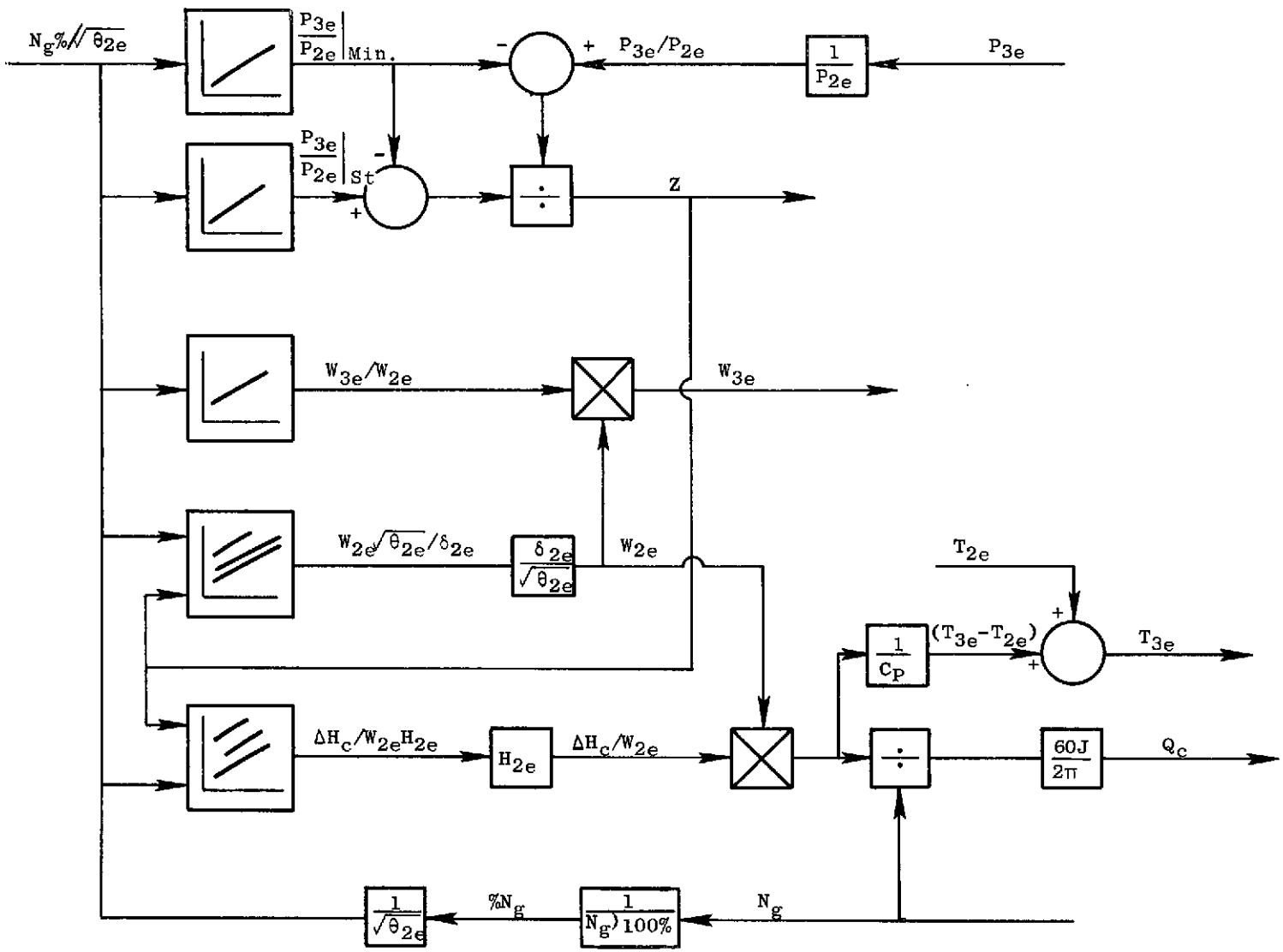


Figure 6. Schematic Diagram of Compressor Model.

where $K = W_{3.1e}/W_{3e}$ (14)

and

$$\alpha_e = \frac{10^{1.3}\sqrt{518.7}}{14.7\ P_{2e}^{1/3}\ T_{2e}^{6/10}}\left(\frac{W_{3e}}{W_{2e}}\right) \quad (15)$$

From the compressor data:

$\frac{W_{3e}}{W_{2e}}$ is a function of $N_g/\sqrt{\theta_{2e}}$.

Thus $\alpha_e$ is a function of $N/\sqrt{\theta_{2e}}$,

and $\frac{W_{2e}\sqrt{\theta_{2e}}}{\delta_{2e}}$, $P_{3e}/P_{2e}$, $T_{3e}/T_{2e}$ and $\beta_e/K$ are functions of $N_g/\sqrt{\theta_{2e}}$ and Z.

Using the above equations for $\beta_e$, and $\alpha_e$, and pressure, temperature, and airflow data from the compressor at various $N_g/\sqrt{\theta_{2e}}$ and Z, the function

$$\frac{\beta_e}{K} = f\left(N_g/\sqrt{\theta_{2e}},\ Z\right) \quad (16)$$

was calculated. Combustor efficiency is a function of $\beta_e$ and fuel/air ratio.

The combustion function Nb is nearly a linear function of $T4_e$ alone and was represented as such. The pressure $P3_e$ was obtained from

$$1 - \frac{P_{4e}}{P_{3e}} = \left[0.856 + 0.85\left(\frac{T_{4e}}{T_{3e}} - 1\right)\right]\left[1 - \left(1 + \frac{\gamma - 1}{2} M_{E3.1}^2\right)^{-\frac{\gamma}{\gamma-1}}\right] \quad (17)$$

In these equations $P_{4e}/P_{3e}$ is a function of Mach number and specific heat ratio. An average value of $\gamma_{3e} = 1.33$ was assumed for the combustor.

The inlet flow $W_{3.1e}$ is:

$$W_{3.1e} = W_{3.0e} - W_{Be} \quad (18)$$

The block diagram of the combustor model is shown in Figure 7.

Turbine Model

The turbine variables to be calculated are:

$P_{4e}$, $T_{5e}$, $Q_T$

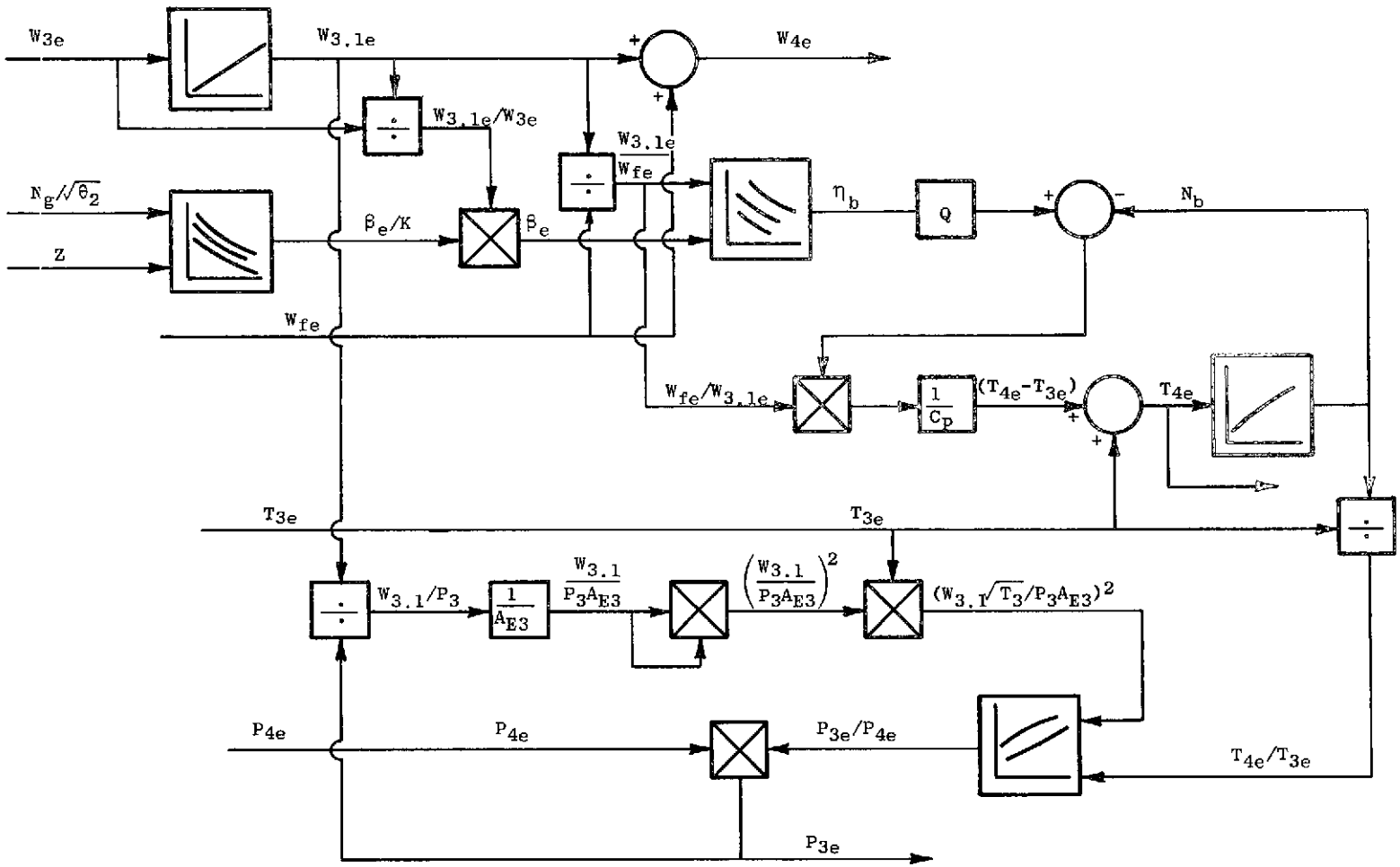


Figure 7. Schematic Diagram of Combustor Model.

and the input variables are:

$$P_{5e},\ T_{4e},\ W_{4e},\ W_{3e},\ N_g$$

The turbine flow map is a function of $N_g/\sqrt{T_{4e}}$ and $\Delta H/T_{4e}$ .

Enthalpy change $\Delta H/T_{4e}$ is a function of speed and turbine pressure drop and is limited by the annulus choke line. The block diagram for the turbine model is shown in Figure 8.

Rotor Dynamics

The variable to be calculated is:

$$N_g$$

and the input variables are:

$$Q_c,\ Q_T$$

Engine speed was obtained by integration of the difference of turbine torque supplied and compressor torque required:

$$Q_T - Q_c = \Delta Q = \frac{2\pi I}{60}\ \frac{dN_g}{dt} \tag{19}$$

where:

$$I = 0.516 \text{ slug-ft}^2\ (0.699\ K_g\text{-m}^2) = \text{J85-13 rotor inertia} \tag{20}$$

Thus,

$$N_g = \int_o^t \frac{60\ \Delta Q}{2\pi I}\ dt \tag{21}$$

The block diagram is shown in Figure 9.

Exhaust Nozzle

The variable to be calculated is $P_{5e}$ and the input variables are

$$W_{5e},\ T_{4e}\ A_{8e},\ P_{oe}$$

Cycle data indicate $P_{8e}$ is approximately 98% of $P_{5e}$, and $P_{8e}$ can be determined as follows:

let

$$C_D = \frac{A_{E8e}}{A_{8e}} \tag{22}$$

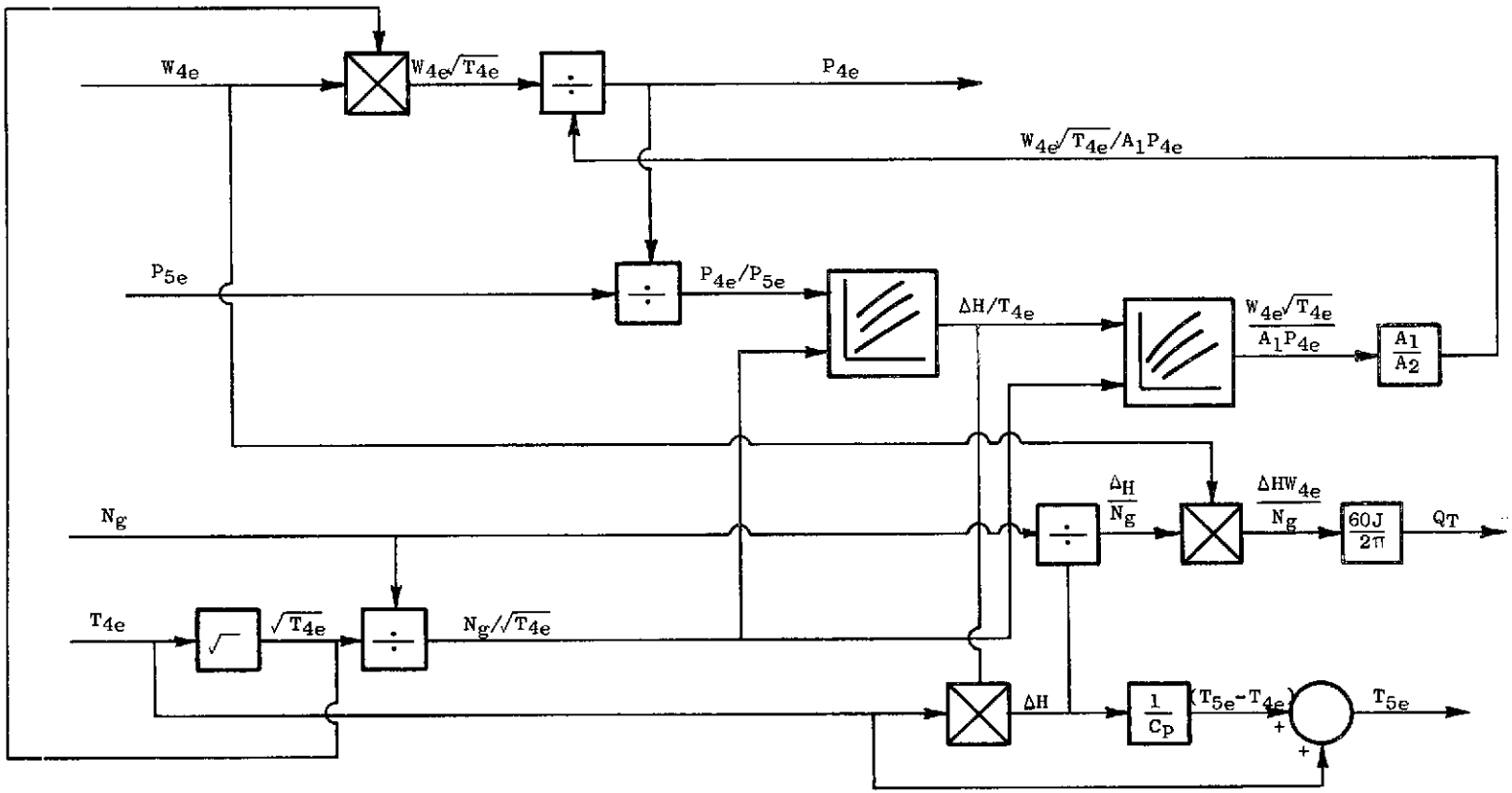


Figure 8. Schematic Diagram of Turbine Model.

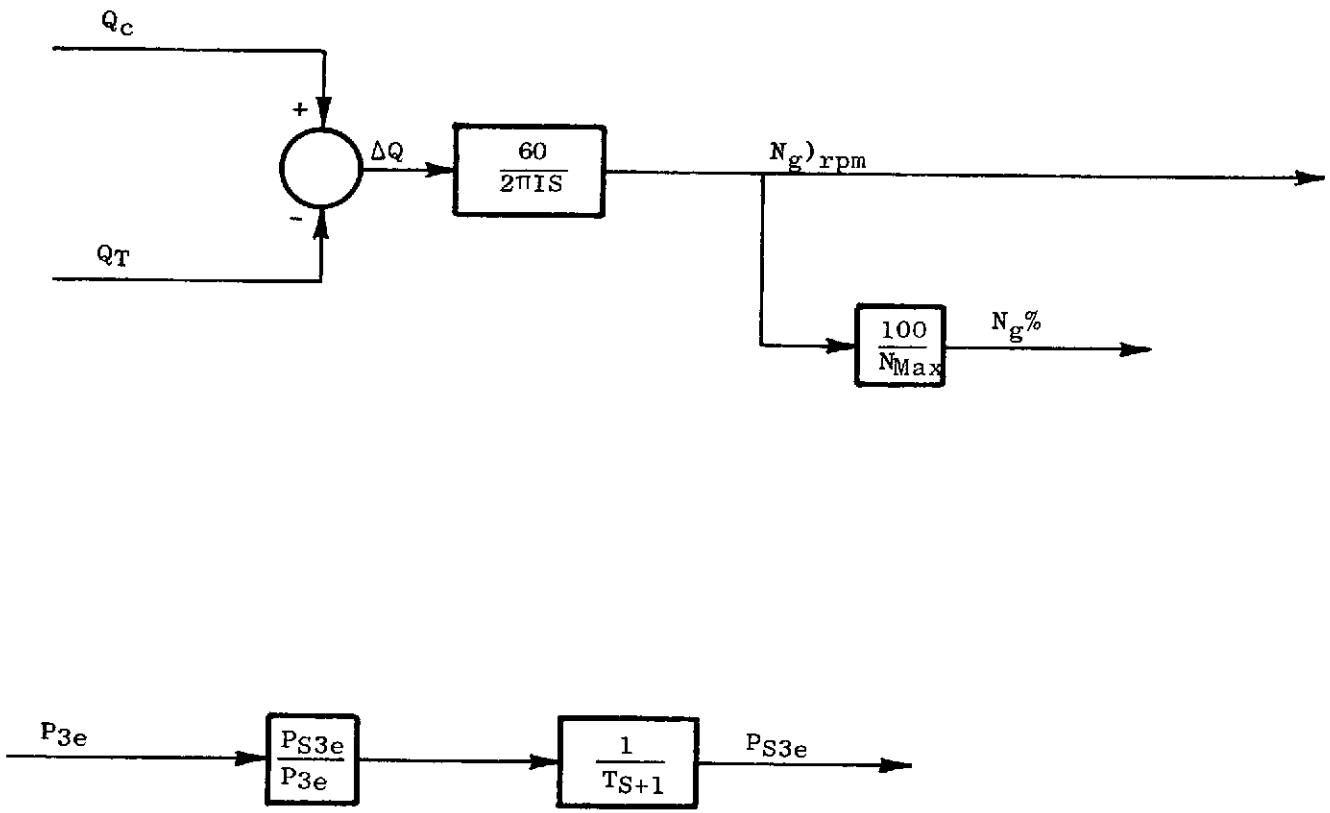


Figure 9. Schematic Diagram of Rotor Model.

A nozzle flow function in terms of static pressure is used to determine nozzle pressure ratios.

Then,

$$0.98\ P_{5e} = \left(\frac{P_{8e}}{P_{oe}}\right) \quad x \quad P_{oe} \tag{23}$$

The block diagram for the nozzle is shown in Figure 10.

The engine model was made operational with a slave fuel control, and adjustments were made to the model in order to obtain better agreement with steady-state cycle data. This operational and checked out model of the J85-13 engine was then used as a design tool in the determination of dynamic requirements for the hydrogen and methane fuel systems.

## Control System Model Development

The control system model is separated into its various components: the pump, heat exchanger, fuel line, pressure regulator, metering valve, and electrical control. The equations describing each of these components involve temperatures, pressures and flows throughout the control system. Figure 11 identifies and shows the relationship of these components and variables.

### Fuel Pump Model

The pump variables to be calculated are:

$W_p$, Np, Wp) calc

and the inputs are:

$V_{Wf}$, $V_{Pp}$, and $P_{fi}$

Pump flow, Wp, is a function of pressure Pp and pump speed. Pump speed Np is modulated to maintain pump pressure Pp. Theoretical pump flow (assuming constant pressure), Wp) calc, is calculated and compared with engine fuel flow $V_{Wf}$ to limit pump speed. A block diagram of the fuel pump is shown in Figure 12.

### Heat Exchanger Model

The heat exchanger variables to be calculated are:

$T_{fo}$, $P_{fi}$, $W_{ai}$, $P_{HE}$, $T_{ai}$, and $T_{fi}$,

and the inputs are:

$\bar{N}_g$, $\bar{W}p$, $\bar{WR}$, and $\bar{W}f$.

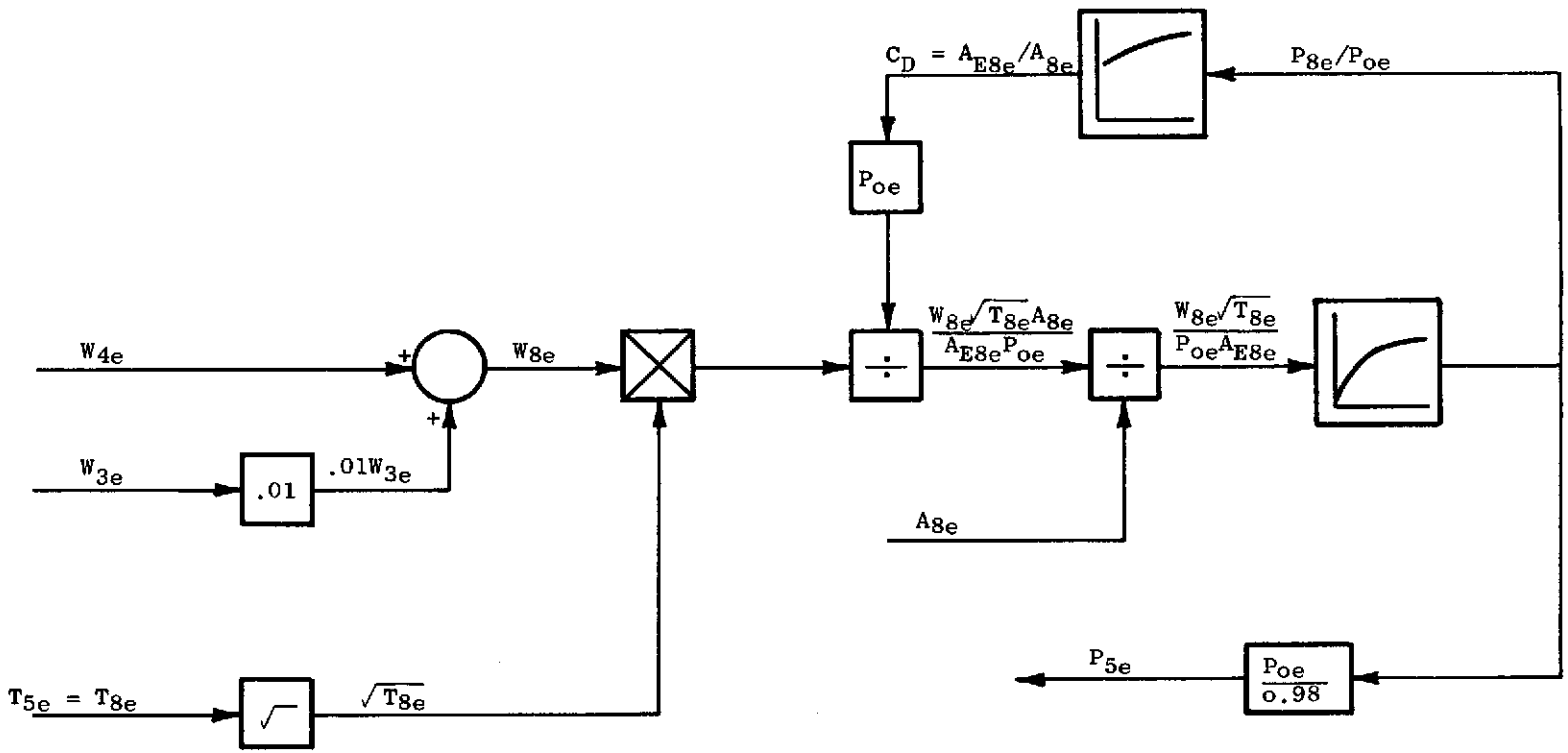


Figure 10. Schematic Diagram of Nozzle Model.

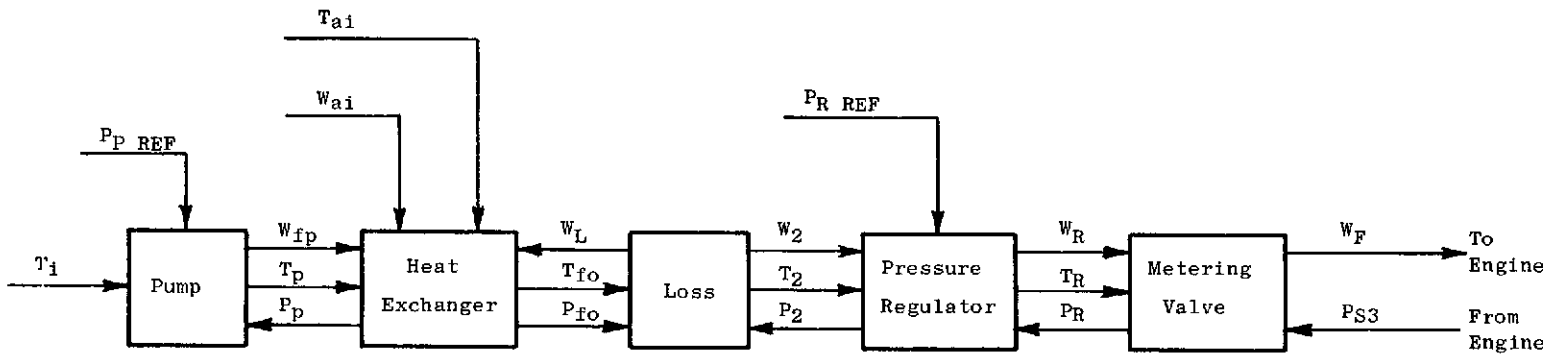


Figure 11. Schematic Diagram of Control System.

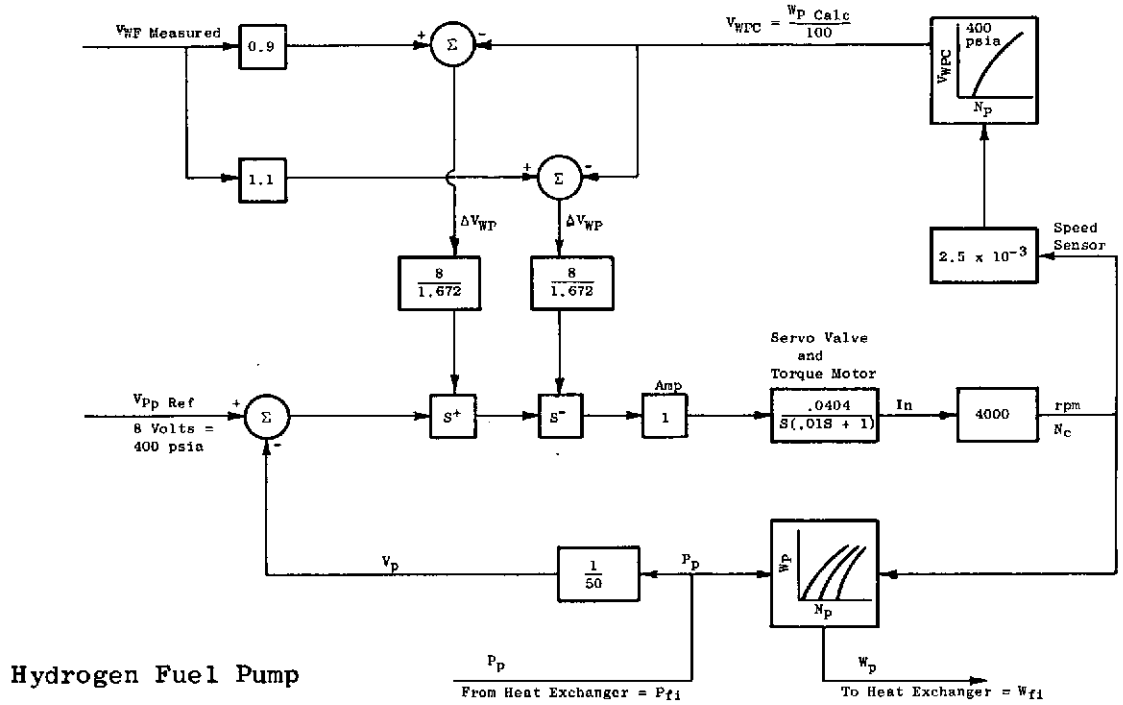


Hydrogen Fuel Pump

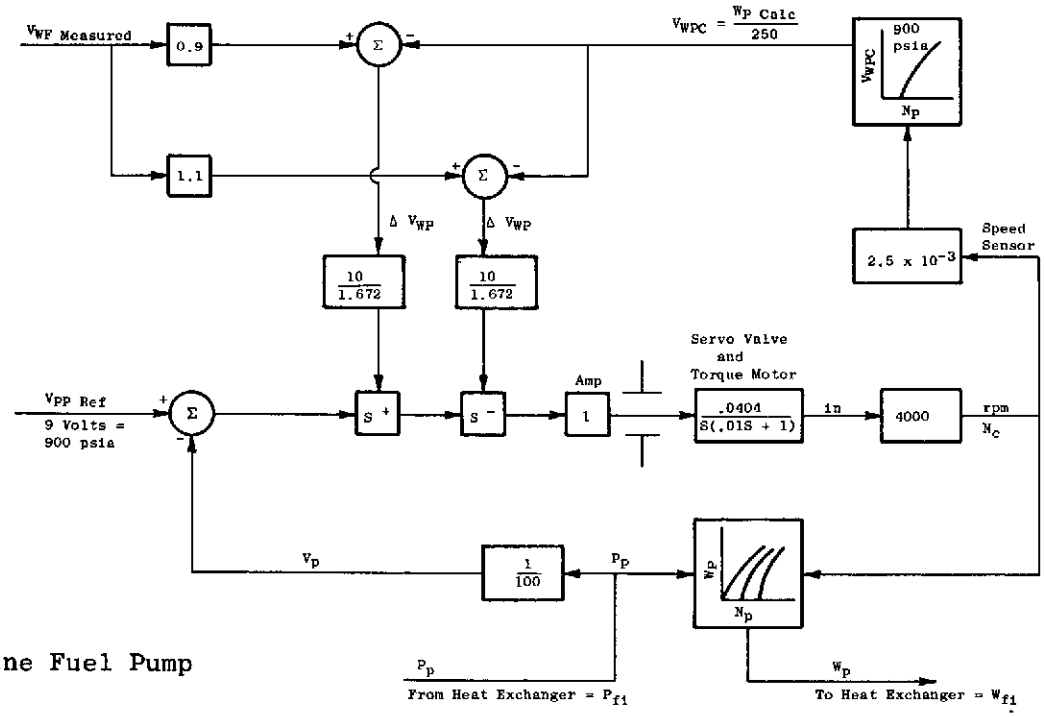


Methane Fuel Pump

Figure 12. Schematic Diagram of Hydrogen and Methane Fuel Pump Model.

Pressure in the heat exchanger ($P_{fo}$) is calculated from the flow unbalance of the heat exchanger (Wp is the flow in and WR is the flow out) and a pressure rise as a function of the heat exchanger flow level. Heat exchanger airflow, $W_{ai}$, is scheduled as a function of speed and fuel flow level. Air ($T_{ai}$) and fuel ($T_{fi}$) temperature are scheduled as a function of engine speed, and temperature of the fuel ($T_{fo}$) is calculated from variations in air temperature and fuel inlet temperature as a complex function of time. Data for the heat exchanger dynamics were obtained from the heat exchanger designer. A block diagram of the heat exchanger is shown in Figure 13.

Pressure Regulator Model

The pressure regulator variables to be calculated are:

$$P_2,\ WR,\ Wf,\ P_R,\ \text{and WF) calc}$$

and the inputs are:

$$WL,\ P_R)_{REF},\ T_R$$

Regulator pressure (PR) and line pressure ($P_7$) are calculated from the flow unbalances into and through the pressure regulator.

Regulator pressure ($P_R$) is controlled to a reference pressure of 700 psia ($4.83 \times 10^6$ N/m$^2$) for methane and 250 psia ($1.72 \times 10^6$ N/m$^2$) for hydrogen. Flow through the regulator is calculated using a flow function and regulator pressure area. Flow is choked through the metering port; hence, flow is calculated using fuel temperature, regulated pressure, and metering valve area. Fuel flow (assuming constant pressure) is calculated for the pump limit circuit. A block diagram of the pressure regulator is shown in Figure 14.

Main Fuel Control Model

The main fuel control variables to be calculated are:

$$N_g)_{DMD},\ V_{\dot{WF}},\ \text{and } A_{MV}$$

and the inputs are:

$$\alpha)_{DMD},\ N_g,\ \text{and Tf}$$

Speed demand is a function of throttle angle ($\alpha_{DMD}$). Accel rate/flow rate is a function of engine speed. The accel rate is calculated by multiplying accel rate/fuel flow by fuel flow. The decel rate is a constant times the accel rate. A comparison is then made between speed error, decel rate, and accel rate to request a change in metering valve area.

Position and rate feedback are used in the metering section of the electronic control which is modeled as shown in Figure 4.

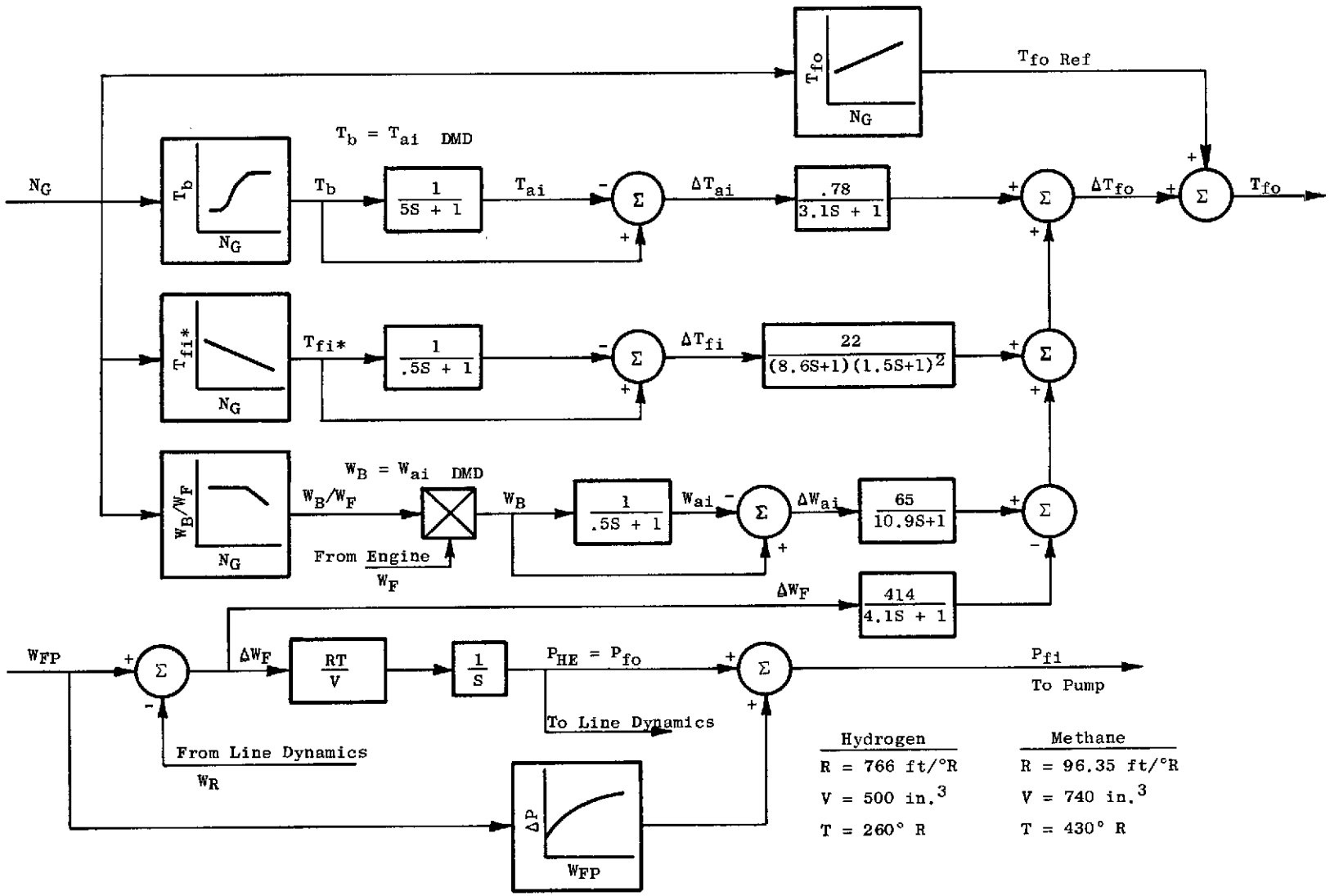


Figure 13. Schematic Diagram of Heat Exchanger Model.

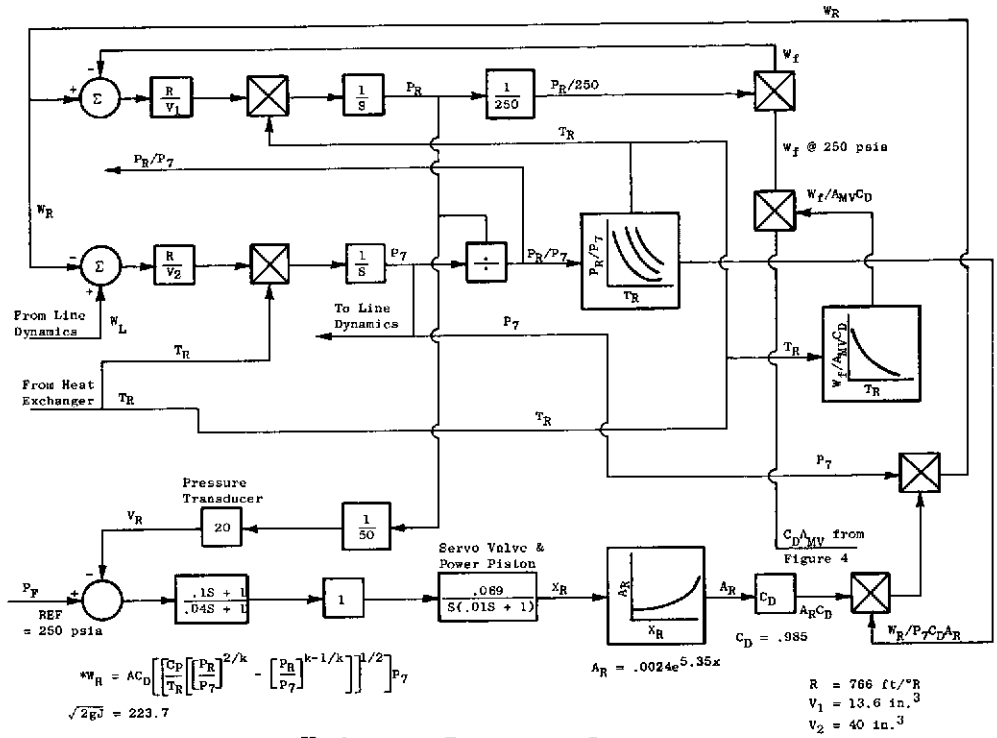


Hydrogen Pressure Regulator

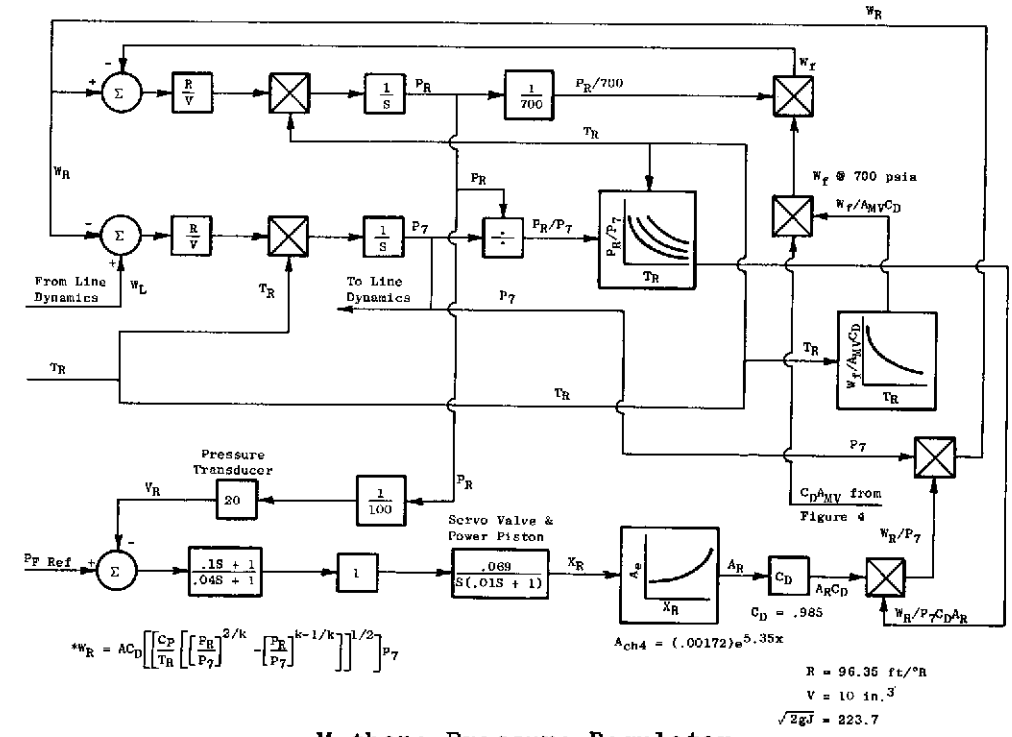


Methane Pressure Regulator

Figure 14. Schematic Diagram of Hydrogen and Methane Pressure Regulators.

Line Dynamics Model

The variable to be calculated is:

$$W_R$$

and the inputs are:

$$P_{fo} \text{ and } P_7$$

Pressure unbalance and fuel flow level are used to calculate flow through the line from the heat exchanger to the pressure regulator as shown in Figure 15.

System Model Results

The evaluation of system dynamic behavior at sea level and selected altitude points for both the hydrogen and methane fuel systems was performed on the engine and fuel system model using the EAI 690 hybrid computer. The computer model was used to verify and optimize preliminary linear analysis of the fuel system. Stable governing and acceptable throttle bursts and chops were attained at all altitudes for both fuels. A typical time history of engine and system parameters obtained at sea level for a throttle-burst acceleration of the methane configuration is shown in Figure 16, sheets 1 and 2. The corresponding deceleration for this configuration is shown in Figure 16, sheets 3 and 4. The sea level acceleration and deceleration of the hydrogen system configuration is shown in Figure 16, sheets 15, 16, 17, and 18. These runs established the values for system gains and time constants for both the hydrogen and methane fuel systems that provided the most compatible system operation over the entire flight envelope.

The computer model was later updated to reflect a reduction in length of fuel transmission line between the air-to-fuel heat exchanger and fuel metering package from 30 feet (9.15 m) to 20 feet (6.1 m) to be more consistent with the fuel piping installation at NASA-Lewis. This reduction permits an improvement in speed governor response which is helpful to improve engine acceleration characteristics in that portion of transients where exhaust nozzle closure significantly affects speed vs fuel flow characteristics. Figure 16, sheets 23 through 26, shows a throttle burst in approximately 7 seconds from 57% to 100% speed for methane at sea level static flight conditions.

The system dynamic model was also temporarily altered to delete the representation of the facility fuel transmission line between the air heat exchanger fuel outlet and fuel metering package inlet. This line run is not expected to be required in an aircraft-type installation, and an assessment was desired of the optimum J85 engine acceleration time obtainable with the fuel system in a flight installation. Removal of the line dynamics permitted an increase in speed governor gain and response; also, a further enriched acceleration fuel schedule was employed. A best effort acceleration time, using

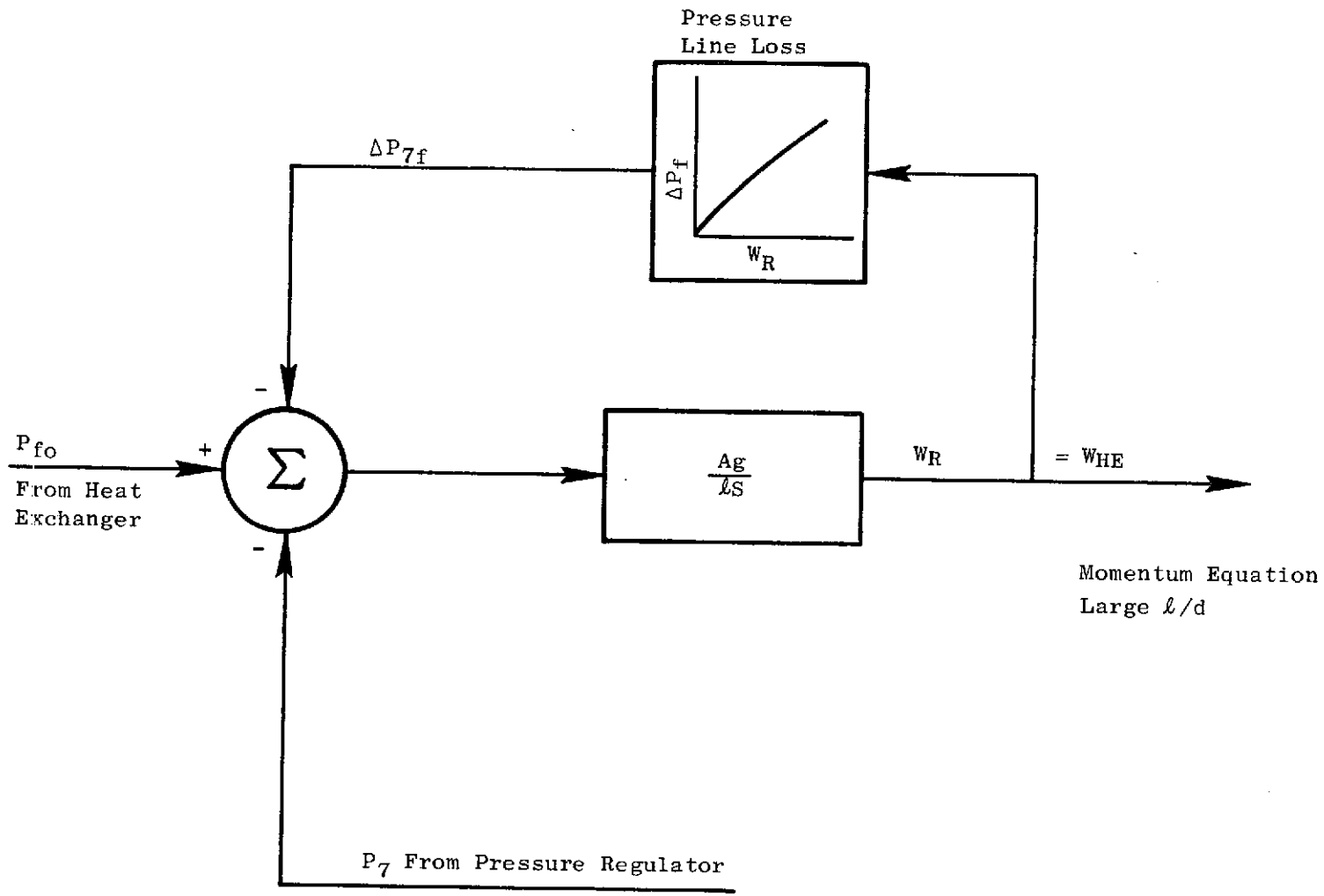


Figure 15. Schematic Diagram of Line Dynamics Model (Between Pressure Regulator and Heat Exchanger).

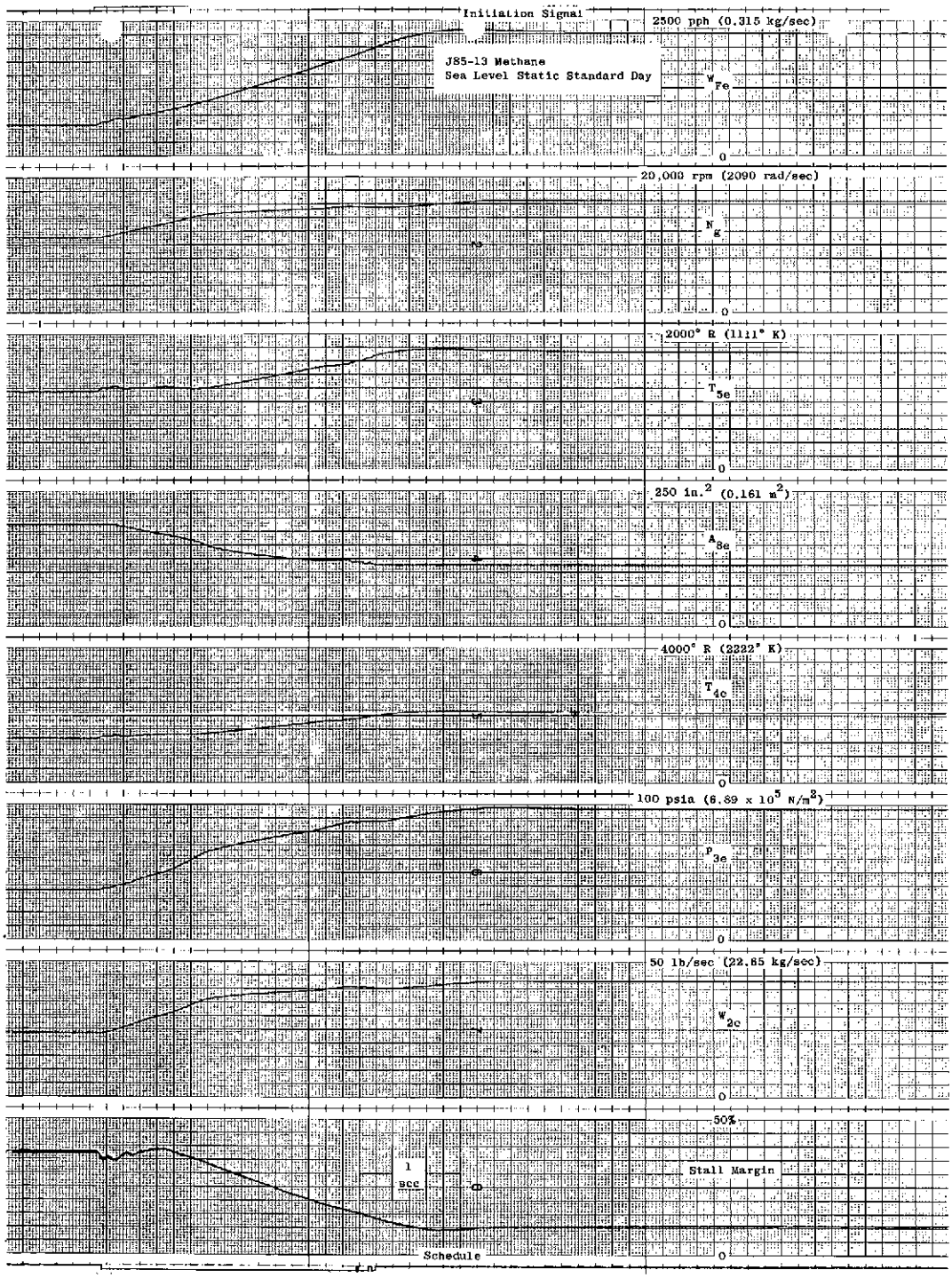


Sheet 1

Figure 16. Typical Time History of Engine and System Parameters for Methane Configuration.

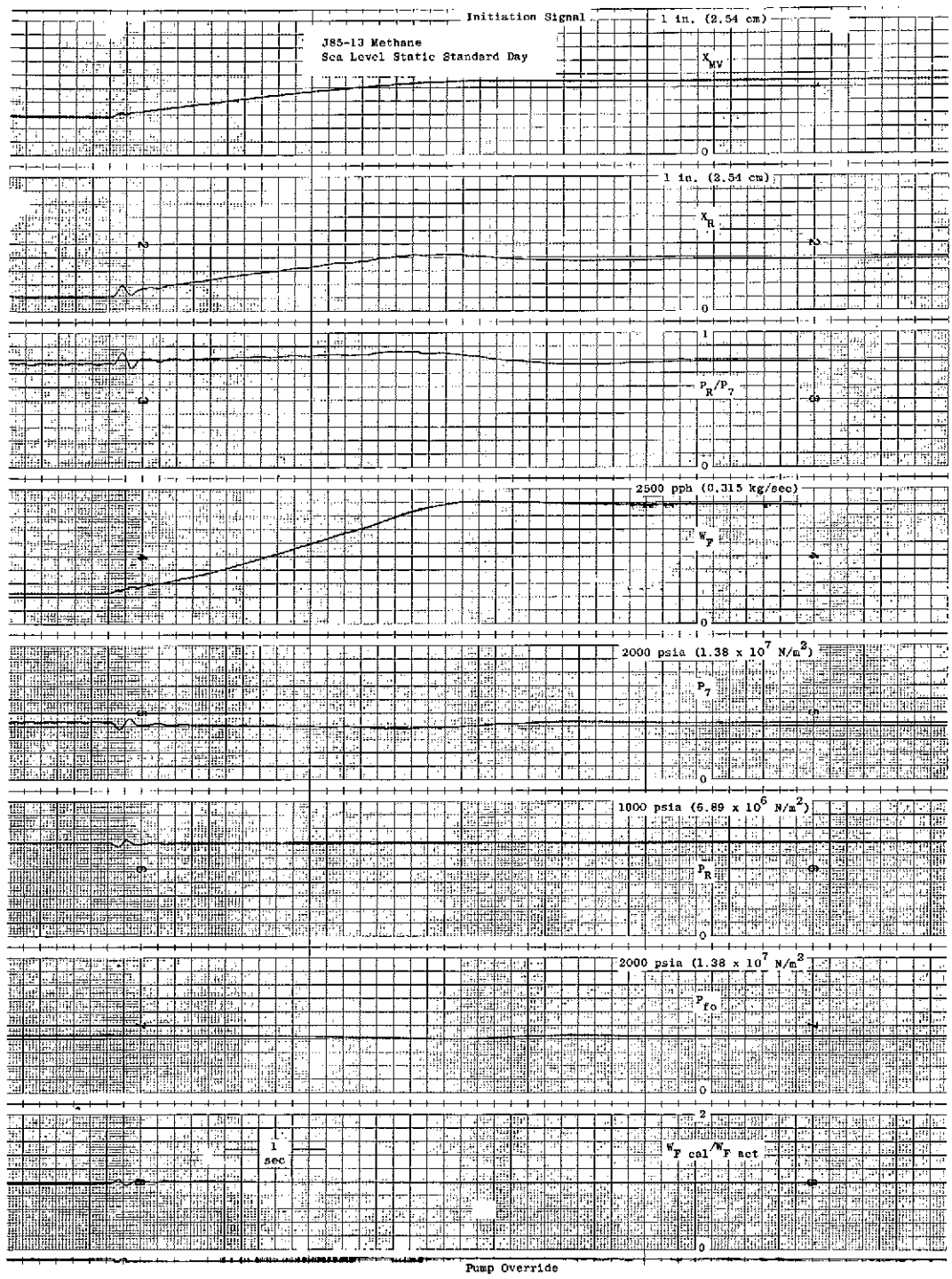


Sheet 2

Figure 16. Typical Time History of Engine and System Parameters for Methane Configuration (Continued).

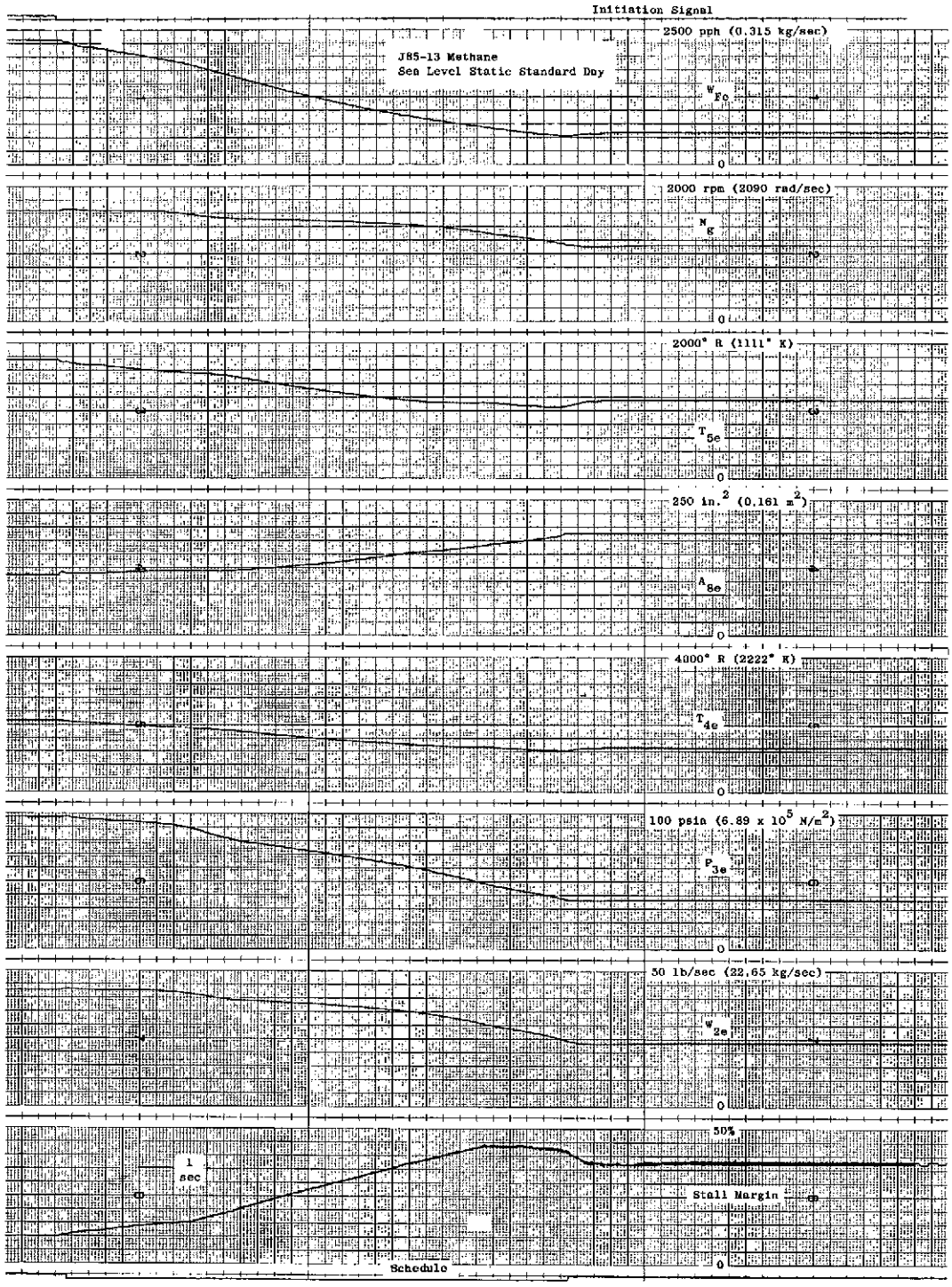


Sheet 3

Figure 16. Typical Time History of Engine and System Parameters for Methane Configuration (Continued).

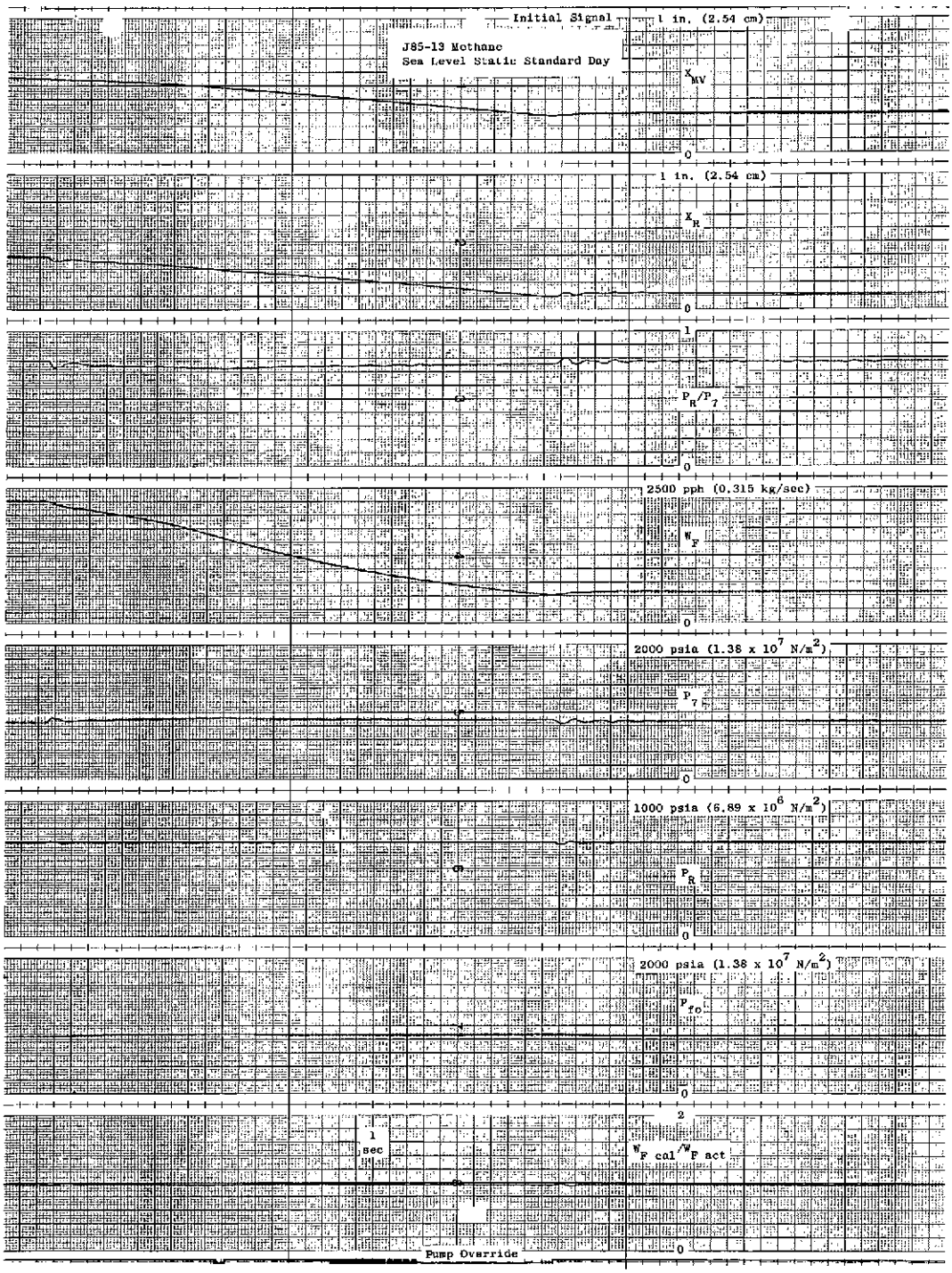


Sheet 4

Figure 16. Typical Time History of Engine and System Parameters for Methane Configuration (Continued).

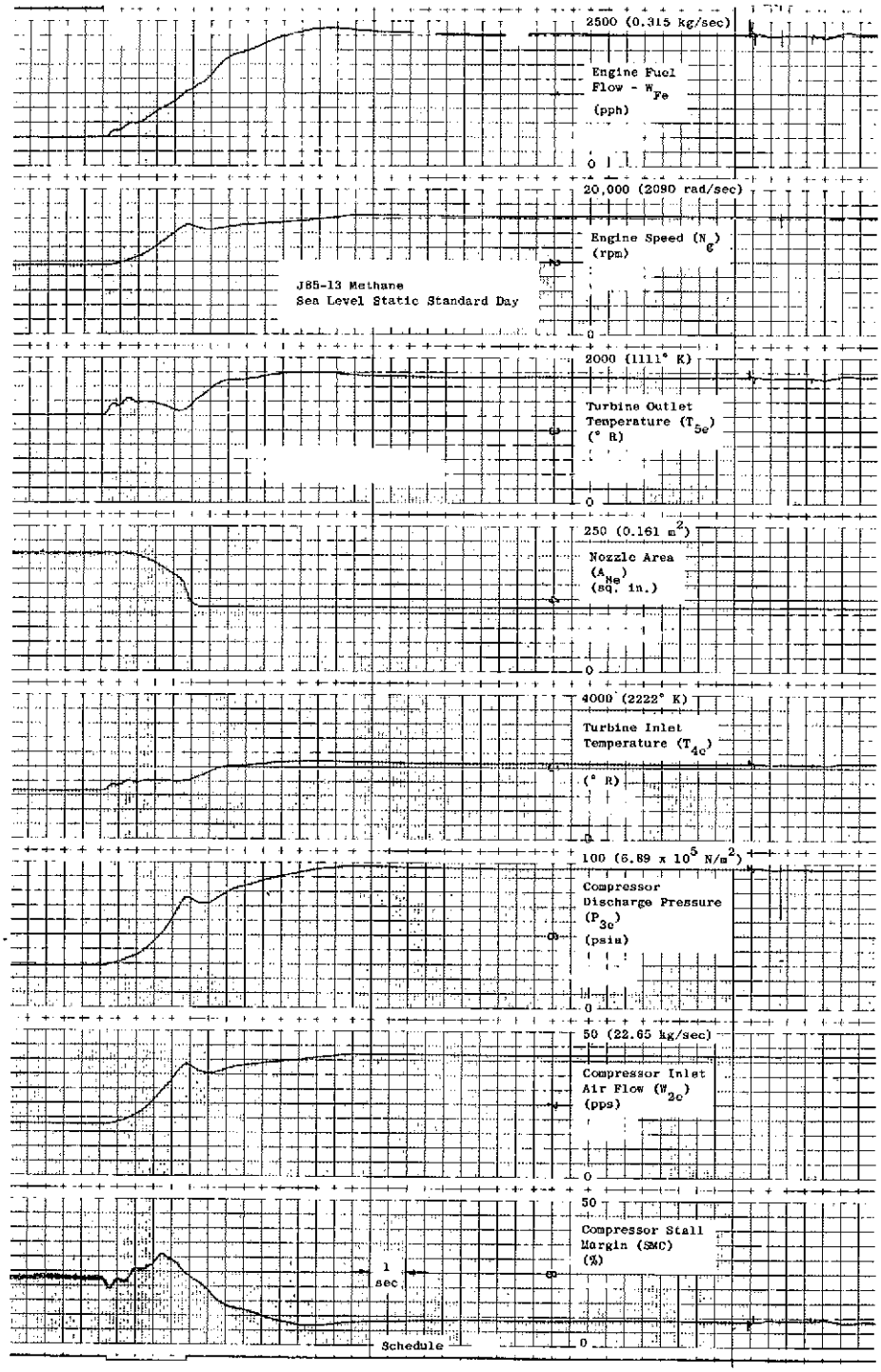


Sheet 15

Figure 16. Typical Time History of Engine and System Parameters for Methane Configuration (Continued).

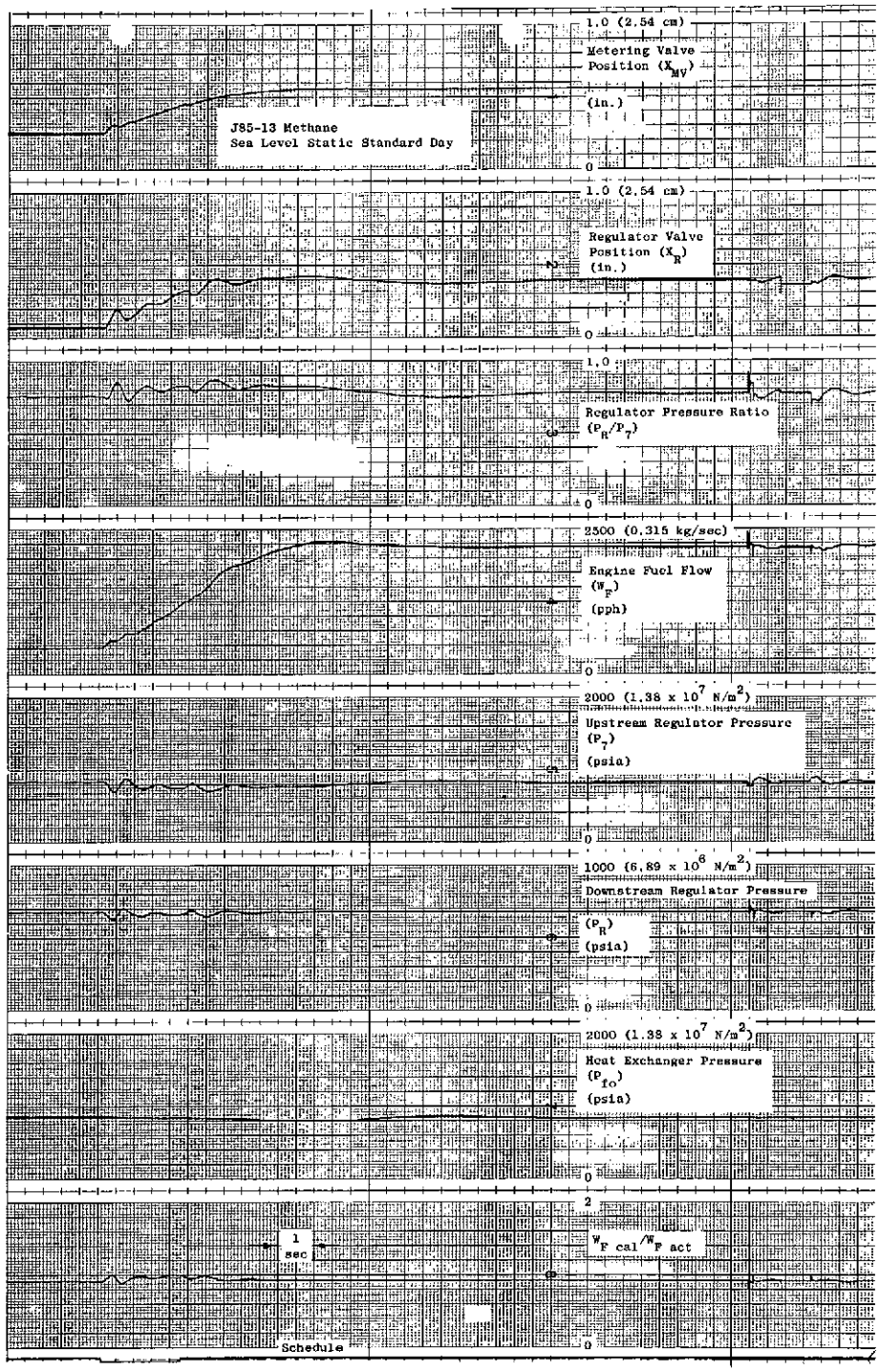


Sheet 16

Figure 16. Typical Time History of Engine and System Parameters for Methane Configuration (Continued).

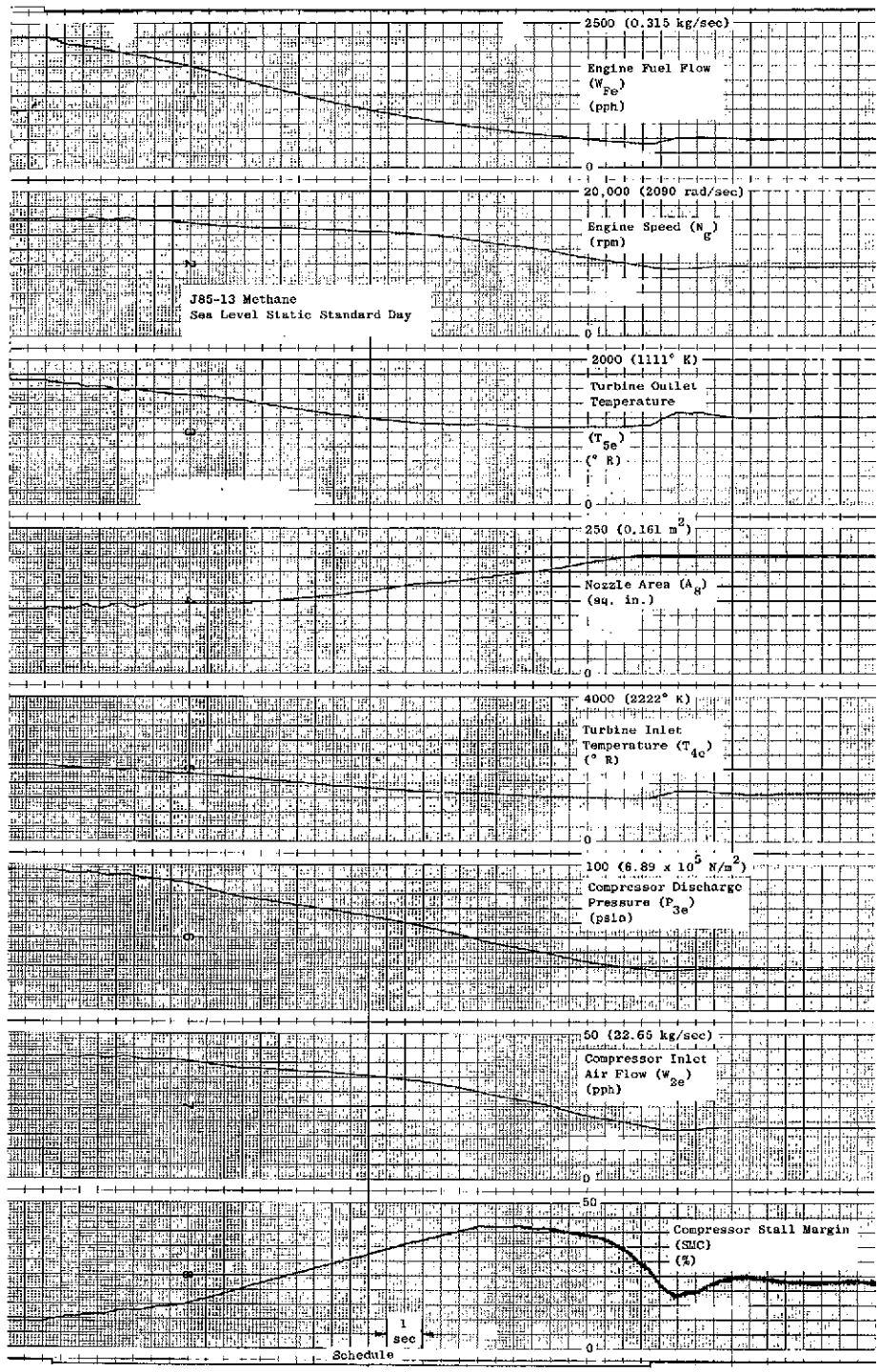


Sheet 17

Figure 16. Typical Time History of Engine and System Parameters for Methane Configuration (Continued).

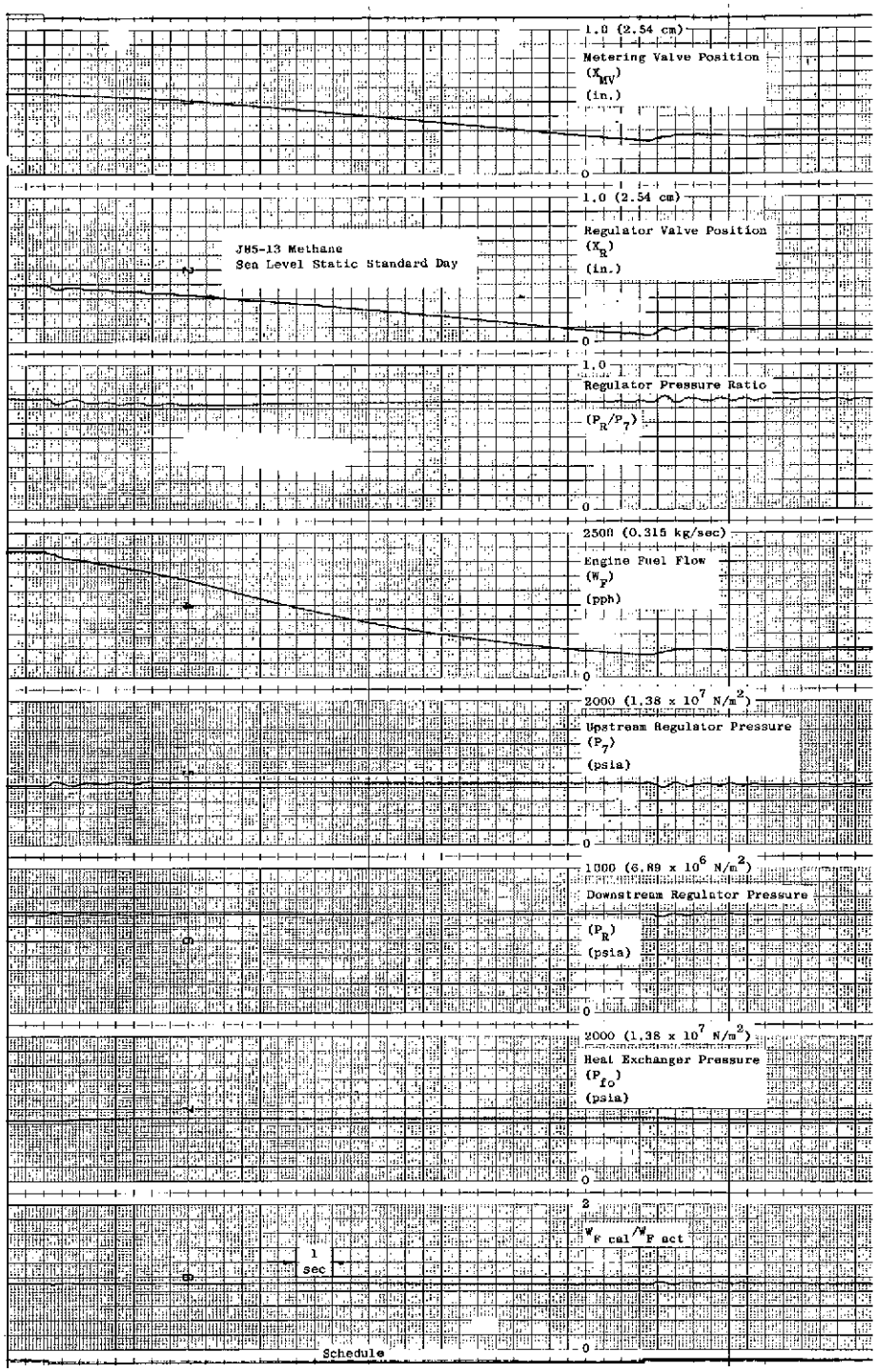


Sheet 18

Figure 16. Typical Time History of Engine and System Parameters for Methane Configuration (Concluded).

methane fuel, of 3.5 seconds from 57% idle to 100% speed was obtained. Figure 17, sheets 1 and 2 shows the engine and fuel system time histories of this run. The traces show that turbine temperature limits are closely approached during the fuel system transient period, so that use of further increased fuel rates of change would be unproductive. The computer model was then run at other points in the flight envelope to map out the expected operating characteristics.

## FLOW METERING STUDY

Since the system conceptual design involved the use of variable area flow metering through a choked, convergent flow passage with variable gas entrance temperatures, it was necessary to define specific flow functions for the $H_2$ and $CH_4$ fuels for use in detail design of the metering valve and electrical flow computation circuits. Useful background data for $H_2$ flow metering in the temperature range 175° R (97.2° K) to 500° R (278° K) were found in Reference (1). This temperature range embraced the metering entrance temperatures expected for all specified engine operating conditions on $H_2$ fuel, but did not cover the temperature below 175° R (97.2° K) which could be encountered during system chilldown.

Reference (1) establishes an expression and data for a real gas flow function for choked hydrogen flow which is equivalent to:

$$\frac{W_8}{A_{x8}} = \frac{C^* P_8 \cdot K_u}{\sqrt{R\ T_8}} \qquad (24)$$

The dimensionless factor, C*, corrects the flow function for real gas effects in the metering. Data extracted or interpolated from Reference (1) for values of C* at selected values of $P_8$ and $T_8$ are tabulated in Table II as are corresponding values of $W_8/A_{x8}$ calculated using Equation (24). These flow function points were used to define the $H_2$ metering flow function in the range of $T_8$ covered by Reference (1).

Table II. $H_2$ Flow Function Values from NASA TN D-2565.

| $T_{\circ 8}$ R | $(T_8)$ (° K) | $P_8$, psia | $(P_8)$ $(N/m^2)$ | C* | $(K\mu)$ | $\frac{R}{\text{ft-lb}_f/\text{lb}_m\text{-°R}}$ | $\frac{(R)}{(J/K_g\text{-°K})}$ | $W_8/A_{x8}$ pps/in$^2$ | $(WA_8/A_{x8})$ $\left(\frac{K_g}{\text{sec-m}^2}\right)$ |
|---|---|---|---|---|---|---|---|---|---|
| 175 | ( 97.2) | 250 | $(1.725\text{x}10^6)$ | 0.7104 | 5.67(1.0) | 767 | $(4.157\text{x}10^3)$ | 2.74 | $(1.93\text{x}10^3)$ |
| 200 | (111.2) | 250 | $(1.725\text{x}10^6)$ | 0.6970 | 5.67(1.0) | 767 | $(4.157\text{x}10^3)$ | 2.52 | $(1.77\text{x}10^3)$ |
| 300 | (166.6) | 250 | $(1.725\text{x}10^6)$ | 0.6747 | 5.67(1.0) | 767 | $(4.157\text{x}10^3)$ | 1.99 | $(1.396\text{x}10^3)$ |
| 500 | (278.0 | 250 | $(1.725\text{x}10^6)$ | 0.6782 | 5.67(1.0) | 767 | $(4.157\text{x}10^3)$ | 1.55 | $(1.087\text{x}10^3)$ |

Since it was desirable to extend the low temperature range of the $H_2$ flow function to include chilldown conditions, another method was used to estimate the flow function from 75° R (41.7° K) to 150° R (83.3° K). An iterative procedure was used to establish metering throat density and velocity corresponding to

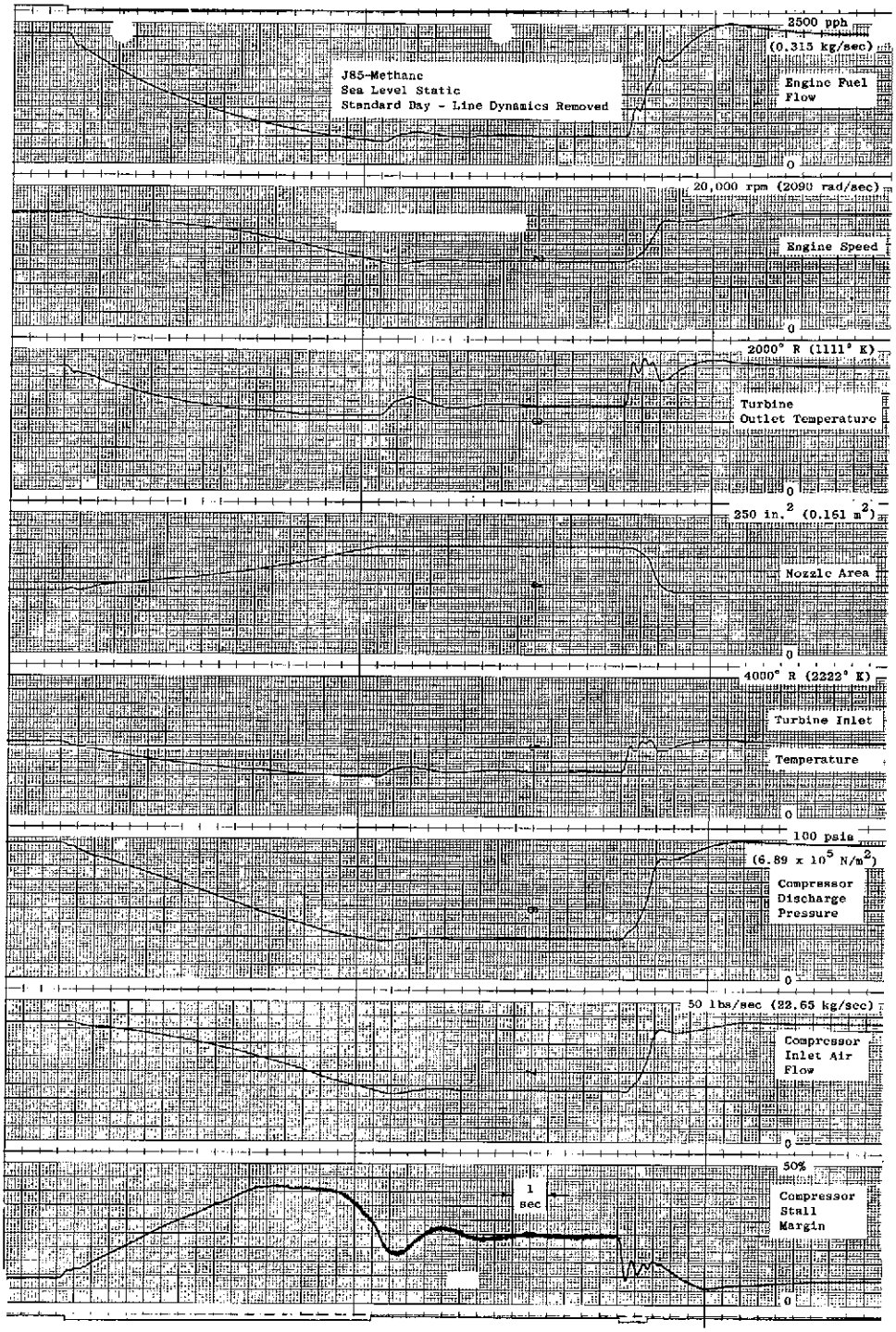


Sheet 1

Figure 17. Time History of Engine and System Parameters for Methane Configuration with Line Dynamics Removed.

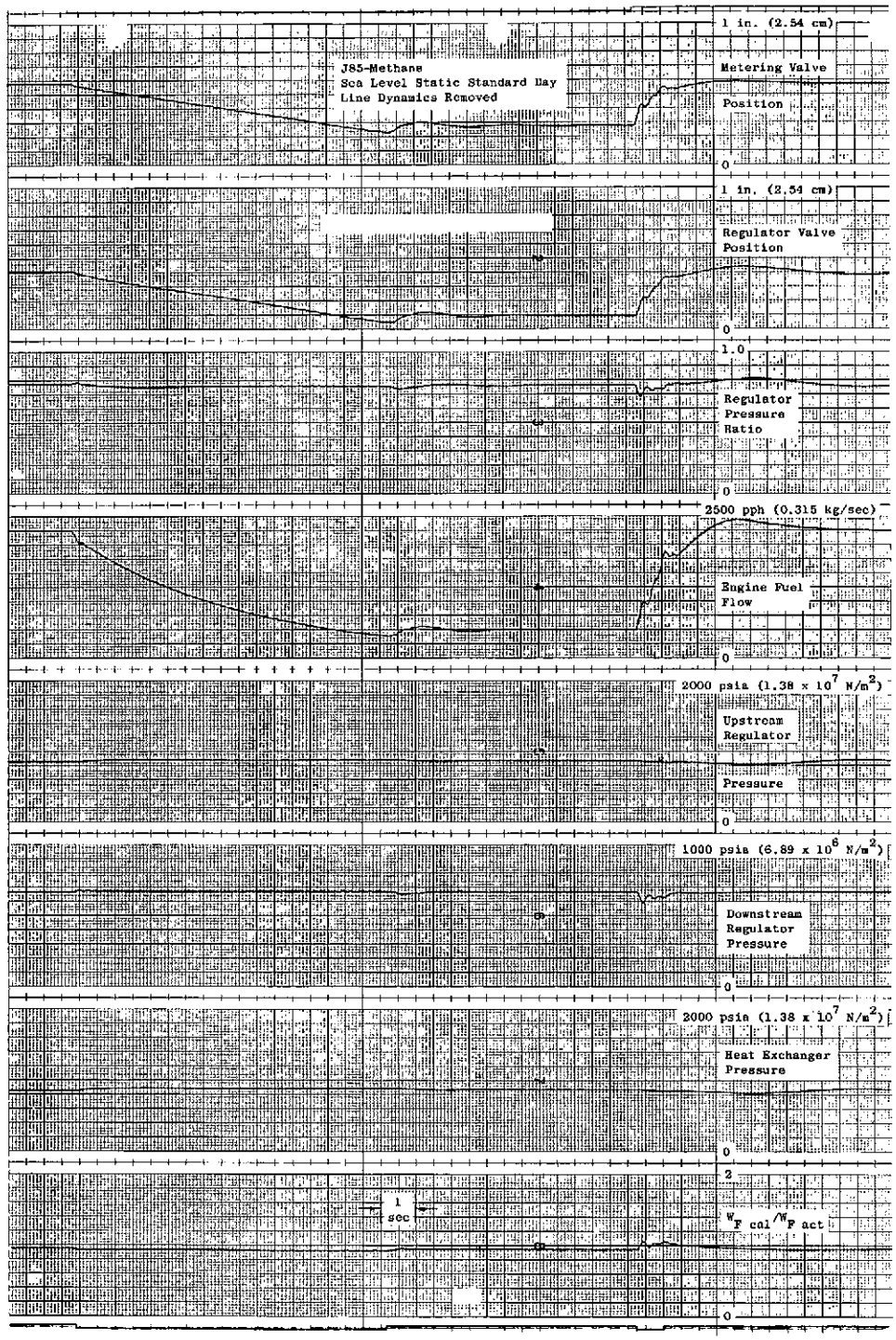


Sheet 2

Figure 17. Time History of Engine and System Parameters for Methane Configuration with Line Dynamics Removed (Concluded).

selected entrance pressure and temperature conditions. An isentropic flow process from metering entrance to metering throat was assumed, and entrance velocity to the metering passage was assumed negligible in relation to throat velocities. The enthalpy change from entrance to throat was determined from the equation:

$$H_8 - H_c = \frac{v_c^2}{2g_o J} \tag{25}$$

Trial estimates of the value of $v_c$ were initially used at each selected entrance case. Graphical property maps for para-hydrogen available in Reference (2) were employed to trace the isentropic process from selected entrance conditions to throat conditions based on the estimated enthalpy change. The velocity estimate was then checked at the trial throat conditions against data for $H_2$ sonic velocity vs. temperature available in Reference (2). The velocity estimation process was repeated until the estimate matched the sonic velocity value from Reference (2) corresponding to the throat temperature, and throat density was then obtained from Reference (2). A value for the flow function at the selected entrance conditions was then established from the equation:

$$\frac{W_8}{A_{x8}} = \frac{\rho_c \, v_c}{144} \tag{26}$$

Values of the flow function established in this manner are tabulated in Table III for entrance temperatures 75° R (41.7°K) to 150° R (83.3° K).

The values of the hydrogen flow function established in Tables II and III were used to draw a continuous flow function versus entrance temperature as plotted on Figure 18. This function was used in design of hydrogen flow metering and computation circuits.

Table III. $H_2$ Flow Function Values from $H_2$ Property Maps.

| $T_8$ ° R | $(T_8)$ (°K) | $P_8$ psia | $(P_8)$ $(N/m^2)$ | $\rho_c$ $lb/ft^3$ | $(\rho_c)$ $(K_g/m^3)$ | $v_c$ ft/sec | $(v_c)$ (m/sec) | $W_8/A_{x8}$ $pps/in^2$ | $(W_8/A_{x8})$ $(\frac{K_g}{sec\text{-}m2})$ |
|---|---|---|---|---|---|---|---|---|---|
| 75 | (41.7) | 250 | $(1.725 \times 10^6)$ | 0.55 | (8.80) | 1245 | (380) | 4.75 | $(3.33 \times 10^3)$ |
| 80 | (44.4) | 250 | $(1.725 \times 10^6)$ | 0.51 | (8.17) | 1375 | (419) | 4.86 | $(3.40 \times 10^3)$ |
| 85 | (47.2) | 250 | $(1.725 \times 10^6)$ | 0.45 | (7.20) | 1450 | (442) | 4.50 | $(3.16 \times 10^3)$ |
| 90 | (50.0) | 250 | $(1.725 \times 10^6)$ | 0.41 | (6.56) | 1500 | (457) | 4.27 | $(3.00 \times 10^3)$ |
| 100 | (55.6) | 250 | $(1.725 \times 10^6)$ | 0.37 | (5.92) | 1650 | (503) | 4.24 | $(2.97 \times 10^3)$ |
| 120 | (66.7) | 250 | $(1.725 \times 10^6)$ | 0.29 | (4.64) | 1850 | (564) | 3.73 | $(2.62 \times 10^3)$ |
| 160 | (88.9) | 250 | $(1.725 \times 10^6)$ | 0.19 | (3.04) | 2200 | (671) | 2.90 | $(2.04 \times 10^3)$ |

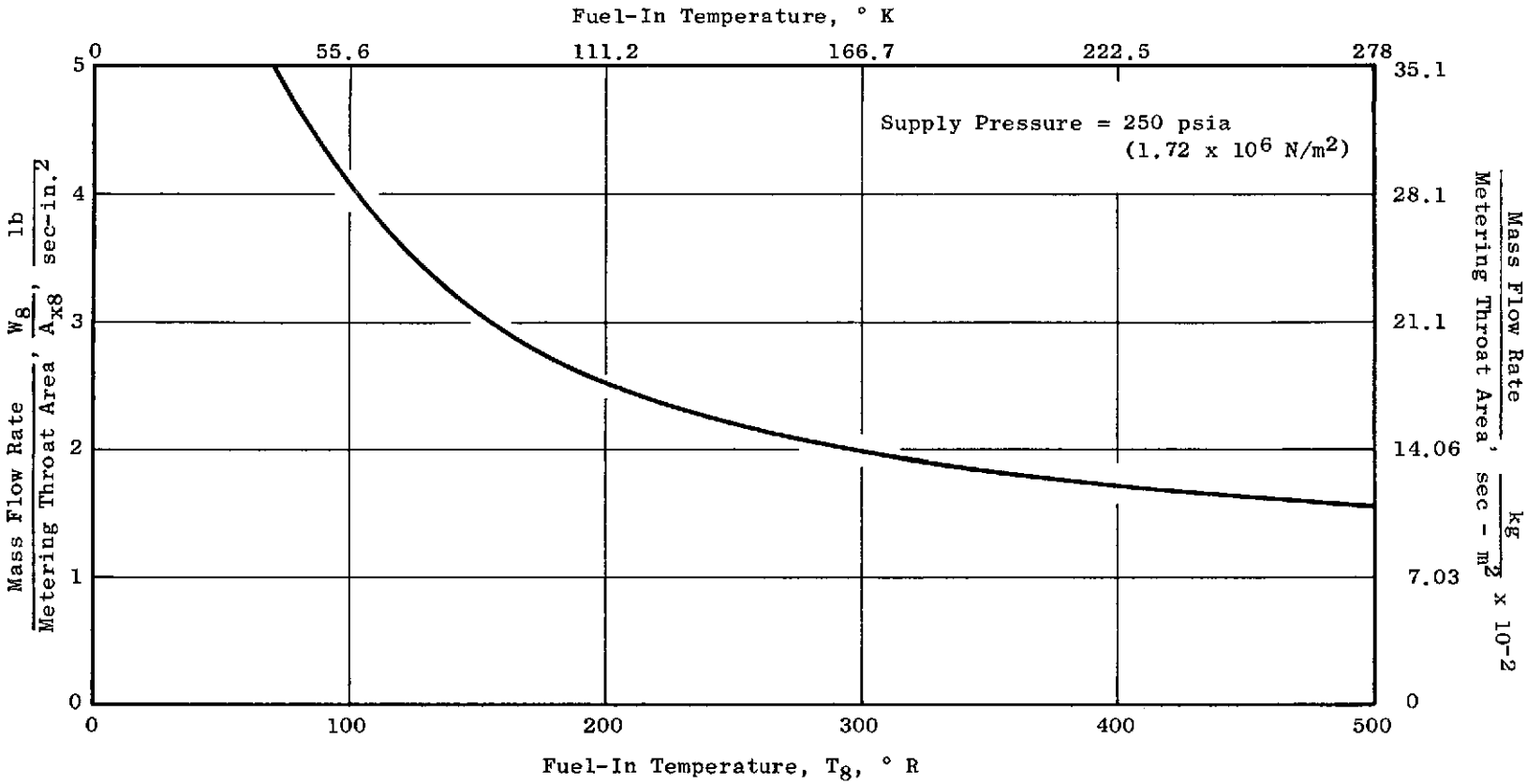


Figure 18. Metering Valve Flow Function, Methane System.

Useful data for defining the methane or natural gas flow functions were found in Reference (3) for the temperature range 450° R (250°K) to 720° R (400°K). Real gas flow effects for natural gas in this temperature range were presented for a natural gas composition by volume consisting of:

| | | |
|---|---|---|
| $CH_4$ = 0.9272 | $iC_4H_{10}$ = 0.0007 | $N_2$ = 0.0218 |
| $C_2H_6$ = 0.0361 | $nC_4H_{10}$ = 0.0010 | $CO_2$ = 0.0077 |
| $C_3H_8$ = 0.0055 | | |

A natural gas flow function and data were established in Reference (3) such that:

$$\frac{W_8}{A_{x8}} = \frac{\phi}{\phi i} \cdot \phi_i \cdot K_u \frac{P_8}{\sqrt{T_8}} \qquad (27)$$

Values of the flow function and data obtained in the temperature range 450° R (250° K) to 720° R (400° K) for natural gas are tabulated in Table IV.

Table IV. Natural Gas Flow Function Values from NASA TMX-52965.

| $T_8$ °R | $(T_8)$ (°K) | $P_8$ psia | $(P_8)$ $(N/m^2)$ | $\phi/\phi_i$ --- | $\phi_i$ $(sec\text{-}°R^{1/2})/ft$ | $(\phi_i)$ $\frac{sec\text{-}°K^{1/2}}{m}$ | $K_u$ - | $(K_u)$ - | $W_8/A_{x8}$ $pps/in^2$ | $\frac{(W_8/A_{x8})}{K_g}$ $\frac{}{sec\text{-}m^2}$ |
|---|---|---|---|---|---|---|---|---|---|---|
| 450 | (250) | 700 | $(4.82x10^6)$ | 1.099 | 0.01249 | (0.03054) | 32.17 | (1.0) | 14.54 | $(1.02x10^4)$ |
| 495 | (275) | 700 | $(4.82x10^6)$ | 1.069 | 0.01247 | (0.03049) | 32.17 | (1.0) | 13.48 | $(0.945x10^4)$ |
| 540 | (300) | 700 | $(4.82x10^6)$ | 1.050 | 0.01244 | (0.03042) | 32.17 | (1.0) | 12.65 | $(0.887x10^4)$ |
| 630 | (350) | 700 | $(4.82x10^6)$ | 1.0295 | 0.01237 | (0.03025) | 32.17 | (1.0) | 11.40 | $(0.801x10^4)$ |
| 720 | (400) | 700 | $(4.82x10^6)$ | 1.018 | 0.01229 | (0.03006) | 32.17 | (1.0) | 10.50 | $(0.737x10^4)$ |

The data presented in Table IV were extrapolated for temperatures above 720° R (400° K) by making the assumption that the value of $\phi/\phi_i$ in Equation (27) remains unity at the higher temperatures, and that $\phi_i$ remains constant at 0.01229 $sec\text{-}°R^{1/2}/ft$ (0.03006 $sec\text{-}°K^{1/2}/m$) for $T_8 \geq$ 720° R (400° K), as would be the case for an ideal gas.

The additional extrapolated values obtained are listed in Table V.

Table V. Natural Gas Flow Function Values Extrapolated from TMX-52965.

| $T_8$ °R | $(T_8)$ (°K) | $P_8$ psia | $(P_8)$ $(N/m^2)$ | $\phi/\phi_i$ | $\phi_i$, sec-° $R^{\frac{1}{2}}$/ft | $(\phi_i)$ $\frac{\text{sec-° } K^{\frac{1}{2}}}{m}$ | $K_u$ | $(K_u)$ | $W_8/A_{x8}$ pps/in$^2$ | $(W_8/A_{x8})$ $\frac{K_g}{\text{sec}/m^2}$ |
|---|---|---|---|---|---|---|---|---|---|---|
| 900 | (500) | 700 | $(4.82\text{x}10^6)$ | 1.000 | 0.01229 | (0.03006) | 32.17 | (1.0) | 9.40 | $(0.66\text{x}10^4)$ |
| 1200 | (667) | 700 | $(4.82\text{x}10^6)$ | 1.000 | 0.01229 | (0.03006) | 32.17 | (1.0) | 8.13 | $(0.57\text{x}10^4)$ |
| 1510 | (839) | 700 | $(4.82\text{x}10^6)$ | 1.000 | 0.01229 | (0.03006) | 32.17 | (1.0) | 7.24 | $(0.508\text{x}10^4)$ |

The data obtained in Tables IV and V were plotted as a smooth curve shown in Figure 19. This flow function was used in design of natural gas flow computation circuits and metering.

Having established the temperature compensation functions to be used in flow computation and the intended mechanization arrangement of the metering valve and flow computer circuits, an estimate of the flow-computing accuracy to be expected from the system was performed. It was obvious that the largest percentage errors in fuel flow computation were to be expected at the minimum values of system fuel flow level as in any flow metering system, but it was not readily apparent as to what influence the temperature compensation function might have in the magnitude of these errors. Graphically, the tangent percentage slopes of the temperature functions were established at various values of $(T_8)$ and $(W_8/A_{x8})$. Percentage errors for the temperature detectors were assumed based on $\pm 10°$ R (5.56° K) error for methane and $\pm 5°$ R (2.78 °K) error for hydrogen. These assumed errors were multiplied by the percentage slopes of the temperature functions to find the worst fuel flow percentage error as a function of temperature. The maximum fuel flow error contributed by the temperature sensor and compensation function occurs at 125° R (69.5° K) for hydrogen metering and at 375° R (208° K) for natural gas metering.

Using the selected worst case $T_8$ conditions for temperature sensor errors in computed fuel flow, estimates were made for the remaining error sources at values of fuel flow ranging from 5% to 100% of system rated fuel flow. The following error sources were considered for hydrogen metering:

- Metering Port Tolerance — $\pm 3.0\%$ $W_8$
- P8 Pressure Regulation Accuracy — $\pm 1.0\%$ $W_8$
- Coefficient of Discharge Variation — $\pm 2.0\%$ $W_8$
- $T_8$ Temperature Sensor Error (125° R) — $\pm 3.08\%$ $W_8$
- $X_8$ LVDT and Demodulator — $\pm 2.68\%$ $W_8$
- $T_8$ Function Electrical Error — $\pm 2.68\%$ $W_8$
- Anti-Ln Generator Electrical Error — $\pm 0.2\%$ Full Scale

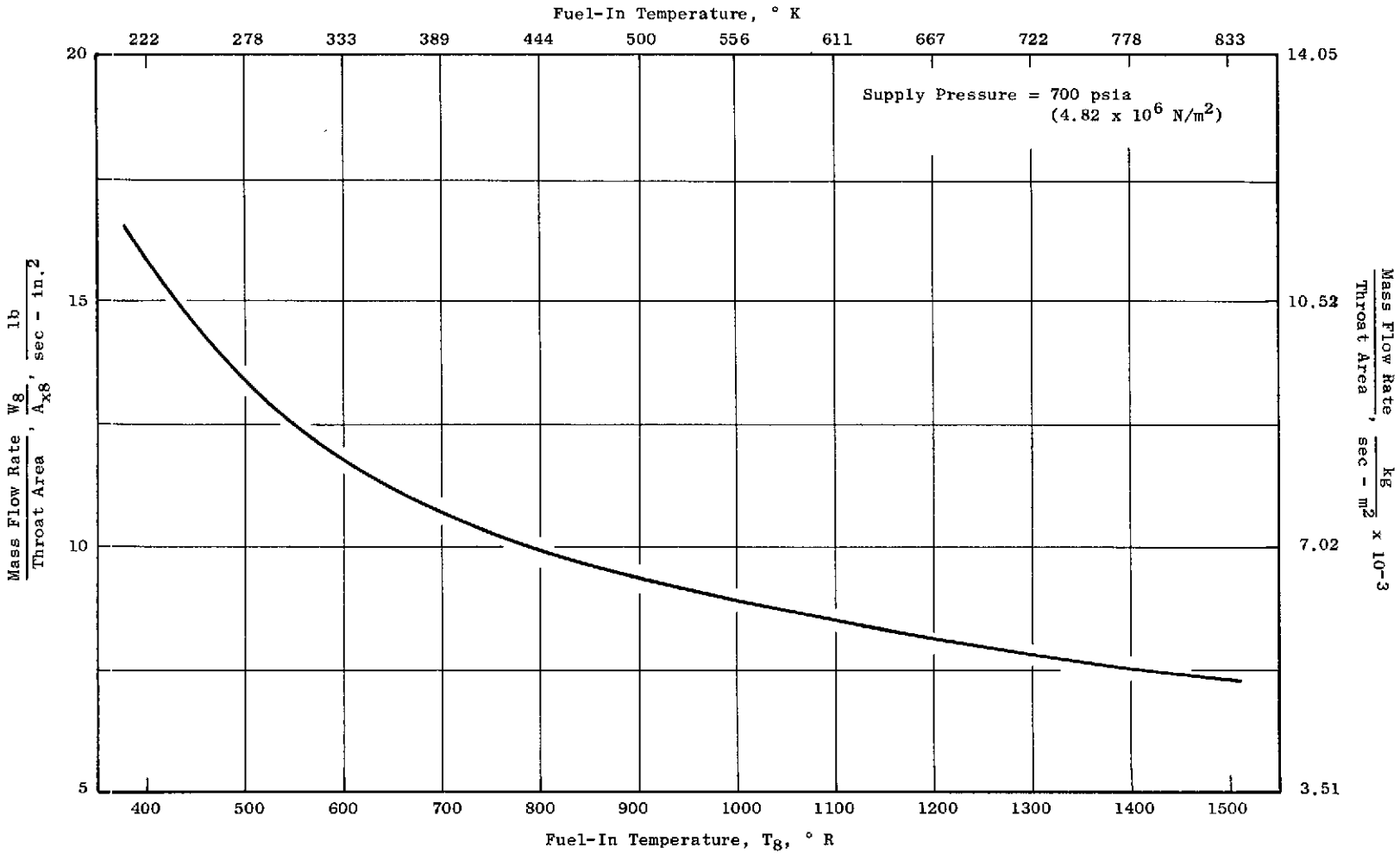


Figure 19. Metering Valve Flow Function, Methane System.

The only source in the above list which could not be estimated as contributing a constant maximum percentage $W_8$ error as a function of fuel flow level was the Anti-Ln Generator. The percentage of full-scale accuracy of the generator converts to $\pm$0.2% $W_8$ at 100% fuel flow, $\pm$1.0% $W_8$ at 20% fuel flow, and $\pm$4.0% $W_8$ at 5% fuel flow.

The errors estimated from the various sources were summed on a root-sum-square basis to yield the following overall computed fuel flow accuracies for hydrogen:

| $T_8$, ° R | $(T_8)$, (°K) | $W_8$ Level, % of Max. | $W_8$ Error (RSS), $\pm$% of $W_8$ |
|---|---|---|---|
| 125 | (69.5) | 5% | $\pm$7.33% |
| 125 | (69.5) | 20% | $\pm$6.23% |
| 125 | (69.5) | 100% | $\pm$6.15% |

For natural gas fuel flow error estimation, the identical error source contributions were used except that the worst case $T_8$ value of 375° R (208° K) was used resulting in a $\pm$2.04% $W_8$ effect due to temperature sensor errors. The root-sum-square summation of these errors for natural gas metering yields the following overall $W_8$ computation errors:

| $T_8$, ° R | $(T_8)$, (° K) | $W_8$ Level, % of Max. | $W_8$ Error (RSS), $\pm$% of $W_8$ |
|---|---|---|---|
| 375 | (208) | 5% | $\pm$6.95% |
| 375 | (208) | 20% | $\pm$5.78% |
| 375 | (208) | 100% | $\pm$5.70% |

These estimated overall fuel flow computation accuracies were considered to be conservatively estimated, and since most operation is expected to occur at $T_8$ temperatures above the worst case selected, the resulting $W_8$ accuracy will be better than the estimates made. The values obtained are well within the $\pm$10% $W_8$ accuracy objective desired for the system. The use of a mode of engine acceleration control which limits fuel flow rate of change rather than fuel flow itself permits use of less stringent accuracy levels in fuel flow computation.

## SYSTEM FAILURE MODES AND EFFECTS ANALYSIS

During design reviews of the conceptual system, it was recognized that safety and equipment protection would be a major concern for the program due to the use of highly flammable fuels in close proximity to high temperature heat sources and due to the overall equipment complexity required to accomplish the intended functions. A system failure mode and effects analysis was performed wherein each major subsystem was analyzed for the possible modes of failure of its input/output parameters, and the resulting effects to be

expected in each of the interrelated subsystems were established. The analysis revealed several undesirable failure effects for the system, and changes or additions were recommended as listed below:

- Latch the engine overspeed-overtemperature trip signal output to prevent cycling of shut-off and vent valves after shutdown, and add valve position signal lights to the shutoff and vent valves.
- Add a temperature logic circuit to the engine control to select engine governing after light-off and deselect governing after blowout, and provide a signal light to indicate engine temperature logic condition.
- Add signal lights to indicate air heater fuel solenoid condition and low burner temperature.
- Add a hydraulic pump overpressure relief valve.
- Add a redundant engine speed sensor for overspeed protection (NASA tachometer).
- Add heat exchanger fuel pressure relief valves.
- Mechanically bias pump and valve torquemotors to the shutdown condition for zero current.
- Add fuel leak or fire detectors in vicinity of fuel package.
- Add fuel leak detectors to airflow side of heat exchangers.
- Surround air-fuel heat exchanger with a blast shield.
- Add fuel leak detectors and high level warning to oil heater surge tank.
- Add blowout discs to oil circuit of oil-methane heat exchanger.

All of these recommended changes were implemented in the detail design and fabrication of system hardware.

## HARDWARE DESIGN AND FABRICATION

### FUEL CONDITIONING PACKAGE

A fuel conditioning package to accomplish the pumping and gasification of the fuels for delivery to the system metering controls was designed and built. Major components were purchased from vendor sources and were assembled and interconnected in a test rig framework designed and fabricated by the contractor. The fuel conditioning package assembly was defined by drawing 4013156-317 and is depicted in the methane configuration in Figure 20.

#### Fuel Pump and Inlet Conditioner

A fuel pumping and inlet conditioner subassembly was purchased from Cosmodyne Division of Cordon International Corp. and was integrated within the fuel conditioning package. The subassembly components include a fuel pump and subcooler as depicted in Figure 21.

A cross section of the variable speed fuel pump and motor assembly is shown in dwg. 2311401. Five reciprocating pistons pump $LH_2$ or $LCH_4$ from intake pressure to discharge through pressure-operated intake and discharge check valves located in the cryogenic cylinder head. Hydraulic motive pressure, which is ported through a rotating sequence valve, is applied to hydraulic pistons directly in line with the cryogenic pistons. Piston reciprocation is tied through ball-jointed connecting links to a nutating plate. As the plate nutates, a Z-crank shaft imparts rotary motion to the sequence valve, establishing a hydraulic timing synchronized with piston motion. Hydraulic flow to the sequence valve is set by an electrohydraulic torquemotor-servovalve to control pump speed and fuel delivery. An electromagnetic pickup senses sequence valve rotational speed for control loop feedback. The vacuum insulated package is 27.5 inches (0.7 m) long x 6.75 inches (0.171 m) O.D. and weighs 60 lbs (27.2 Kg).

Saturated liquid $LH_2$ or $LCH_4$ at 30 psia ($2.07 \times 10^5$ $N/m^2$) minimum is received at the conditioner inlet. The inlet conditioner subcools the incoming fuel by heat exchange with a bath of the fuel which is vented to ambient. The subcooled fuel is delivered directly into pump inlet from the conditioner discharge. The outer bath is vacuum insulated. A bath level control valve intermittently ports liquid fuel from the heat exchanger header to the outer bath to maintain the boiling bath level at a preselected value to assure maximum cooling.

The rated performance for which the fuel pumping and inlet conditioning equipment was designed is listed as follows:

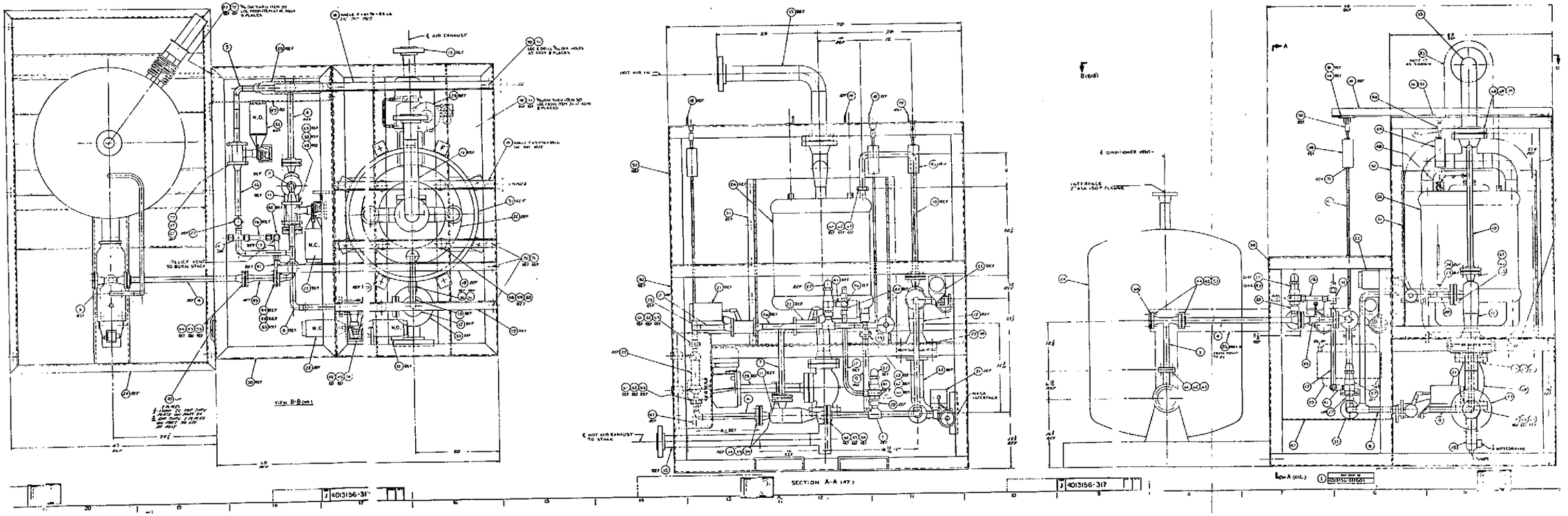




FOLDOUT FRAME

FOLDOUT FRAME 2

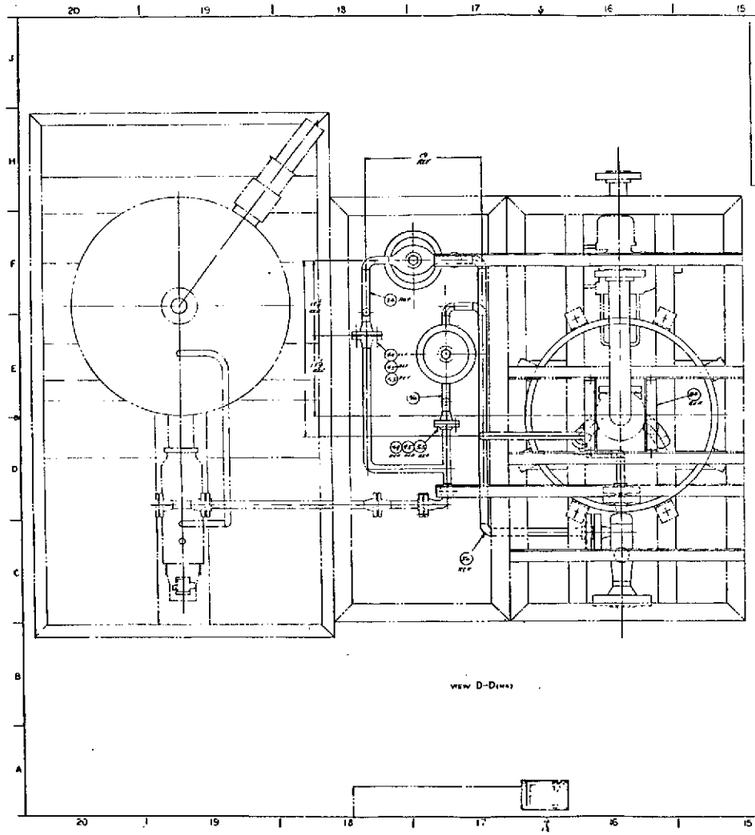

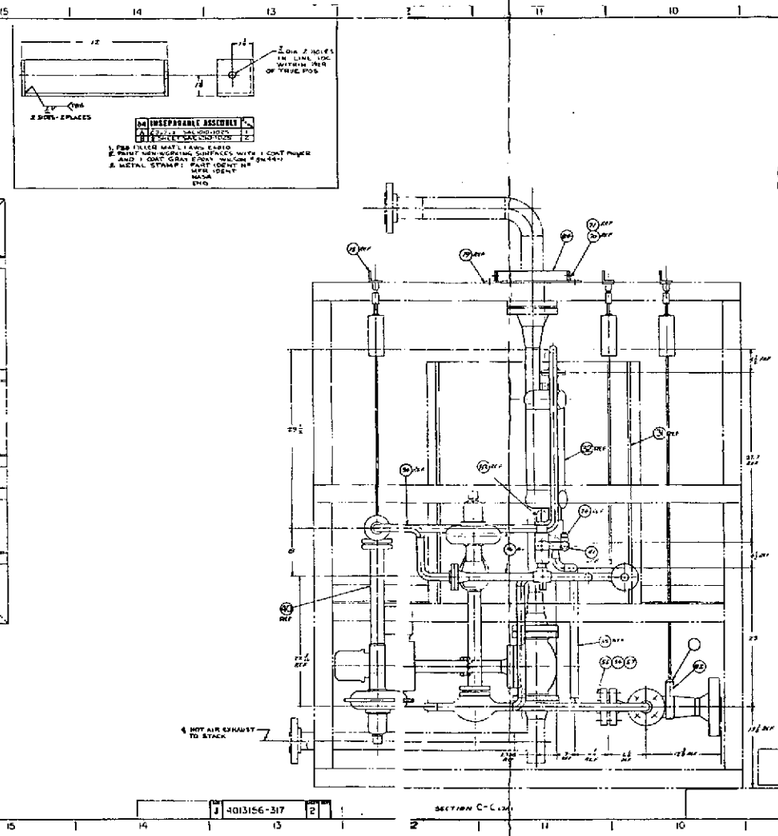

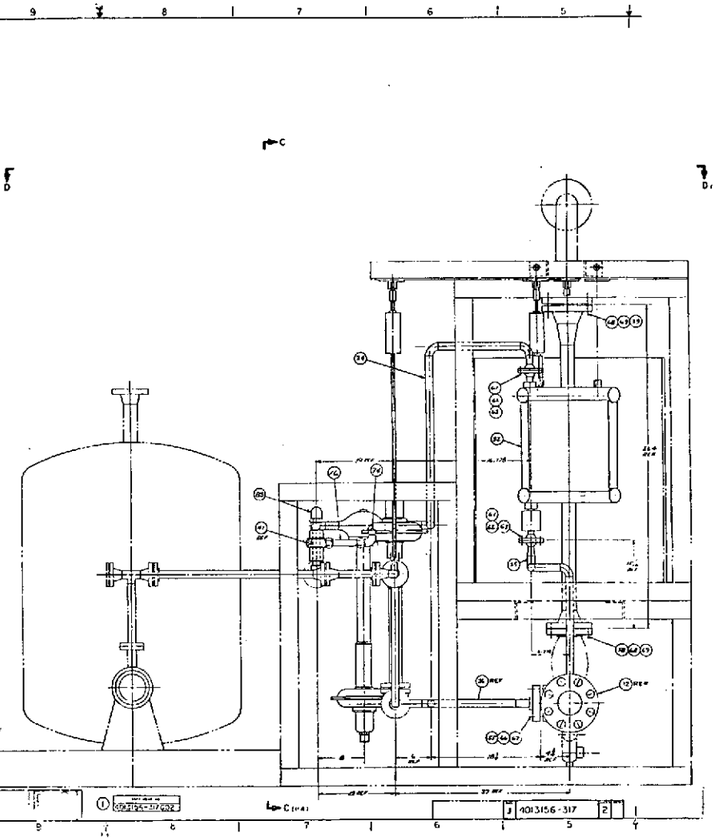



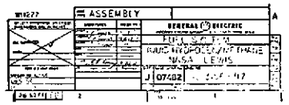



FOLDOUT FRAME

FOLDOUT FRAME 2

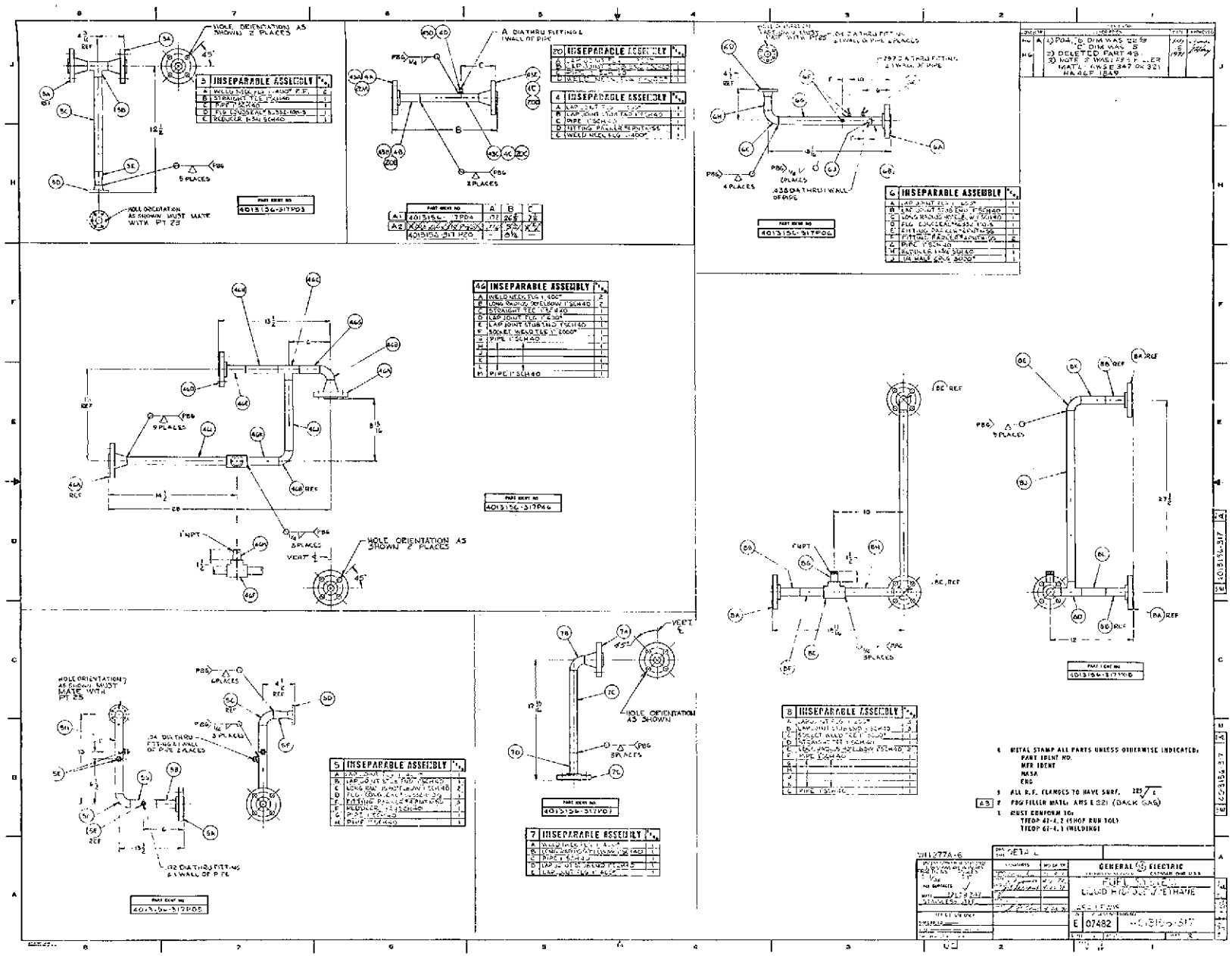
3 INSEPARABLE ASSEMBLY
4 INSEPARABLE ASSEMBLY
20 INSEPARABLE ASSEMBLY
6 INSEPARABLE ASSEMBLY
44 INSEPARABLE ASSEMBLY
8 INSEPARABLE ASSEMBLY
5 INSEPARABLE ASSEMBLY
7 INSEPARABLE ASSEMBLY
HOLE ORIENTATION AS SHOWN 2 PLACES
HOLE ORIENTATION AS SHOWN MUST MATE WITH PT 25
5 PLACES
2 PLACES
4 PLACES
9 PLACES
3 PLACES
.438 DIA THRU WALL OF PIPE
.172 DIA THRU FITTING & WALL OF PIPE
4013156-317P03
4013156-317P04
4013156-317P05
4013156-317P06
4013156-317P07
4013156-317P08
1) P04 - B DIM WAS 12.59 C DIM WAS 5
2) DELETED PART 48
3) NOTE 2 WAS FEP FILLER MATL: AMS-R-3417 OR 321 HASA P 1849
GENERAL ELECTRIC
FUEL MANIFOLD
LIQUID HYDROJET/METHANE
E 07482

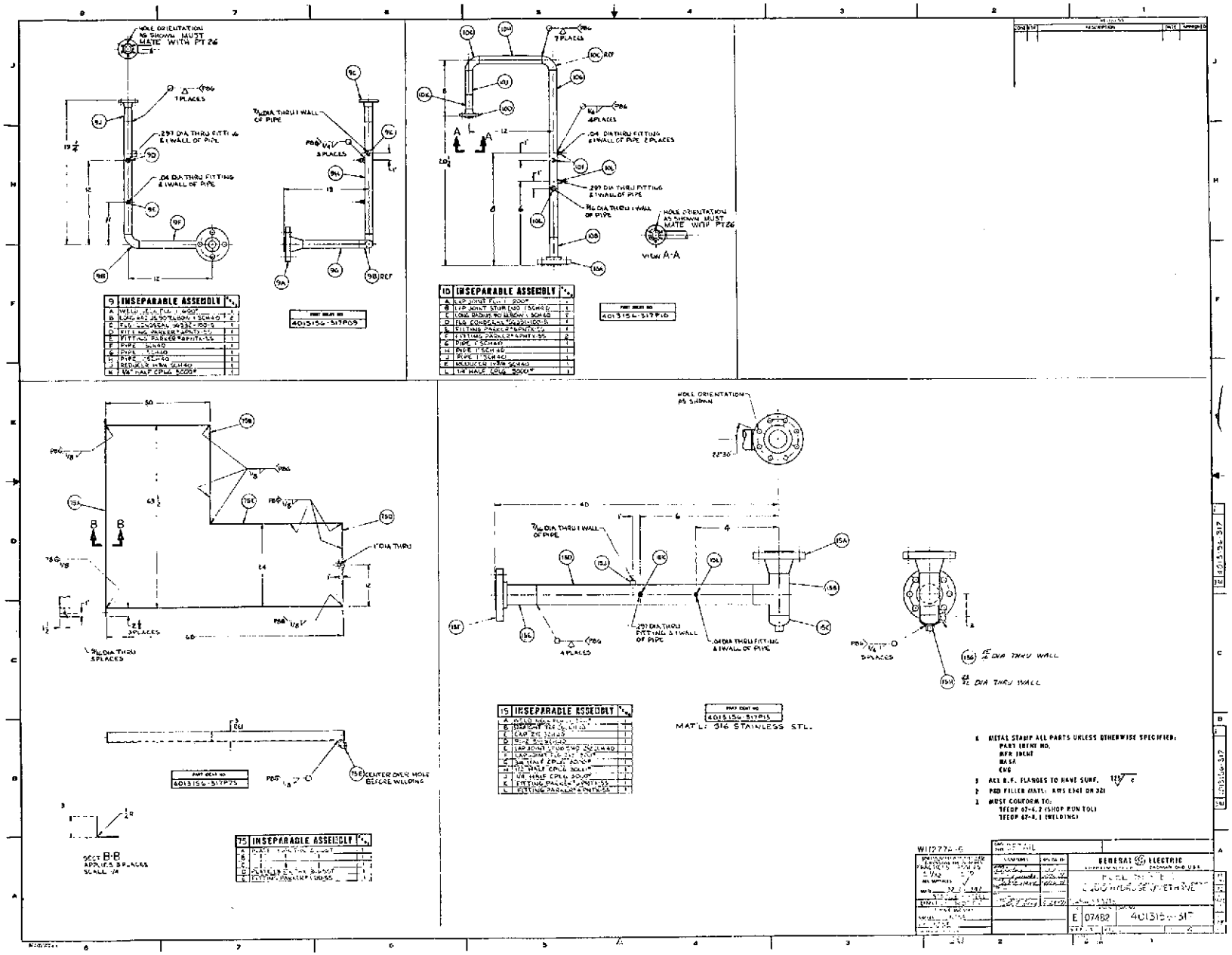
HOLE ORIENTATION AS SHOWN MUST MATE WITH PT 26
7 PLACES
.297 DIA THRU FITTING & 1 WALL OF PIPE
.06 DIA THRU FITTING & 1 WALL OF PIPE
3/16 DIA THRU 1 WALL OF PIPE
3 PLACES
4013156-517P09
9 INSEPARABLE ASSEMBLY
4013156-517P10
10 INSEPARABLE ASSEMBLY
VIEW A-A
50
63 1/2
3 PLACES
3/8 DIA THRU 3 PLACES
1" DIA THRU
4013156-517P75
75 INSEPARABLE ASSEMBLY
SECT B-B APPLIES 3 PLACES SCALE 1/4
CENTER DRILL HOLE BEFORE WELDING
40
4 PLACES
.297 DIA THRU FITTING & 1 WALL OF PIPE
.06 DIA THRU FITTING & 1 WALL OF PIPE
4013156-517P15
15 INSEPARABLE ASSEMBLY
MAT'L: 316 STAINLESS STL.
22°30'
5/8 DIA THRU WALL
11/16 DIA THRU WALL
3 PLACES
1. METAL STAMP ALL PARTS UNLESS OTHERWISE SPECIFIED: PART IDENT NO. MFR IDENT MASK CNG
2. ALL R.F. FLANGES TO HAVE SURF. 125 √ c
3. PRD FILLER MATL: AWS E4043 OR 321
4. MUST CONFORM TO: TECOP 07-6.2 (SHOP RUN TOL) TECOP 07-8.1 (WELDING)
W112774-6
GENERAL ELECTRIC
E 07482
4013156-517

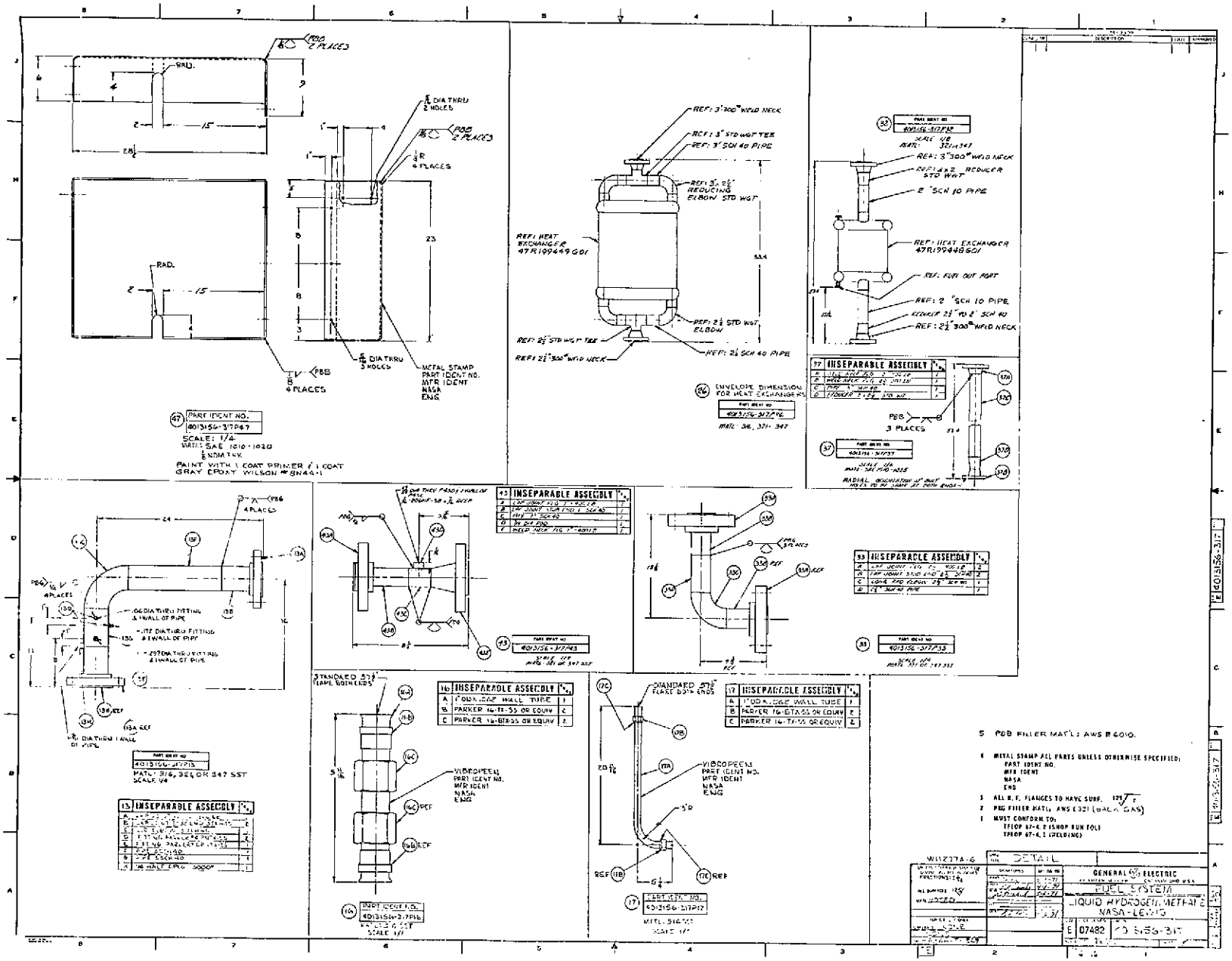
PART IDENT NO. 401356-317P47
SCALE: 1/4
MATL: SAE 1010-1020
PAINT WITH 1 COAT PRIMER & 1 COAT GRAY EPOXY WILSON # 8N441
PART IDENT NO. 401356-317P48
MATL: 316, 321, 347
INSEPARABLE ASSEMBLY
PART IDENT NO. 401356-317P49
MATL: 316, 321 OR 347 SST
SCALE: 1/4
PART IDENT NO. 401356-317P16
MATL: 316, 321 OR 347 SST
SCALE: 1/1
PART IDENT NO. 401356-317P17
MATL: 316 SST
SCALE: 1/1
PART IDENT NO. 401356-317P43
SCALE: 1/1
PART IDENT NO. 401356-317P53
SCALE: 1/1
PART IDENT NO. 401356-317P37
SCALE: 1/1
PART IDENT NO. 401356-317P52
SCALE: 1/8
MATL: 321 OR 347
ENVELOPE DIMENSION FOR HEAT EXCHANGERS
PART IDENT NO. 401356-317P46
MATL: 316, 321, 347
REF: HEAT EXCHANGER 47R199449 G01
REF: HEAT EXCHANGER 47R199448 G01
REF: 3" 300# WELD NECK
REF: 3" STD WGT TEE
REF: 3" SCH 40 PIPE
REF: 3" x 2½" REDUCING ELBOW STD WGT
REF: 2½" STD WGT ELBOW
REF: 2½" STD WGT TEE
REF: 2½" 300# WELD NECK
REF: 2½" SCH 40 PIPE
REF: 2" x 2" REDUCER STD WGT
2" SCH 10 PIPE
REF: FUEL OUT PORT
REDUCE 2½" TO 2" SCH 10
MATERIAL SPECIFICATIONS
1 MATERIAL SAE 1010-1020
2 MATERIAL AMS 4911 (SHEET) AMS 4910 (PLATE)
3 MATERIAL AMS 4911 (SHEET) AMS 4910 (PLATE) AMS 4921 (FORGINGS)
4 MATERIAL AMS 5504 (SHEET) AMS 5501 (PLATE) AMS 5589 (FORGINGS)
5 PCB FILLER MATL: AWS B 6010.
6 METAL STAMP ALL PARTS UNLESS OTHERWISE SPECIFIED: PART IDENT NO. MFR IDENT NASA ENG
7 ALL R.F. FLANGES TO HAVE SURF. 125√
8 PCB FILLER MATL: AWS E 321 (BALA GAS)
9 MUST CONFORM TO: EFLOP 67-4.2 (SHOP RUN FOIL) EWOP 67-4.1 (WELDING)
WL1277A-6
DETAIL
GENERAL ELECTRIC
FUEL SYSTEM
LIQUID HYDROGEN/METHANE
NASA-LEWIS
E 07482
401356-317

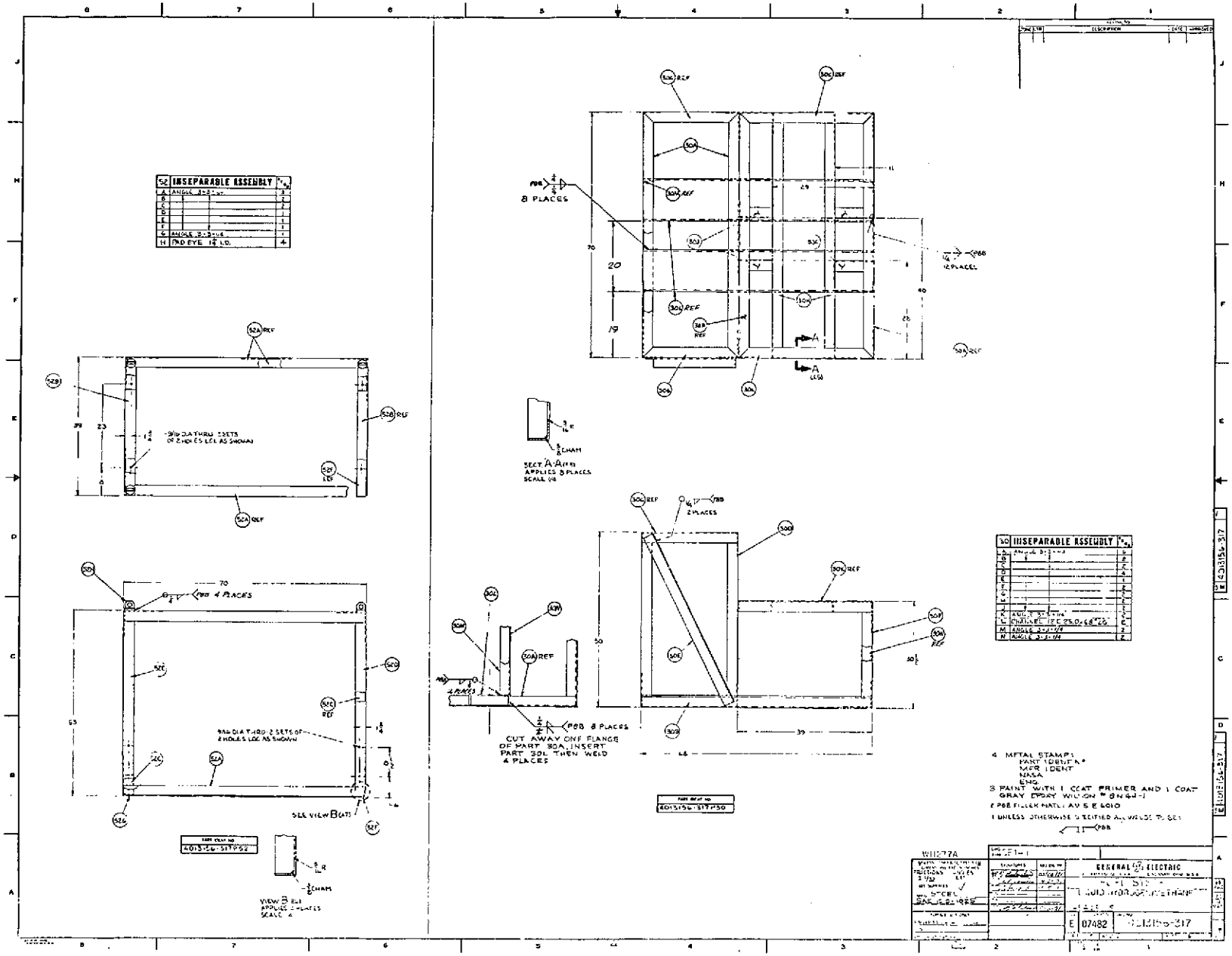
52 INSEPARABLE ASSEMBLY
A ANGLE 3-1/2 x 3-1/2 x 1/4
G ANGLE 3-1/2 x 3-1/2 x 1/4
H PAD EYE 1/4 I.D.
8 PLACES
12 PLACES
SECT A-A
APPLIES 8 PLACES
SCALE 1/4
70
20
19
-3/16 DIA THRU 2 SETS OF 2 HOLES LOC AS SHOWN
4 PLACES
SEE VIEW B
VIEW B
APPLIES 2 PLACES
SCALE 4
30 INSEPARABLE ASSEMBLY
CHANNEL 12 C 25.0 x 6.8 x 20
ANGLE 3-1/2 x 3-1/2 x 1/4
CUT AWAY ONE FLANGE OF PART 30A, INSERT PART 30L THEN WELD
4 PLACES
4 METAL STAMPS
PART IDENT NO
MFR IDENT
NASA
ENG
3 PAINT WITH 1 COAT PRIMER AND 1 COAT GRAY EPOXY WILSON # 8N64-1
5 PAINT WITH 1 COAT PRIMER AND 1 COAT GRAY EPOXY WILSON # 8N64-1
6 P68 FILLER MATL: AV 5 E 6010
7 UNLESS OTHERWISE SPECIFIED ALL WELDS TO BE
GENERAL ELECTRIC
E 07482
E403156-317

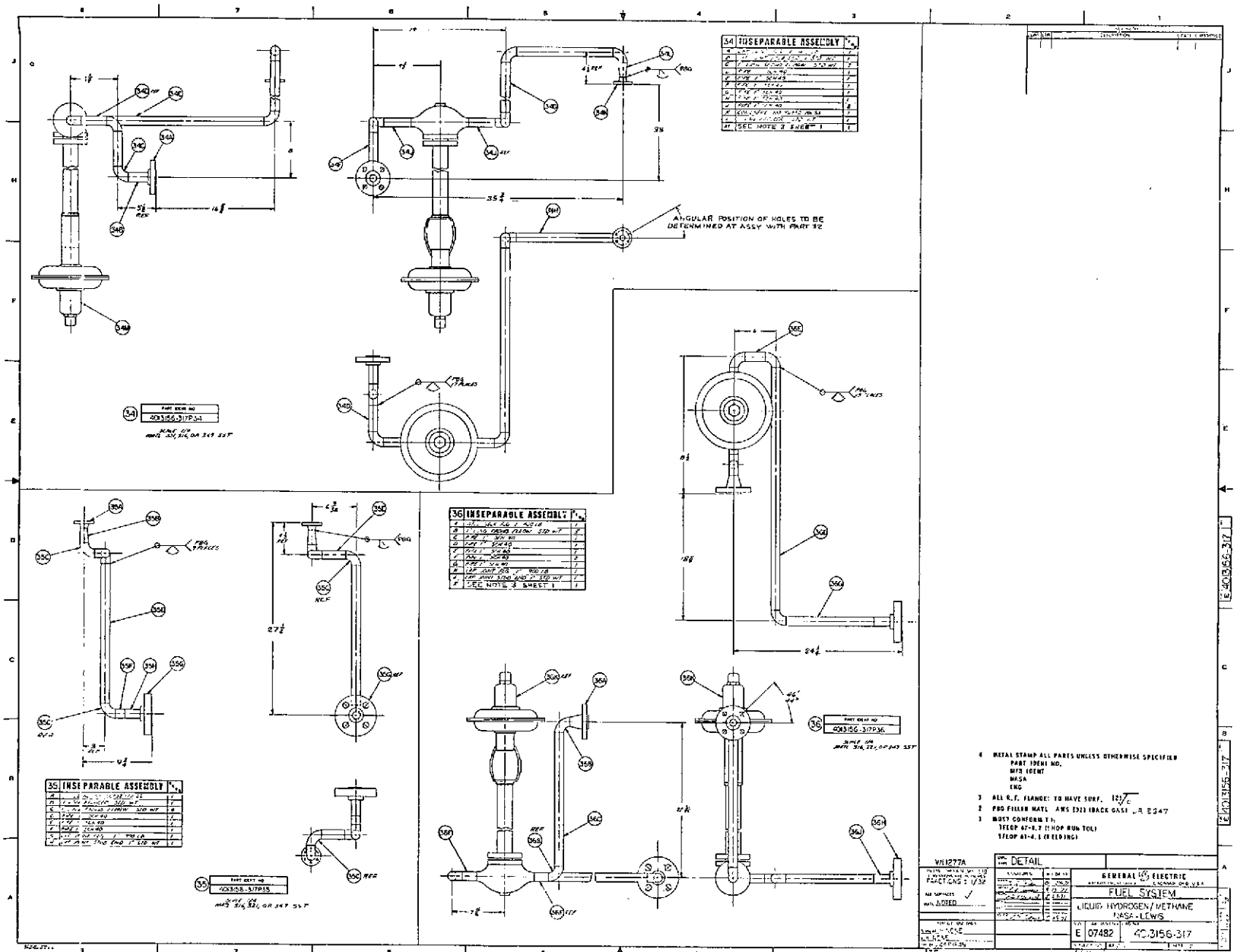
ANGULAR POSITION OF HOLES TO BE DETERMINED AT ASSY WITH PART 32
DETAIL
GENERAL ELECTRIC
FUEL SYSTEM
LIQUID HYDROGEN/METHANE
NASA-LEWIS
E 07482
40.3156-317

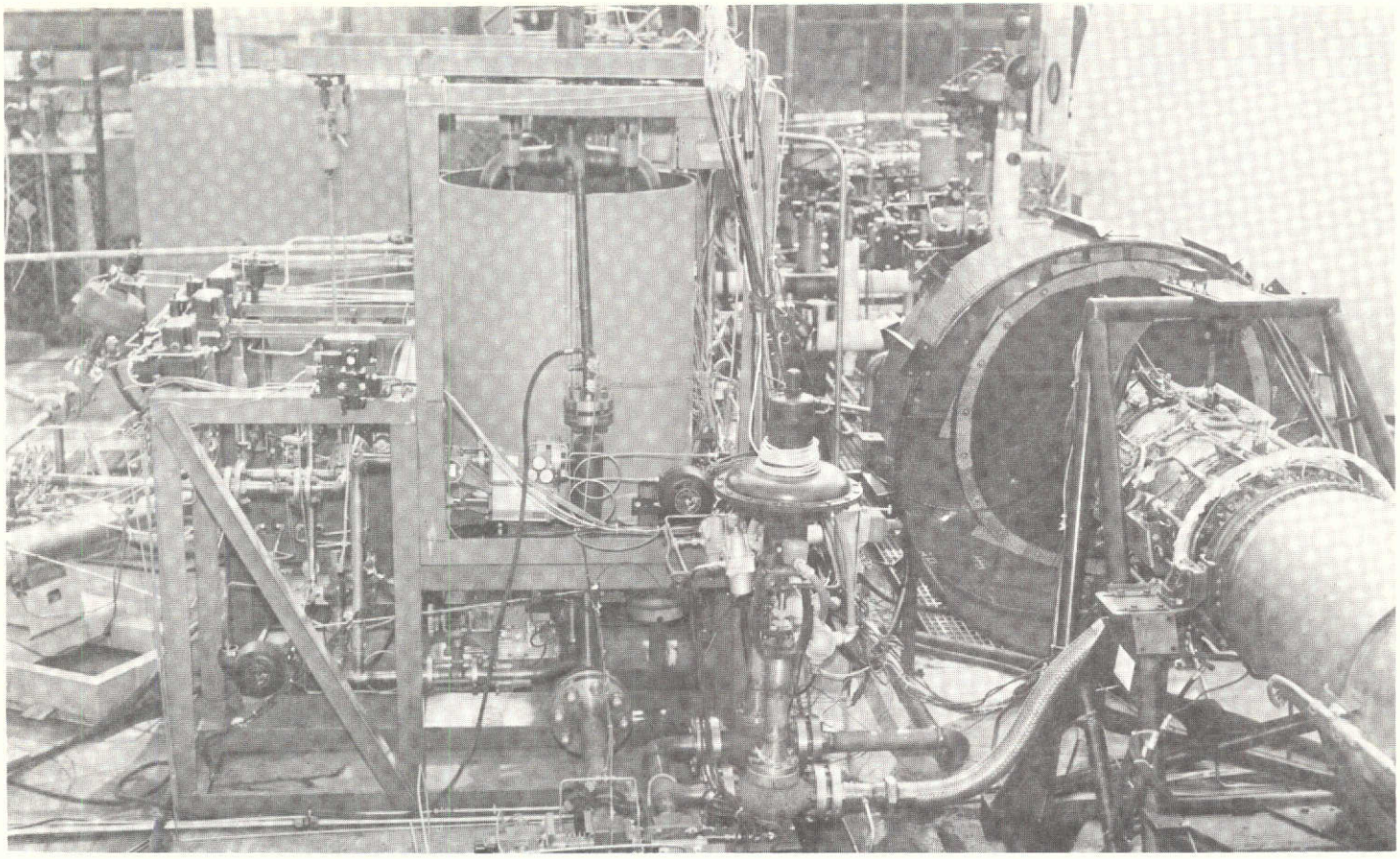

Figure 20. Fuel Conditioning Package Assembly.

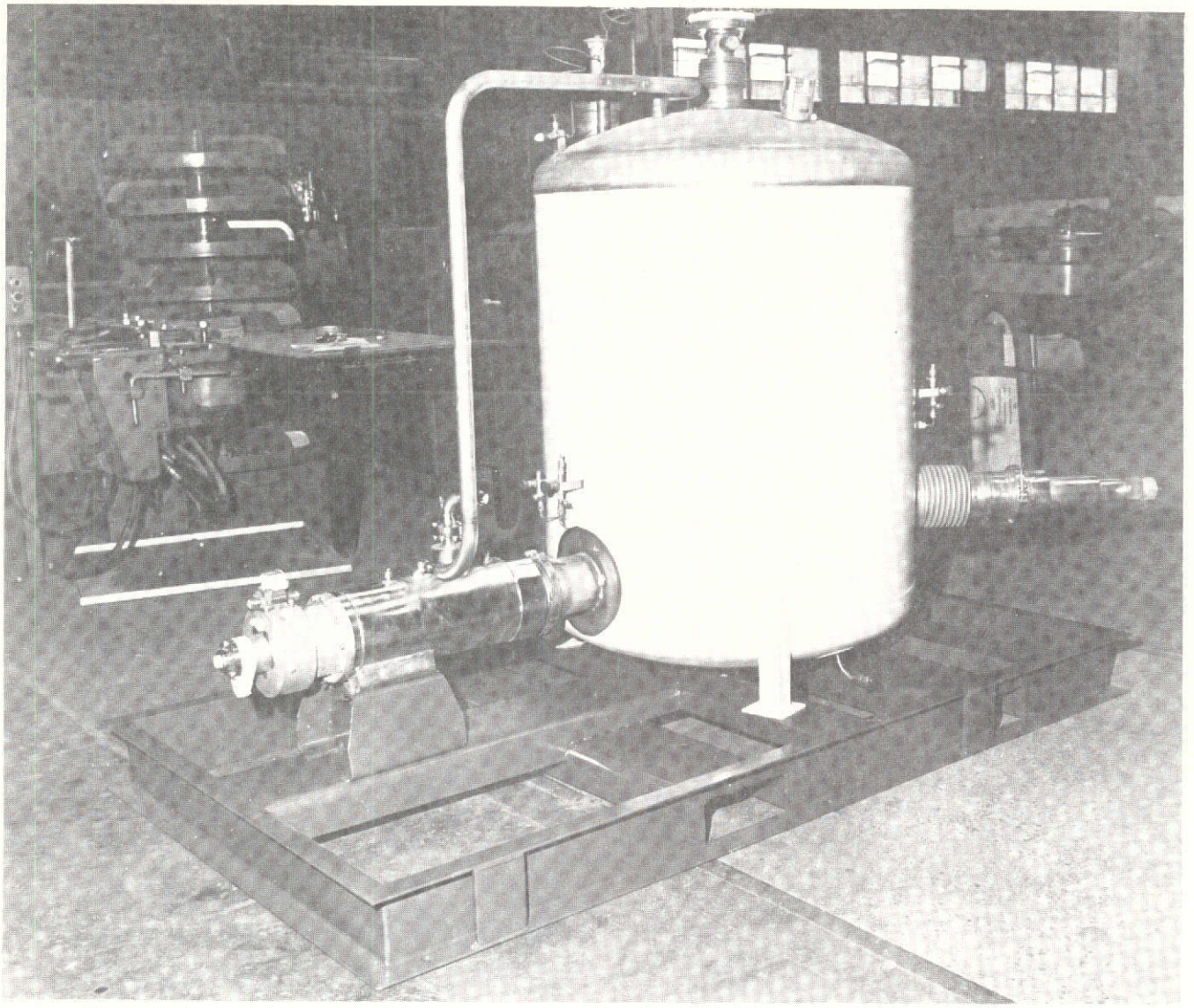

Figure 21. Fuel Pumping and Inlet Conditioner Subassembly, Fuel Pump and Subcooler.

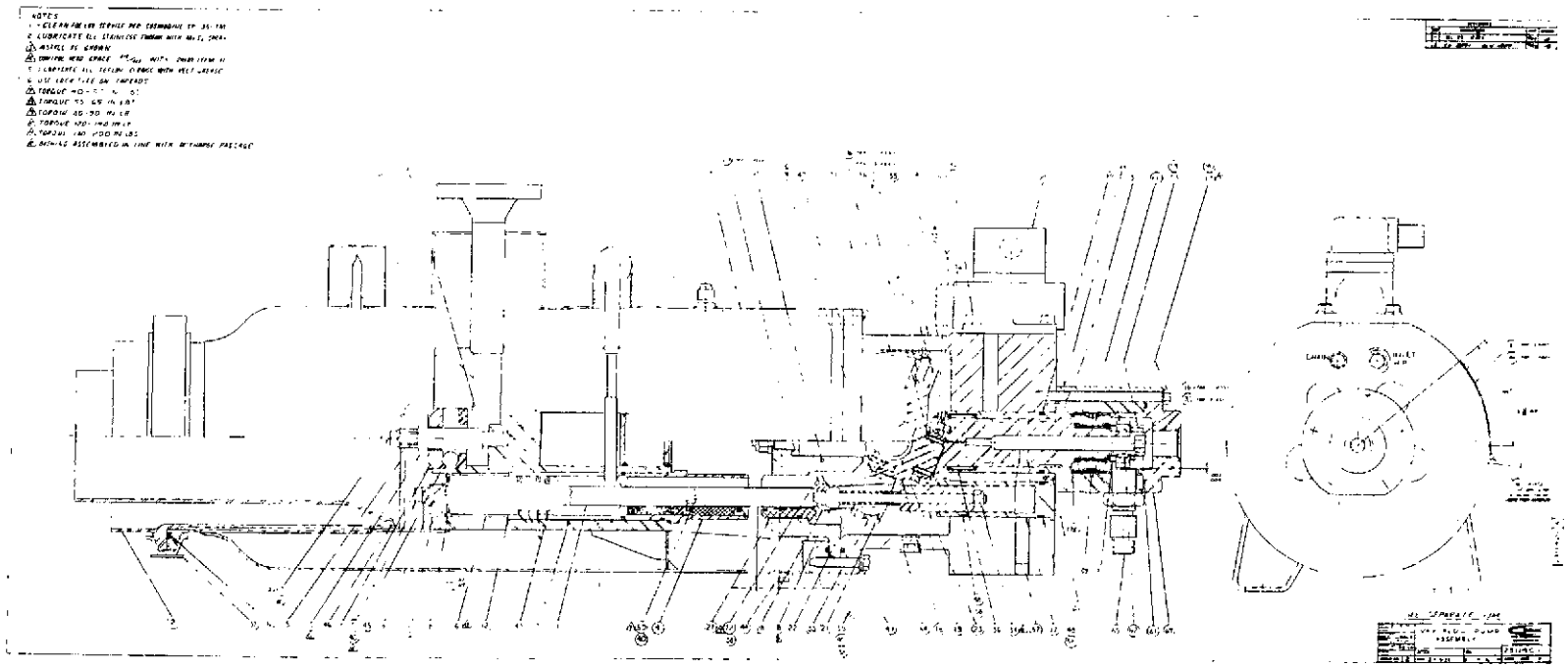

## Cryogenic Fluid

### Inlet Conditions

| | |
|---|---|
| Pressure | 20 to 60 psia ($1.38 \times 10^5$ to $4.14 \times 10^5$ $N/m^2$) |
| Temperature | Saturated liquid |

### Subcooler Bath

| | |
|---|---|
| Pressure | Ambient |
| Temperature | Saturated liquid |
| Capacity | 65 gallons (0.246 $m^3$) |
| Vent Flow rate (maximum) | 282 scfm $H_2$ (0.133 $m^3$/sec) |
| | 165 scfm $CH_4$ (0.078 $m^3$/sec) |

| Discharge Conditions | $LH_2$ | $LCH_4$ |
|---|---|---|
| Pressure | 400 $\pm$ 100 psia ($2.76 \times 10^6 \pm .69 \times 10^6$ $N/m^2$) | 900 $\pm$ 200 psia ($6.21 \times 10^6 \pm 1.38 \times 10^6$ $N/m^2$) |
| Delivered Flow | 1080 pph (0.136 Kg/sec) 27 gpm ($17 \times 10^{-4}$ $m^3$/sec) | 2410 pph (0.304 Kg/sec) 12 gpm ($7.56 \times 10^{-4}$ $m^3$/sec) |

## Hydraulic Fluid (MIL-H-5606)

### Supply Conditions

| | |
|---|---|
| Pressure | 3000 psig ($20.7 \times 10^6$ $N/m^2$) |
| Flow | 16 gpm ($LH_2$ configuration) ($10.1 \times 10^{-4}$ $m^3$/sec) |
| | 9 gpm ($LCH_4$ configuration) ($5.67 \times 10^{-4}$ $m^3$/sec) |
| Temperature | 50 to 120° F (283 to 322 ° K) |

### Return Conditions

| | |
|---|---|
| Pressure | 100 psia ($6.89 \times 10^5$ $N/m^2$) |
| Flow | 15.5 gpm ($LH_2$ configuration) ($9.77 \times 10^{-4}$ $m^3$/sec) |
| | 8.5 gpm ($LCH_4$ configuration) ($5.35 \times 10^{-4}$ $m^3$/sec) |
| Temperature | 65 to 140° F (286 to 333 ° K) |

Hydraulic Motor Cavity Drain

| | |
|---|---|
| Pressure | Ambient |
| Flow | 0.5 gpm ($0.315 \times 10^{-4}$ $m^3$/sec) |
| Temperature | 65 to 140° F (286 to 333° K) |

Servo Valve (Abex Model 420)

| | |
|---|---|
| Input Current | 80 ma/coil |

Pump Speed Sensor (Airpax Model 721-001)

| | |
|---|---|
| Output waveform | Sinusoidal |
| Output frequency | 38.4 Hz/100 rpm |
| Output voltage (min) | 0.130 vrms at 100 rpm |

## Air-Methane Heat Exchanger

### Mechanical Design

The air-methane heat exchanger is shown in the drawing of Figure 22. The heat exchanger has a counterflow arrangement with a single pass of air through the cylindrical annulus formed between the inner and out shells, and two passes of methane through the tube core bundle. This arrangement was selected to minimize the icing problems associated with air heat exchangers operating at cryogenic temperatures.

The tube bundle consists of 804, 0.188 inch-OD ($0.478 \times 10^{-2}$ m) by 0.016-inch ($0.0406 \times 10^{-2}$ m) wall tubes with an average tube length of 28 inches ($71.2 \times 10^{-2}$ m). The Inconel 625 tube bundle is arranged in a cylindrical array with a core diameter of 20 inches (0.508 m) and is approximately 18 inches (0.458 m) long. This wraparound configuration was selected because of its low profile and the adaptability of this configuration to future engine installations where the core could be either partially or completely wrapped around the engine.

The methane enters the heat exchanger though a 1-inch ($2.54 \times 10^{-2}$ m) inlet to a distributing manifold whose cross-sectional flow area is sufficiently large to achieve a fairly uniform pressure across the face of both core sections. The inlet manifold has a divider plate that separates the inlet from the outlet to prevent the methane from bypassing the core. A 0.040-inch ($0.103 \times 10^{-2}$ m) diameter orifice is brazed into the inlet of each tube to further equalize the flow rate of each tube. After passing through the rear section, the methane from each half discharges into the common return manifold. The methane from

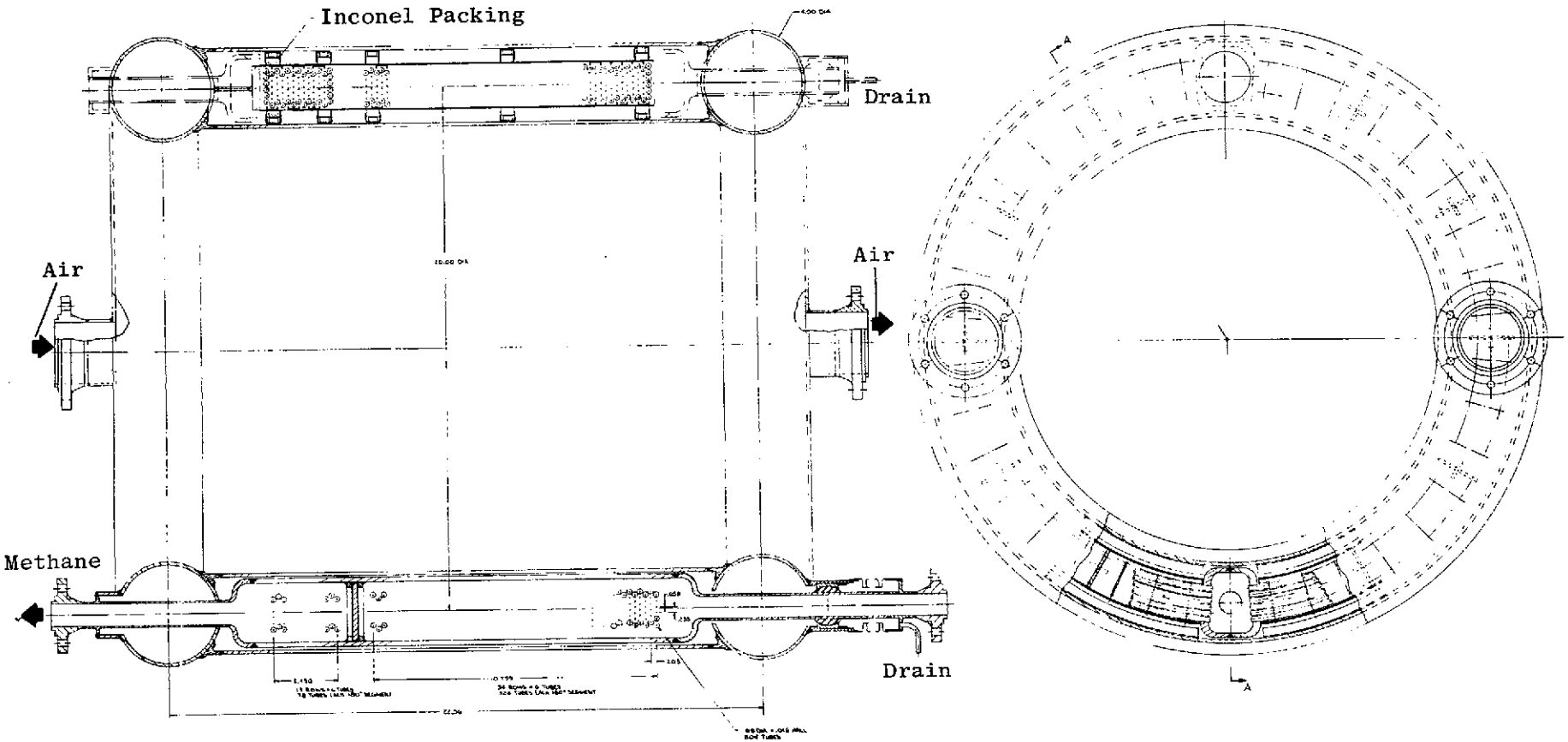


Figure 22. Air-to-Methane Heat Exchanger.

each half is thoroughly mixed and then flows to the inlet side of the forward tube section to start its second pass. A 0.070-inch ($0.178 \times 10^{-2}$ m) orifice is brazed into the inlet of each tube to equalize the flow rate of each tube in the second pass of the methane through the core. The methane discharges into the common exit header and is discharged through a 1-inch ($2.54 \times 10^{-2}$ m) outlet.

The hot air enters the heat exhanger through two, 2-1/2-inch ($6.35 \times 10^{-2}$ m) inlets into a 4-inch ($10.3 \times 10^{-2}$ m) diameter toroidal air manifold. The air leaves the air manifold through 36 slots evenly distributed over the face of the core. The air passes through the forward section of the core and discharges into a mixing chamber between the two sections before completing the pass through the rear section. The cooled air then passes through the slots into the outlet toroidal manifold and discharges through two 2-1/2-inch ($6.35 \times 10^{-2}$m) outlets.

A summary of the mechanical design features of the air-methane heat exchanger is shown in Table VI.

Thermal and Hydraulic Design

The air-methane heat exchanger was designed to meet the performance requirements summarized in the contract Statement of Work. This specification requires that the heat exchanger performance be not significantly impaired by the formation of ice in the heat exchanger that could partically block the free-flow area on the air side of the heat exchanger. The no-icing condition can be met even with an inlet methane temperature of -215° F (131° K) by designing the heat exchanger so that the tube wall is always above 32° F (273° K) for all operating conditions. This is accomplished in the heat exchanger by controlling the ratio of the film heat transfer coefficient at the inner and outer surface of the tube wall (i.e., a high-heat transfer coefficient on the hot air side and a low-heat transfer coefficient on the cold methane side of the tube). The resultant heat exchanger size and weight are larger than that which would be designed if the no-freeze criteria were not required. The required "no-freeze" resistance ratios for the two cases where significant thermal resistance is present in the tube, and for the case where it is negligible, are presented in Figure 23.

The general calculational method used for determining the thermal design with the no-freeze restriction is illustrated in Figure 24. A series of parametric curves were generated as a function of the tube diameter using the thermal rating required for the TAKE-OFF condition. In addition to the bare tubes study, a parametric study was made using finned tubes. Several arrangements using finned tubes were considered, but none showed a significant improvement in core geometry from the bare tubes. Based on the parametric studies, a reference design was selected with 2240 core tubes of 0.188-inch ($0.478 \times 10^{-2}$ m) diameter. The core was arranged for a two-pass flow system with each bank equal in size and number of tubes.

Table VI. Air-to-Methane Heat Exchanger Mechanical Design.

Type - One-Pass Air, Two-Pass Methane, Counter Flow

Overall Core Dimensions - 20-inch (0.508 m) Diameter by 18-inch (0.457 m) Length

Unit Weight (without facility air ducting):

| | Estimated | | Actual | |
|---|---|---|---|---|
| Core | 112 lb | (50.8 kg) | 100 lb | (45.4 kg) |
| Shell | 160 lb | (72.6 kg) | 200 lb | (90.8 kg) |
| Total | 272 lb | (123.4 kg) | 300 lb | (132.2 kg) |

Methane Side

No. of Tubes = 804

Tube Size - 0.188-inch (0.478 cm) Dia x 0.016-inch (0.0406 cm) Wall x 28-inch (0.711 m) Long

Arrangement - Triangular Array, P/D = 1.25

Pressure - 1150 psia ($7.92 \times 10^6$ N/m$^2$)

Temperature Range - -215° F (136° K) to +854° F (730° K)

Air Side

Pressure - 155 psia ($1.07 \times 10^6$ N/m$^2$)

Temperature Range - 1180° F (912° K) ⟵ 115° F (320° K)

Core Pressure Drop - 5 psi ($3.45 \times 10^4$ N/m$^2$)

Design Features

(1) Wrap-Around Configuration

(2) Floating Core

(3) Curved Tubes to Accommodate Large Differential Thermal Expansion

(4) Toroidal Air Manifold

(5) Asymmetric Core

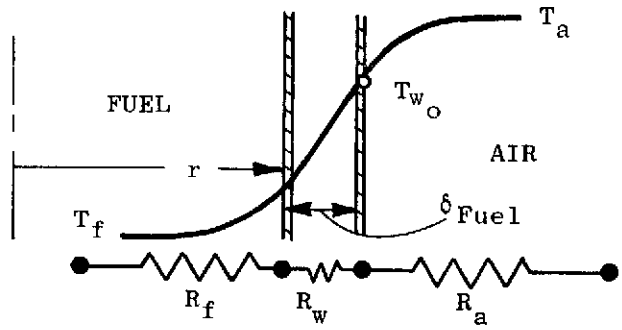


TEMPERATURE DROP AIR-SIDE WALL TO FUEL:

$$T_{w_o} - T_f = q\ (R_f + R_w) \qquad (a)$$

Temperature Drop from Air to Fuel:

$$T_a - T_f = q\ (R_f + R_w + R_a) \qquad (b)$$

Combining Equations (a) and (b) and Rearranging:

$$\frac{R_f + R_w}{R_a} = \frac{F}{1 - F} \text{ where } F \equiv \frac{T_{w_o} - T_f}{T_a - T_f},$$

the Freeze Coefficient

For no Freezing of Water, $T_{w_o} \geq 32°$ F

Then $$\boxed{\frac{R_f + R_w}{R_a} \geq \frac{F}{1 - F}, \text{ No Freezing}}$$

where $$R_w = \frac{\delta_{Fuel}}{k_{Fuel}} + \frac{\delta_{SS}}{k_{SS316}}$$

For Bare Tubes, $\delta_{fuel} = 0$ and $R_f >> R_w$

$$\boxed{\frac{R_f}{R_a} \geq \frac{F}{1 - F}, \text{ No Freezing}}$$

Figure 23. Air-to-Methane Heat Exchanger Performance, Derivation of No-Freeze Criterion.

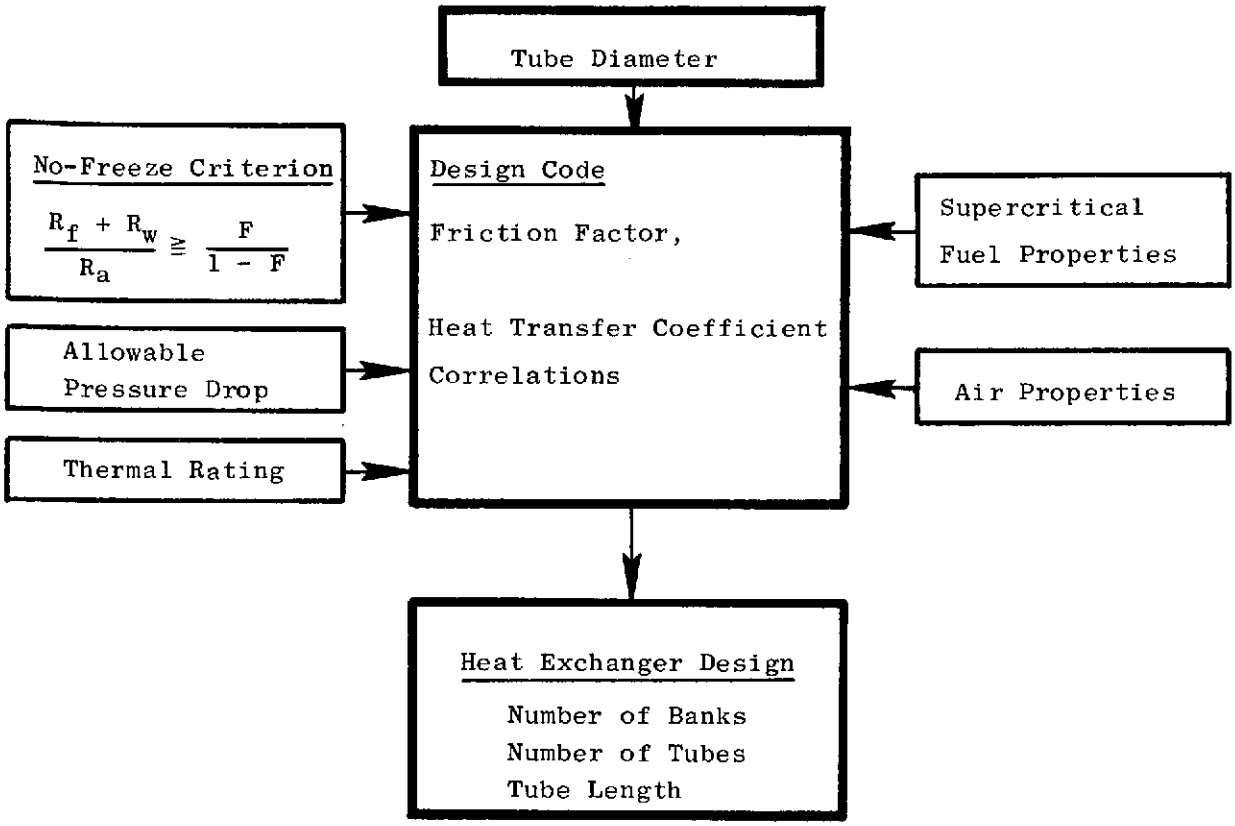


Figure 24. Heat Exchanger Calculational Method with No-Freeze Criterion.

Additional design studies indicated that an asymmetric bank design would show a significant improvement and meet the no-ice formation criteria. The increased efficiency of the asymmetric core resulted in a reduced-core volume. The number of tubes was reduced from 2240 to 804. This significant reduction in the number of tubes resulted in a more compact and reliable heat exchanger design. The calculated performance of the air-methane heat exchanger is shown in Table VII.

## Oil-Methane Heat Exchanger

### Mechanical Design

The oil-methane heat exchanger is shown in the drawing of Figure 25. The heat exchanger has a co-flow arrangement with the fuel making one pass through the tubes and the oil making five shell-side passes in cross flow.

The core consists of 342, 0.188-inch-OD ($0.478 \times 10^{-2}$ m) by 0.016-inch-wall ($0.0406 \times 10^{-2}$ m) tubes 5.5 inches ($14 \times 10^{-2}$ m) long. The Inconel 625 tubes are arranged in a triangular array with a pitch-to-diameter ratio of 1.25. There are 57 rows with six tubes in each row. The overall core dimensions are 1.6 inches ($4.06 \times 10^{-2}$ m) thick by 12 inches ($30.5 \times 10^{-2}$ m) wide and 5.5 inches ($14 \times 10^{-2}$ m) long.

The shell of the heat exchanger consists of five shallow U-shaped members that are circumferentially welded to the flow baffles and the headers. The shell holds the baffles in place and maintains a constant flow area for the oil. The shell design is sufficiently flexible to accommodate the small differential thermal expansion between the shell and core.

The methane enters the heat exchanger through a 1-inch ($2.54 \times 10^{-2}$ m) inlet and a tee-shaped distributor at -230° F (128° K) and 1150 psi ($7.93 \times 10^{6}$ N/m$^2$). The methane passes into the tube core through a 0.040-inch ($.103 \times 10^{-2}$ m) orifice designed to equalize the flow rates between tubes. The methane, after cooling the oil, discharges into the outlet header and discharges through a 1-inch ($2.54 \times 10^{-2}$ m) outlet.

A summary of the mechanical design features of the oil-methane heat exchanger is given in Table VIII.

### Thermal and Hydraulic Analysis

The pour point of an oil is determined by cooling a sample of oil in a test jar until, when the jar is displaced from the vertical to the horizontal position, no perceptible movement of the oil will occur within 5 seconds. Tube wall temperatures in the vicinity of the pour point must be avoided since stagnant oil films at that temperature could result and lead to stratification, poor local heat transfer, and reduced flow area. The minimum allowable tube wall temperature is a matter of judgement. Both 0° F (255° K) and -50° F

Table VII. Calculated Performance of Air-Methane Heat Exchanger.

| | Engine[1] Start | Idle | Takeoff[2] | Climb | Acceleration | Cruise | Deceleration | Descent |
|---|---|---|---|---|---|---|---|---|
| Methane | | | | | | | | |
| Inlet Temp,[3] ° F | -200 | -175 | -215 | -193 | -188 | -116 | +330 | 170 |
| (° K) | (144.5) | (158) | (136) | (148) | (151) | (191) | (439) | (350) |
| Calculated Outlet Temp, ° F | 265 | 260 | 430 | 415 | 548 | 1050 | 820 | 420 |
| (° K) | (402) | (400) | (494) | (486) | (560) | (838) | (711) | (489) |
| Flow, lbm/sec | 0.065 | 0.133 | 0.665 | 0.266 | 0.465 | 0.200 | 0.033 | 0.033 |
| (kg/sec) | (0.0295) | 0.0603) | (0.0302) | (0.121) | (0.211) | (0.0908) | (0.015) | (0.015) |
| Air | | | | | | | | |
| Inlet Temp, ° F | 290 | 290 | 680 | 630 | 1080 | 1180 | 830 | 425 |
| (° K) | (417) | (417) | (633) | (605) | (856) | (912) | (717) | (492) |
| Inlet Press, psia | | 60 | 155 | 60 | 130 | 65 | 30 | 45 |
| ($N/m^2 \times 10^{-6}$) | | (0.414) | (1.07) | (0.414) | (0.896) | (0.449) | (0.207) | (0.310) |
| Calculated Outlet Temp, ° F | 182 | 146 | 150 | 125 | 548 | 760 | 780 | 404 |
| (° K) | (356) | (337) | (339) | (325) | (560) | (677) | (688) | (480) |
| Flow, lbm/sec | 0.78 | 1.59 | 2.65 | 1.06 | 2.92 | 1.46 | 0.795 | 0.928 |
| (kg/sec) | (0.354) | (0.722) | (1.205) | (0.481) | (1.325) | (0.662) | (0.361) | (0.422) |

(1) Engine start condition received 11/10/70.

(2) Actual methane inlet temperatures may be higher in system performance of oil-methane unit.

(3) Fuel-side pressure drop at takeoff is 16 psi ($1.102 \times 10^5$ $N/m^2$), due to four flow restrictors; air-side core pressure drop at takeoff is 4.5 psi ($3.1 \times 10^4$ $N/m^2$) plus 10 psi ($6.89 \times 10^4$ $N/m^2$) total for inlet and exit toroids.

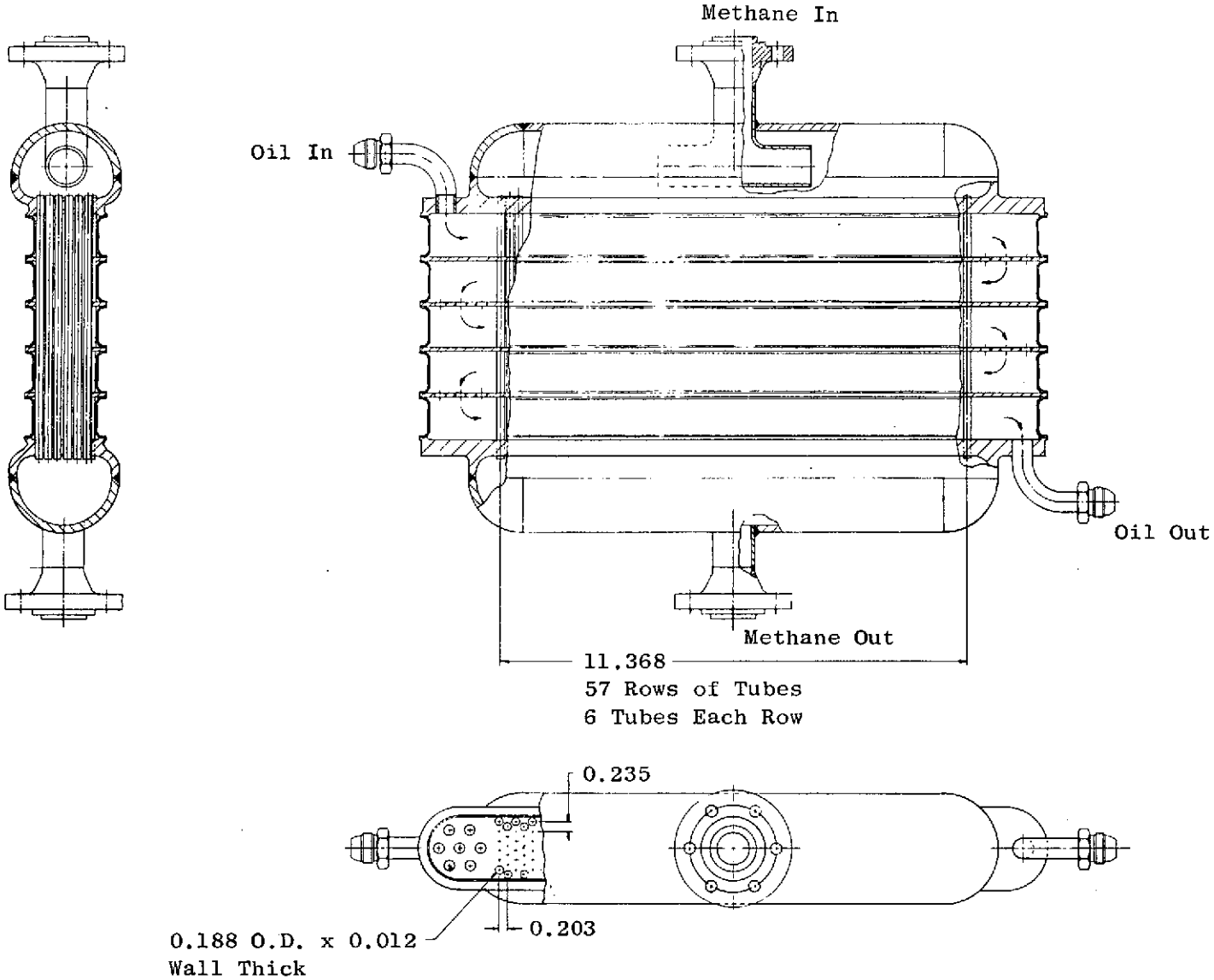


Figure 25 Oil-to-Methane Heat Exchanger.

Table VIII. Oil-to-Methane Heat Exchanger Mechanical Design.

Type - Five-Pass Oil, One-Pass Methane, CO Flow

Overall Core Dimensions - 1.6 in. (4.06 cm) x 12 in. (30.5 cm) x 5.5 in. (14 cm) Long

Unit Weight (without facility piping):

| | Estimated | | Actual | |
|---|---|---|---|---|
| Core | 16.8 lb | (7.62 kg) | 16.4 lb. | (7.45 kg) |
| Shell | 6.0 lb | (2.73 kg) | 9.7 lb | (4.40 kg) |
| Total | 22.8 lb | (10.35 kg) | 26.1 lb | (11.85 kg) |

Methane Side

No. of Tubes - 342

Tube Size - 0.188-in. (0.478 cm) Dia x 0.016-in. (0.0406 cm) Wall x 5.5-in. (14 cm) Long

Arrangement - Triangular Array, P/D = 1.25

Pressure - 1150 psia ($7.9 \times 10^6$ N/m$^2$)

Temperature - 230° F (128° K)

Oil Side

Pressure - 165 psia ($1.137 \times 10^6$ N/m$^2$)

Temperature Rnage - 200° F (367° K) to 500° F (533° K)

Maximum $\Delta P$ - 25 psi ($1.72 \times 10^5$ N/m$^2$)

Design Features

(1) Flexible Shell

(2) Straight Tubes

(3) Minimum Bypass Design

(228° K) were considered for this application with a pour point of -120°F (189° K).

The oil-methane heat exchanger was overspecified in that two different thermal designs were defined by the specification (i.e., "Take-Off" and "Cruise" condition). The heater exchanger was designed for the "Cruise" condition which is the point of maximum heat transfer. The resultant design will overperform at the "Take-Off" condition in that the oil will be cooled below the required 290° F (416° K) as shown in Table IX. The exit bulk oil temperature is predicted to be approximately 164° F (347° K), but the minimum tube wall temperature will be as low as -50° F (228° K). The heat exchanger was designed for silicon-base oil SF 8150 (dimethyl polysiloxane) which has a pour point of -120° F (189° K).

Control of the tube wall temperature is accomplished in the same manner as that used to prevent freezing in the fuel-air heat exchangers. The ratio of the film heat transfer coefficients at the inner and outer surface of the tube wall must be above a required value. Using the general calculation method discussed for the air-methane heat exchanger, a series of parametric curves was generated as functions of the assumed tube diameter.

Table X shows a comparison of the heat exchanger core parameters for the assumed 3/16 inch ($0.478 \times 10^{-2}$ m) tube size with 6 oil passes for the two assumed minimum tube wall temperatures. For this table, zero oil leakage is assumed. Overall consideration of all factors led to the selection of the -50° F (228° K) tube wall design. Primary items influencing this selection were: The low pour point temperature of -120° F (189° K), the predicted minimum exit bulk oil temperature of +25° F (269° K), and geometric considerations.

The number of oil passes was reduced from 6 to 5 in the final design so that the oil inlet and outlet tubes would be on opposite sides. This ensured that all the oil, regardless of the amount of bypass leakage, would cross the core bundle at least once.

The calculated performance of the oil-methane heat exchanger is shown in Table XI.

---

Table IX. Operation of Oil-Methane Unit at Takeoff when Sized for Cruise

| | Cruise | Takeoff |
|---|---|---|
| Inlet Oil Temperature | 400° F (478° K) | 400° F (478° K) |
| Outlet Oil Temperature | 170° F (350° K) | 290° F specified (417° K)<br>164° F actual (347° K) |
| Inlet Fuel Temperature | -231° F (127° K) | -235° F (125° K) |
| Outlet Fuel Temperature | -100° F (200° K) | -215° F specified )136° K)<br>-189° F actual (151° K) |

Table X. Oil-Methane Heat Exchanger Core Parameters

| Min. Tube Temp. @ TO | Total Tubes | Tube Length | Oil Flow Length/Pass | Transverse Length | Oil Passes |
|---|---|---|---|---|---|
| -50° F (228° K) | 184 | 4" (0.102 m) | 7" (0.178 m) | 1 3/16" (0.0302 m) | 6 |
| 0° F (255° K) | 505 | 3" (0.0762 m) | 10 1/2" (0.267 m) | 2 3/8" (0.0603 m) | 6 |

## Air-Hydrogen Heat Exchanger

### Mechanical Design

The air-hydrogen heat exchanger is similar in construction to the air-methane unit except it is designed for a 100° arc sector rather than the complete 360° wraparound configuration of the air-methane unit. The reduced size is due to the lower thermal capacity requirement for the air-hydrogen heat exchanger. The air-hydrogen heat exchanger is shown in the drawing of Figure 26.

The air-hydrogen heat exchanger core is arranged in a one-pass air, two-pass fuel configuration similar to the air-methane heat exchanger. The air-hydrogen unit is co-flow where the air-methane unit was counterflow. Another basic difference is the use of a fuel tube assembly consisting of two concentric tubes with a stagnant layer of fuel in the annulus. The additional thermal resistance in the tube is used effectively to meet the "no-icing" requirement needed to operate an air heat exchanger with cryogenic fuel.

The tube bundle or core consists of 235 fuel tubes with an average length of 12.6 inches (0.32 m). Each tube assembly consists of an 0.188-inch-OD ($0.478 \times 10^{-2}$ m) outer tube with a 0.016-inch ($0.0407 \times 10^{-2}$ m) wall and 0.136-inch ($0.346 \times 10^{-2}$ m) inner tube with a 0.008-inch ($0.0203 \times 10^{-2}$ m) wall separated by a spirally wound 0.008-inch-diameter ($0.0203 \times 10^{-2}$ m) spacer wire. The tubes are arranged in a 7.5-inch (0.19 m) radius sector having an overall dimension of 1.5 inches (0.0381 m) thick by 13 inches (0.33 m) wide by 12 inches (0.305 m) long. The core is divided into two asymmetric sections. The first bank or forward section consists of 13 rows of five tubes across; the second bank or rear section consists of 34 rows of five tubes across. The tubes are arranged in a triangular array with a pitch-to-diameter ratio of 1.25. The spacing between tubes is maintained by five baffle plates which are 1.3 inches (0.033 m) wide and 0.100 inch ($0.254 \times 10^{-2}$ m) thick and run the length of the core bundle to join the rear and forward banks together. The baffle plates have positioning holes for each tube and are match drilled to the same triangular pattern as the tube headers. The baffles are used only for tube support and maintain the spacing between tubes and limit

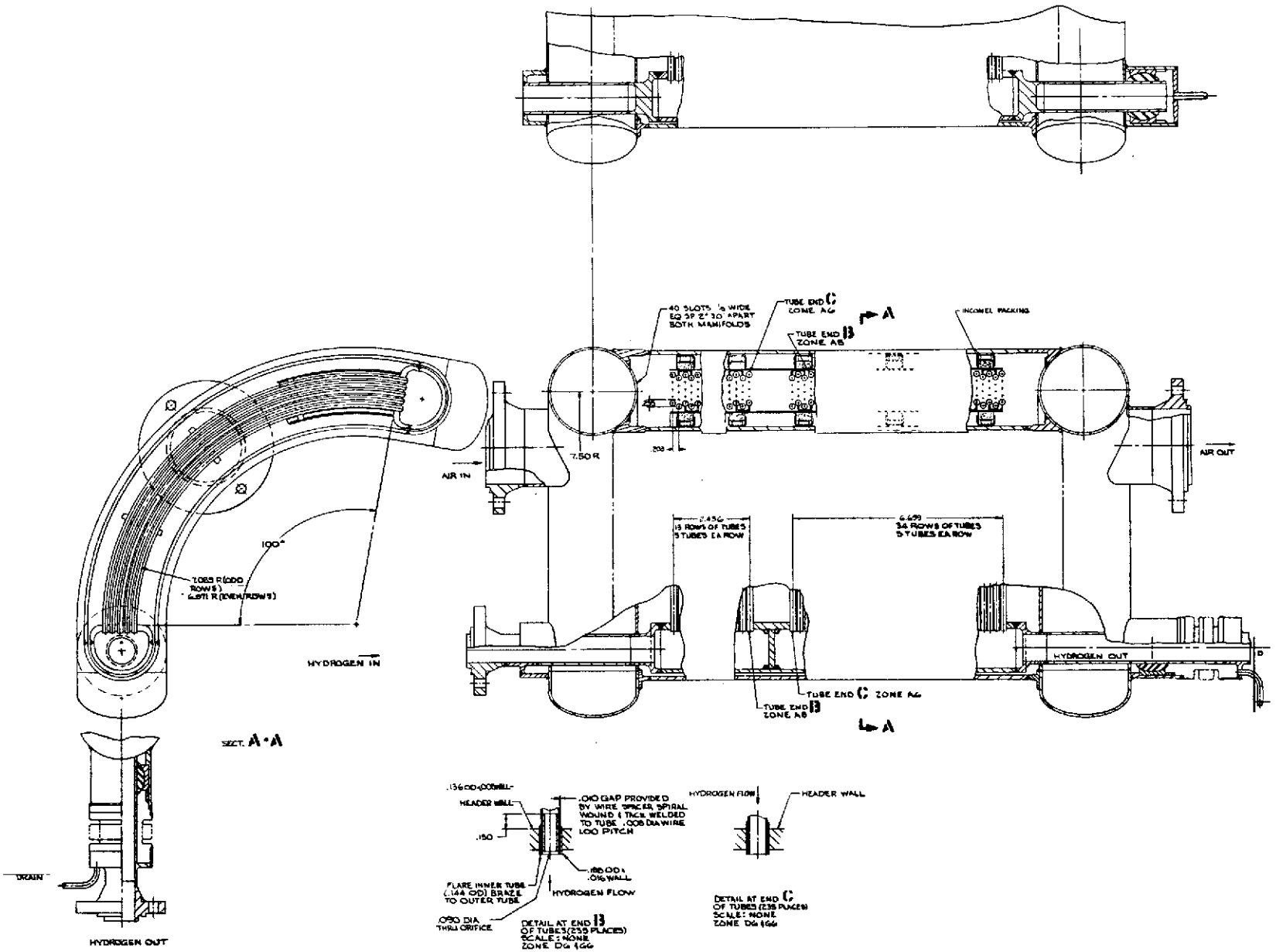


Figure 26. Air-to-Hydrogen Heat Exchanger.

Table XI. Oil-Methane Unit Calculated Performance of Present Five-Pass Design

| | Idle | Takeoff ** | Climb | Accel-eration | Cruise | Decel-eration | Descent |
|---|---|---|---|---|---|---|---|
| Methane | | | | | | | |
| Inlet Temp, ° F (° K) | -230 (128) | -235 (125) | -232 (127) | -233 (126) | -231 (127) | -210 (139) | -210 (139) |
| Calculated Outlet Temp, ° F (° K) | -132 (182) | -189 (151) | -120 (189) | -174 (159) | -106 (197) | 256 (397) | 180 (355) |
| Flow, lbm/sec (Kg/sec) | 0.133 (0.0603) | 0.655 (0.297) | 0.266 (0.121) | 0.465 (0.211) | 0.20 (0.0907) | 0.033 (0.015) | 0.033 (0.015) |
| Oil* | | | | | | | |
| Inlet Temp, ° F (° K) | 200 (366) | 400 (477) | 400 (477) | 400 (477) | 400 (477) | 500 (533) | 400 (477) |
| Calculated Outlet Temp, ° F (° K) | 2 (256) | 164 (346) | 174 (352) | 167 (348) | 167 (348) | 341 (445) | 252 (395) |
| Flow, lbm/sec (Kg/sec) | 0.195 (0.0885) | 0.325 (0.148) | 0.325 (0.148) | 0.325 (0.148) | 0.325 (0.148) | 0.292 (0.133) | 0.260 (0.118) |

* Oil is silicone fluid, SF 8150; nominal specific heat is 0.4 Btu/lbm - °F ($1.67 \times 10^3$ J/Kg-°K). Oil $\Delta T$ meets the specification at cruise and exceeds the specification at all other conditions.

** Oil-side pressure drop at takeoff is 20 psi ($1.38 \times 10^5$ N/m$^2$), including 18 velocity heads for inlet, pass expansion, turning, and exit losses. Fuel-side pressure loss is 8 psi ($5.52 \times 10^4$ N/m$^2$) (due to 2 flow restrictors).

the vibrational amplitude and frequency of the individual tubes during operation. The three center baffles are welded to the inlet air manifold to support the core and dampen the tube bundle from flow-induced vibrations.

A summary of the mechanical design features of the air-hydrogen heat exchanger is given in Table XII.

Thermal and Hydraulic Design

The air-hydrogen heat exchanger was designed to meet the performance requirements summarized in the Statement of Work. This specification requires that the heat exchanger performance be not significantly impaired by the formation of ice in the heat exchanger that could partially block the free-flow area on the air side of the heat exchanger. A thermal inconsistency relative to the "non-freeze" design was found in the specification; if the heat exchanger is designed to meet the "take-off" condition, the exit air temperature at "cruise" will be -19° F (245° K) which is inconsistent with the "non-freeze" icing condition. The solution to the problem was to design a smaller capacity heat exchanger which does not cool the air below 32° F (273° K) at the "cruise" condition.

The no-icing condition can be met using the same criteria as described in detail for the air-methane heat exchanger. In addition to controlling the convective heat transfer coefficients, a stagnant layer of fuel between two concentric tubes is used to decrease the heat transfer rate through the fuel tube in order to maintain the air-side temperature of the fuel tube above 32° F (273° K).

The initial analysis of the air-hydrogen heat exchanger was made for bare tubes without the thermal sleeves. The short length of the tubes, from 2 (0.0508 m) to 8 (0.203 m) inches long, made it impossible to achieve the desired mechanical configuration of curved tubes in a sector arrangement. To increase the tube length, sleeves were added. The next design refinement included asymmetric banks as previously discussed in the air-methane section.

The calculated performance of the air-hydrogen heat exchanger is shown in Table XIII.

Table XII. Air-to-Hydroagen Heat Exchanger Mechanical Design.

Type - One-Pass Air, Two-Pass Hydrogen, CO Flow

Overall Core Dimensions - 1.5 in. (3.81 cm) x 13 in. (33 cm) x 12 in. (30.5 cm)

Estimated Weight (without facility piping):

| | | |
|---|---|---|
| Core | 30.5 lb | (13.8 kg) |
| Shell | 31.7 lb | (14.4 kg) |
| Total | 62.2 lb | (28.2 kg) |

Hydrogen Side

No. of Tubes - 235

Tube Size - 0.188-in. (0.478 cm) Dia x 0.016-in. (0.0406 cm) Wall x 12.6-in. (32 cm) Long

Arrangement - Triangular Array, P/D = 1.25

Pressure - 400 psia ($2.76 \times 10^6$ N/m$^2$)

Temperature Range - -420° F (22.2° K) to -200° F (144.5° K)

Tube Insert - 0.136-in. (0.345 cm) OD x 0.008-in. (0.020 cm) Wall (0.009 in., 0.0228 cm Gap)

Air Side

Pressure - 150 psia ($1.033 \times 10^6$ N/m$^2$)

Temperature Range - 950° F (784° K) to 115° F (319° K)

Core Pressure Drop - 15 psi ($1.033 \times 10^5$ N/m$^2$)

Design Features

(1) Annular Configuration

(2) Floating Core

(3) Curved Tube to Accommodate Large Differential Expansion

(4) Flow Baffles at Core/Shell Boundary

(5) Asymmetric Core

Table XIII. Air-Hydrogen Unit, Calculated Performance of Present Asymmetric-Bank Design with Sleeves (12 Mil Gap)

| | Engine* Start** | Ground Idle | Takeoff | Cruise | Altitude Idle** |
|---|---|---|---|---|---|
| Hydrogen | | | | | |
| Inlet Temp, ° F (° K) | -410 (27.8) | -410 (27.8) | -420 (22.2) | -415 (25.0) | -400 (33.3) |
| Outlet Temp, ° F (° K) | -130 (183) | -263 (109.5) | -298 (09.2) | -248 (118) | -93 (204) |
| Flow, lbs/sec, (Kg/Sec) | 0.029 (0.0132) | 0.06 (0.0272) | 0.3 (0.136) | 0.135 (0.0613) | 0.03 (0.0136) |
| Air | | | | | |
| Inlet Temp, ° F (° K) | 315 (431) | 600 (590) | 960 (790) | 810 (707) | 400 (478) |
| Inlet Pressure, psi ($N/m^2$) | - - | 150 ($1.034 \times 10^6$) | 150 ($1.034 \times 10^6$) | 150 ($1.034 \times 10^6$) | 150 ($1.034 \times 10^6$) |
| Outlet Temp, ° F (° K) | -33 (237) | 75 (297) | 494 (530) | 110 (317) | 16 (265) |
| Flow, lbs/sec, (Kg/Sec) | 0.35 (0.159) | 0.72 (0.327) | 1.2 (0.545) | 0.48 (0.218) | 0.36 (0.163) |

* Engine Start Condition Received 11/10/70.

** Fuel Bypassing Can be Used to Correct Air Enthalpy Problem During Engine Start and Altitude Idle.

Bypass and Restrictor Valves - Methane Heat Exchanger

Standard commercial cyrogenic gas valves were procured with appropriate electro-pneumatic controls and plumbed into the fuel conditioning package to accomplish upstream restriction and bypass of the fuel side of each of the methane heat exchangers. Valves ROV-5, ROV-6, ROV-7 and ROV-8 of the fuel conditioning package are of a single model series, Masoneilan series 35000. Pneumatic positioners provided with these valves are Masoneilon series 7600. Pneumatic control logic solenoid valves were provided for safety logic interface with the system mode control panel. These solenoid valves are ASCO #8302A58 valves.

Valves ROV-6 and ROV-8 were equipped with electrical-to-pneumatic signal transducers of the Fisher Governor type 546/67FR. These transducers are signalled by the air-to-fuel heat source control system to effect automatic fuel bypass for use in controlling heater fluid exit temperature of the heat exchangers. These transducers are 3 to 15 psi ($2.07 \times 10^4$ to $1.07 \times 10^5$ $N/m^2$) output with 1 to 5 milliamp input and utilize a 2500 ohm coil.

Air signals for ROV-5 and ROV-7 were to be customer provided. Any standard panel loader or EP transducer with 3 to 15 psi ($2.07 \times 10^4$ to $1.07 \times 10^5$ $N/m^2$) output may be used to manually effect remote control of these valves. All valves were equipped with air pressure filter-regulators which are Masoneilan No. 77-4.

Bypass and Restrictor Valves - Hydrogen Heat Exchanger

Values ROV-5B and ROV-6B for the hydrogen configuration of the fuel conditioning package were provided in a single model series, Masoneilan series 20,000. These valves were selected to obtain actuator shaft sealing capable of operation at liquid hydrogen temperatures. The electrical-to-pneumatic signal transducer used for ROV-6 in the methane configuration was also used to control ROV-6B for hydrogen. A customer panel loader of 3 to 15 psi ($2.07 \times 10^4$ to $1.07 \times 10^5$ $N/m^2$) output must be provided to control ROV-5B.

Fuel Pressure Relief Valves

Two fuel pressure relief valves were provided for the methane fuel conditioning package. These are Consolidated model #1975 valves. Relief settings at 1160 psig ($8 \times 10^6$ $N/m^2$) were used to protect the heat exchanger. Relief flow was intended to be routed to the system vent stack.

The hydrogen fuel system package was provided with a single Anderson-Greenwood model 81S88-3 relief valve to protect the heat exchanger. A relief setting of 550 psig ($3.79 \times 10^6$ $N/m^2$) was used.

## Heat Exchanger Exhaust Airflow Control Valve

Airflow control valve ROV-4 was physically mounted with the fuel conditioning package at the air heat exchanger exhaust. Functionally the valve acts as a component of the air-to-fuel heat source and control subsystem.

The valve body provided is a Fisher Controls model series ES. The valve was equipped with a type 476U actuator, a type 3570 valve positioner, and a type 546 E-P transducer. A type 3550 electronic valve stem position indicator was also included. The E-P transducer for ROV-4 is signalled from the air control system electrical panel for automatic heat exchanger airflow control.

## FUEL METERING AND PRESSURE REGULATING PACKAGE

The Fuel Metering and Pressure Regulating Valve Package is depicted in the lower right foreground of Figure 20. Components contained in this package include:

Pressure Regulating Valve (PRV)

Metering Valve

$P_8$ Pressure Sensor

$T_8$ Temperature Detector

Engine Fuel Shutoff Valve (ROV-2A)

System Vent Valve (ROV-2B)

This package interconnects the heat exchanger exit fuel with the engine manifold and system vent stack.

## Pressure Regulating and Metering Valves & Sensors

The Pressure Regulating and Metering Valve assembly cross section is shown on layout 4013094-539. These valves were designed and assembled by the contractor from purchased piece parts.

The configuration of the valves is a rotary slide valve. Instead of nozzles, there is a valve plate with two shaped ports. A rotating member, with ceramic pads, is spring and pressure loaded against the flat surface on the valve plate. As these pads rotate, port opening varies.

The valve plate has a wear resistance surface coating applied by Malcomizing (nitriding). The valve plate also has a vented groove around the port which reduces the bearing area sensing the pressure drop. Logarithmic ports are provided with relief on the back side.

Referring to Drawing 4013094-539, the rotating member is driven by a rotary actuator through a shaft and bellows coupling. The bellows coupling is attached to the shaft by means of an adapter which is keyed and clamped to a taper. The bellows coupling is large in diameter to provide a high torsional

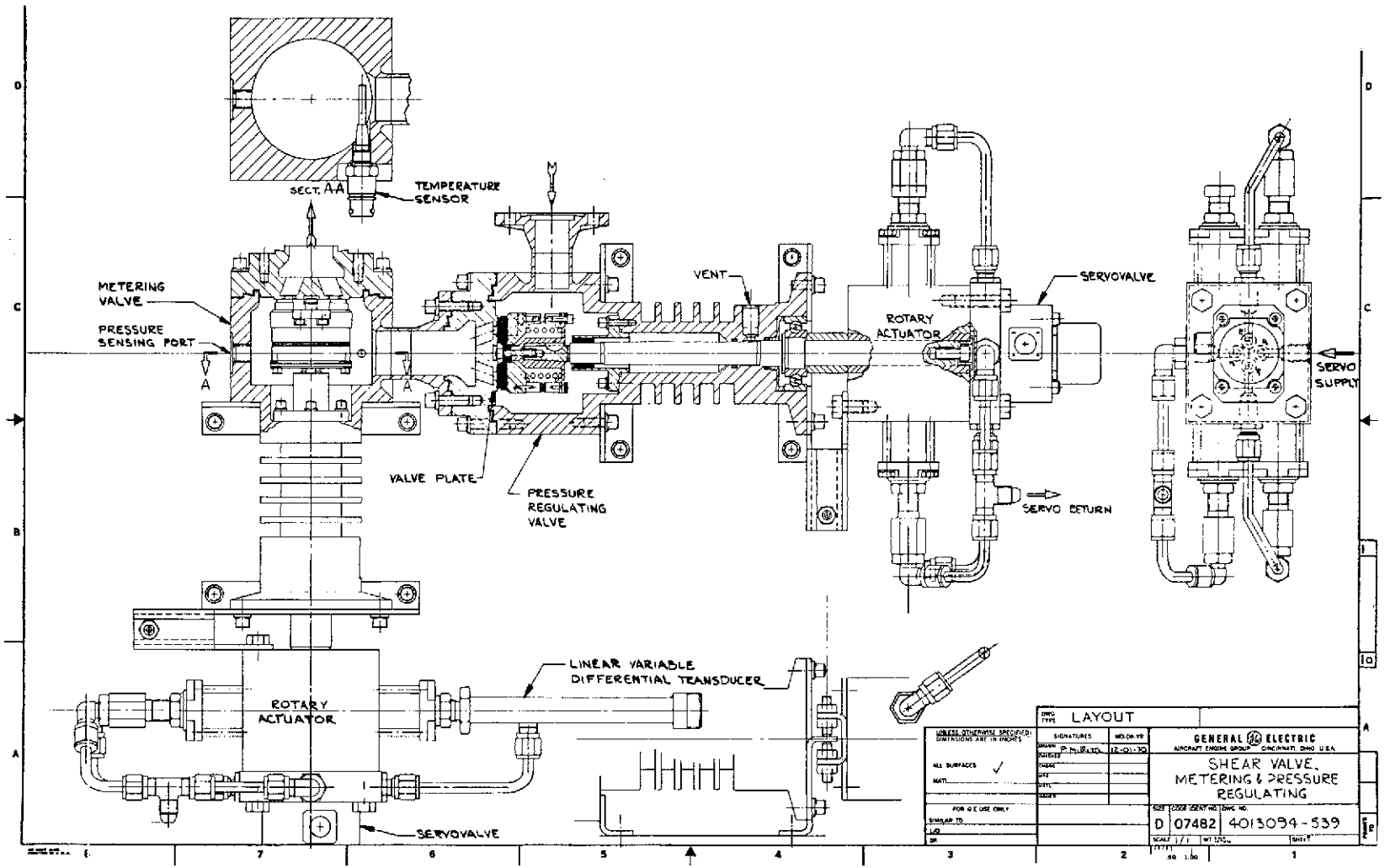
SECT. A-A
TEMPERATURE SENSOR
METERING VALVE
PRESSURE SENSING PORT
A
A
VENT
ROTARY ACTUATOR
SERVOVALVE
SERVO SUPPLY
VALVE PLATE
PRESSURE REGULATING VALVE
SERVO RETURN
LINEAR VARIABLE DIFFERENTIAL TRANSDUCER
ROTARY ACTUATOR
SERVOVALVE
LAYOUT
GENERAL ELECTRIC
AIRCRAFT ENGINE GROUP CINCINNATI, OHIO U.S.A.
SHEAR VALVE, METERING & PRESSURE REGULATING
D
07482
4013094-539

spring rate. The windup for 30 in-lbs (3.39 N-m) torque is calculated to be 2.4 minutes. The bellows coupling allows axial shaft motion relative to the rotating member which will occur because of expected temperature differences in the parts involved. The shaft is supported at the valve end by a carbon journal bearing. This bearing also acts as a clearance seal which will reduce fuel circulation along the shaft. A carbon radial bearing with large clearance is provided between the rotating member and the shaft. The bellows coupling is rigid in shear so it will position the rotating member normally. The general scheme is to avoid metal-to-metal rubbing at the valve end of the assembly.

The rotary actuator shown is a catalog item with minor modifications for adjustable stops and the position transducer (LVDT). The actuator has a hollow shaft which allows mounting it to the valve shaft. The joint at this end of the shaft is an axial clamp for zero backlash plus a key for redundancy. Brackets prevent relative rotation between the actuator and valve housing. The rotary shaft seals are near the actuator where temperatures will be moderate. The seals are of filled Teflon with a metallic expanding spring. These seals have a temperature range of -423° (20.6° K) to +500° F (533° K). Two seals with a vent between them are provided.

The servo valve is mounted to the actuator by means of a machined manifold. This manifold provides porting for all the hydraulic interconnectins. The servo valves have a mechanical bias which will drive the vapor control or pressure regulating valves closed when no electrical signal exists. This servo valve is a standard ABEX model 410.

The linear variable differential transformer was procured from G.L. Collins Corporation under GE Drawing HCD-1008. The temperature sensors ($T_8$) are Rosemount model 150 MA ($H_2$) and model 177MA ($CH_4$). Both pressure and temperature are sensed upstream of the metering ports. The pressure sensors ($P_8$) utilized were Statham model PA-822.

The two valves operate on both fuels, requiring only changes in sensors and stop settings for conversion. Refer to Figure 27 for calibration and stop settings of the metering valve.

## Engine Fuel Shutoff and Vent Valves

The shutoff and vent valves, ROV-2A and ROV-2B, are Masoneilan series 20000 valves. The solenoid logic valves which control shutoff and venting are ASCO #8302 A58 valves. Valve positions are controlled electrically from the system mode control panel.

## ENGINE ELECTRICAL CONTROL

The engine electrical control package provided consists of an Electrical Control breadboard panel and a Power Lever package. A photographic view of the electrical control panel and power lever package is shown in Figure 28. These circuits and devices were designed and assembled by the contractor from purchased piece parts.

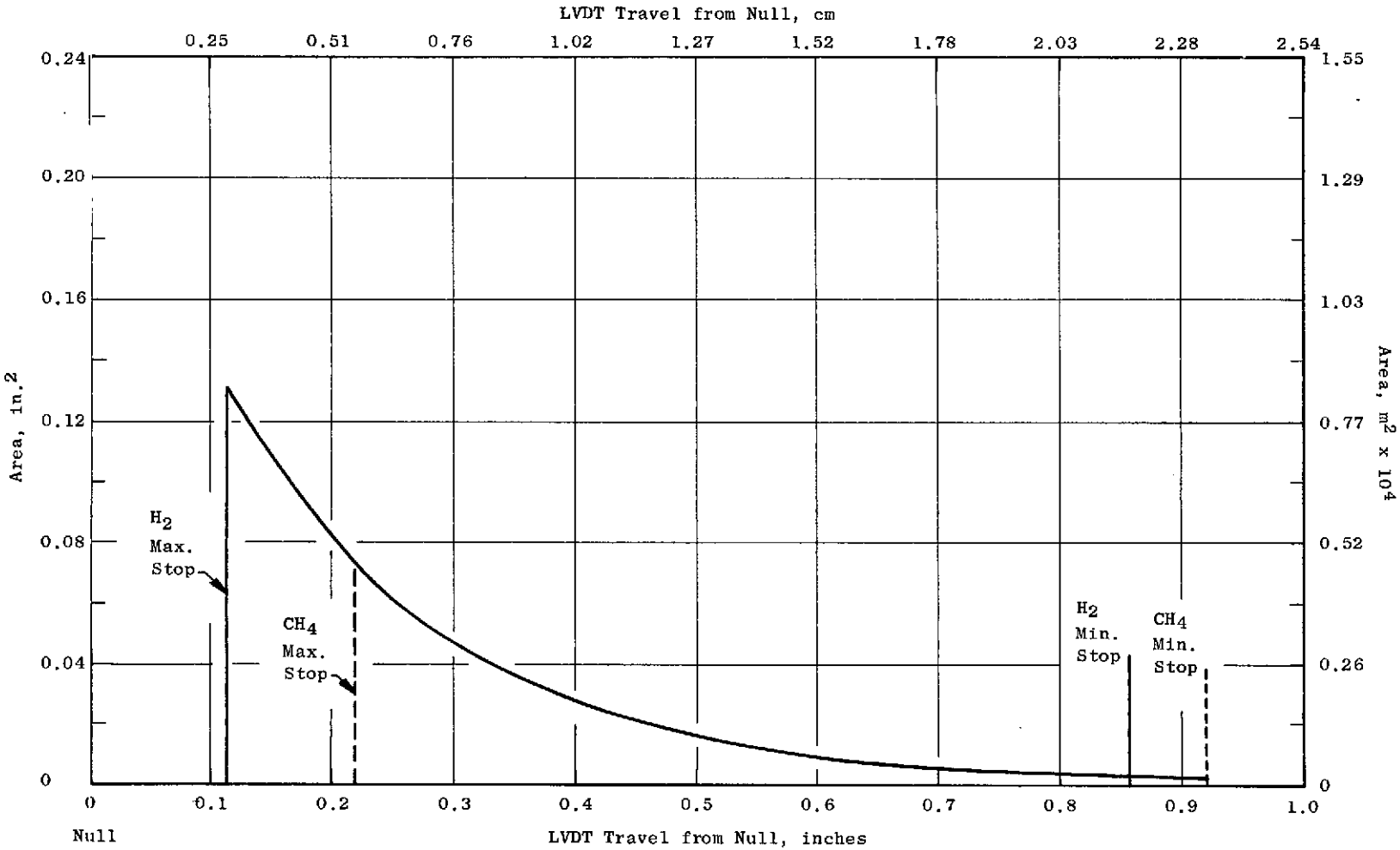


Figure 27. Metering Valve Calibration Curve.

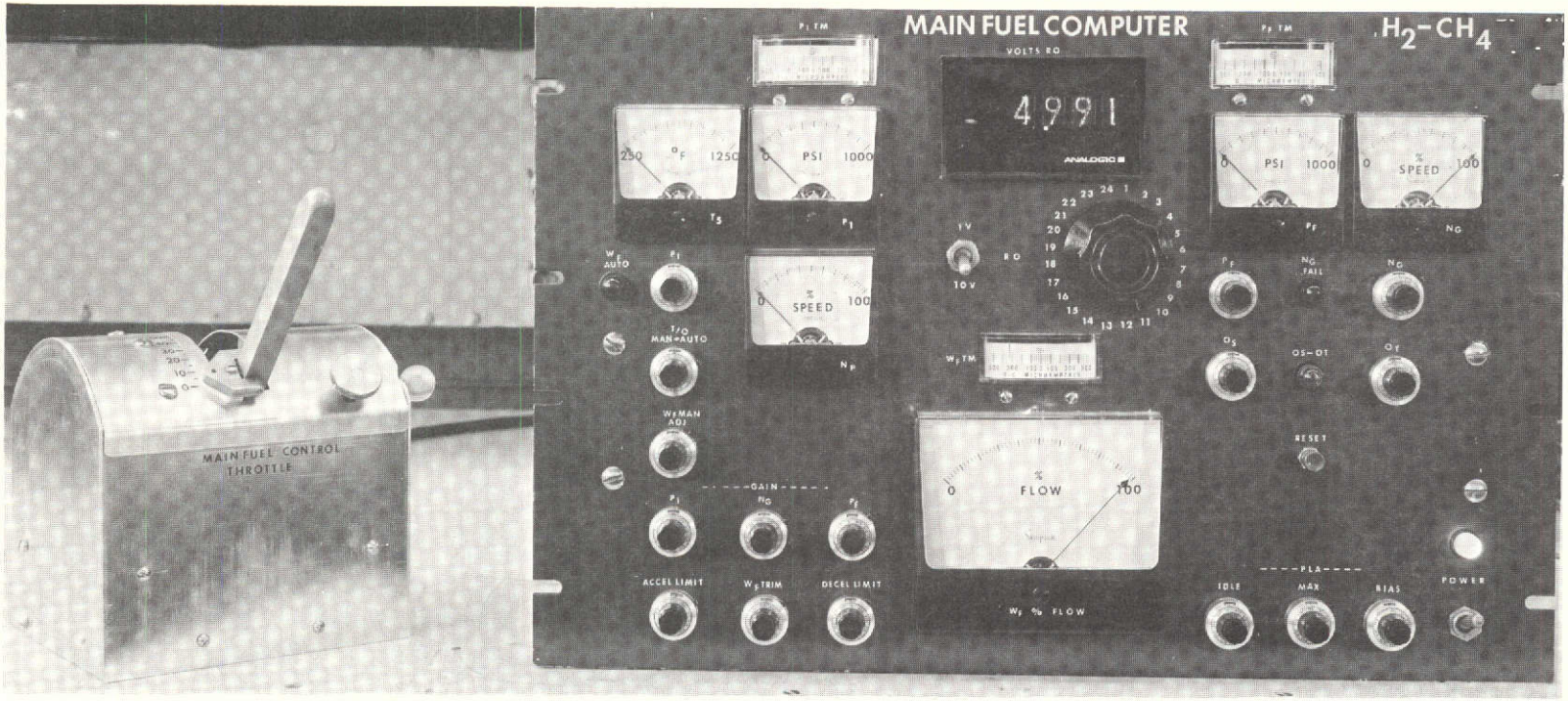


Figure 28. Electronic Control Computer Breadboard and Power Lever Quadrant.

## Circuit Functional Description

Circuit functions are described in reference to schematic CED 29000.

### Speed Governing Loop

Governor speed request signals are provided to the loop by the Power Lever Transducer position. The power lever package also contains a shutdown switch which is interlocked with the Mode Control Panel logic to shut off engine fuel and vent the system (through ROV-2A and 2B) whenever the power lever is below 10° angle.

A circuit board contains shaping circuits for the power lever speed request schedule, signal selectors for acceleration and deceleration limit signals, the fuel flow rate loop integrater - amplifier, a manual-automatic signal selector, and the fuel flow position loop driver amplifier. Output current of the driver amplifier signals the metering valve torque motor. Torque motor current in the electrohydraulic servo valve ports hydraulic flow to the metering valve actuator, and the signal is integrated hydraulically to move the metering valve position.

Governor speed feedback signals are generated by the standard J85 Control Alternator. One half of a circuit board serves as a frequency-to-DC converter for the Ng speed signal. The output serves as speed feedback to the governor error amplifier.

Metering valve actuator position is sensed by the $W_f$ LVDT. The alternating output signal of the LVDT is demodulated and the DC output signal, which is proportional to the log of metering valve area, is sent to the fuel temperature compensation circuit board. A function log $W_f/A$ vs $T_f$ is generated using the $W_f$ RTD output as the measure of metering valve fuel temperature. The function output log $W_f/A$ is added to log A to yield an output which is proportional to log $W_f$. The log $W_f$ signal is input to an anti-log generator such that the resulting output signal becomes the analog of $W_f$. The $W_f$ output voltage is used as feedback to close the metering valve position loop and also as input to the fuel flow rate feedback network.

In addition, the computed fuel flow signal is used as input to generate acceleration and deceleration limits on fuel flow rate and is read out for display.

### Acceleration-Deceleration Limits

The acceleration control mode used in the control is such that $\dot{W}_f/W_f = f(N_g)$. The fixed function is generated using $N_g$ output signal from the governor feedback. The $W_f$ signal is also multiplied by the function output $\dot{W}_f/W_f$ to yield a limit signal voltage proportional to $\dot{W}_f$. This acceleration limit signal is compared to governor speed error at the acceleration limit

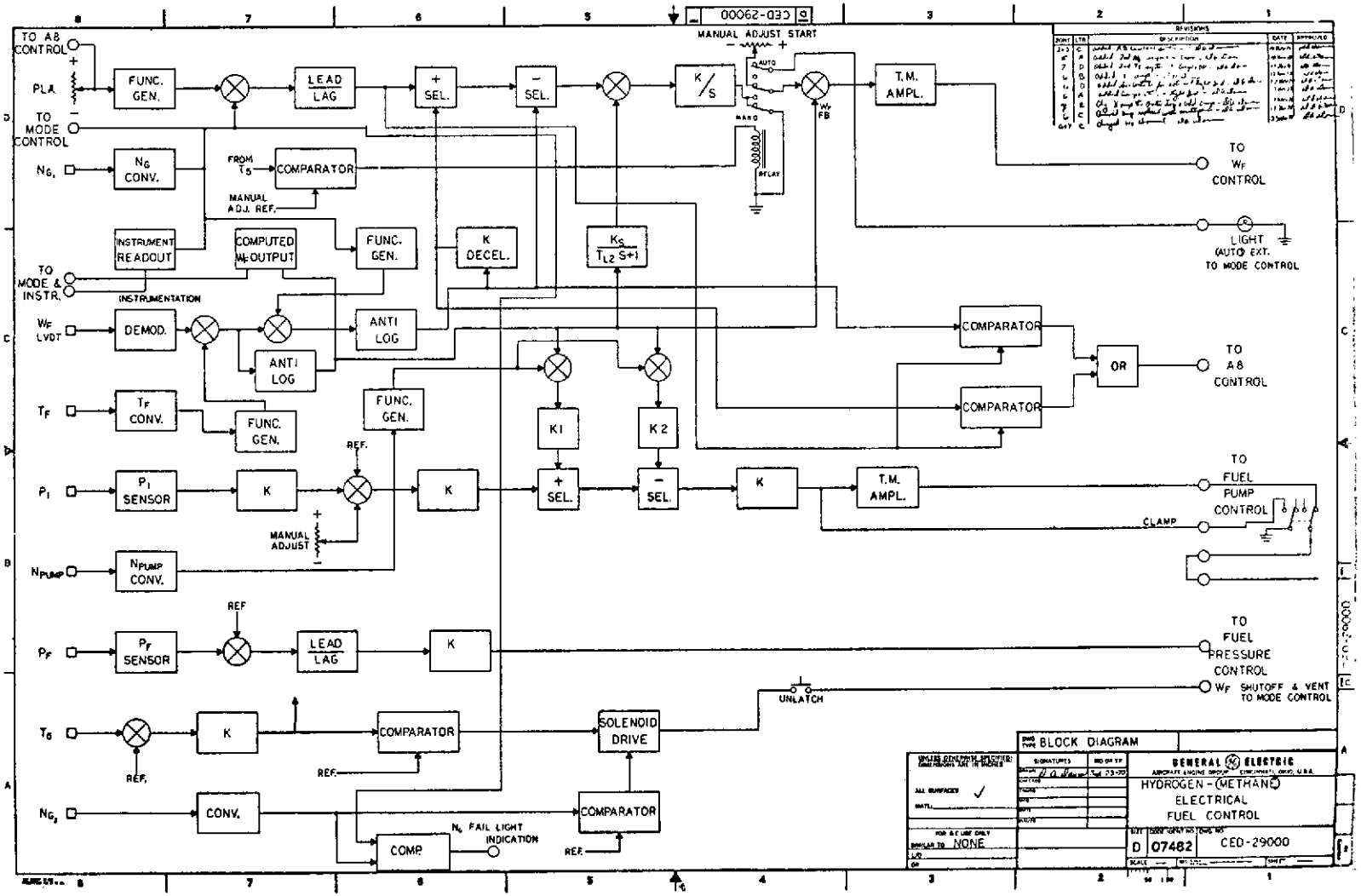
CED-29000
MANUAL ADJUST START
TO A8 CONTROL
PLA
TO MODE CONTROL
FUNC. GEN.
LEAD LAG
+ SEL.
- SEL.
K/S
AUTO
HARD
RELAY
T.M. AMPL.
TO WF CONTROL
LIGHT (AUTO EXT. TO MODE CONTROL
NG
NG CONV.
FROM T5
COMPARATOR
MANUAL ADJ. REF.
INSTRUMENT READOUT
COMPUTED WF OUTPUT
FUNC. GEN.
K DECEL.
Ks/(TL2 S+1)
TO MODE & INSTR.
INSTRUMENTATION
WF LVDT
DEMOD.
ANTI LOG
ANTI LOG
COMPARATOR
COMPARATOR
OR
TO A8 CONTROL
TF
TF CONV.
FUNC. GEN.
FUNC. GEN.
K1
K2
P1
P1 SENSOR
K
REF.
K
+ SEL.
- SEL.
K
T.M. AMPL.
TO FUEL PUMP CONTROL
CLAMP
MANUAL ADJUST
NPUMP
NPUMP CONV.
REF
PF
PF SENSOR
LEAD LAG
K
TO FUEL PRESSURE CONTROL
WF SHUTOFF & VENT TO MODE CONTROL
UNLATCH
T6
K
COMPARATOR
SOLENOID DRIVE
REF.
REF.
NG
CONV.
COMPARATOR
NG FAIL LIGHT INDICATION
COMP
REF.
BLOCK DIAGRAM
GENERAL ELECTRIC
AIRCRAFT ENGINE GROUP
HYDROGEN-(METHANE) ELECTRICAL FUEL CONTROL
D 07462
CED-29000
NONE

selector. The $\dot{W}_f$ acceleration limit signal is scaled and inverted to provide a deceleration limit voltage such that $W_f$ decel equals - K x $\dot{W}_f$ accel. The deceleration limit signal is applied to the appropriate selector to compare with governor speed error. These limit signals are also used as input to a logic circuit to provide permission logic for the exhaust area control system.

Overspeed - Overtemperature Protection

One circuit board provides overspeed and overtemperature protection for the engine. The standard J85 thermocouple harness output is provided to the circuit. The circuit amplifies the $T_5$ temperature signal and compares the amplified signal to an adjustable temperature limit reference voltage. When limit temperature is exceeded, a relay driver stage is triggered, which switches the engine shutoff and vent valves (ROV-2A & 2B) and shuts off fuel pump hydraulic power.

The circuit also senses an engine overspeed signal obtained from a magnetic pickup tachometer package provided by NASA. The signal is converted to DC and applied to the relay driver stage. When the speed level exceeds the overspeed reference voltage, the relay is energized and shutdown occurs. The converted speed output is also compared to the $N_g$ speed output. If the two tachometer signals do not agree within preselected limits, a comparator energizes a relay which lights a tach failure indicator light on the front panel.

The circuit also contains a temperature reference adjustment for manual-automatic switching of fuel valve control. When $T_5$ exceeds a preselected value, the temperature error is amplified and sent to the governor circuit energizing a relay. The relay then unclamps the governor integrator amplifier and switches out the manual reference ajustment input to the fuel valve position loop which is used to set starting fuel flow. The relay also provides an engine light logic to the Safety and Mode Controller.

Exhaust Area Control Signals

Exhaust area control signals and processing are provided for a NASA electrohydraulic exhaust area actuation system for the J85 engine. The engine $T_{5e}$ temperature signal is compared to a fixed $T_{5e}$ reference voltage to generate a $T_{5e}$ temperature error signal for exhaust area control. Lead compensation is applied to the error signal, and the error is integrated and applied to a limit selector. The $T_{5e}$ error is selected whenever the error is positive and larger than the $A_{8e}$ position command voltage at the selector. The selector output is buffered and provided to the NASA electrohydraulic control.

The circuit also contains the logic circuitry required for the exhaust area control. Governor speed error is applied as input to two comparators. The acceleration and deceleration limit signal voltages are also applied to these comparators. Whenever speed error reaches a value such that the acceleration or deceleration limit is selected in the governor, the comparators fire a driver amplifier which energizes a relay. The relay then selects the output

of an $A_{8e}$ position command which is scheduled as a function of engine speed signal.

When the engine is operating in the steady-state speed condition with small governor speed error, the $A_{8e}$ position command selected is a function of the power lever position voltage. The position command schedule selected by the relay is applied to a signal selector circuit. Thus, when the engine is undergoing a speed transient, $A_{8e}$ is scheduled from engine speed, and when the engine is operating steady-state, $A_{8e}$ is scheduled by power lever. Either schedule can be overridden by $T_5$ error to open the exhaust nozzle in event of overtemperature conditions. This circuit was not used during the contractor test demonstrations for the J85 engine.

Fuel Pump Control Circuit

The fuel pump is operated as a variable-speed, variable-delivery, pressure regulated flow source. Pump discharge fuel pressure is sensed by the P1 pressure transducer and the output signal is amplified. A variable pressure reference ajustment is also provided and is compared with the sensed discharge pressure signal to generate a pressure error signal. The error signal is amplified, applied to limit selectors, and integrated to generate a torque motor driver current to the electrohydraulic servo valve mounted on the fuel pump hydraulic motor. The integrated pressure error signal modulates serve valve current and hydraulic flow to vary pump speed and delivery to satisfy the pump pressure reference. The torque motor driver current can be interrupted by permission relay contacts in the Mode Control and by overspeed-overtemperature action.

The fuel pump pressure servo action is bounded by limits on fuel pump speed and delivery which are established in relation to the system fuel valve fuel flow signal. Pump speed is sensed by an electromagnetic speed pickup which senses rotation of a gear attached to the pump motor hydraulic sequencing valve. The pump speed sensor signal is demodulated and converted to a DC voltage and is then applied to a function generator circuit. The function generator circuit generates an analog output of fuel pump delivery as a function of sensed pump speed, based on prior delivery calibration of the pump. The fuel valve fuel flow voltage is applied as input to two comparators, and the comparator outputs are fed to the positive and negative selectors which pass pump pressure servo error. When the fuel pump delivery violates a pre-established limit ratio with fuel valve flow, the comparators apply suitable voltages to the limit selectors to deselect pressure error and cause the pump speed to be limited to upper and lower bounds in relation to fuel valve flow.

Pressure Regulator Valve Control Circuit

The electrohydraulically operated fuel pressure regulating valve immediately upstream of the system flow metering valve serves to regulate metering valve entrance pressure to a constant value and provides the throttling required to reduce from pump discharge pressure level to metering valve entrance

pressure. Metering valve entrance pressure is sensed by the $P_F$ transducer. The sensor output is demodulated and compared to an ajustable pressure reference voltage. The pressure error signal is amplified and generates a driver current for the $P_F$ torque-motor in the electrohydraulic servo valve which controls the fuel pressure regulating valve. The error signal is integrated hydraulically in the fuel valve actuator, which positions valve area to satisfy the electrical pressure reference.

Engine and System Operation

Engine fuel shutoff and venting can always be achieved by retarding the Power Lever Quadrant to 0° angle. The power lever switch which opens below 10° PLA is interlocked with the Mode Control Panel to prevent engine fuel admission through the action of ROV-2A and 2B.

The engine starting and ignition sequence is controlled primarily by the Mode Control Panel. The only settings required at the Electrical Control during starting procedure are to preselect the Manual $W_f$ pot setting for start fuel level and to place the power lever angle at 15° - 18° for idle speed request. The control automatically accelerates the engine from light-off to idle speed during the start.

Any part speed or maximum speed power lever setting called for in the test plan can be set as rapidly as desired. The control automatically controls acceleration transients and steady-state governing. Automatic shutdown for overspeed and overtemperature is also provided.

HYDRAULIC SUPPLY

The hydraulic power supply equipment purchased for the system consists of the following components:

- Engine-driven, high pressure hydraulic pump
- High pressure relief valve
- Return pressure regulating valve
- Boost conditioning cart

These items were purchased from vendors and plumbed into the system at the point of test set up. The system utilizes MIL-H-5606 hydraulic oil.

Engine-Driven High Pressure Hydraulic Pump

An Abex model AP6VSC-16 Airborne Hydraulic Pump was procured for the engine-driven high pressure supply. The pump was mounted on the overspeed governor pad of the J85 engine gearbox which turns at 7088 rpm (743 rad/sec) for 100% engine speed. The pump is pressure compensated and a setting of 3000 psig ($2.07 \times 10^7$ N/m$^2$) was selected. The compensator stroke was adjusted to permit 27 gpm ($17 \times 10^{-4}$ m$^3$/sec) delivery at the selected speed and pressure.

### High Pressure Relief Valve

A Rexroth model DBDS10EA 4500/5 high pressure relief valve was procured to protect the control system against overpressure. The relief valve was installed between the engine pump high pressure discharge line and the case drain line. A relief pressure setting of 3200 psig ($2.21 \times 10^7$ N/m$^2$) was selected.

### Return Pressure Regulating Valve

A Republic relief valve model 628XB was provided in series with the hydraulic system return flow to the reservoir for the purpose of regulating system back pressure to the control servos. A 90 psig ($6.2 \times 10^5$ N/m$^2$) relief setting was selected for the regulated level.

### Boost Conditioning Cart

An off-engine oil boost conditioning cart of standard industrial type was procured to provide inlet pressure boost, oil cooling, and a supply reservoir for the engine-driven hydraulic pump. The boost cart was procured from PABCO Fluid Power Company to General Electric Specification W-11277-29.

The cart consists of a 60 gallon (0.227 m$^3$) standard reservoir, a motor-driven boost pump providing 25 gpm ($15.75 \times 10^{-4}$ m$^3$/sec) flow at 75 to 150 psid ($0.517$ to $1.034 \times 10^6$ N/m$^2$) boost level, and a water-cooled return flow heat exchanger sized to dissipate heat rate equivalent to 36 HP ($2.68 \times 10^4$ W). Filtration and electrical service connections were also provided on the cart.

## AIR HEATER SUBSYSTEM

An air supply heating and control subsystem was designed and fabricated as planned in concept studies for supply of hot air to the air-to-fuel heat exchangers. The heater subsystem was designed to accept facility input air at ambient temperature and 150 psig ($1.034 \times 10^6$ N/m$^2$) pressure and to handle flow rates up to 3 pps (1.36 Kg/sec). The system automatically controls heat exchanger airflow rate, entrance pressure, and entrance temperature. The system includes: 1) an air heater combustor, valving, and piping assembly, 2) at set of electrical control panels. The pneumatic and electrical equipment was designed and assembled by the contractor from procured industrial standard piece parts.

### Air Heater

The arrangement of the air heater and control equipment is shown by drawing 4013157-233. The air heater and valving is depicted by Figure 29. Entrance air to the system is throttled by valve ROV-3 and associated electropneumatic controls to establish heat exchanger entrance pressure and combustor pressure level. Dual fuel control valves ROV-10 and ROV-11, with associated electropneumatic controls,

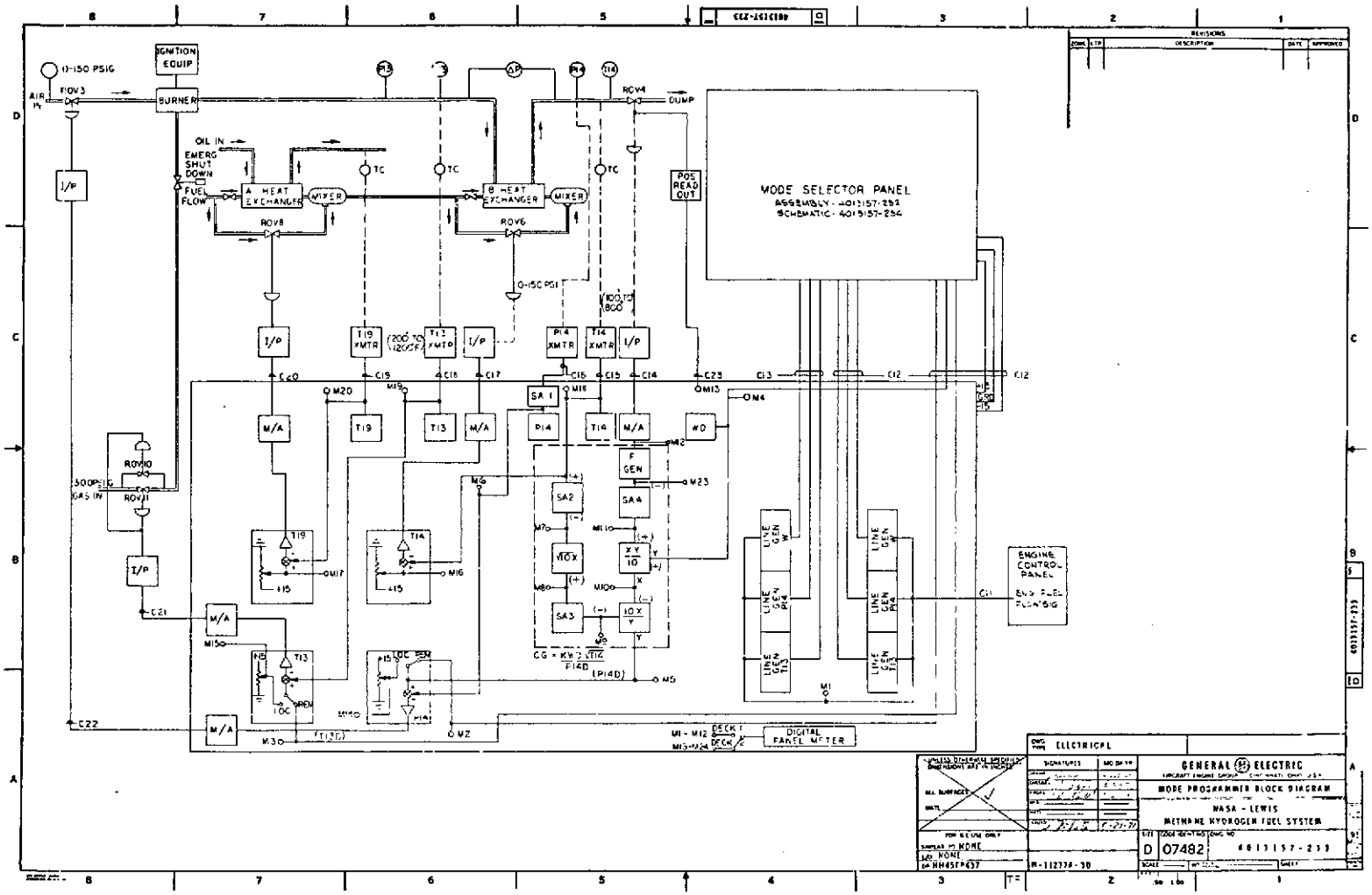
0-150 PSIG
IGNITION EQUIP
AIR IN
FIOV3
BURNER
OIL IN
EMERG SHUT DOWN
FUEL FLOW
A HEAT EXCHANGER
MIXER
B HEAT EXCHANGER
MIXER
ROV8
ROV6
ROV4
DUMP
POS READ OUT
MODE SELECTOR PANEL
ASSEMBLY - 4013157-253
SCHEMATIC - 4013157-254
0-150 PSI
100 TO 800
T19 XMTR
(200 TO 1200°F)
T13 XMTR
PI4 XMTR
T14 XMTR
I/P
M/A
SA 1
SA2
SA3
SA4
F GEN
WD
√10X
XY/10
10X
LINE GEN
ROV10
ROV11
300PSIG GAS IN
ENGINE CONTROL PANEL
END FUEL FLOW SIG
DIGITAL PANEL METER
DECK 1
DECK 2
ELECTRICAL
GENERAL ELECTRIC
MODE PROGRAMMER BLOCK DIAGRAM
NASA - LEWIS
METHANE HYDROGEN FUEL SYSTEM
D
07482
4013157-253

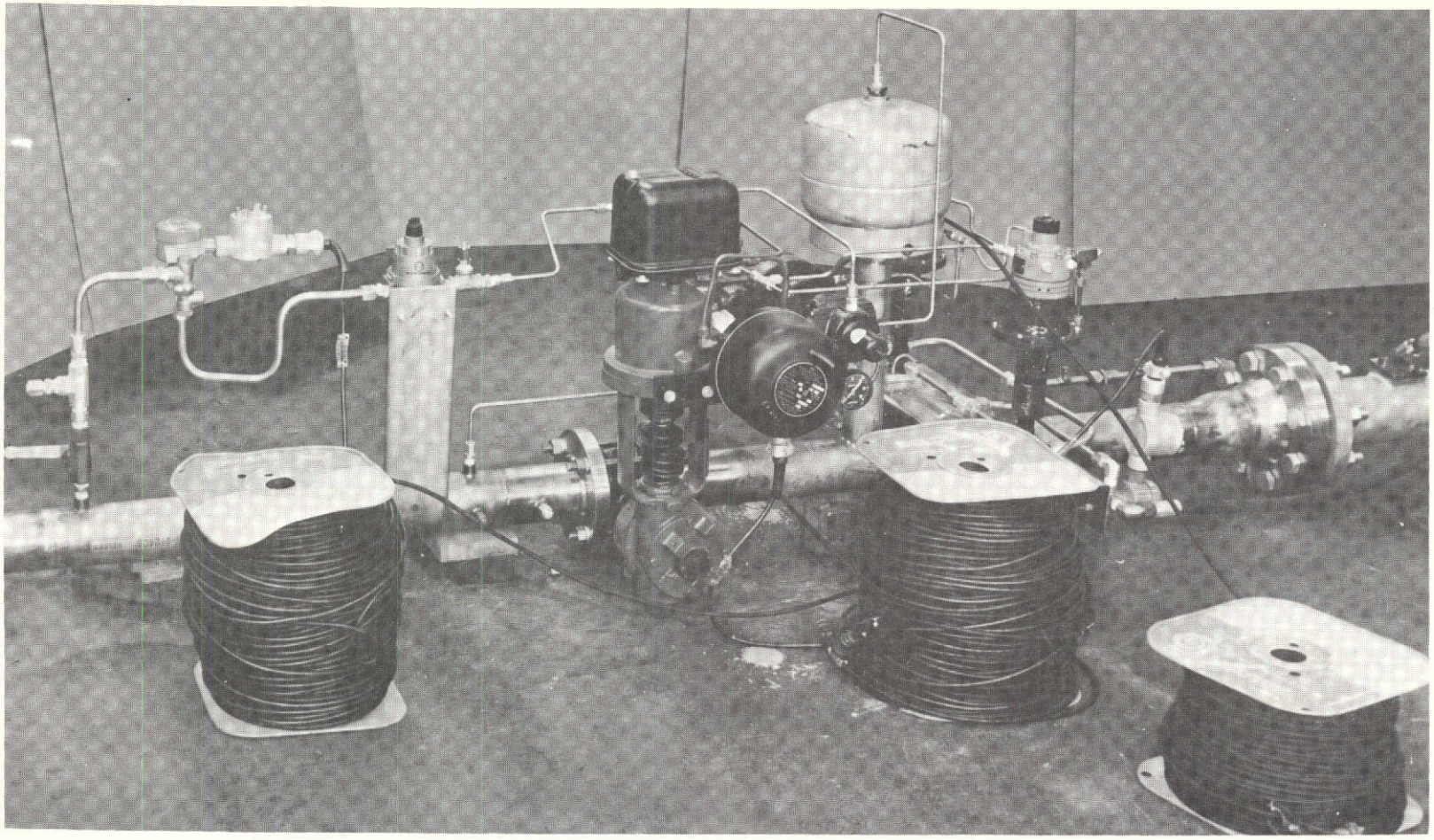

Figure 29. Air Heater and Control Equipment.

meter gaseous hydrogen to the burner injector from a pressure regulated bottle-gas source. The fuel valves are automatically modulated to regulate burner exit temperature or heat exchanger entrance temperature. Airflow of the system is set by modulation of the area of valve ROV-4 mounted in the fuel conditioning package at the heat exchanger air exhaust. A 28V DC ignition unit similar to engine equipment was provided for lighting the burner. The required temperature and pressure sensors for control loop feedback were also provided with the equipment.

Electrical Control Panel

Electrical control panels and circuits for computation and control of air system parameters were designed and fabricated from procured industrial electronic components. The panels provided accomplish the control and computation functions depicted schematically by drawing 4013157-233.

Heat exchanger A and B heater fluid discharge temperatures ($T_{19}$ and $T_{14}$) are controlled by means of fuel bypass valves ROV-8 and ROV-6 which are operated by means of set-point controllers with direct temperature feedback. The temperature demand is set manually from the controller set point. Air inlet temperature ($T_{13}$) to heat exchanger B is controlled by burner gas valves ROV-10 and ROV-11. These valves are operated by the $T_{13}$ controller with direct temperature feedback. The $T_{13}$ demand or set point is generated by the Mode Select circuit and is a function of engine fuel flow. An option is provided whereby "local" or "manual" set point operation can be used. Heat exchanger B discharge pressure is controlled by valve ROV-3 which is operated by the $P_{14}$ controller with direct pressure feedback. The $P_{14}$ demand is generated by the Mode Select circuit and is a function of fuel flow. An option is provided whereby "manual" set point operation can be used. Heat Exchanger B airflow is controlled in the following manner:

The minimum value of $P_{14}$ is about 30 psia ($2.07 \times 10^5$ N/m$^2$) and, therefore, critical flow conditions always exist through valve ROV-4. If the valve flow coefficient (Cg) is known, airflow can be calculated by the formula:

$$W_{14} = \frac{C_g P_{14}}{K \sqrt{T_{14}}} \tag{28}$$

Values of Cg versus percent stroke are published by the valve manufacturer accurate to within 1%. Therefore, a known value of Cg can be set by setting valve stroke. A required value of Cg is determined by analog computer solution of the following equation:

$$C_g = \frac{K W_d \sqrt{T_{14}}}{P_{14d}} \tag{29}$$

where:

$W_d$ is airflow demand (from Mode Select)

$P_{14d}$ is pressure demand (from Mode Select)

K is a constant

Substituting Equation (28) into Equation (29) yields:

$$W_{14} = W_d \times \frac{P_{14}}{P_{14d}} \tag{30}$$

As the $P_{14}$ controller acts to make $P_{14}$ equal to $P_{14d}$, actual airflow ($W_{14}$) will be equal to demand airflow ($W_d$). The actual value of Cg is derived from the demand value of Cg by means of a function generator which positions the valve so that the required value of Cg results.

The demand signals, $P_{13d}$, $P_{14d}$, and $W_d$ are adjustable linear functions of engine fuel flow. Two sets of three line generators are provided to furnish these functions. Each line generator has a zero and a slope adjustment associated with it, located in the Mode Selector circuit. The zero intercept and slope of a line between two moded points is determined by manual programming and mode selection so that the air parameter demand variables are varied in response to engine fuel flow automatically. Sequential switching from one set of schedules to another may be accomplished during engine test by setting engine fuel flow to a value corresponding to the intersection of two schedules dialed on the mode selection panel.

## OIL HEATER SUBSYSTEM

An oil heat supply source for heat input to Heat Exchanger A of the methane fuel system was designed and procured. The system consists of an electrically powered oil heating and recirculating cart coupled with associated flow controls and piping to interconnect with Heat Exchanger A in the fuel conditioning package. The heat source system is depicted schematically by drawing 4013156-300. The package utilizes SF8150 (dimethyl polysiloxane) oil as the heater fluid.

The basic oil heating and recirculating cart was procured as a vendor package to GE Specification W11277-2. A Youngstown-Miller model HT60-IERS cart was selected. The unit employs 60kw electrical power in strip-heater columns to heat recirculated oil pumped through a relief system. External flow to Heat Exchanger A is throttled by a manually set remote flow control valve, and return oil from Heat Exchanger A joins the recirculation return to the heater columns. The system provides oil flow up to 0.325 pps (0.147 Kg/sec) at temperatures ranging from 200 to 500° F (367 to 533° K) and pressures up to 100 psig ($6.39 \times 10^5$ N/m$^2$) at the entrance to Heat Exchanger A. Rupture discs were provided in the oil piping circuit to protect the heat exchanger shell from overpressure.

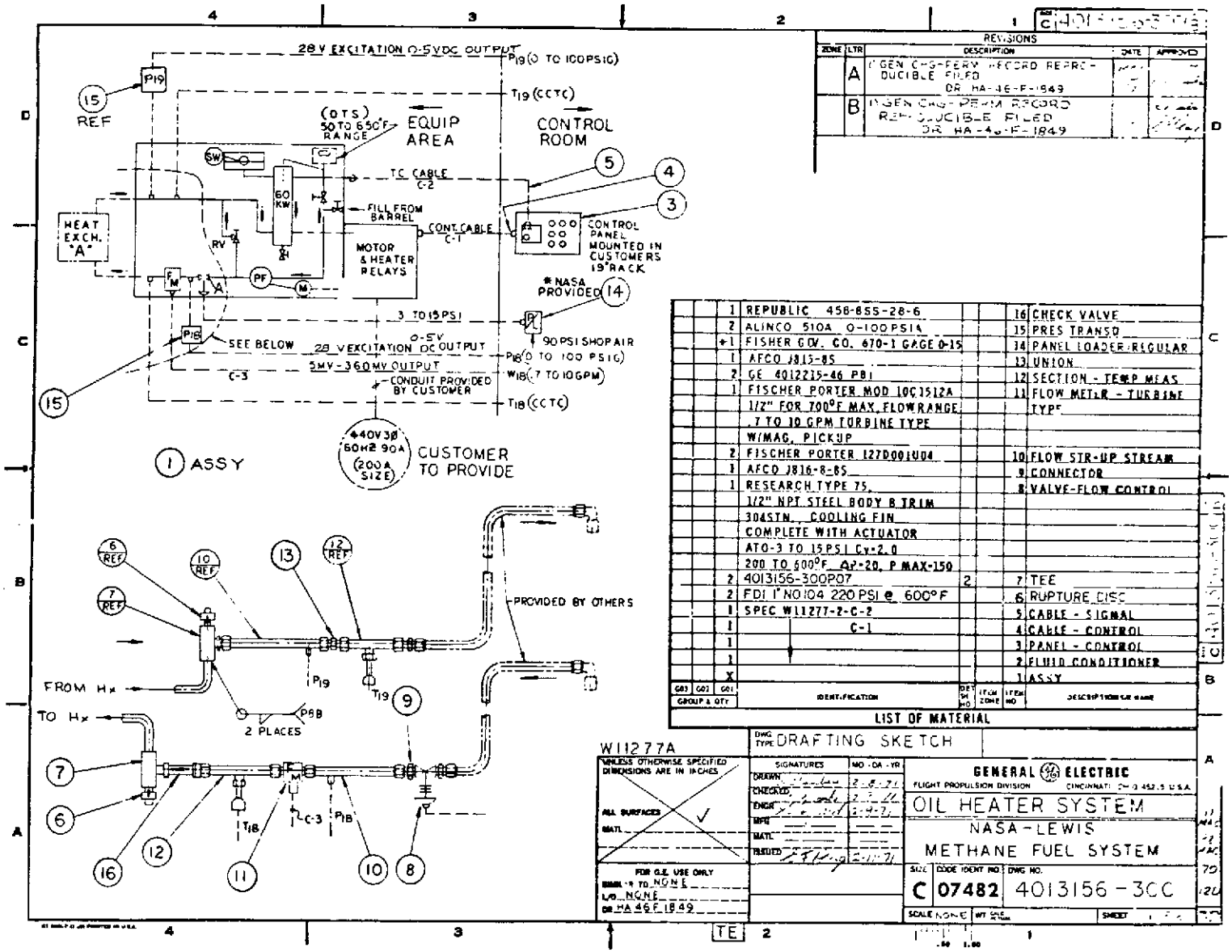


| ZONE | LTR | DESCRIPTION | DATE | APPROVED |
|---|---|---|---|---|
| | A | IGEN CHG-PERM RECORD REPRODUCIBLE FILED DR HA-46-F-1849 | | |
| | B | IGEN CHG-PERM RECORD REPRODUCIBLE FILED DR HA-46-F-1849 | | |

REVISIONS

| | | | | | | | |
|---|---|---|---|---|---|---|---|
| | | 1 | REPUBLIC 458-855-28-6 | | 16 | CHECK VALVE |
| | | 2 | ALINCO 510A 0-100PSIG | | 15 | PRES TRANSD |
| | | +1 | FISHER GOV. CO. 670-1 GAGE 0-15 | | 14 | PANEL LOADER-REGULAR |
| | | 1 | AFCO J815-8S | | 13 | UNION |
| | | 2 | GE 4012215-46 PB1 | | 12 | SECTION - TEMP MEAS |
| | | 1 | FISCHER PORTER MOD 10C3512A 1/2" FOR 700°F MAX. FLOW RANGE .7 TO 10 GPM TURBINE TYPE W/MAG. PICKUP | | 11 | FLOW METER - TURBINE TYPE |
| | | 2 | FISCHER PORTER 127D001U04 | | 10 | FLOW STR-UP STREAM |
| | | 1 | AFCO J816-8-8S | | 9 | CONNECTOR |
| | | 1 | RESEARCH TYPE 75, 1/2" NPT STEEL BODY B TRIM 304STN. COOLING FIN COMPLETE WITH ACTUATOR ATO-3 TO 15PSI Cv=2.0 200 TO 600°F ΔP=20, P MAX-150 | | 8 | VALVE-FLOW CONTROL |
| | | 2 | 4013156-300P07 | 2 | 7 | TEE |
| | | 2 | FDI 1" NO104 220 PSI @ 600°F | | 6 | RUPTURE DISC |
| | | 1 | SPEC W11277-2-C-2 | | 5 | CABLE - SIGNAL |
| | | 1 | C-1 | | 4 | CABLE - CONTROL |
| | | 1 | | | 3 | PANEL - CONTROL |
| | | 1 | | | 2 | FLUID CONDITIONER |
| | | X | | | 1 | ASSY |
| GO3 GROUP & QTY | GO1 GO2 | | IDENTIFICATION | PART OR IND NO | ITEM ZONE | ITEM NO | DESCRIPTION OR NAME |

LIST OF MATERIAL

W11277A

DWG TYPE DRAFTING SKETCH

UNLESS OTHERWISE SPECIFIED DIMENSIONS ARE IN INCHES

ALL SURFACES ✓

| SIGNATURES | MO - DA - YR |
|---|---|
| DRAWN | 2-16-71 |
| CHECKED | 2-16-71 |
| ENGR | 2-19-71 |
| MFR | |
| MATL | |
| RELEASED | 2-19-71 |

FOR G.E. USE ONLY
ENGR-Y TO NONE
L/O NONE
DR HA 46 F 1849

GENERAL ELECTRIC
FLIGHT PROPULSION DIVISION CINCINNATI OHIO 45215 U.S.A.

OIL HEATER SYSTEM
NASA-LEWIS
METHANE FUEL SYSTEM

| SIZE | CODE IDENT NO. | DWG NO. |
|---|---|---|
| C | 07482 | 4013156-3CC |

SCALE NONE WT SHEET

## SAFETY AND MODE CONTROL PANEL

An electrical safety and mode control panel was designed and constructed from procured piece parts to provide supervisory logic for overall system operation. The control panel is arranged schematically as shown by drawing 4013157-231. The control permits orderly selection of the system operating modes listed in Table I.

## J85 ENGINE MODIFICATIONS

A J85-13 engine, serial number 230-023, was obtained by NASA on bailment from US Air Force and made available to the contractor for use in engine test demonstrations of the hydrogen-methane fuel system. Reassembly and modification of the engine required to accommodate the planned system test was performed by the contractor.

Engine modifications were required in these areas: (1) fuel manifolds and injectors to accommodate gaseous fuel, (2) mounting of a NASA-furnished overspeed tachometer, (3) mounting of input equipment to operate the exhaust area control as a two-position area control, (4) modification of the JP-4 main fuel control system to allow normal operation of the engine compressor variable geometry.

### Engine Fuel Injectors and Manifold

The fuel injectors for the methane configuration of the engine were furnished by NASA. Figure 30 illustrates the injector provided and the manner of providing retention safety for the screw-on nozzle tips. This injector configuration had been selected by NASA based upon comparative combustion test rig results conducted under Phase IV of the contract.

The fuel injector selected for the hydrogen configuration utilized a nozzle tip design which had previously been used successfully by the contractor to operate a J85-5 engine on gaseous hydrogen. Spare injector tubes provided by NASA for the Phase IV combustor tests of candidate methane injectors were modified to install the hydrogen nozzle tips. Figure 31 illustrates the modification performed to construct the hydrogen injectors.

The gaseous fuel manifold selected for the engine was a production fuel manifold designed for the LM350 industrial engine which has a J85 core. An evaluation of the flow distribution effects of the manifold was conducted prior to assembly by observing water flow spouting head distribution. From these observations, flow balancing orifices consisting of drilled Voi-Shan inserts located at the manifold B-nut flare connection to the pigtails were selected.

### NASA Overspeed Tachometer

NASA provided a tachometer package which had been used at NASA-Lewis for J85 engine test operation. The tachometer assembly was made to NASA drawing

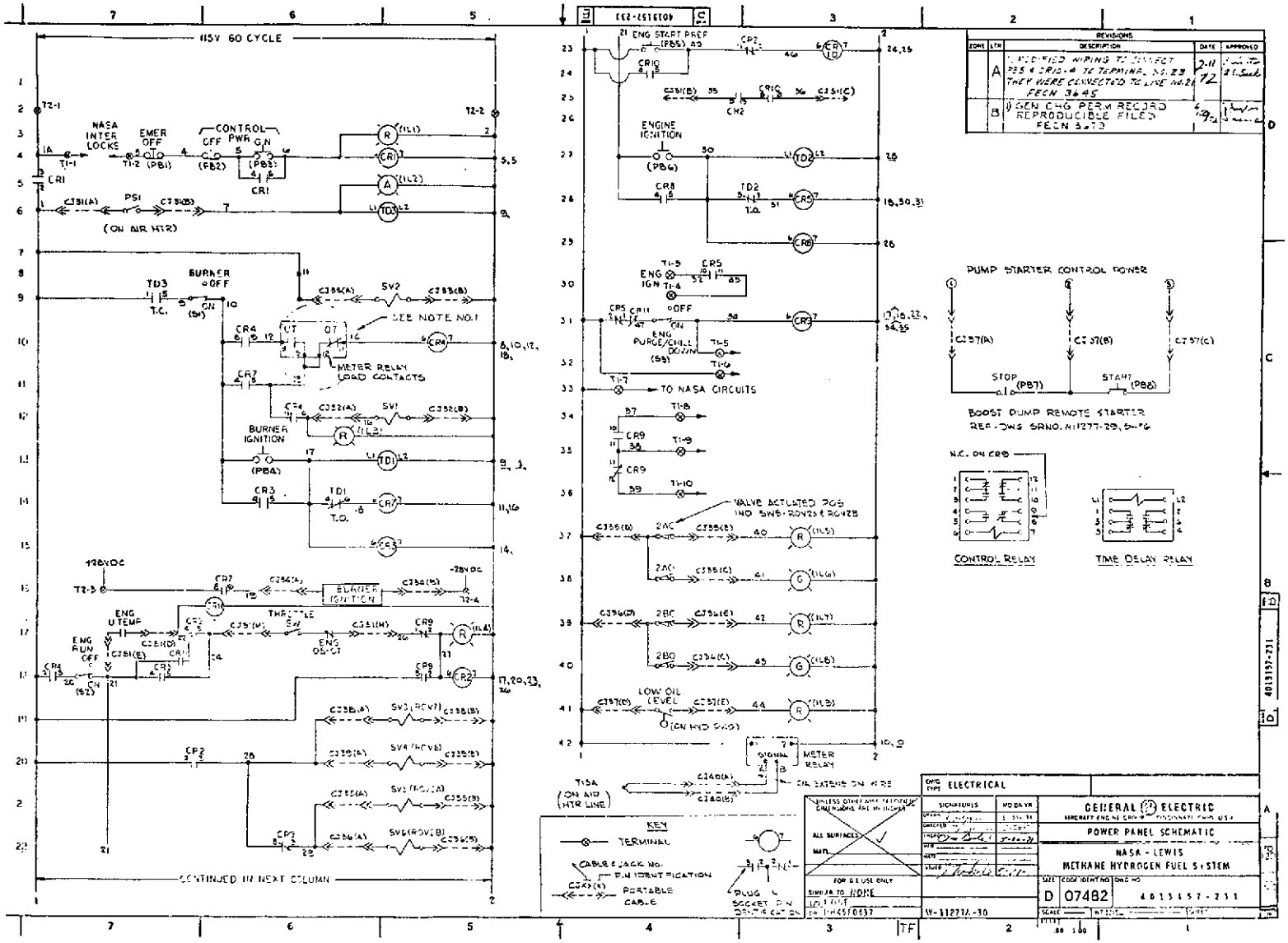
115V 60 CYCLE
NASA INTER LOCKS
EMER OFF
CONTROL
OFF PWR ON
ENGINE IGNITION
ENG START PREF
PUMP STARTER CONTROL PANEL
STOP (PB7)
START (PB6)
BOOST PUMP REMOTE STARTER
REF DWG SRNO. N11277-29, SH 6
N.C. ON CR9
CONTROL RELAY
TIME DELAY RELAY
BURNER IGNITION
BURNER OFF
SEE NOTE NO.1
METER RELAY LOAD CONTACTS
TO NASA CIRCUITS
VALVE ACTUATED POS IND SWS-ROV2S & ROV2B
LOW OIL LEVEL
(ON HYD SWG)
METER RELAY
CONTINUED IN NEXT COLUMN
KEY
TERMINAL
PORTABLE CABLE
PLUG & SOCKET P/N
REVISIONS
DESCRIPTION
DATE
APPROVED
GENERAL ELECTRIC
POWER PANEL SCHEMATIC
NASA - LEWIS
METHANE HYDROGEN FUEL SYSTEM
ELECTRICAL
D 07482
4013157-231
W-11277A-30

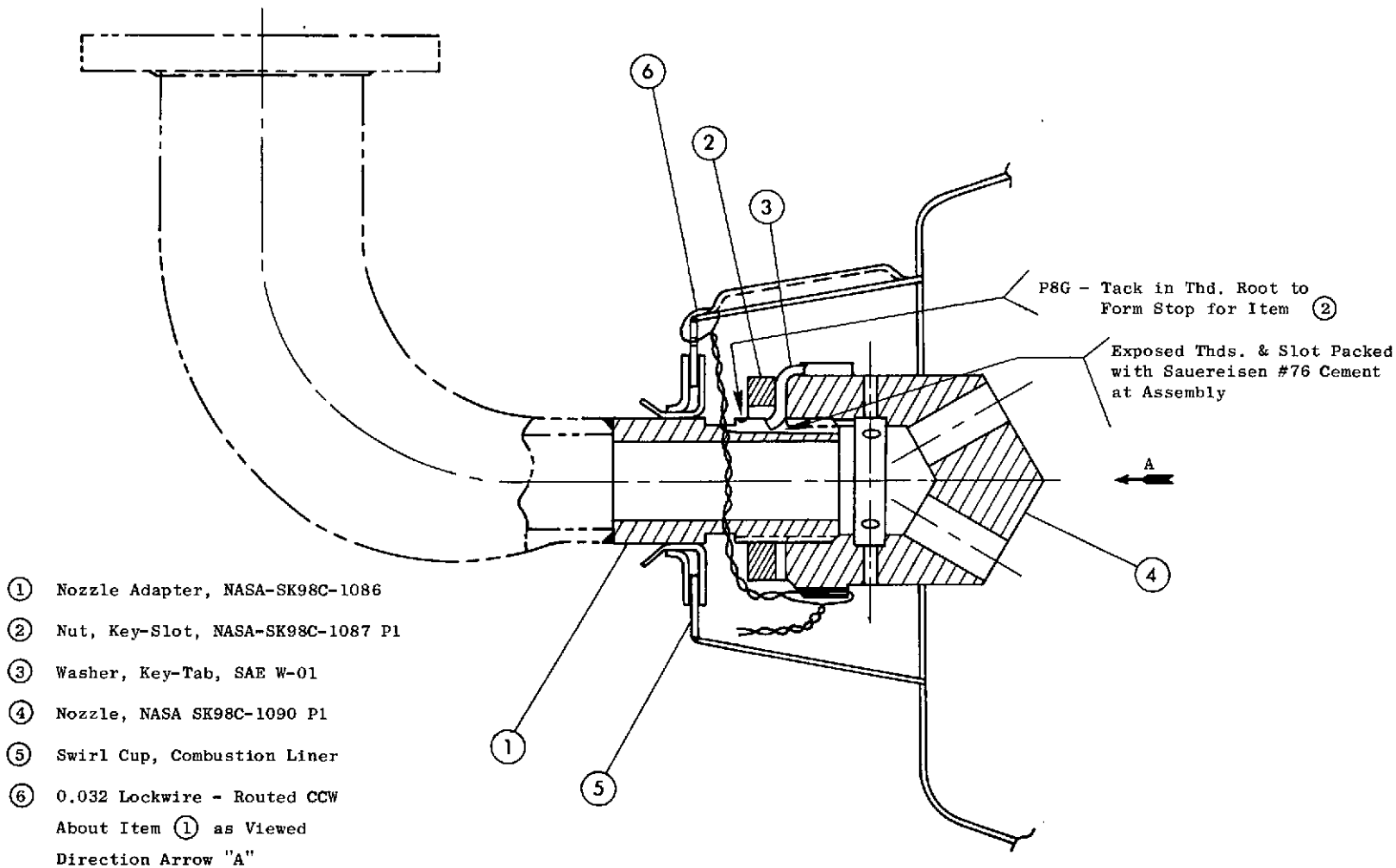


Figure 30. Methane Fuel Injector.

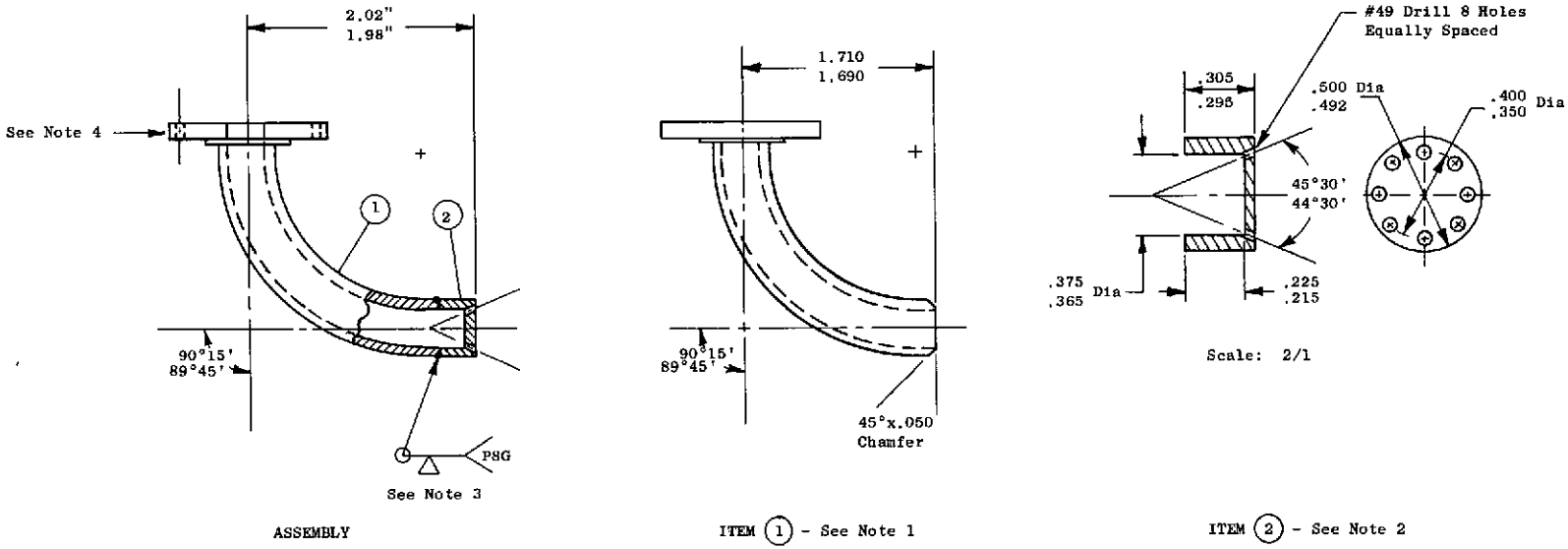


NOTES:

1. Make Item (1) from Existing Injectors Provided - Material 321 SS
2. Item (2) Material 321 SS
3. P8G Filler AMS 5680, Grind Weld OD to $\begin{matrix}.500\\.492\end{matrix}$ Dia
4. Electro-Etch Dwg No. on Edge of Pad

Figure 31. Hydrogen Fuel Injector.

CF641391 and consisted of a shaft-driven gear exciting an electromagnetic speed pickup. This tachometer package was mounted on the J85 gearbox PTO pad, and the signal was used for overspeed protection in the engine electrical control system.

Slave Exhaust Area Control

It was originally planned that an electrohydraulic slave exhaust area control for the engine would be provided at NASA-Lewis, and appropriate logic and exhaust temperature control circuits to interface with the NASA control were provided in the Engine Electrical Control. When the contract was modified to include J85 engine running at the Contractor's facility rather than at NASA-Lewis, an alternate means of effecting exhaust area control was needed.

It was decided that the standard J85-13 mechanical exhaust control servo and actuation would be employed to effect exhaust area variation. A means of interfacing with the mechanical servo input link to establish nozzle position commands was provided by mounting a 28V DC electromechanical gear motor, with appropriate brackets, supported on the afterburner fuel pump pad of the J85 gearbox. A relay logic circuit was constructed to control 28V power to the gearmotor as shown by Figure 32. Engine speed and power lever intelligence available in the Engine Electrical Control were used to establish two-position exhaust area logic as shown in the diagram. Slew rate of the exhaust area servo was adjusted by variation of the DC voltage supply level to the gearmotor. End point exhaust areas for the two-position mode of control were established by adjustment of the motor limit switches and by mechanical rigging of the screwjack output of the mechanical servo. A slew time of 2 - 4 seconds from idle exhaust area to military exhaust area was intended for the system.

Compressor Variable Geometry Control

Compressor inlet guide vane and 8th stage bleed valve actuation for the J85-13 are normally controlled by the standard main fuel control as a function of compressor corrected speed. For this purpose, the standard JP-4 main fuel supply and control were retained on the engine with the JP-4 operated in a recirculated mode. Figure 33 illustrates the repiping of the JP-4 main fuel system used to maintain normal operation of the compressor variable geometry. The augmentor fuel supply and controls were removed from the engine as was the hydromechanical overspeed governor.

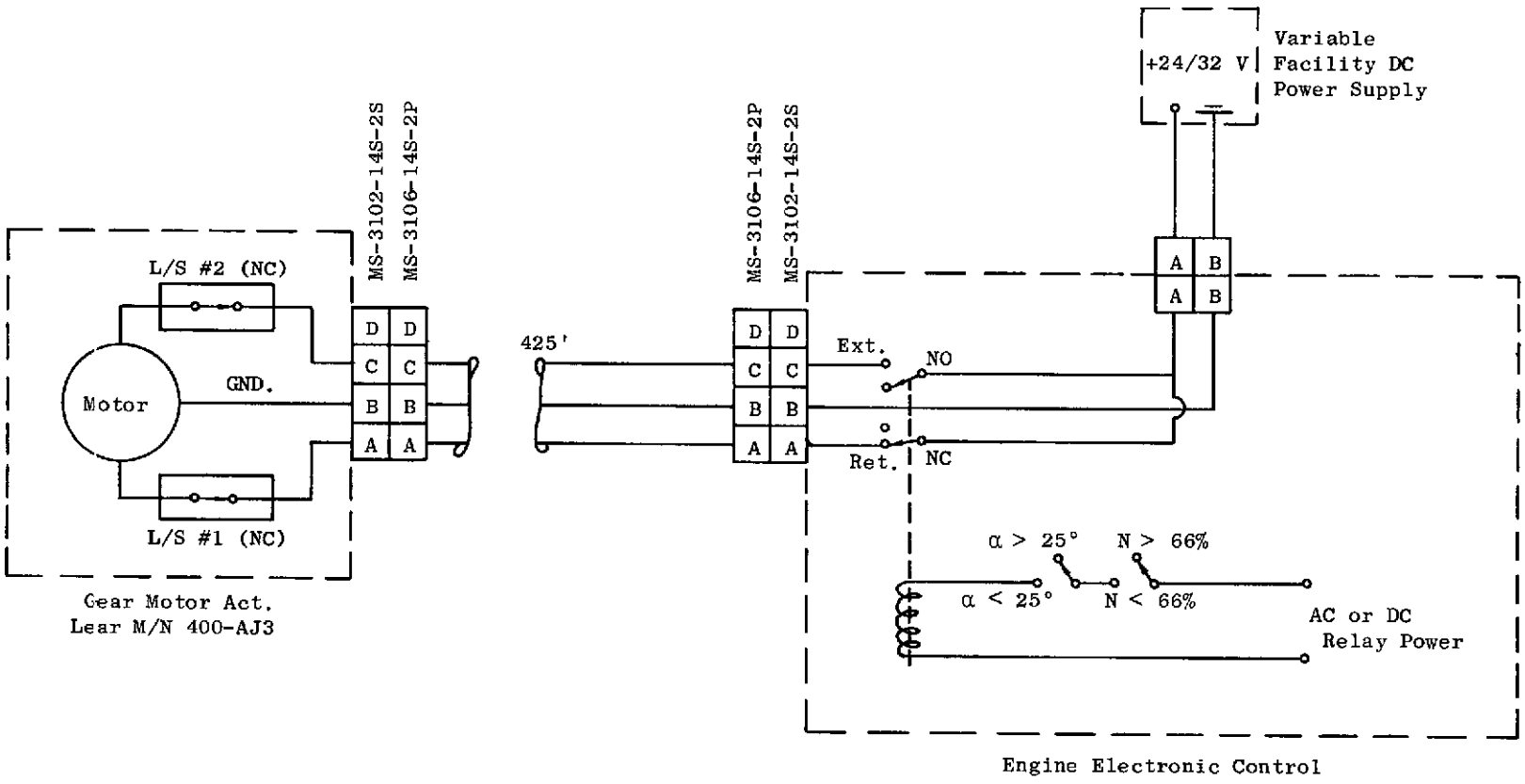


L/S #2 Limits Extend Motion (Open Ag)

L/S #1 Limits Retract Motion (Close Ag)

Figure 32. Wiring Schematic, Exhaust Nozzle Control Logic.

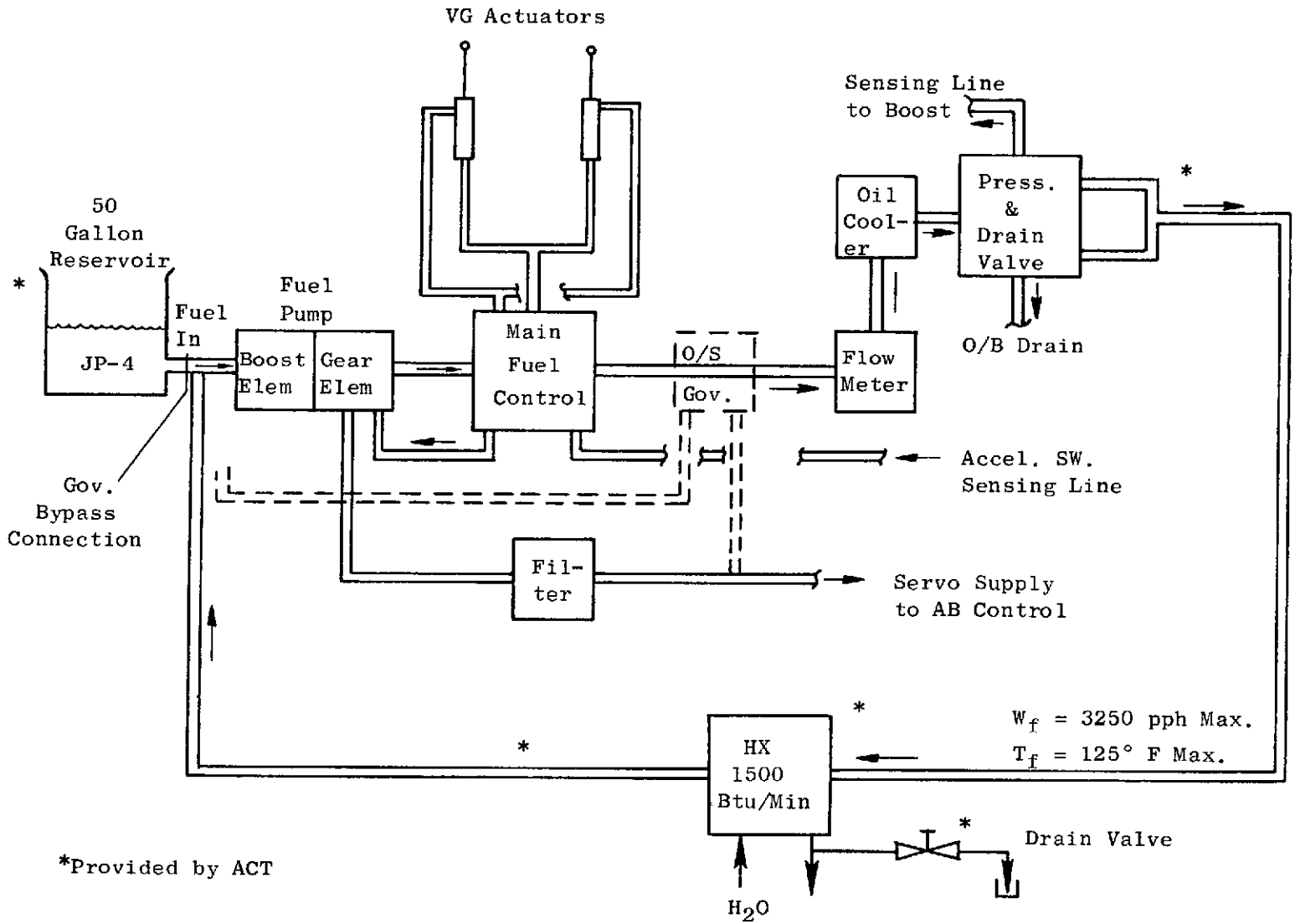


Figure 33. JP-4 Fuel System for Variable Geometry.

## TESTING AND RESULTS

### FUEL PUMP COMPONENT TEST

As part of the procurement program for design and delivery of the Cosmodyne Variflow Fuel Pump, component performance tests were conducted by the vendor. Liquid nitrogen was used as the cryogenic fluid for testing delivery performance in both the methane and hydrogen stroke configurations. The hydraulic motor section was operated on MIL-H-5606 oil per design intent from a high pressure hydraulic supply cart. All pump performance conducted by the vendor was done with the system subcooler operational.

During initial calibration attempts of the Variflow pump, seizure of the hydraulic timing valve occurred on several occasions. Following one such seizure, a fracture of the nutating plate occurred. A redesign of the hydraulic motor feedback drive train and hydraulic sequence valve was undertaken to improve the capability of the feedback mechanism to withstand maximum cyclic loads imposed by piston pressure imbalance. The feedback design shown in Drawing 2311401 resulted.

Subsequent checkout testing of the redesigned pump was satisfactory and no further failures occurred. The cryogenic performance calibration shown in Figure 34 was obtained for the methane stroke configuration, and the hydraulic calibration is shown in Figure 35.

For the hydrogen stroke configuration, the delivery performance shown in Figure 36 was obtained with the corresponding hydraulic calibration shown in Figure 37. As a result of these tests, the performance ratings of the two configurations were established as follows:

100% $LCH_4$ - 12.0 gpm ($7.56 \times 10^{-4}$ $M^3$/sec) delivery at 1430 rpm (150 rad/sec) and 900 psid ($6.21 \times 10^6$ $N/M^2$) head rise.

100% $LH_2$ - 27.0 gpm ($17 \times 10^{-4}$ $M^3$/sec) delivery at 1600 rpm (167.5 rad/sec) and 400 psid ($2.76 \times 10^6$ $N/M^2$)

Following the calibration performance tests, an additional 10 hours of endurance running was performed in the methane stroke configuration at various speeds and pressure rises to gain some assurance of an acceptable redesign in the hydraulic motor section.

Selection of the Variflow piston pumping element resulted from earlier unsuccessful attempts to demonstrate $LH_2$ pumping with a close-clearance vane pump design provided by Pesco. Recirculation leakages to inlet of the vane element limited $LH_2$ head rise to 260 psid ($1.79 \times 10^6$ $N/M^2$), and the volumetric efficiency obtained was inadequate for a 20/1 variable speed turndown.

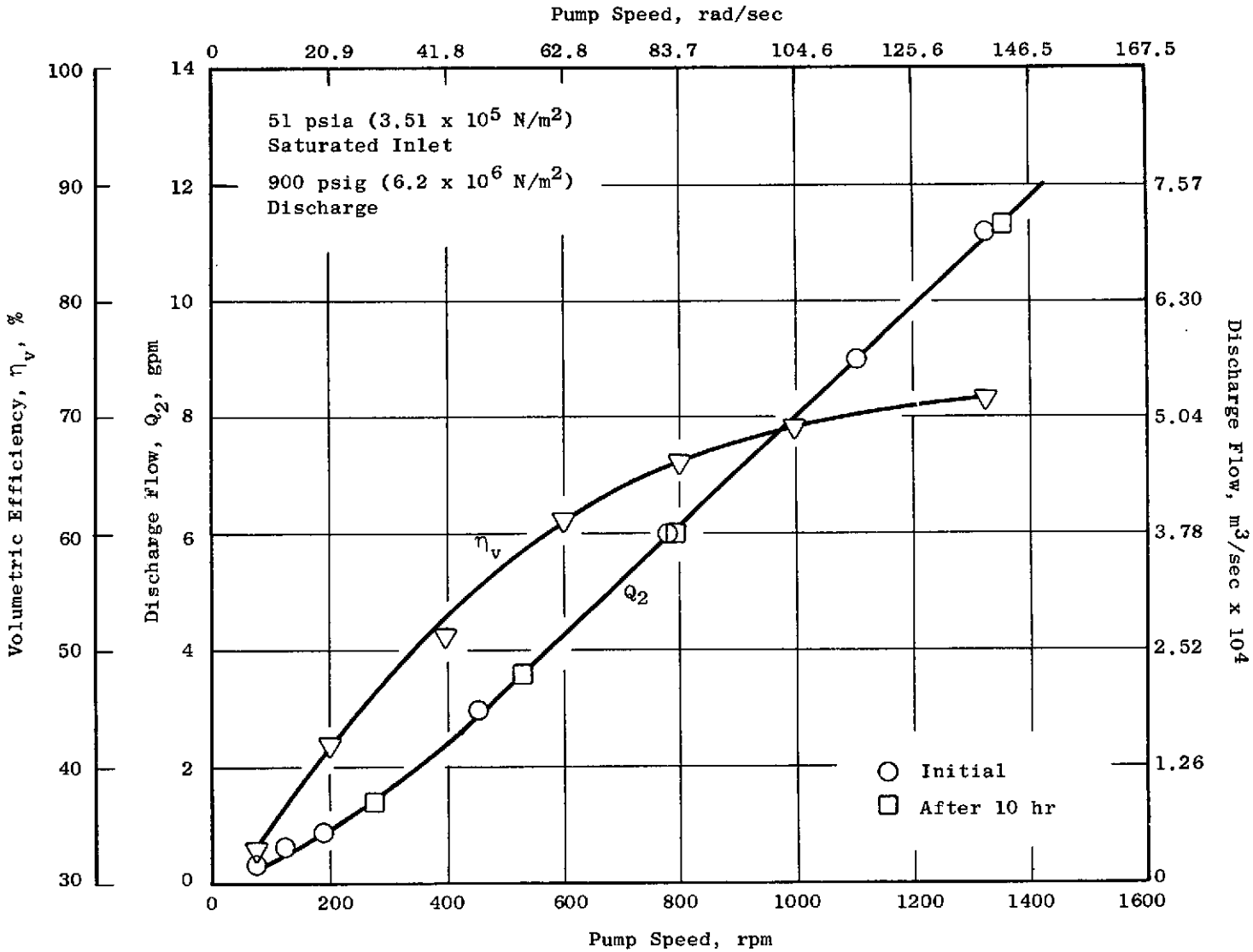


Figure 34. Cosmodyne Methane Fuel Pump Cryogenic Performance Calibration with Liquid Nitrogen.

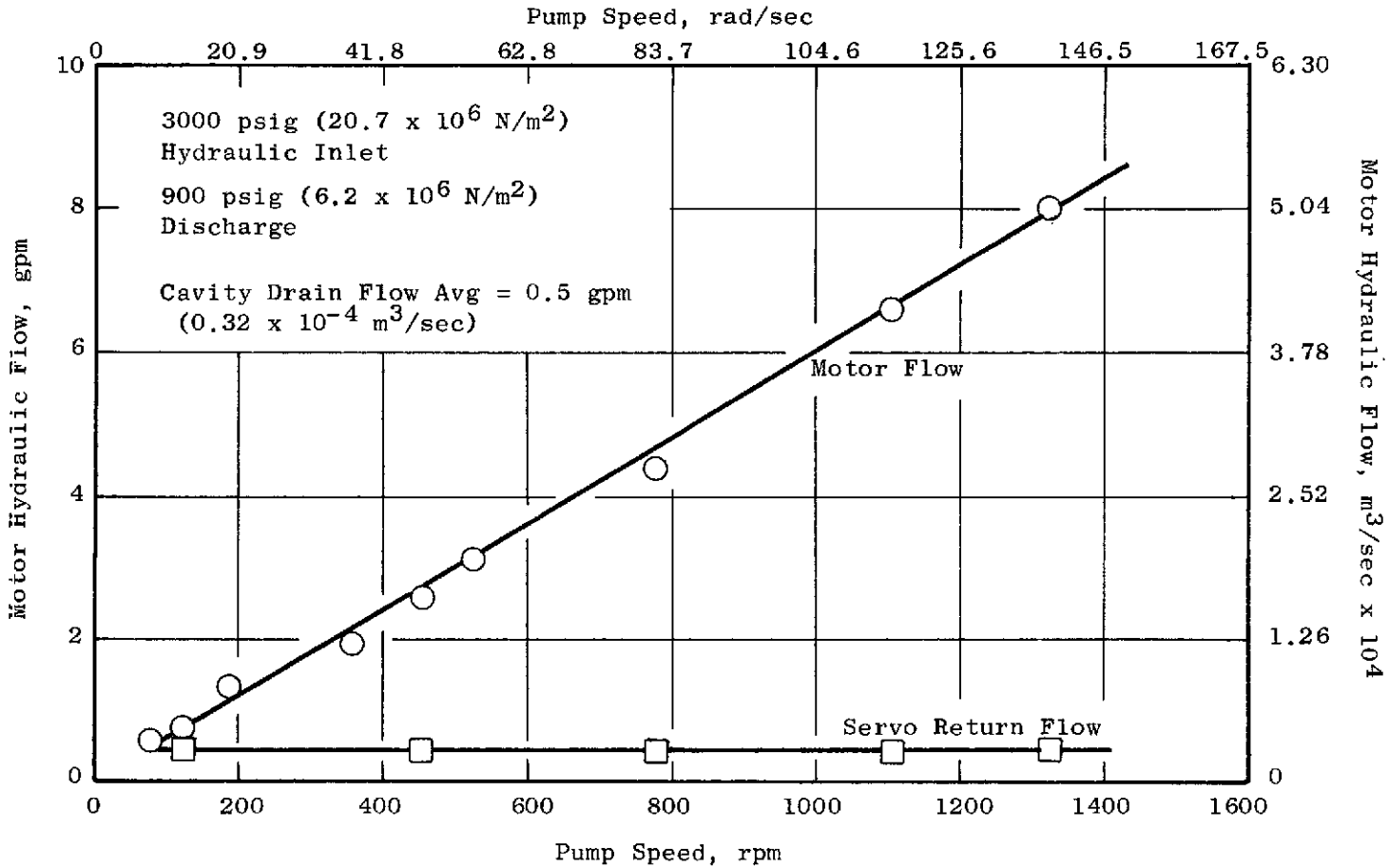


Figure 35. Cosmodyne Methane Fuel Pump Hydraulic Performane Calibration wih Liquid Nitrogen.

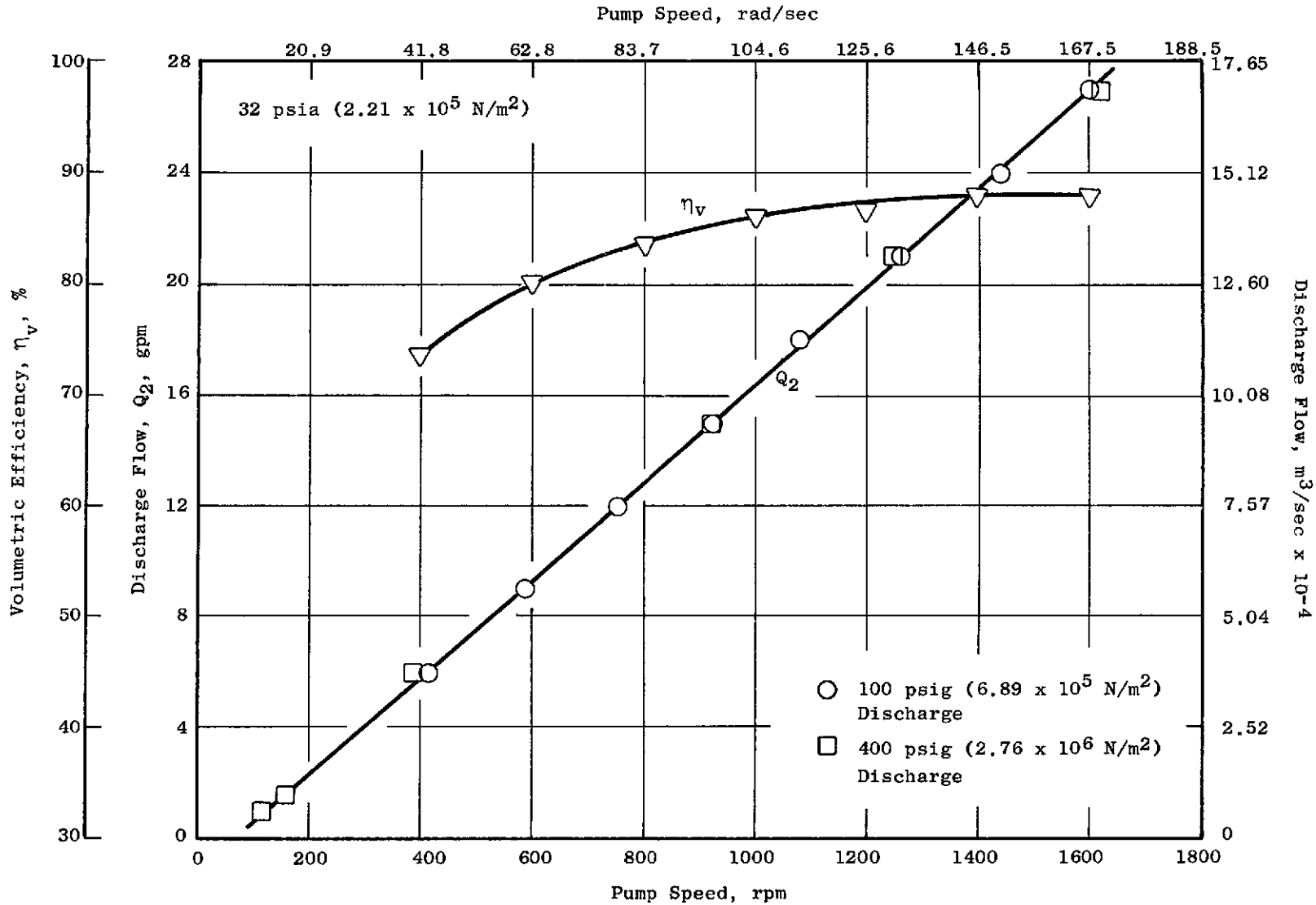


Figure 36. Cosmodyne Hydrogen Fuel Pump Cryogenic Performance Calibration with Liquid Nitrogen.

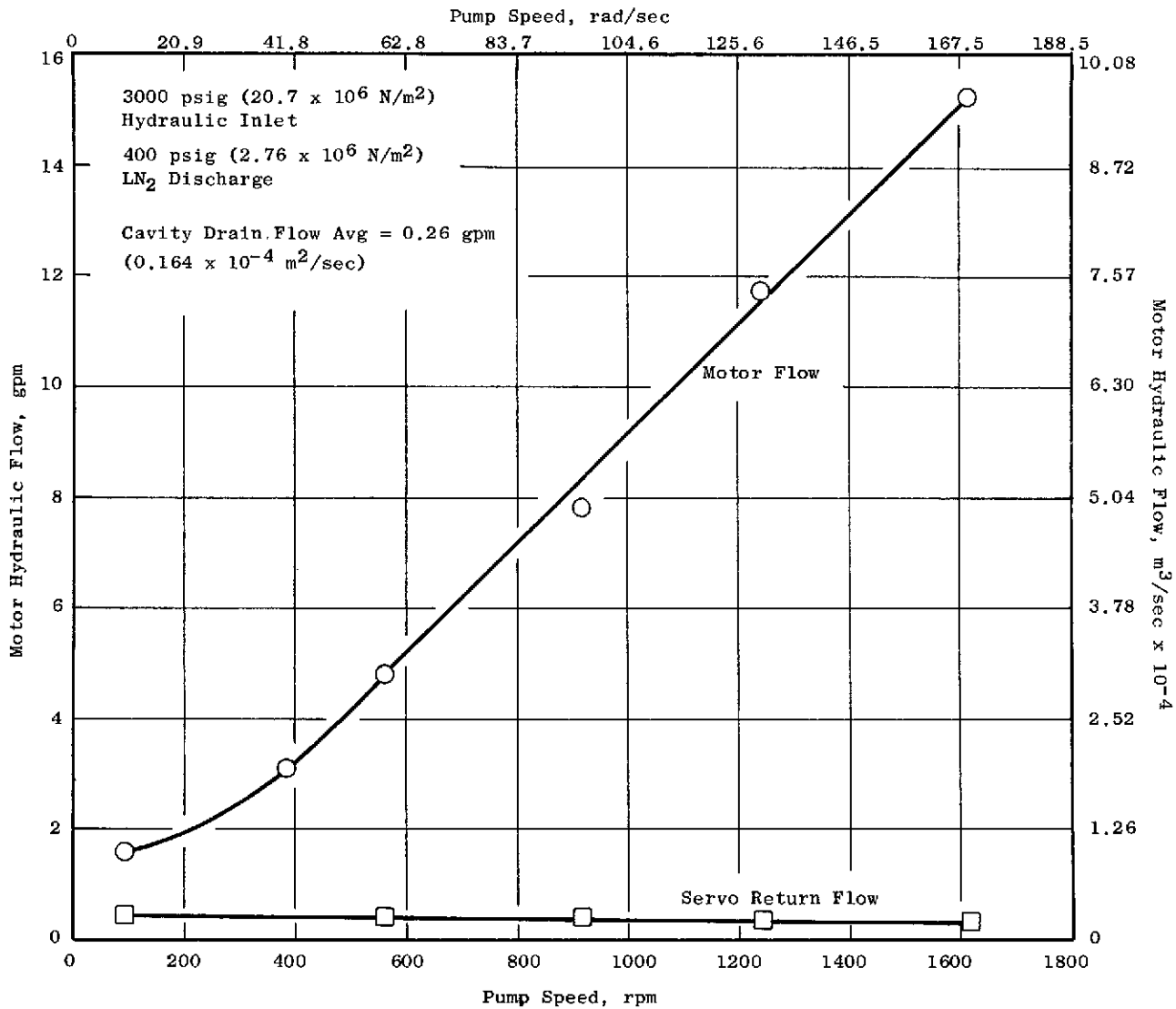


Figure 37. Cosmodyne Hydrogen Fuel Pump Hydraulic Performance Calibration with Liquid Nitrogen.

## METHANE INJECTOR COMBUSTION TESTS

Phase IV of the contract program was established to provide combustor rig testing of several candidate methane fuel injectors provided by NASA. Six candidate configurations were subjected to ignition tests in a J85 combustor. The configuration selected by NASA for use in engine build displayed superior ignition characteristics in terms of heat rise available at light-off conditions and combustion efficiency. Performance mapping of the injector which showed superior ignition characteristics was completed at simulated ground idle, takeoff, cruise, and flight idle descent conditions. Performance of this injector appeared suitable for engine use with methane or natural gas fuel. Data from this test phase were forwarded to NASA in accordance with the contract amendment.

## FUEL METERING AIRFLOW TESTS

Component checkout tests of the fuel metering and pressure regulating valves in conjunction with the associated control circuits of the Engine Electrical Control were performed after fabrication and assembly of these devices. Shop air was supplied to the valves as the flowing medium, while hydraulic servos were supplied from a facility hydraulic source. Stable and responsive control of the valves was established, and calibration of the metering valve electrical position readout was made in comparison to a dial indicator reading of valve positions. Airflow measurements through the valves were made with a calibration orifice at various metering valve area settings. Metering valve area calculated from measured airflow was compared to theoretical valve area as a function of valve position as shown in Figure 38. The theoretical and measured areas were in agreement at all stroke settings within $\pm 3\%$, which is within the airflow measurement accuracy.

## SYSTEM AND ENGINE TESTS

The approach to testing of the system and J85 engine using cryogenic fuels was to assemble all system equipment including the engine into a single test setup which permitted the choice of operating the fuel system alone using a vent stack discharge or of operating the entire system including the engine. All component, system, and engine checkout and problem solving using these fuels was thus accomplished in a single test assembly for each fuel.

### Test Installation

The test system was installed on an outdoor test pad. Electrical control panels used in the system were rack-mounted in the control room of the test cell and electrical cable connections were run for approximately 425 ft. (129.6 M) to electrical interface devices located on the outdoor pad. A schematic of the major test equipment interconnections and services supplied for the methane system configuration is shown in Figure 39. The comparable schematic for the hydrogen system configuration is shown in Figure 40. NASA provided the transport trailers used for fuel storage for both fuels. A photographic view of the engine and test equipment installation for the methane system configuration is shown in Figure 41.

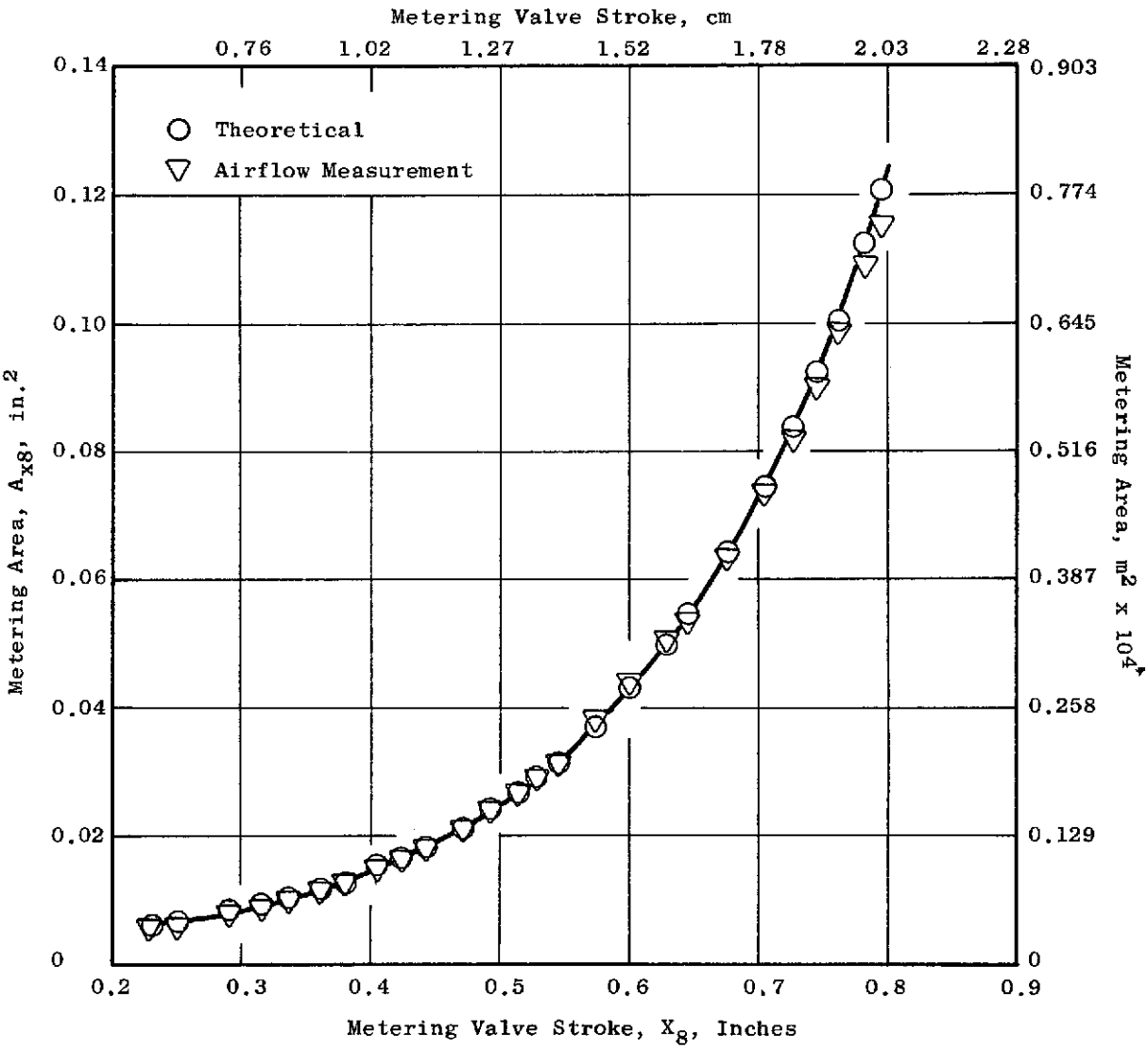


Figure 38. Fuel Metering Aiflow Calibration Test Results.

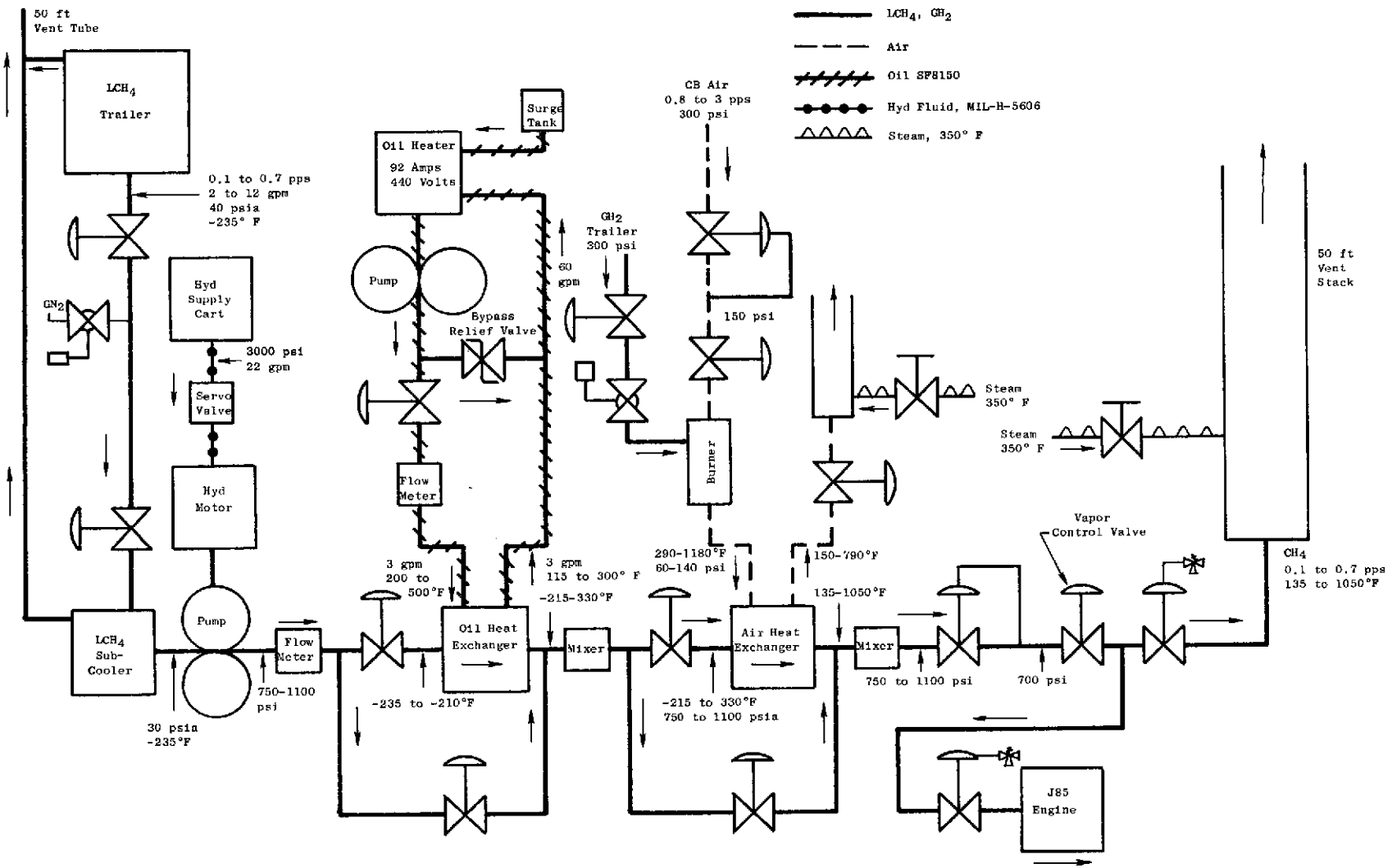


Figure 39. Schematic Diagram of Methane Fuel System.

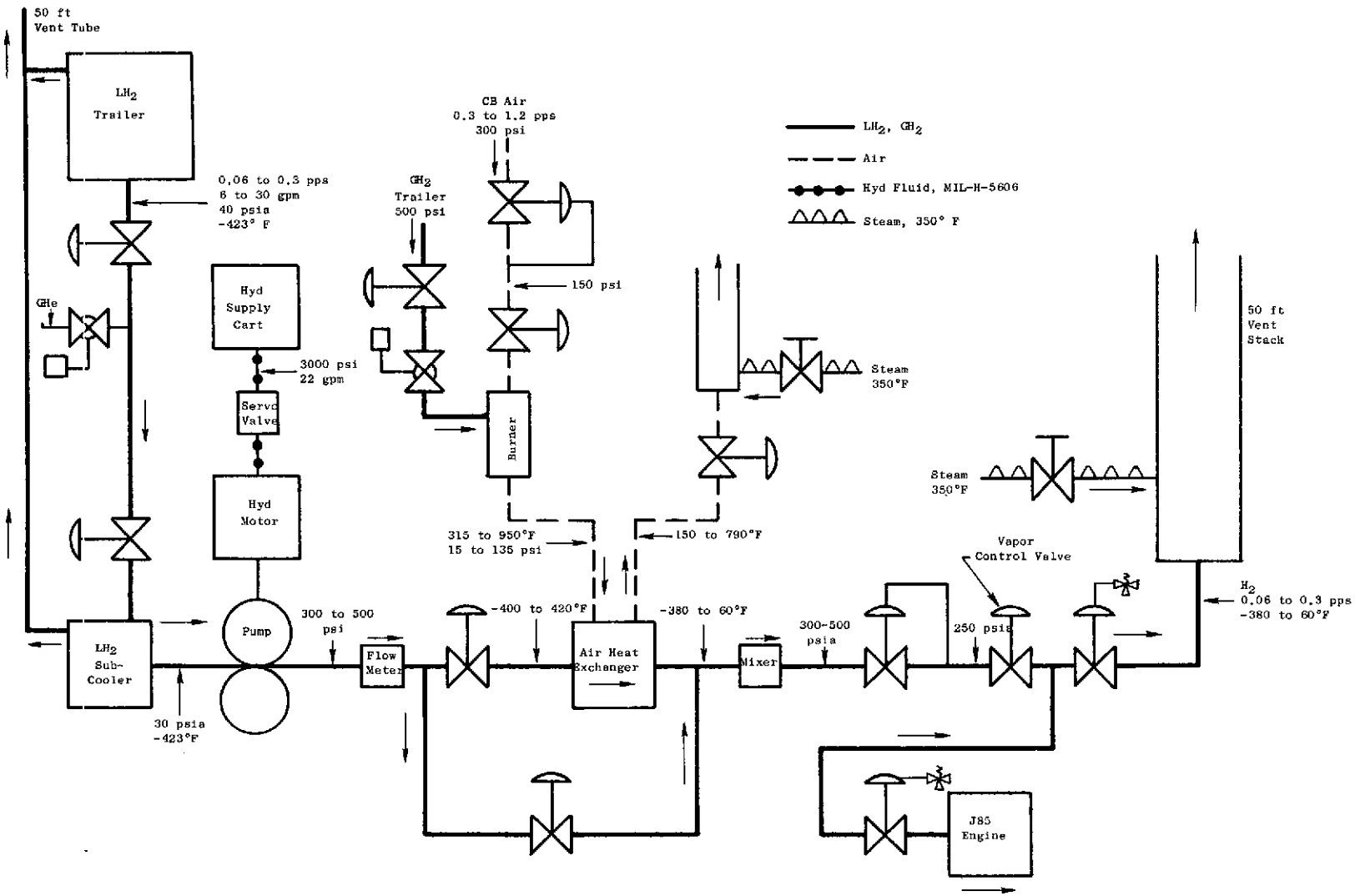


Figure 40. Schematic Diagram of Hydrogen Fuel System.

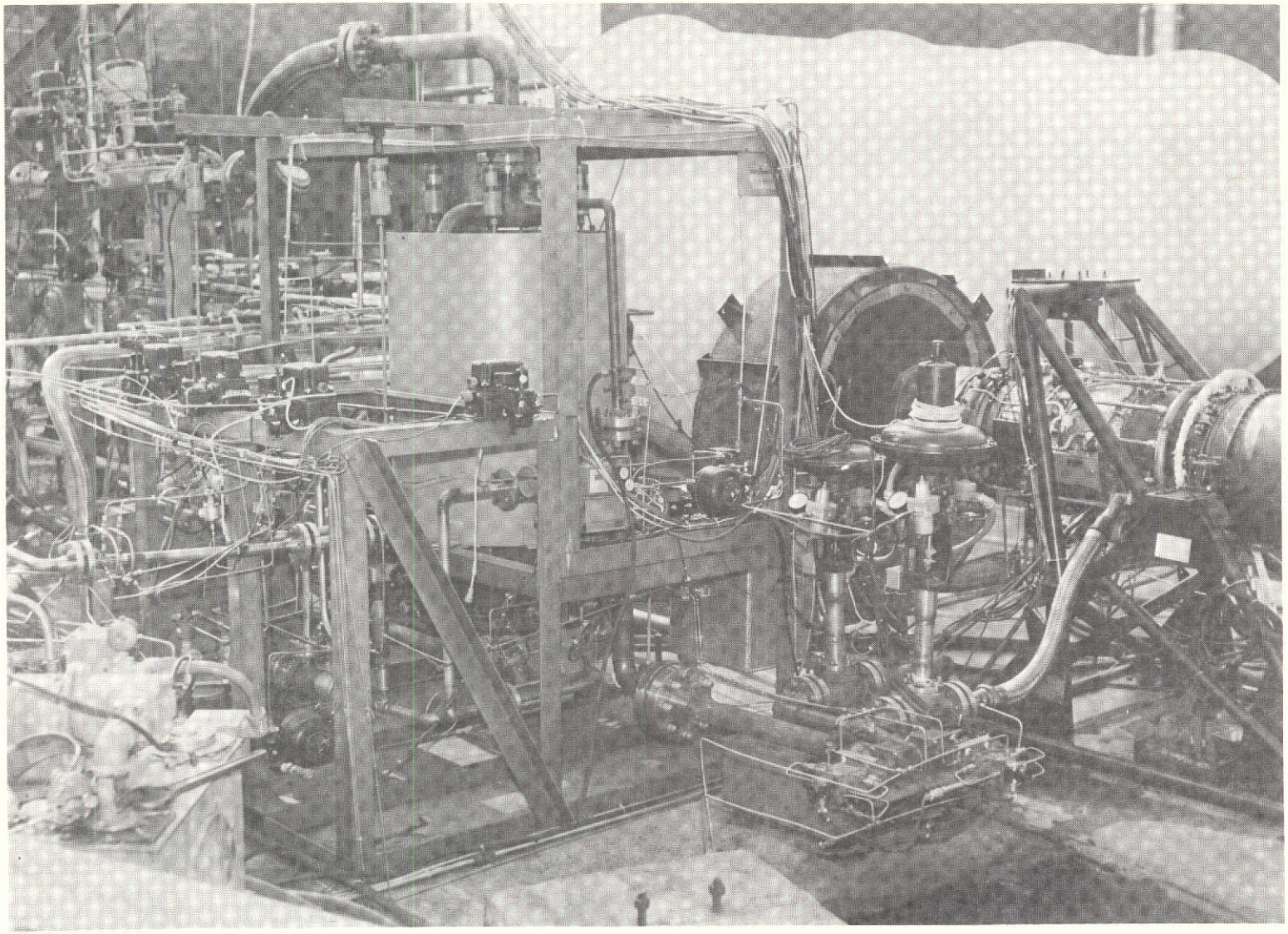

Figure 41. Engine and Test Equipment Installation for Methane Fuel System.

The contract was amended during the program to provide for sampling and measurement of J85 engine exhaust gas emission constituents. Sampling rakes were installed on the engine at the turbine discharge, and the gas sampling and measurement equipment shown in Figure 42 was installed for the methane system configuration. For the hydrogen system configuration, the gas sampling and analysis setup shown in Figure 43 was installed for measurement of $NO_x$ concentrations.

## Instrumentation

Instrumentation required for customer data recording was provided as listed in Table XIV for the methane system and as listed in Table XV for the hydrogen system. In addition, steady-state panel displays of the Engine Electrical Control and Air Mode Programmer panels were monitored, as was basic engine safety instrumentation. Transient data were recorded on Sanborn chart recorders as coded in Tables XIV and XV.

## Test Procedure

System check-out and testing were planned in six procedural increments which progressed from trial check-out of controls and facility equipment through engine and system acceptance demonstrations on both fuels. The methane configuration of the system was assembled first, followed by conversion to the hydrogen configuration. Detailed charts of test steps and control settings were prepared for each procedural phase. The sequence of test procedural phases was as follows:

- Air Heater Hot Check-out
- No Fuel Check-out
- LNG Flow and Thermal Calibration
- LNG System Transient and Steady-State Acceptance (Engine Run)
- $LH_2$ Flow and Thermal Calibration
- $LH_2$ System Transient and Steady-State Acceptance (Engine Run)

Modifications to the engine test procedures were planned at appropriate points to insert steady-state engine speed settings for exhaust emissions data. Emissions data were planned for 50, 75, 85, 95, and 100% engine speed settings.

## TEST RESULTS

System tests were performed generally in the chronological order planned for the detailed test procedure steps. Some of the procedure phases were repeated at various times because of problems encountered with the system or components.

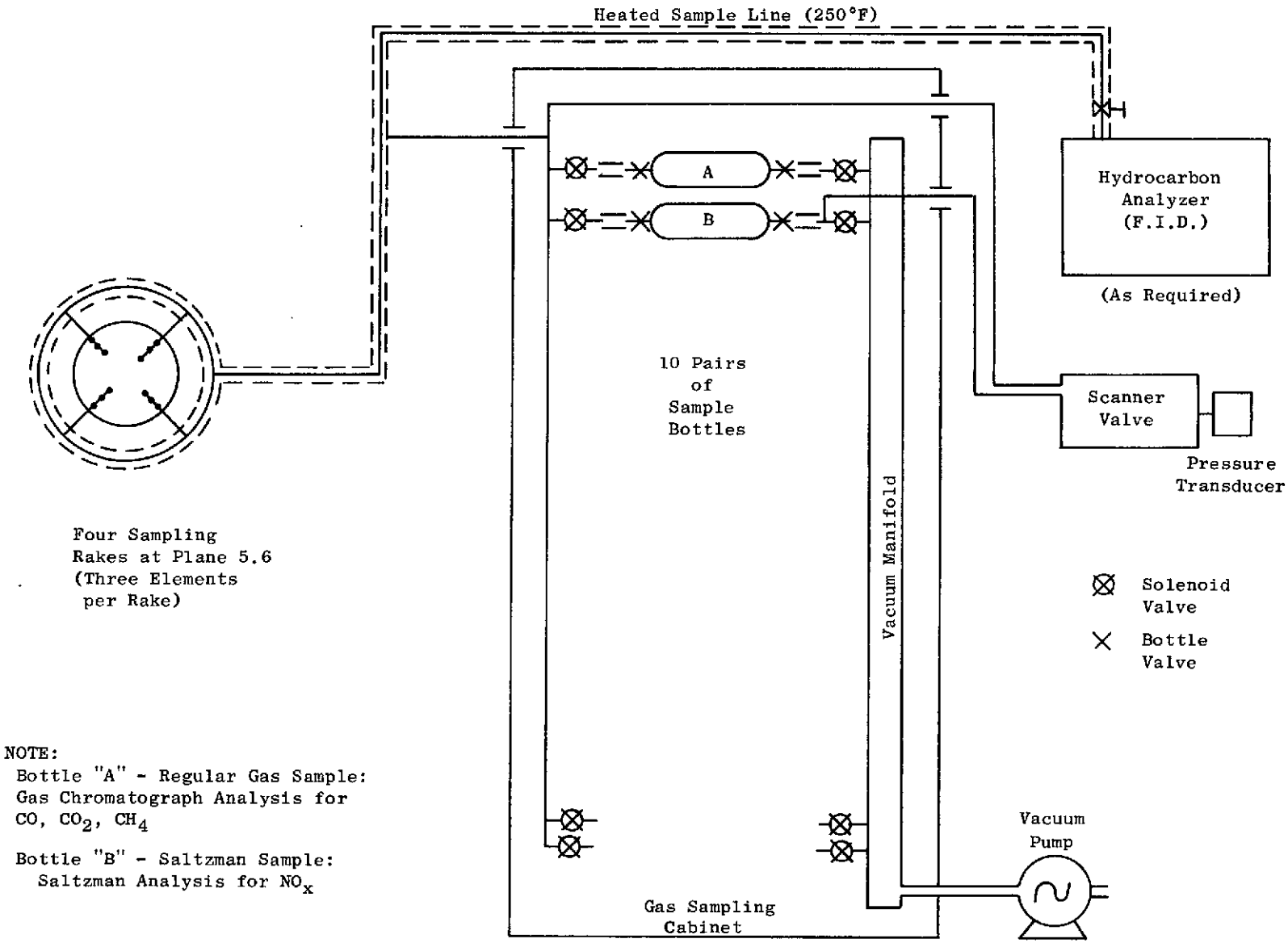


Figure 42. Schematic Diagram of Methane Fueled J85 Engine Exhaust Gas Sampling System.

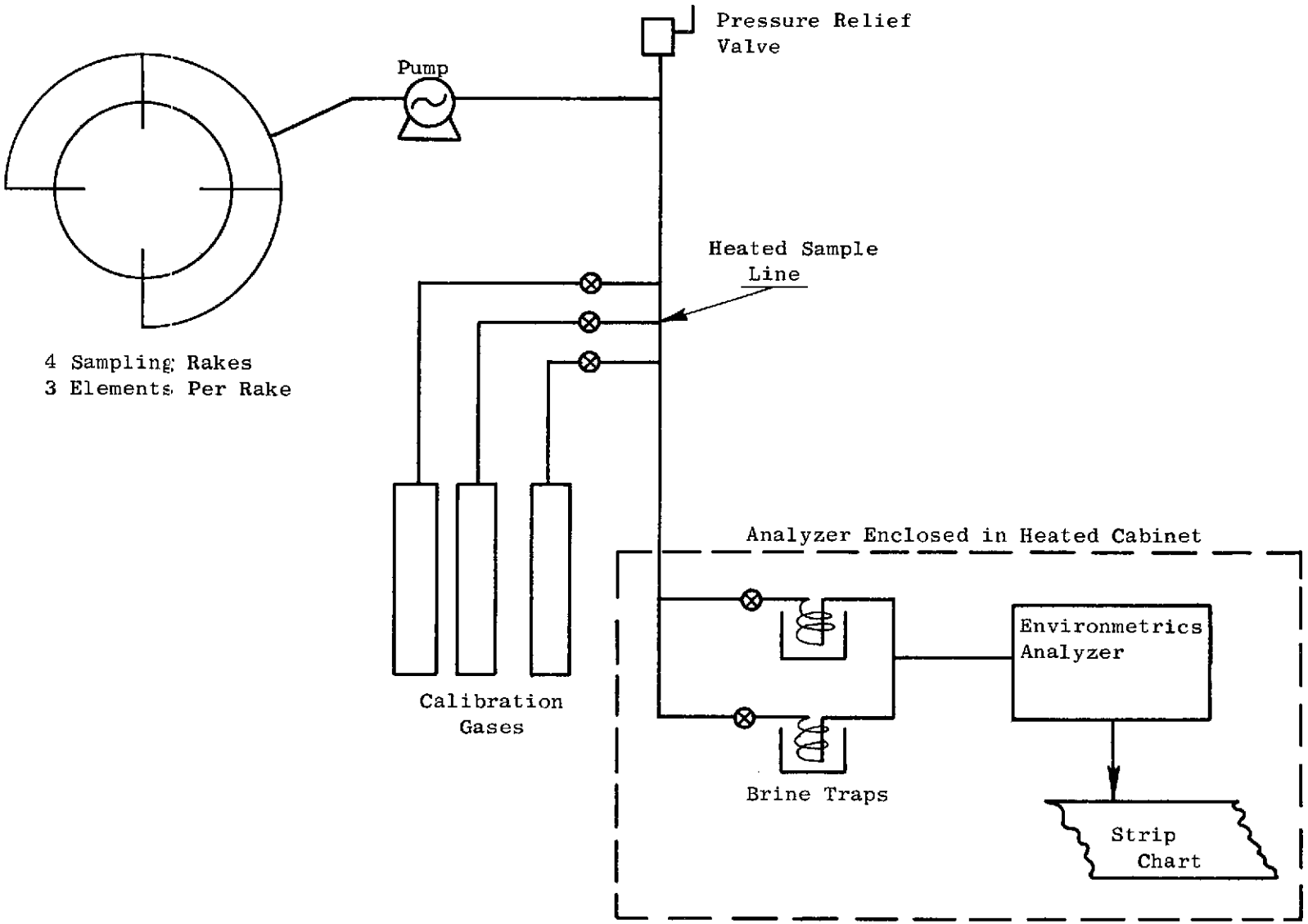


Figure 43. Schematic Diagram of Hydrogen Fueled J85 Engine Exhaust Gas Sampling System.

# Table XIV. NASA Instrument Plan, $CH_4$ Fuel, Steady State and Transient.

Code:
*Vapor Bulb
1 - ADR - NASA
2 - S.S. Display - NASA
3 - Transient Recorder - NASA
4 - S.S. - GE

| Symbol | System Parameter | Range & Units | Acquisition Location | Sensor Interface Description | Sensor Type | Sensor Source | GE Designer | Est. Accuracy | Display Code |
|---|---|---|---|---|---|---|---|---|---|
| $P_o$ | Sub-Cooler Inlet Static Pressure | 15-70 psia | Sub-Cooler Inlet Bayonet | Probe - 1/4" AN Male | DAMPR | NASA | Davis | ±0.1% | 1 |
| $P_o$ | Sub-Cooler Inlet Static Pressure | 15-70 psia | Sub-Cooler Inlet Bayonet | PTX Connector | PTX | GE | Rader/Davis | ±2% | 2 |
| $P_{To}$ | Sub-Cooler Inlet Vapor Pressure | 15-70 psia | Sub-Cooler Inlet Bayonet | *Probe - 1/4" AN Male | DAMPR | NASA | Davis | ±0.1% | 1 |
| $P_{To}$ | Sub-Cooler Inlet Vapor Pressure | 15-70 psia | Sub-Cooler Inlet Bayonet | PTX Connector | PTX | GE | Rader/Davis | ±2% | 2 |
| $P_i$ | Fuel Pump Inlet Static Pressure | 15-70 psia | Pump Inlet Bayonet | Probe - 1/4" AN Male | DAMPR | NASA | Davis | ±0.1% | 1 |
| $P_{Ti}$ | Fuel Pump Inlet Vapor Pressure | 15-70 psia | Pump Inlet Bayonet | *Probe - 1/4" AN Male | DAMPR | NASA | Davis | ±0.1% | 1 |
| $P_2$ | Fuel Pump Disch. Static Pressure | 15-1100 psia | Pump Disch. Line | Voltage from Elec. Control | PTX | GE | Owens/Rader | ±1% | 1,4 |
| $T_2$ | Fuel Pump Disch. Temperature | -230 - +100°F. | Pump Disch. Line | RTD Connector | RTD150MA | GE | Rader | ±3% | 1,2,3 |
| $P_3$ | HX-A Fuel Inlet Static Pressure | 15-1100 psia | HX-A Fuel Inlet Line | Wall Tap - 1/4" AN Male | DAMPR | NASA | Rader | ±0.1% | 1 |
| $P_4$ | HX-A Fuel Disch. Static Pressure | 15-1100 psia | "A" Flow Mixer Gas Inlet | Wall Tap - 1/4" AN Male | DAMPR | NASA | Rader | ±0.1% | 1 |
| $P_4$ | HX-A Fuel Disch. Static Pressure | 15-1100 psia | "A" Flow Mixer Gas Inlet | PTX Connector | PTX | GE | Rader | ±2% | 2 |
| $P_5$ | HX-B Fuel Inlet Static Pressure | 15-1100 psia | HX-B Fuel Inlet Line | Wall Tap - 1/4" AN Male | DAMPR | NASA | Rader | ±0.1% | 1 |
| $P_6$ | HX-B Fuel Disch. Static Pressure | 15-1100 psia | "B" - Flow Mixer Gas Inlet | Wall Tap - 1/4" AN Male | DAMPR | NASA | Rader | ±0.1% | 1 |
| $P_6$ | HX-B Fuel Disch. Static Pressure | 15-1100 psia | "B" - Flow Mixer Gas Inlet | PTX Connector | PTX | GE | Rader | ±2% | 2,3 |
| $P_7$ | PRV Fuel Inlet Static Pressure | 15-1100 psia | PRV Fuel Inlet Body | 1/4" AN Male | DAMPR | NASA | Kast | ±0.1% | 1 |
| $P_8$ | VCV Fuel Inlet Static Pressure | 15-750 psia | VCV Fuel Inlet Body | Voltage from Elec. Control | PTX | GE | Owens | ±1% | 1,3,4 |
| $P_9$ | SOV Fuel Inlet Static Pressure | 5-125 psia | SOV Fuel Inlet Adapter | Wall Tap - 1/4" AN Male | DAMPR | NASA | Rader | ±0.1% | 1 |
| $P_{10}$ | SOV Engine Fuel Disch. Static Press. | 5-125 psia | SOV Engine Fuel Disch. Adapter | Wall Tap - 1/4" AN Male | DAMPR | NASA | Rader | ±0.1% | 1 |
| $P_{10}$ | SOV Engine Fuel Disch. Static Press. | 5-125 psia | SOV Engine Fuel Disch. Adapter | PTX Connector | PTX | GE | Rader | ±2% | 2,3 |
| $W_2$ | Fuel Pump Disch. Flow Rate | .028-.665 pps | Fuel Pump Disch. Line | Voltage From Elec. Control | NTX | GE | Owens | ±3% | 1,2,3 |
| $W_8$ | VCV Fuel Flow Rate | .028-.695 pps | VCV Throat | Voltage from Elec. Control | $T_8$, $X_8$ | GE | Owens | ±3% | 1,3,4 |
| $T_4$ | HX-A Fuel Disch. Temperature | 225-640°R | "A" Flow Mixer Gas Inlet | T/C Connector | T/C - ? | GE | Rader | ±1% | 1,2,3 |
| $T_5$ | HX-B Fuel Inlet Temperature | 225-640°R | HX-B Fuel Inlet Line | T/C Connector | T/C - ? | GE | Rader | ±1% | 1,2,3 |
| $T_6$ | HX-B Fuel Disch. Temperature | 225-1810°R | "B" Flow Mixer Gas Inlet | T/C Connector | T/C - CA | GE | Rader | ±1% | 1,2,3 |
| $T_7$ | PRV Fuel Inlet Temperature | 225-1810°R | PRV Fuel Inlet Body | T/C Connector | T/C - CA | GE | Rader | ±1% | 1,2 |
| $T_8$ | VCV Fuel Inlet Temperature | 225-1810°R | VCV Fuel Inlet Body | Voltage from Elec. Control | RTD | GE | Owens | ±3% | 1,2,3 |
| $T_{10}$ | SOV Engine Fuel Disch. Temperature | 225-1810°R | SOV Engine Fuel Disch. Adapter | T/C Connector | T/C - CA | GE | Rader | ±1% | 1,2 |
| $X_3$ | HX-A Fuel Bypass Valve Position | 0-100% | HX-A Fuel Bypass Valve Stroke | None | XTX | GE | Rader | ±3% | 1,4 |
| $X_6$ | HX/B Fuel Bypass Valve Position | 0-100% | HX-B Fuel Bypass Valve Stroke | None | XTX | GE | Rader | ±3% | 1,4 |

## Table XIV. NASA Instrument Plan, $CH_4$ Fuel, Steady State and Transient (Concluded).

1 - ADR - NASA
2 - S.S. Display - NASA
3 - Trans. Recorder - NASA
4 - S.S. - GE

| Symbol | System Parameter | Range & Units | Acquisition Location | Sensor Interface Description | Sensor Type | Sensor Source | GE Designer | Est. Accuracy | Display Code |
|---|---|---|---|---|---|---|---|---|---|
| $P_{11}$ | Air Supply Static Pressure | 0-165 psia | Inlet Line to Airflow Cont. Valve | Wall Tap - 1/4" AN Male | DAMPR | NASA | Rader | ±0.1% | 1 |
| $P_{12}$ | Burner Inlet Static Pressure | 0-165 psia | Inlet Line to Air Heater Burner | Wall Tap - 1/4" AN Male | DAMPR | NASA | Rader | ±0.1% | 1 |
| $P_{13}$ | HX-B Air Supply Static Pressure | 0-150 psia | Inlet Air Line to HX-B | Wall Tap - 1/4" AN Male | DAMPR | NASA | Rader | ±0.1% | 1 |
| $P_{13}$ | HX/B Air Supply Static Pressure | 0-150 psia | Inlet Air Line to HX-B | PTX Connector | PTX | GE | Rader | ±2% | 2,3 |
| $P_{14}$ | HX-B Air Exhaust Static Pressure | 0-135 psia | Exhaust Air Line from HX-B | Wall Tap - 1/4" AN Male | DAMPR | NASA | Rader | ±0.1% | 1 |
| $\Delta P_{13-14}$ | HX-B Core Air Differential Pressure | 0-5 psid | HX-B Shell ΔP Taps | PTX Connector | PTX | GE | Rader | ±2% | 1,2 |
| $T_{13}$ | HX-B Air Supply Temperature | 200-1200°F | Inlet Air Line to HX-B | T/C Connector | T/C - CA | GE | Rader | ±1% | 1,2,3 |
| $T_{14}$ | HX-B Air Exhaust Temperature | 100-800°F | Exhaust Air Line form HX-B | T/C Connector | T/C - CA | GE | Rader | ±1% | 1,2,3 |
| $W_{14}$ | HX-B Air Flow Rate | .319-2.92 pps | Air Flow Control Computer | Voltage from Air Control | None | GE | Rader | ±7% | 1,3,4 |
| $X_{14}$ | Air Flow Control Valve Position | 0-100% | Air Flow Control Computer | None | XTX | GE | Rader | ±1% | 1,4 |
| $P_{15}$ | Hyd. Pump Inlet Pressure | 0-100 psia | Hyd. Pump Inlet Housing | 1/4" AN Male | DAMPR | NASA | St. Clair | ±0.1% | 1 |
| $P_{15}$ | Hyd. Pump Inlet Pressure | 0-100 psia | Hyd. Pump Inlet Housing | PTX Connector | PTX | GE | Rader | ± 2% | 2 |
| $P_{16}$ | Hyd. Pump Disch. Pressure | 0-4000 psia | Hyd. Pump Disch. Housing | 1/4" AN Male | DAMPR | NASA | St. Clair | ±0.1% | 1 |
| $P_{16}$ | Hyd. Pump Disch. Pressure | 0-4000 psia | Hyd. Pump Disch. Housing | PTX Connector | PTX | GE | Rader | ±2% | 2 |
| $P_{17}$ | Hyd. Reservoir Pressure | 0-100 psia | Hyd. Reservoir Housing | 1/4" AN Male | DAMPR | NASA | Rader | ±0.1% | 1 |
| $T_{15}$ | Hyd. Pump Inlet Temperature | 0-125°F | Inlet Line to Hyd. Pump | None | T/C | NASA | - - - | - - - | 1,2 |
| $T_{16}$ | Hyd. Pump Disch. Temperature | 0-160°F | Disch. Line from Hyd. Pump | None | T/C | NASA | - - - | - - - | 1,2 |
| $T_{17}$ | Hyd. Return Temperature | 0-175°F | Hyd. HX Oil Inlet Line | T/C Connector | T/C - CC | GE | Rader | ±1% | 1,2 |
| $I_8$ | VCV Torquemotor Current | 0 ± 100 ma | Electronic Control | None | Meter | GE | Owens | ±5% | 4 |
| $I_2$ | Fuel Pump Torquemotor Current | 0-100 ma | Electronic Control | None | Meter | GE | Owens | ±5% | 4 |
| $I_7$ | PRV Torquemotor Current | 0 ± 100 ma | Electronic Control | None | Meter | GE | Owens | ±5% | 4 |
| $N_2$ | Fuel Pump Speed | 0-110% | Electronic Control | None | NTX | GE | Owens | ±2% | 4 |
| $T_{5e}$ | Engine Exhaust Gas Temperature | 650-1250°F | Engine $T_5$ Harness | Engine $T_5$ Connector | T/C - CA | NASA | Owens | ±20°F | 1,3,4 |
| $N_g$ | Engine Rotor Speed | 0-110% | Engine Driven Tachometer | Elec. Connector on Tach. | NTX | NASA | Owens | ±0.2% | 1,3,4 |
| $X_8$ | VCV Position | 0-100% | Electronic Control | Voltage from Elec. Control | XTX | GE | Owens | ±1% | 1,2 |
| $A_8$ | Engine Exhaust Nozzle Area | 0-100% | $A_8$ Actuator Stroke | None | XTX | NASA | - - - | - - - | 1,2,3 |
| PLA | Power Lever Angle | 0-90° | Electronic Control | Voltage from Elec. Control | XTX | GE | Owens | ±1% | 1,2,3 |
| $P_{18}$ | HX-A Oil Inlet Pressure | 0-100 psig | HX-A Oil Inlet Line | PTX Connector | PTX | GE | Rader | ±2% | 1,2 |
| $P_{19}$ | HX-A Oil Disch. Pressure | 0-100 psig | HX-A Oil Disch. Line | PTX Connector | PTX | GE | Rader | ±2% | 1,2 |
| $T_{18}$ | HX-A Oil Inlet Temperature | 50-600°F | HX-A oil Inlet Line | T/C Connector | T/C - CC | GE | Rader | ±1% | 1,2 |
| $T_{19}$ | HX-A Oil Disch. Temperature | -50 to 600°F | HX-A Oil Disch. Line | T/C Connector | T/C - CC | GE | Rader | ±1% | 1,2 |
| $W_{18}$ | HX-A Oil Flow Rate | 0.7-10 gpm | HX-A Oil Inlet Line | TFM Connector | TFM | GE | Rader | ±2% | 1,2 |

# Table XV. NASA Instrument Plan, $H_2$ Fuel, Steady State and Transient.

Display Code: *Vapor Bulb
1. ADR - NASA
2. S.S. Display - NASA
3. Transient Recorder - NASA
4. S.S. - GE

| Symbol | System Parameter | Range & Units | Acquisition Location | Sensor Interface Description | Sensor Type | Sensor Source | GE Designer | Est. Accuracy | Display Code |
|---|---|---|---|---|---|---|---|---|---|
| $P_o$ | Sub-Cooler Inlet Static Pressure | 15-70 psia | Sub-Cooler Inlet Bayonet | Probe - 1/4" AN Male | DAMPR | NASA | Davis | ±0.1% | 1 |
| $P_o$ | Sub-Cooler Inlet Static Pressure | 15-70 psia | Sub-Cooler Inlet Bayonet | PTX Connector | PTX | GE | Rader/Davis | ±2% | 2 |
| $P_{To}$ | Sub-Cooler Inlet Vapor Pressure | 15-70 psia | Sub-Cooler Inlet Bayonet | *Probe - 1/4" AN Male | DAMPR | NASA | Davis | ±0.1% | 1 |
| $P_{To}$ | Sub-Cooler Inlet Vapor Pressure | 15-70 psia | Sub-Cooler Inlet Bayonet | PTX Connector | PTX | GE | Rader/Davis | ±2% | 2 |
| $P_1$ | Fuel Pump Inlet Static Pressure | 15-70 psia | Pump Inlet Bayonet | Probe - 1/4" AN Male | DAMPR | NASA | Davis | ±0.1% | 1 |
| $P_{T1}$ | Fuel Pump Inlet Vapor Pressure | 15-70 psia | Pump Inlet Bayonet | *Probe - 1/4" AN Male | DAMPR | NASA | Davis | ±0.1% | 1 |
| $P_2$ | Fuel Pump Disch. Stator Pressure | 15-500 psia | Pump Disch. Line | Voltage from Elec. Control | PTX | GE | Owens/Rader | ±1% | 1,4 |
| $T_2$ | Fuel Pump Disch. Temperature | -420 - +100°F | Pump Disch. Line | RTD Connector | RTD -150 MA | GE | Rader | ±3% | 1,2,3 |
| $P_5$ | HX-B Fuel Inlet Static Pressure | 15-500 psia | HX-B Fuel Inlet Line | Wall Tap - 1/4" AN Male | DAMPR | NASA | Rader | ±0.1% | 1 |
| $P_8$ | HX-B Fuel Disch. Static Pressure | 15-500 psia | "B" - Flow Mixer Gas Inlet | Wall Tap - 1/4" AN Male | DAMPR | NASA | Rader | ±0.1% | 2,3 |
| $P_6$ | HX-B Fuel Disch. Static Pressure | 15-500 psia | "B" - Flow Mixer Gas Inlet | PTX Connector | PTX | GE | Rader | ±2% | 2,3 |
| $P_7$ | PRV Fuel Inlet Static Pressure | 15-500 psia | PRV Fuel Inlet Body | 1/8" AN Male | DAMPR | NASA | Kast | ±0.1% | 1 |
| $P_8$ | VCV Fuel Inlet Static Pressure | 15-300 psia | VCV Fuel Inlet Body | Voltage from Elec. Control | PTX | GE | Owens | ±1% | 1,3,4 |
| $P_9$ | SOV Fuel Inlet Static Pressure | 5-125 psia | SOV Fuel Inlet Adapter | Wall Tap - 1/4" AN Male | DAMPR | NASA | Rader | ±0.1% | 1 |
| $P_{10}$ | SOV Engine Fuel Disch. Static Pressure | 5-125 psia | SOV Engine Fuel Disch. Adapter | Wall Tap - 1/4" AN Male | DAMPR | NASA | Rader | ±0.1% | 1 |
| $P_{10}$ | SOV Engine Fuel Disch. Static Pressure | 5-125 psia | SOV Engine Fuel Disch. Adapter | PTX Connector | PTX | GE | Rader | ±2% | 2,3 |
| $W_2$ | Fuel Pump Disch. Flow Rate | .012-0.30 pps | Fuel Pump Disch. Line | Voltage from Elec. Control | NTX | GE | Owens | ±3% | 1,2,3 |
| $W_8$ | VSV Fuel Flow Rate | .012-0.30 pps | VCV Throat | Voltage from Elec. Control | $T_8$, X | GE | Owens | ±7% | 1,3,4 |
| $T_6$ | HX-B Fuel Disch. Temperature | -300 - +100°F | "B" Flow Mixer Gas Inlet | T/C Connector | T/C - CA | GE | Rader | ±1% | 1,2,3 |
| $T_7$ | PRV Fuel Inlet Temperature | -300 - +100°F | PRV Fuel Inlet Body | T/C Connector | T/C - CA | GE | Rader | ±1% | 1,2 |
| $T_8$ | VCV Fuel Inlet Temperature | -390 - +100°F | VCV Fuel Inlet Body | Voltage from Elec. Control | RTD | GE | Owens | ±3% | 1,2,3 |
| $T_{10}$ | SOV Engine Fuel Disch. Temperature | -390 - +100°F | SOV Engine Fuel Disch. Adapter | RTD Connector | RTD | GE | Rader | ±3% | 1,2 |
| $X_5$ | HX-B Fuel Bypass Valve Position | 0-100% | HX-B Fuel Bypass Valve Stroke | None | XTX | GE | Rader | ±3% | 1,4 |
| $P_{11}$ | Air Supply Static Pressure | 0-165 psia | Inlet Line to Airflow Cont.Valve | Wall Tap - 1/4" AN Male | DAMPR | NASA | Rader | ±0.1% | 1 |
| $P_{12}$ | Burner Inlet Static Pressure | 0-165 psia | Inlet Line to Air Htr.Burner | Wall Tap - 1/4" AN Male | DAMPR | NASA | Rader | ±0.1% | 1 |
| $P_{13}$ | HX-B Air Supply Static Pressure | 0-150 psia | Inlet Air Line to HX-B | Wall Tap - 1/4" AN Male | DAMPR | NASA | Rader | ±0.1% | 1 |
| $P_{13}$ | HX-B Air Supply Static Pressure | 0-150 psia | Inlet Air Line to HX-B | PTX Connector | PTX | GE | Rader | ±2% | 2,3 |
| $P_{14}$ | HX-B Air Exhaust Static Pressure | 0-135 psia | Exhaust Air Line from HX-B | Wall Tap - 1/4" AN Male | DAMPR | NASA | Rader | ±0.1% | 1 |
| $T_{13}$ | HX-B Air Supply Temperature | 200°-1000°F | Inlet Air Line to HX-B | T/C Connector | T/C - CA | GE | Rader | ±1% | 1,2,3 |
| $T_{14}$ | HX-B Air Exhaust Temperature | 0°-600°F | Exhaust Air Line from HX-B | T/C Connector | T/C - CA | GE | Rader | ±1% | 1,2,3 |
| $W_{14}$ | HX/B Air Flow Rate | 0.144-1.2 pps | Air Flow Control Computer | Voltage from Air Control | None | GE | Rader | ±7% | 1,3,4 |
| $X_{14}$ | Air Flow Control Valve Position | 0-100% | Air Flow Control Computer | None | XTX | GE | Rader | ±1% | 1,4 |

# Table XV. NASA Instrument Plan, $H_2$ Fuel, Steady State and Transient (Concluded).

Display Code
1. ADR - NASA
2. S.S. Display - NASA
3. Trans. Recorder - NASA
4. S.S. - GE

| Symbol | System Parameter | Range & Units | Acquisition Location | Sensor Interface Description | Sensor Type | Sensor Source | GE Designer | Est. Accuracy | Display Code |
|---|---|---|---|---|---|---|---|---|---|
| $P_{15}$ | Hyd. Pump Inlet Pressure | 0-100 psia | Hyd. Pump Inlet Housing | 1/4" AN Male | DAMPR | NASA | St. Clair | ±0.1% | 1 |
| $P_{15}$ | Hyd. Pump Inlet Pressure | 0-100 psia | Hyd. Pump Inlet Housing | PTX Connector | PTX | GE | Rader | ±2% | 2 |
| $P_{16}$ | Hyd. Pump Disch. Pressure | 0-4000 psia | Hyd. Pump Disch. Housing | 1/4" AN Male | DAMPR | NASA | St. Clair | ±0.1% | 1 |
| $P_{16}$ | Hyd. Pump Disch. Pressure | 0-4000 psia | Hyd. Pump Disch. Housing | PTX Connector | PTX | GE | Rader | ±2% | 2 |
| $P_{17}$ | Hyd. Reservoir Pressure | 0-100 psia | Hyd. Reservoir Housing | 1/4" AN Male | DAMPR | NASA | Rader | ±0.1% | 1 |
| $T_{15}$ | Hyd. Pump Inlet Temperature | 0-125°F | Inlet Line to Hyd. Pump | None | T/C | NASA | - - - | - - - | 1,2 |
| $T_{16}$ | Hyd. Pump Disch. Temperature | 0-160°F | Disch. Line from Hyd. Pump | None | T/C | NASA | - - - | - - - | 1,2 |
| $T_{17}$ | Hyd. Return Temperature | 0-175°F | Hyd. HX Oil Inlet Line | T/C Connector | T/C - CA | GE | Rader | ±1% | 1,2 |
| $I_8$ | VCV Torquemotor Current | 0 ± 100 ma | Electronic Control | None | Meter | GE | Owens | ±5% | 4 |
| $I_2$ | Fuel Pump Torquemotor Current | 0-100 ma | Electronic Control | None | Meter | GE | Owens | ±5% | 4 |
| $I_7$ | PRV Torquemotor Current | 0 ± 100 ma | Electronic Control | None | Meter | GE | Owens | ±5% | 4 |
| $N_2$ | Fuel Pump Speed | 0-110% | Electronic Control | None | NTX | GE | Owens | ±2% | 4 |
| $T_{5e}$ | Engine Exhaust Gas Temperature | 650-1250°F | Engine $T_5$ Harness | Engine $T_5$ Connector | T/C - CA | NASA | Owens | ±20°F | 1,3,4 |
| $N_g$ | Engine Rotor Speed | 0-110% | Engine Drives - Tachometer | Elec. Connector on Tach. | NTX | NASA | Owens | ±0.2% | 1,3,4 |
| $X_8$ | VCV Position | 0-100% | Electronic Control | Voltage from Elec. Control | XTX | GE | Owens | ±1% | 1,2 |
| $A_8$ | Engine Exhaust Nozzle Area | 0-100% | $A_8$ Actuator Stroke | None | XTX | NASA | - - - | - - - | 1,2,3 |
| PLA | Power Lever Angle | 0-90° | Electronic Control | Voltage from Elec. Control | XTX | GE | Owens | ±1° | 1,2,3 |

DEFINITION OF ABBREVIATIONS:

DAMPR - NASA pressure conversion system for automatic data recording of pressures
PTX - Electrical pressure transducer
RTD - Resistance Temperature Detector
XTX - Electrical position transducer
T/C - Thermocouple
NTX - Electrical speed sensor
HX - Heat exchanger
PRV - Pressure regulating valve
VCV - Vapor control valve
SOV - Shutoff & vent valve

## Check-Out Tests

In June 1972, the test procedure check-outs were initiated using the methane system configuration. The procedural phases for Air Heater Hot Check-Out and No Fuel Check-Out of control functions were performed. Minor problems with instrumentation and control settings were discovered and corrected. Air heater operation and control functions were established as suitable to proceed with testing of the system on LNG fuel.

## LNG Flow and Thermal Calibrations

A trial flow and thermal calibration run using liquid natural gas fuel was initiated on June 19, 1972. While attempting to fill the system subcooler and chilldown, an overfill of the subcooler occurred which resulted in LNG spill from the vent stack, aborting the run. Investigation revealed that the subcooler bath level control valve was either stuck open or had a broken connection causing overfill of the bath. The subcooler was removed from the system since adequate storage trailer pressurization was available to prime the fuel pump intake directly.

A second LNG calibration run was attempted on July 5, 1972. This run was aborted by a problem with overspeed of the fuel pump motor when the pump start mode was selected. A malfunctioning module in the pump speed limit circuit of the Engine Electrical Control was isolated and repaired, correcting the problem.

A third flow and thermal calibration of the system equipment using LNG was performed on July 10, 1972, and the test procedure was completed with a full set of data obtained.

Performance of the system was acceptable in these respects:

- Adequate fuel pump priming was obtained without the subcooler.
- The fuel pump operated successfully over a flow range of 5% to 100% of system rated flow at discharge pressures ranging from 430 to 800 psia ($2.9 \times 10^6$ to $5.51 \times 10^6$ $N/M^2$).
- The metering valve operated without difficulty, and the control computed flow as intended, judging by comparison with Cosmodyne pump calibration data.
- The air-to-fuel heat exchanger met or exceeded required heat transfer rates at all specified conditions, and no evidence of icing was indicated during a one half hour run at the rated take-off fuel-flow point.

Significant problems encountered during the run were:

- System pressure levels at the pump discharge and the metering valve entrance sagged below the intended steady-state levels, particularly at small values of system fuel flow.

- The oil-to-fuel heat exchanger froze and reduced oil flow to zero whenever fuel flows in excess of 20% of rated were passed through.

The problem with pressure levels falling out of regulation was believed to be due to a slight shift in the fuel pump delivery characteristic coupled with the existence of excessively tight pump speed limits set at 110% of requested system flow. Because of the tight limits, the pump could not adjust speed sufficiently to provide the real flow necessary to reach rated pressures at the smaller values of pump speed and flow. Figure 44 illustrates the comparison of the Cosmodyne LN2 calibration used to define the pump characteristic and the LNG flow as determined by metering valve computation corrected for pressure errors. A reduction in delivery of about 5% at 100% rated pump speed was apparent. This problem was correctable by expanding the pump speed limit settings.

The problem encountered with freezing in the oil-to-fuel heat exchanger was apparently a tendency to overperform at large values of fuel flow which was inherent in the design. No correction for this condition appeared feasible other than to utilize the fuel bypass valving around the exchanger to limit through flow to partial values.

In Table XVI the successive heat exchanger performance readings measured during a 30-minute icing run at the take-off condition are shown. Heat exchanger air-side entrance temperature, $T_{13}$, did not record properly in digital data for this run. The $T_{14}$ air outlet temperature remained at a steady value throughout the run.

A fourth flow and thermal calibration run of the system using liquid natural gas was performed on August 2, 1972. A successful run was obtained yielding a complete set of data. System pressure levels regulated properly at all steady-state operating points from 10% to 100% rated system fuel flow; the fuel pump control circuit speed limits had been widened prior to the run.

Operation of the heat exchanger fuel bypass servos in the automatic mode was attempted during this run. The air-to-methane heat exchanger was successfully bypassed, with the automatic servo regulating air exhaust temperature stable. Regulated temperatures were varied at the system idle fuel flow point such that fuel metering valve entrance temperatures were varied from a value of +245° F (392° K) at zero bypass to a value of -65° F (219° K) at the highest bypass setting.

Automatic fuel bypass operation of the oil-to-methane heat exchanger was attempted by setting up the oil outlet temperature regulator reference at +50° F (283° K) with the system at idle fuel flow and with oil outlet temperature operating at +70° F (294° K). Oil supply conditions were then reset to the take-conditions and system fuel flow was advanced to the take-off condition (100% flow). Freeze-up of the oil flow path occurred, reducing oil flow to zero, before 100% fuel flow was reached. The bypass servo was never able to act to prevent the freeze-up because oil flow stopped before the sensed oil outlet temperature fell below the +50° F (283° K) regulating reference. Further automatic operation was abandoned, and manual bypass of the heat exchanger fuel path was used for the remainder of the run.

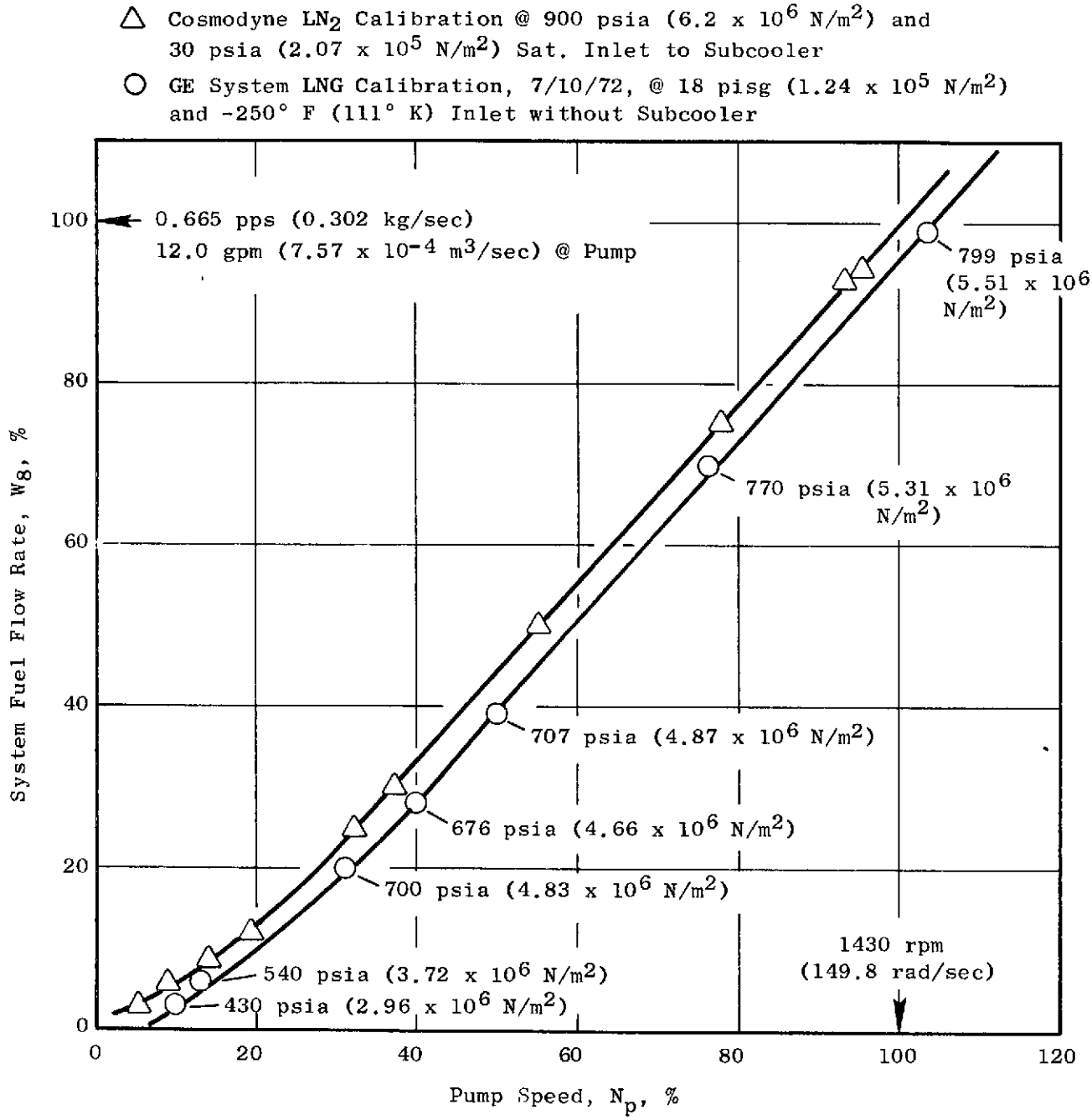


Figure 44. Fuel Pump Performance Comparison Between Cosmodyne Liquid Nitrogen Calibration and GE System Liquid Natural Gas Calibration Data.

Table XVI. Heat Exchanger B Icing Run $CH_4$ System Configuration Take-Off Flow Conditions.

| Time Min. | Fuel Side | | | | | | | | Air Side | | | |
|---|---|---|---|---|---|---|---|---|---|---|---|---|
| | $T_5$ Fuel In ° F | $T_5$ Fuel In (° K) | $T_6$ Fuel Out ° F | $T_6$ Fuel Out (° K) | $W_2$ Fuel Flow pps | $W_2$ Fuel Flow (Kg/sec) | $P_2$ Fuel Press. psia | $P_2$ Fuel Press. ($N/M^2$) | $W_A$ Air Flow pps | $W_A$ Air Flow (Kg/sec) | $T_{14}$ Air Out ° F | $T_{14}$ Air Out (° K) |
| 0 | -240.2 | (122.0) | 399.5 | (478) | 0.683 | (0.310) | 985.1 | ($6.79 \times 10^6$) | 2.81 | (1.275) | 186.9 | (359) |
| 10 | -242.7 | (121.0) | 416.0 | (486) | 0.671 | (0.305) | 1012.4 | ($6.99 \times 10^6$) | 2.81 | (1.275) | 185.0 | (358) |
| 20 | -243.5 | (120.4) | 413.6 | (485) | 0.678 | (0.308) | 1009.1 | ($6.96 \times 10^6$) | 2.80 | (1.270) | 186.5 | (359) |
| 30 | -241.8 | (121.3) | 413.1 | (485) | 0.680 | (0.309) | 1045.8 | ($7.21 \times 10^6$) | 2.80 | (1.270) | 186.7 | (359) |

Additional thermal performance data on Heat Exchanger B were obtained as tabulated in Table XVII. Thermal performance in terms of heat rates, temperature changes, and air-side pressure drops correlated quite well with predicted values. Heat Exchanger A was bypassed for these data points. No evidence of icing in Heat Exchanger B was noted.

LNG Engine Run

An operational demonstration run of the J85 engine using the liquid natural gas fuel system was successfully completed on August 16, 1972. The oil heat exchange system was not operated during this run because the oil heater package had experienced a severe overheating during a previous attempt to run.

The engine was successfully started and accelerated to idle several times during the run. A fuel flow level of 8% at engine motoring speed of 10% was found to provide reliable light-off and acceleration. At the initially planned motoring speeds of 15% and higher, the engine would not light. Figure 45 (sheets 1, 2, and 3) illustrates the typical engine start transient obtained.

A complete set of steady-state operating points for the engine was recorded, and exhaust emission gas samples were obtained at these points. Stable governing and fuel system pressure regulation were obtained as planned. At 100% speed, the engine required only 80%-90% of rated fuel flow, and engine exhaust gas temperature was approximately 200° F (111° K) lower than the expected value. Apparently the rigging of the two-position engine exhaust area control was not set far enough closed to bring the engine up to rated temperature at 100% speed. The air heater system and air-to-fuel heat exchanger continued to operate normally during the run.

Several throttle-bursts of the engine from idle power to 100% speed were successfully made. The engine was quite responsive and no transient problems with fuel system regulation were encountered. Acceleration fuel schedule adjustments and exhaust area control slew rate adjustments were made to attempt to minimize the engine acceleration time. Figure 46 (sheets 1, 2, and 3) illustrates the last throttle burst made. The engine reached an initial speed peak at 96% speed in 3.5 seconds, followed by a slight speed rollback and recovery to 100% speed. The speed rollback and long recovery time reflect an excessive amount of anticipation in the governor circuit and a conservatively low governor gain. Further experimentation to tune the governor dynamics for optimized anticipation should improve the characteristic recovery from rollback; however, the system ran out of fuel at this point and the run was terminated.

Several engine decelerations were also made by chopping the power lever setting to idle from the 100% speed setting. These decelerations were free of any problems and consumed approximately 15-20 seconds due to the conservative deceleration schedule used in the control.

Table XVII(a). Heat Exchanger B Performance - LNG Fuel.

| Parameter | Gnd. Idle | Takeoff | Climb | Accel. | Cruise | Decel. | Descent |
|---|---|---|---|---|---|---|---|
| **Air Side (Pred/Actual)** | | | | | | | |
| Airflow - pps | 1.59/1.35 | 2.65/2.71 | 1.06/1.28 | 2.92/2.87 | 1.46/1.28 | 0.795/0.93 | 0.928/1.10 |
| Temp in - ° F | 290/309 | 680/691 | 630/649 | 1080/1071 | 1180/1143 | 830/793 | 425/415 |
| Temp out - ° F | 146/146 | 150/176 | 125/184 | 548/513 | 760/463 | 780/558 | 404/352 |
| Press in - psia | 60/58.4 | 150/153 | 60/65 | 130/120.4 | 65/68.3 | 35/36.5 | 45/46.4 |
| Press out - psia | 51.6/55.2 | 138.8/147.5 | 56.4/60.0 | 105/110.8 | 50.8/64.2 | 30.9/34.5 | 40.3/43.5 |
| Heat Rate - Btu/sec | 44/53 | 360/344 | —/146.5 | —/410 | 150/223.5 | 8/55.3 | —/16.9 |
| **Fuel Side (Pred/Actual)** | | | | | | | |
| Fuel Flow - pps | 0.133/0.133 | 0.665/0.661 | 0.266/0.265 | 0.465/0.467 | 0.200/0.199 | 0.033/0.046 | 0.033/0.033 |
| Temp in - ° F | -175/-149 | -215/-242 | -193/-235 | -188/-240 | -116/-219 | +330/+32 | +170/+44 |
| Temp out - ° F | 260/250 | 430/409 | 415/308 | 548/902 | 1050/916 | 820/741 | 420/405 |
| Pressure - psia | 900/920 | 900/935 | 900/941 | 900/935 | 900/935 | 900/432 | 900/870 |

Table XVII(b). Heat Exchanger B Performance - LNG Fuel.

| Parameter | Gnd. Idle | Takeoff | Climb | Accel | Cruise | Decel | Descent |
|---|---|---|---|---|---|---|---|
| **Air-Side (Pred/Actual)** | | | | | | | |
| Airflow - Kg/sec | 0.722/0.613 | 1.203/1.23 | 0.481/0.581 | 1.320/1.300 | 0.662/0.581 | 0.360/0.421 | 0.420/0.499 |
| Temp. in - ° K | 416/427 | 633/639 | 606/616 | 856/851 | 912/892 | 717/696 | 491/486 |
| Temp out - ° K | 337/337 | 339/353 | 325/358 | 561/541 | 678/513 | 689/566 | 480/451 |
| Press. in - $N/M^2 \times 10^{-5}$ | 4,14/4.02 | 10,34/10.54 | 4.14/4,48 | 8.97/8,30 | 4.48/4.71 | 2.41/2.52 | 3.10/3.20 |
| Press. out - $N/M^2 \times 10^{-5}$ | 3.56/3.81 | 9.56/10.2 | 3,89/4.14 | 7.24/7.65 | 3.50/4.43 | 2.13/2.38 | 2.82/3.00 |
| Heat Rate - $w \times 10^{-3}$ | 46.5/55.9 | 380/353 | —/155 | —/433 | 158.3/236 | 8.44/58.4 | —/17.8 |
| **Fuel-Side (Pred/Actual)** | | | | | | | |
| Fuel Flow - kg/sec | 0.0603/0.0603 | 0.302/0.300 | 0.121/0.120 | 0.211/0.212 | 0.0908/0.0903 | 0.0150/0.0209 | 0.0150/0.0150 |
| Temp. in - ° K | 158/173 | 136/121 | 148/125 | 151/122 | 191/134 | 439/273 | 350/280 |
| Temp. out - ° K | 400/394 | 494/483 | 486/427 | 561/757 | 840/765 | 712/668 | 489/481 |
| Pressure - $N/M^2 \times 10^{-6}$ | 6.21/6,34 | 6.21/6.44 | 6,21/6.48 | 6.21/6.44 | 6.21/6.44 | 6.21/2.98 | 6.21/6.00 |

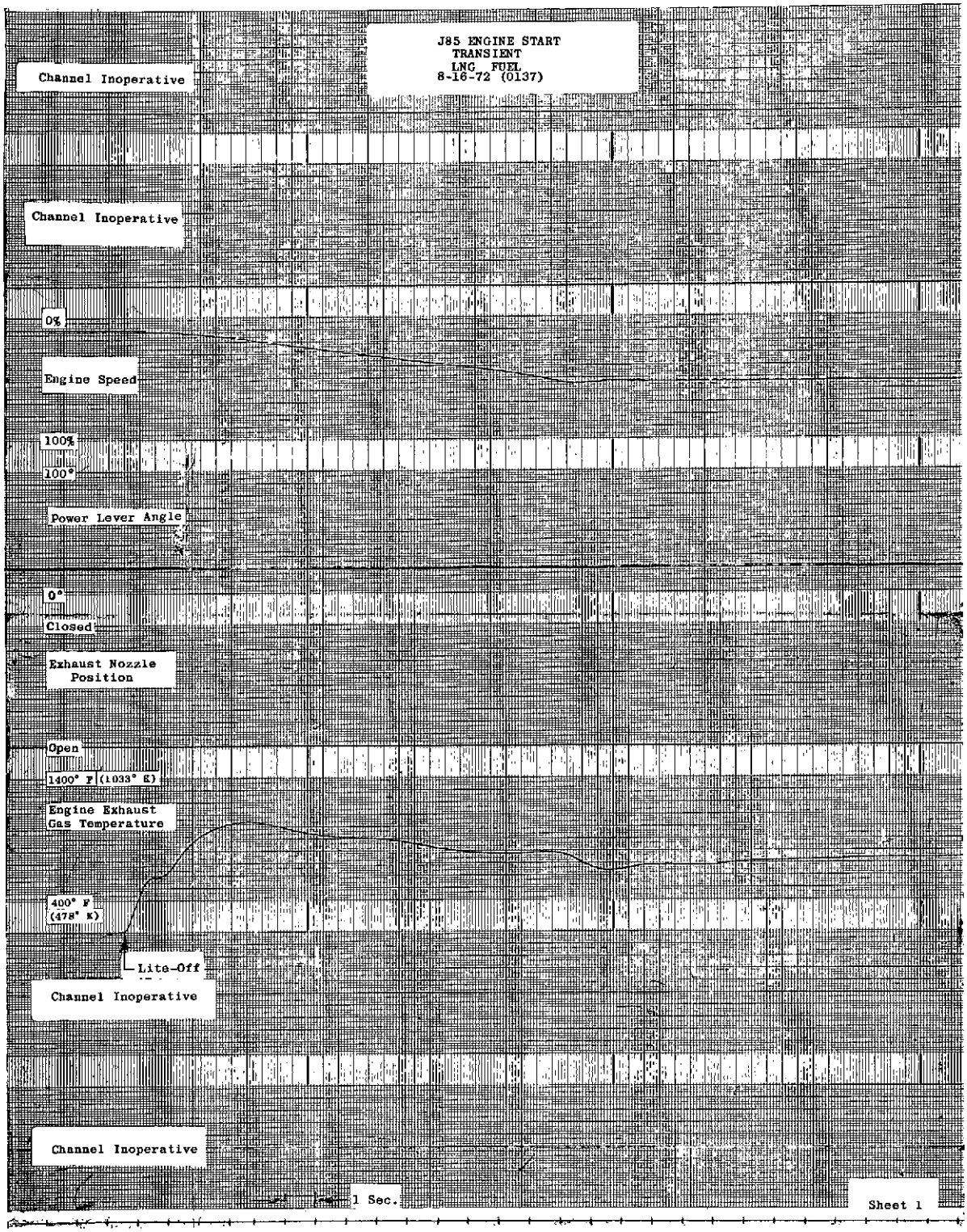


Figure 45. Engine Start Transient for Methane Fuel System Using Liquid Natural Gas, Demonstration Run.

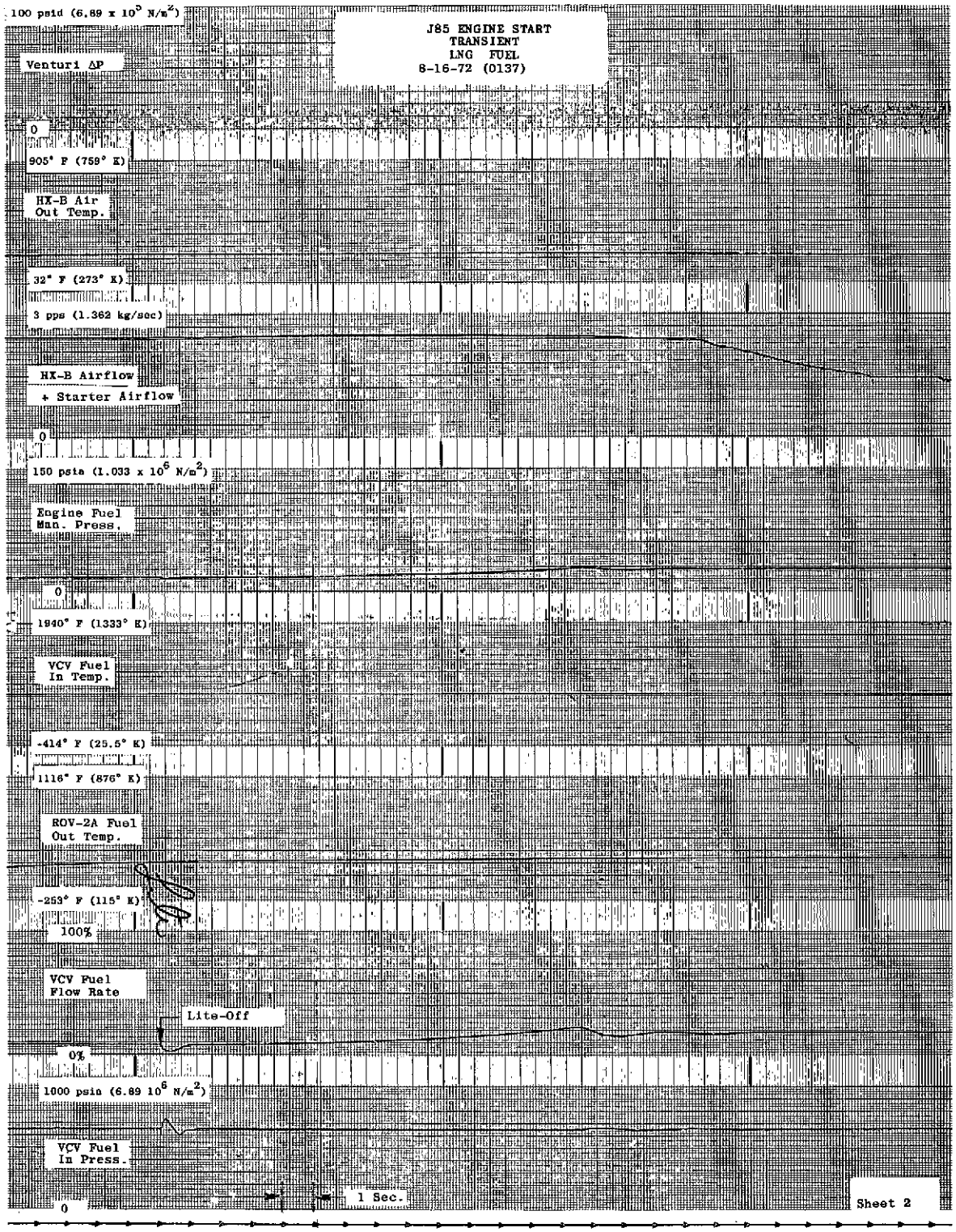


Figure 45. Ergine Start Transient for Methane Fuel System Using Liquid Natural Gas, Demonstration Run (Continued).

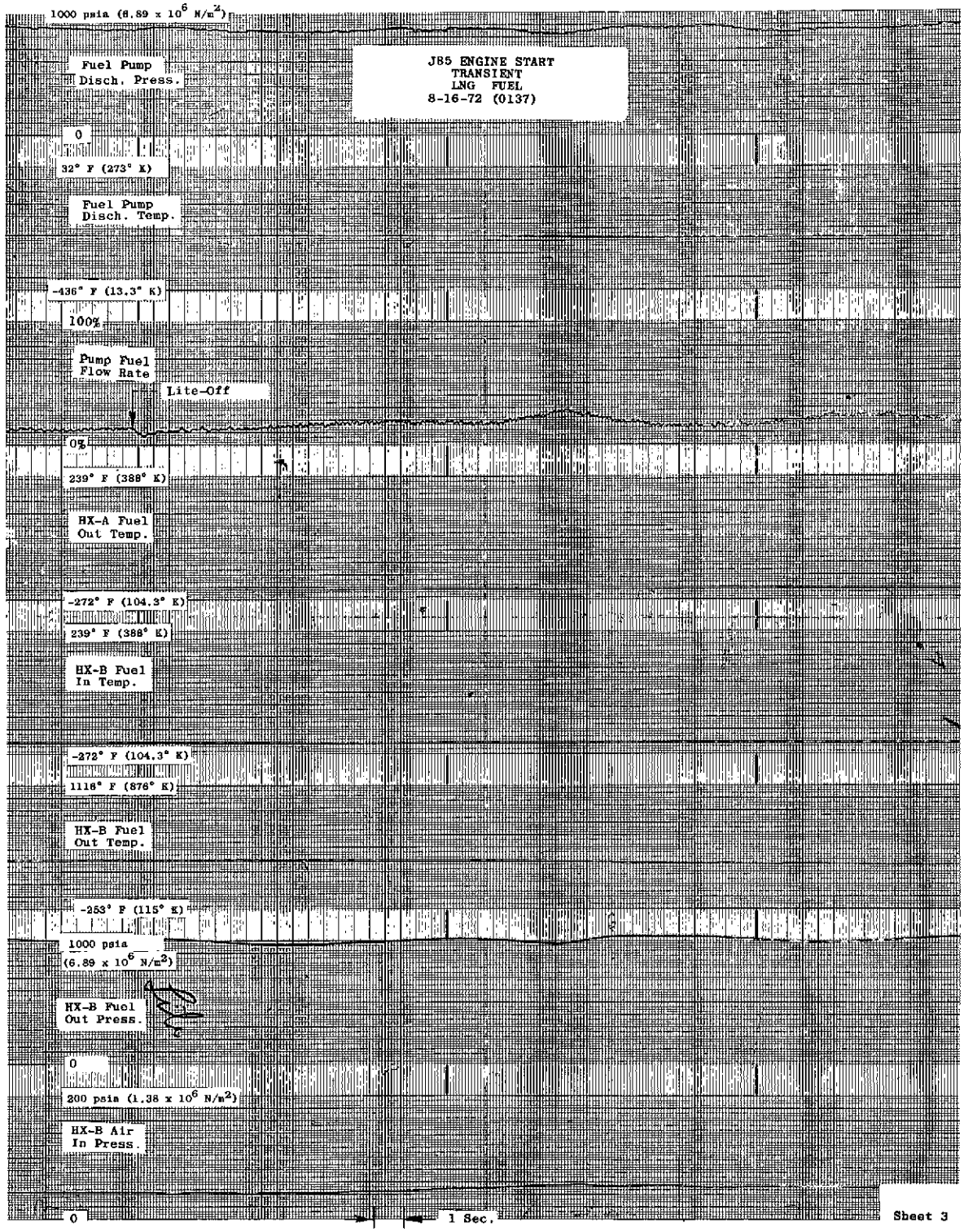


Figure 45. Engine Start Transient for Methane Fuel System Using Liquid Natural Gas, Demonstration Run (Concluded).

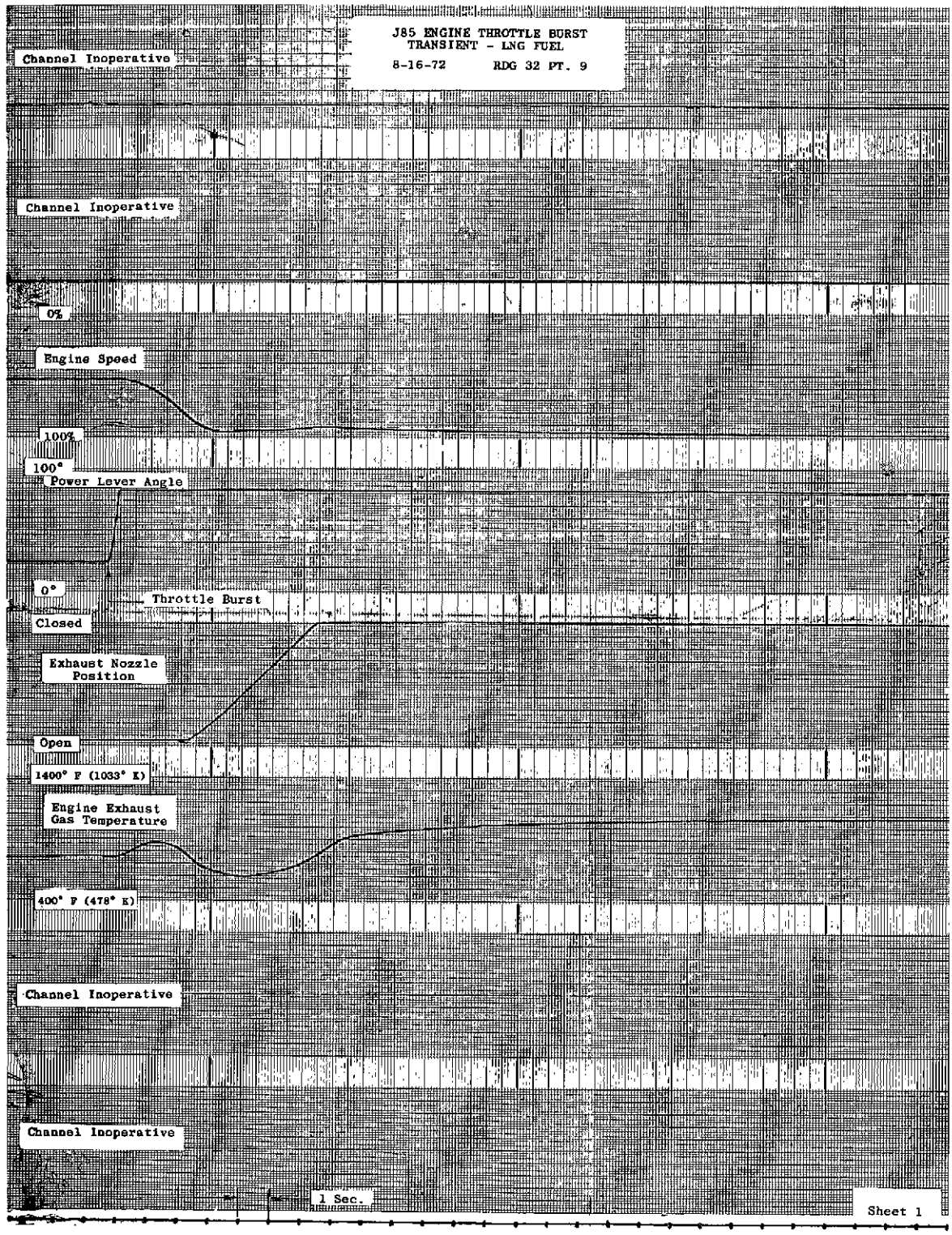


Figure 46. Engine Throttle Burst Transient for Methane Fuel System Using Liquid Natural Gas, Demonstration Run.

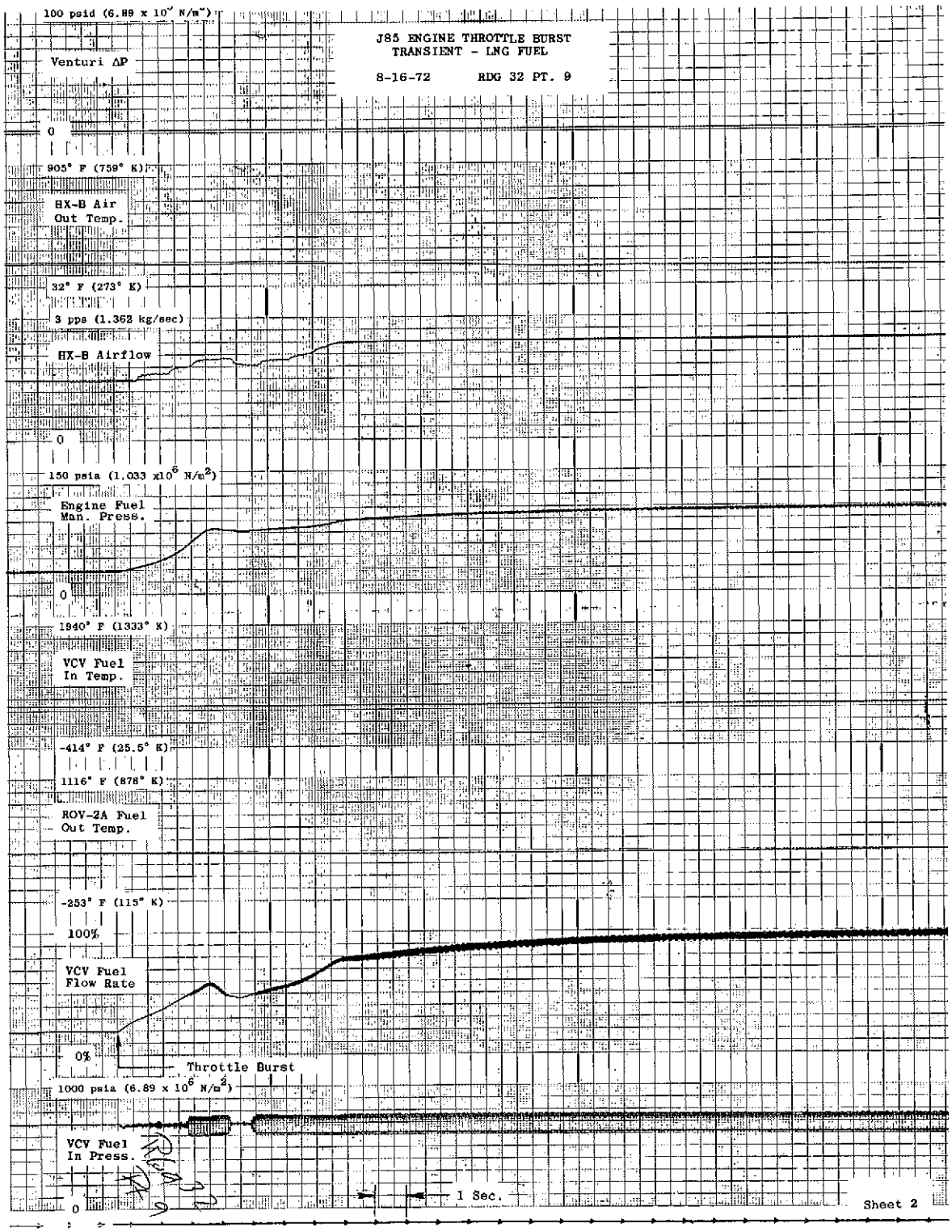


Figure 46. Engine Throttle Burst Transient for Methane Fuel System Using Liquid Natural Gas, Demonstration Run (Continued).

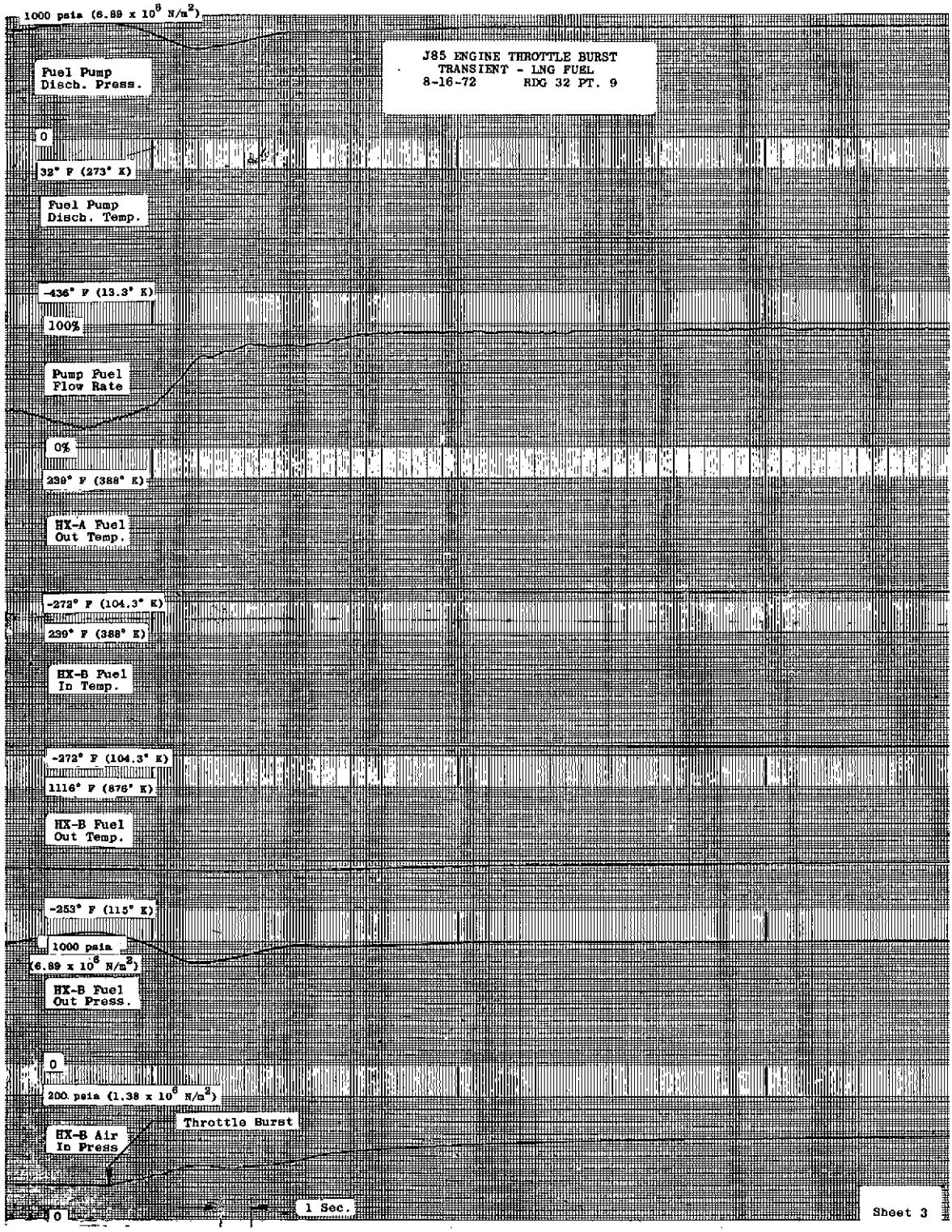


Figure 46. Engine Throttle Burst Transient for Methane Fuel System Using Liquid Natural Gas, Demonstration Run (Concluded).

It was determined during the run that the resistance temperature detector used to sense metering valve fuel entrance temperature was developing a short-to-ground failure. Near the end of the run this failure was generating excessive error in the metered fuel flow computation. Since the sensor could not be physically removed, it was decoupled and replaced with a fixed resistance simulating the average metering valve fuel temperature encountered in accelerations from idle to 100% speed. Throttle-bursts made near the end of the run were performed with this simulated temperature output.

Metering valve flow rate computations obtained with the failing temperature detector have been corrected for steady-state points based on the temperature ($T_7$) measured at the entrance to the pressure regulating valve immediately upstream of the metering valve. These corrected fuel flow rates are compared to the Cosmodyne calibration of the system fuel pump in Figure 47. Flow measured by venturi at the fuel pump discharge is also compared.

Exhaust gas emission samples were taken during the engine run and analysis was performed after completion of the test. A gas chromatograph was used to analyze collected samples for CO, $CO_2$, and unburned $CH_4$. A modified Saltzman analysis was performed to analyze for $NO_x$. The results of these analyses are plotted in Figures 48 through 52 as a function of both engine speed and combustor inlet temperature.

## $LH_2$ Flow and Thermal Calibrations

As a result of the generally successful operation of the system and J85 engine using LNG fuel, verbal permission was obtained from NASA to convert the equipment and engine to hydrogen configuration. The engine was returned to GE Lynn for disassembly and installation of $H_2$ fuel injectors.

A disassembly of the Cosmodyne fuel pump and drive motor assembly was made in order to convert the pump stroke to hydrogen requirements. The heat exchanger and valving of the fuel conditioning package were converted to the hydrogen configuration. An $LH_2$ storage trailer loaned by NASA was installed to replace the $CH_4$ supply trailer.

Two attempts to initiate $LH_2$ flow calibration in October 1972 were made, but both were aborted by overboard fuel leaks at the fuel pump inlet bayonet connector. The pump diameter mating the radial seal on the bayonet tip was found to be over print by 0.021 inch. The leak was stopped by building up the seal groove diameter at the radial seal to effect more positive squeeze.

A system flow and thermal calibration test using $LH_2$ was performed on November 8, 1972. The overboard leakage previously encountered was not experienced.

System operation during the calibration test was normal except that fuel pump $LH_2$ delivery was lower than expected, requiring that the pump be operated at higher than normal speeds to achieve desired metering valve flow rates. Maximum system fuel flow of only 70% could be obtained with the pump speed operating at 120% of rated. Thermal data were taken at the lower fuel flow points. The air-to-fuel heat exchanger performed satisfactorily, and a 30

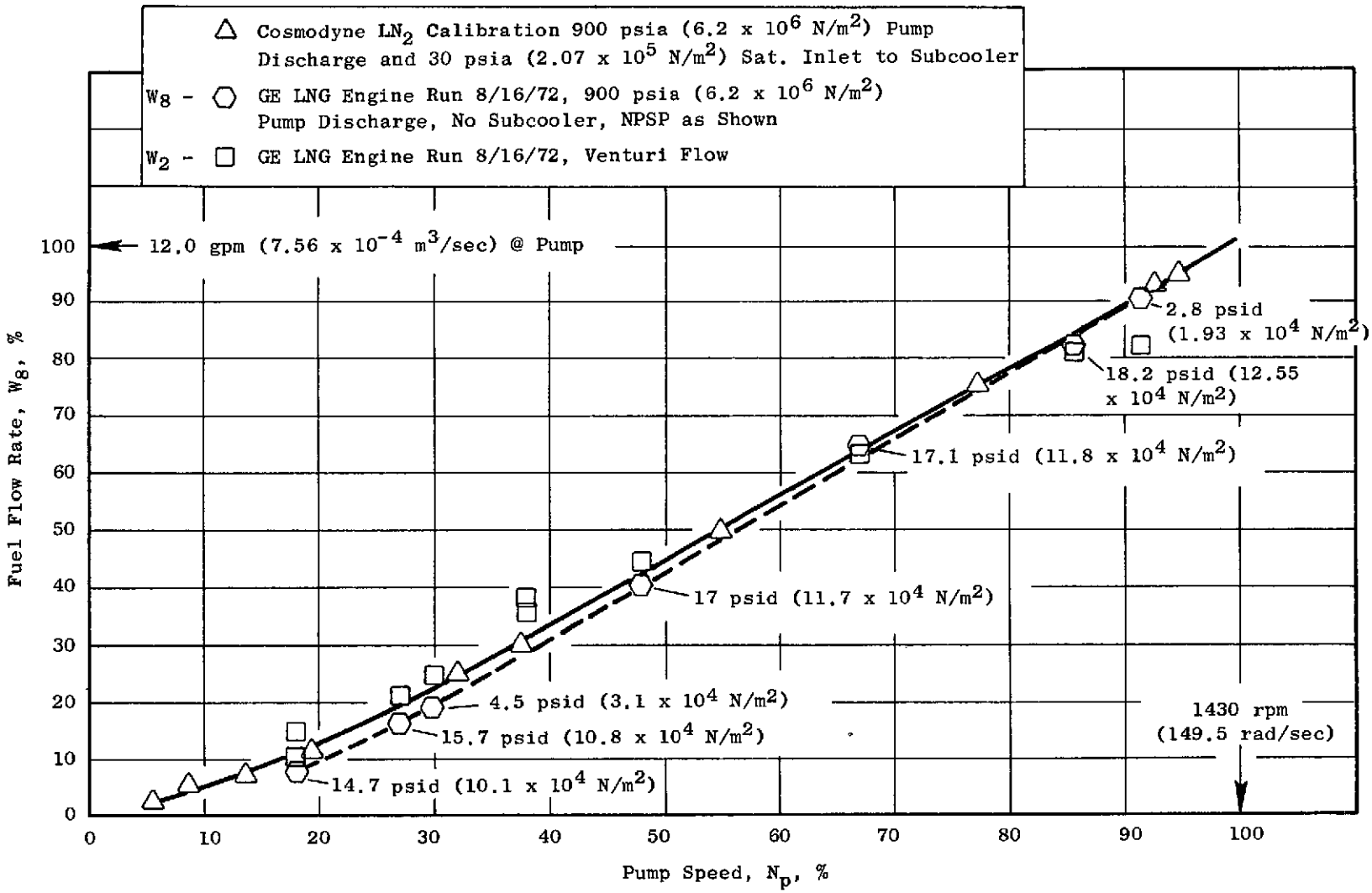


Figure 47. Methane Fuel Pump Performance, Corrected Fuel Flow Rates Compared to Cosmodyne Calibration Data.

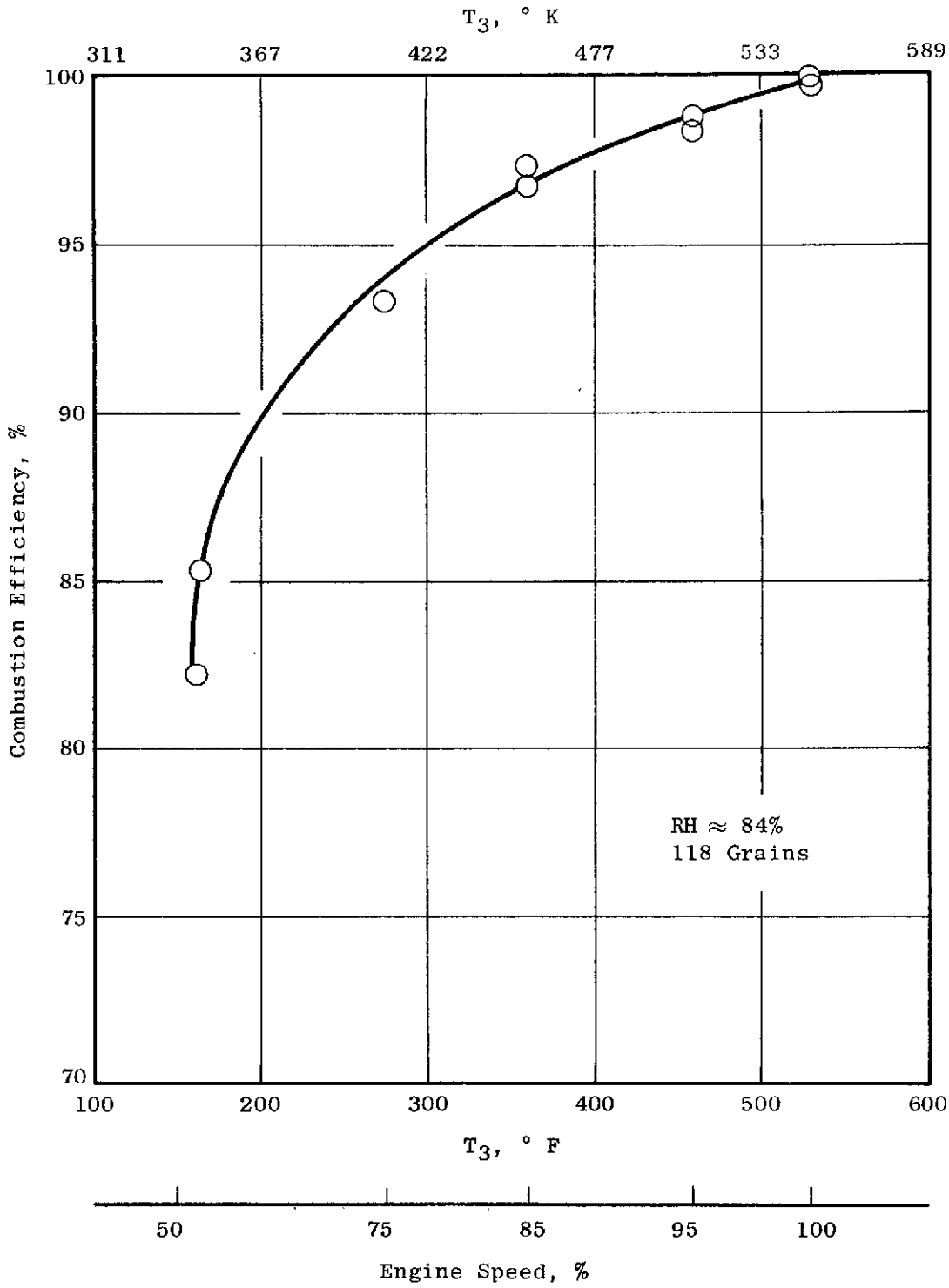


Figure 48. Methane Fueled J85 Engine Combustion Efficiency.

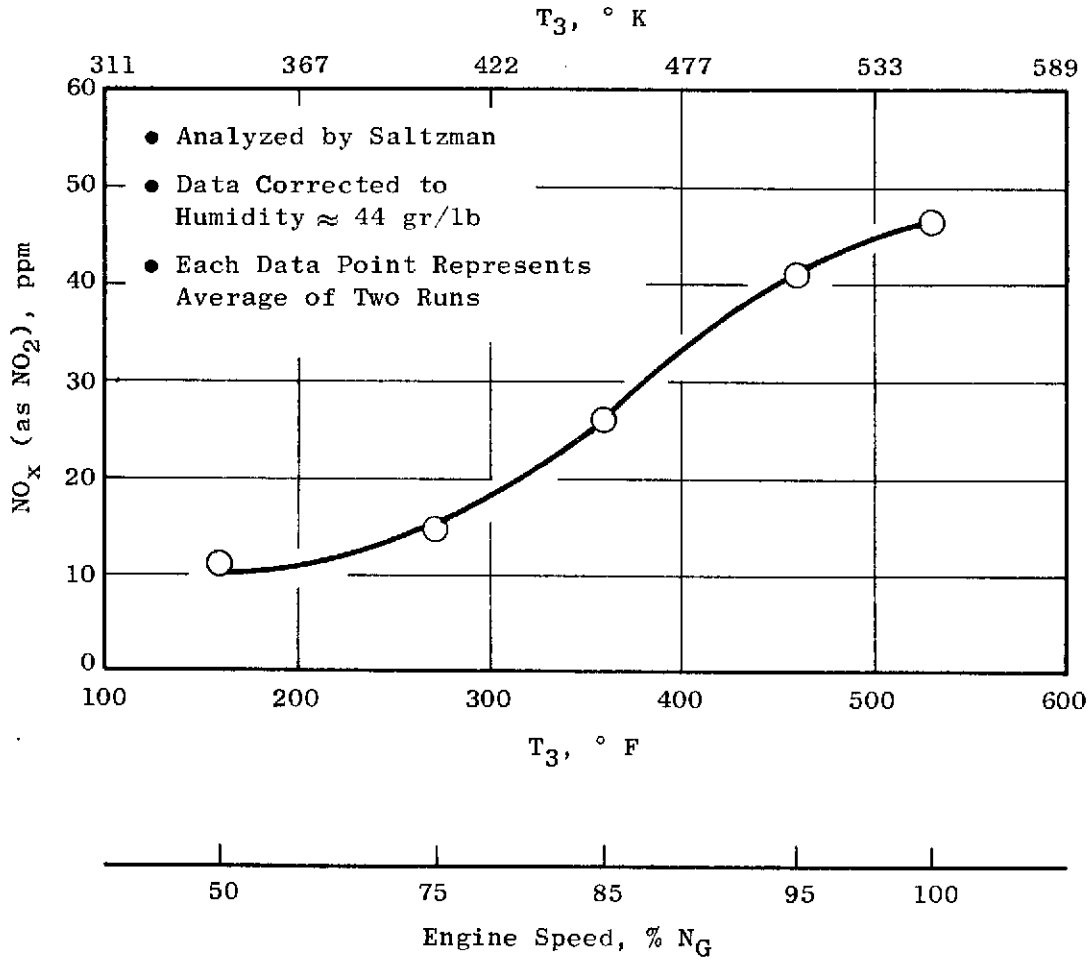


Figure 49. Methane Fueled J85 Engine $NO_x$ Emissions Analysis.

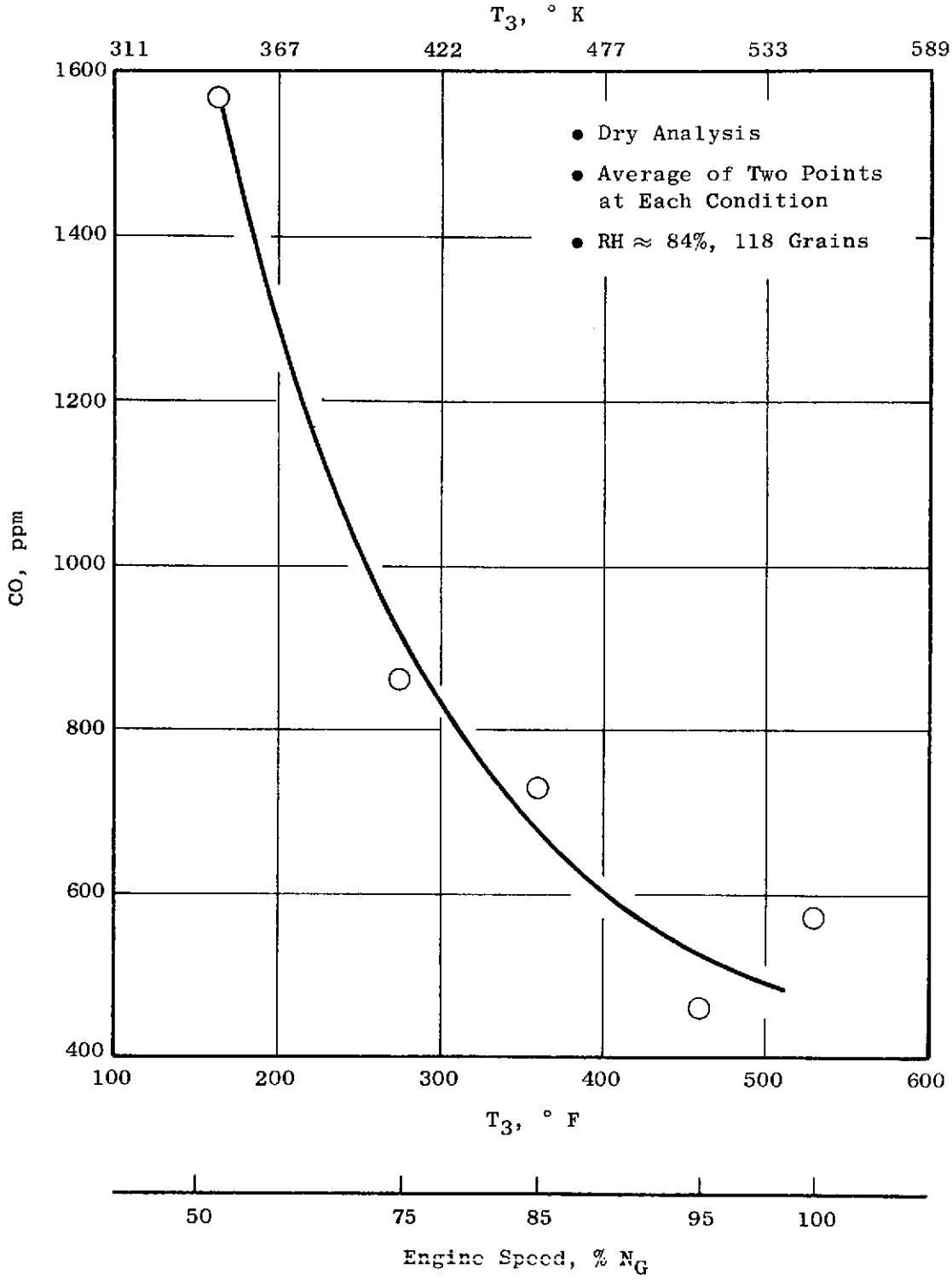


Figure 50. Methane Fueled J85 Engine CO Emissions Analysis.

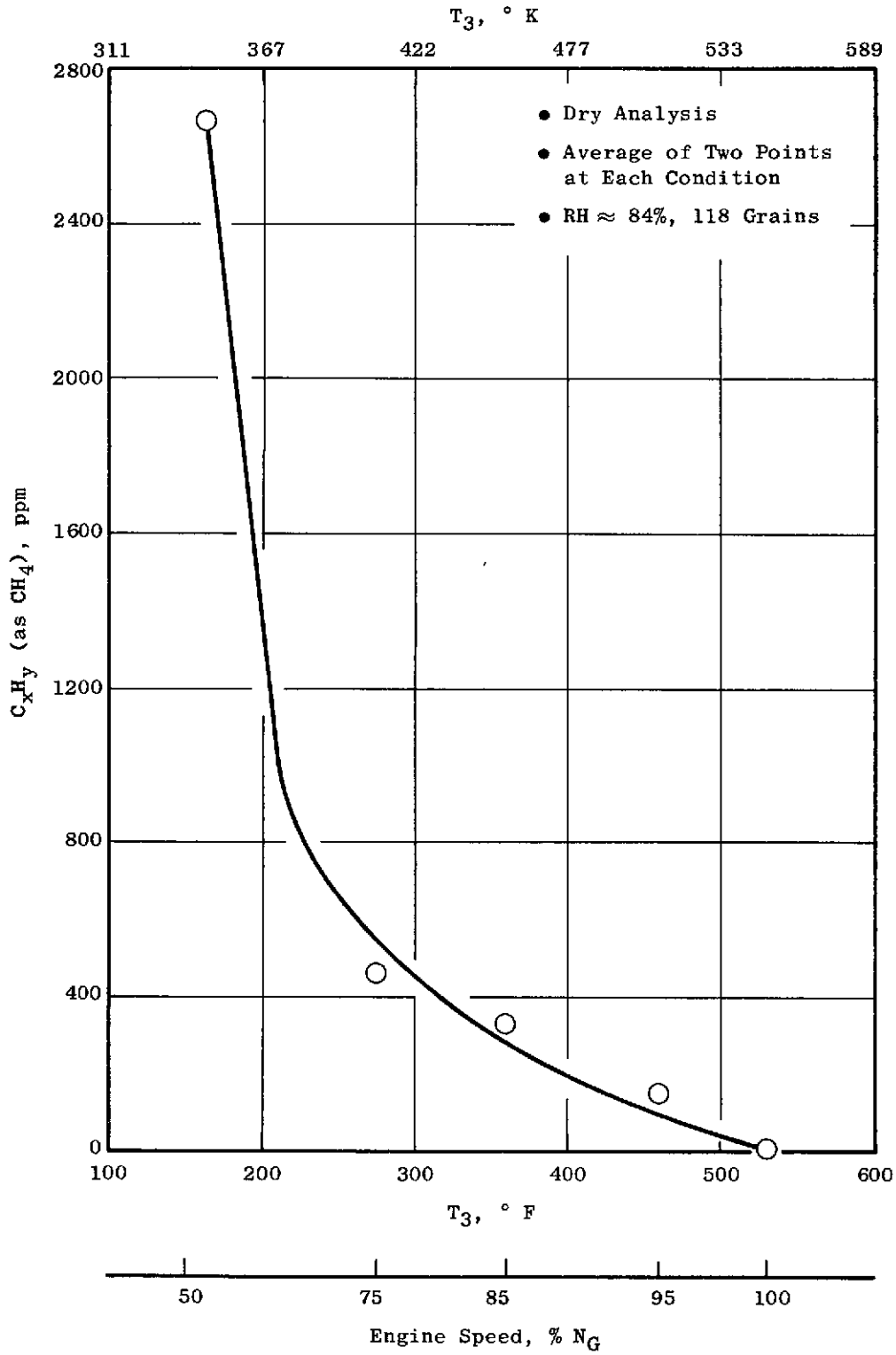


Figure 51. Methane Fueled J85 Engine $CH_4$ Emissions Analysis.

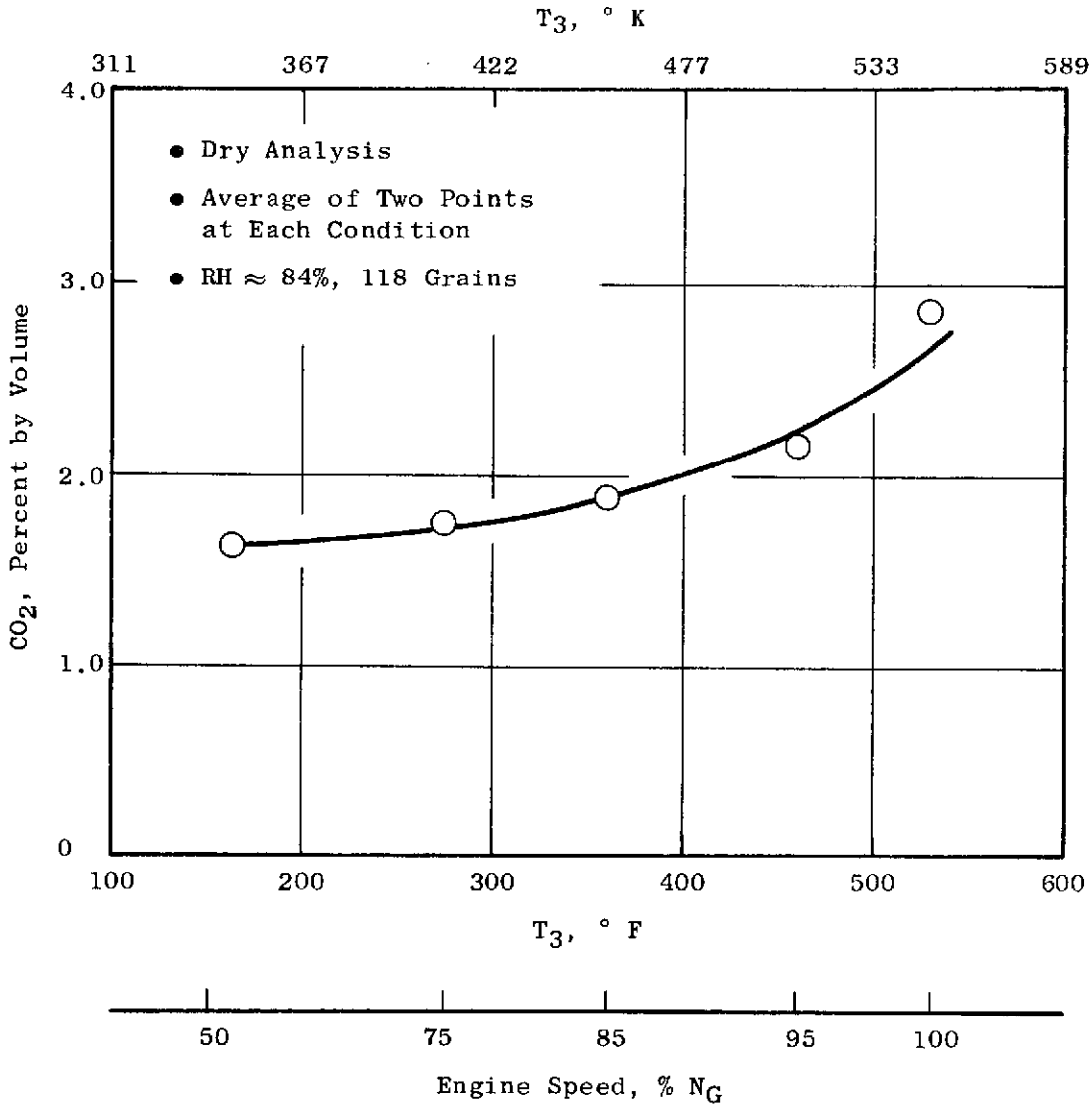


Figure 52. Methane Fueled J85 Engine $CO_2$ Emissions Analysis.

minute non-icing run was successfully completed at the Altitude Idle fuel flow point. Thermal performance data are plotted in Figure 53. Table XVIII lists heat exchanger parameters recorded during the 30 minute icing run.

To investigate possible causes of low fuel pump delivery, the system was instrumented with an orifice plate to measure piston seal vent cavity flow to the exhaust stack. Another calibration run was performed on November 14, 1972. The fuel pump delivery was again low as a function of pump speed, and substantial piston seal cavity leakage to the exhaust stack was indicated by the orifice measurement. Figure 54 illustrates the pump flows measured in comparison to the Cosmodyne calibration originally performed using liquid nitrogen. It appeared that piston seal leakage accounted for nearly all of the reduction in $LH_2$ delivery.

The pump was then disassembled for piston seal investigation. The piston ring seals, cylinder liner crush washers, and rod seal cartidges were all intact. The following observations were made:

- Rod seal cartridges were not tight, and the seal lip inner diameter was worn 0.007 in. ($1.78 \times 10^{-4}$ M) oversize on the primary Teflon seal scraper. Also, traces of hydraulic oil were found at the piston ring seals. The oil could have drained to this region during vertical handling.

- Piston ring seals were not apparently worn and exhibited normal radial compression loading.

- The cylinder liner crush washer seals were adequately deformed and loaded, but had been reused after the previous disassembly.

No positive conclusion could be drawn as to what caused the apparent excessive piston leakage. Discussion with the piston ring seal vendor (Shamban, Inc.) led to a recommendation that the wave washer used underneath the Teflon piston seal rings be changed from 0.003 in. ($0.762 \times 10^{-4}$ m) stock thickness to 0.005 in. ($1.27 \times 10^{-4}$ m) stock to increase radial spring loading. The pump was rebuilt with all new seal elements, including the stronger wave washer under the piston ring seals.

The pump was reinstalled in the system, and preparations were completed for a run of the system and J85 engine.

$LH_2$ Engine Run

A test run using $LH_2$ fuel was conducted on the system and J85 engine on December 8, 1972.

The system and J85 engine operated as expected except that the fuel pump $LH_2$ delivery was again low, repeating the values of fuel flow that had been previously observed as a function of pump speed. Sufficient $LH_2$ flow to maintain system regulating pressures up to 88% engine speed was available. System data and engine exhaust emission samples were taken at 50%, 75%, and

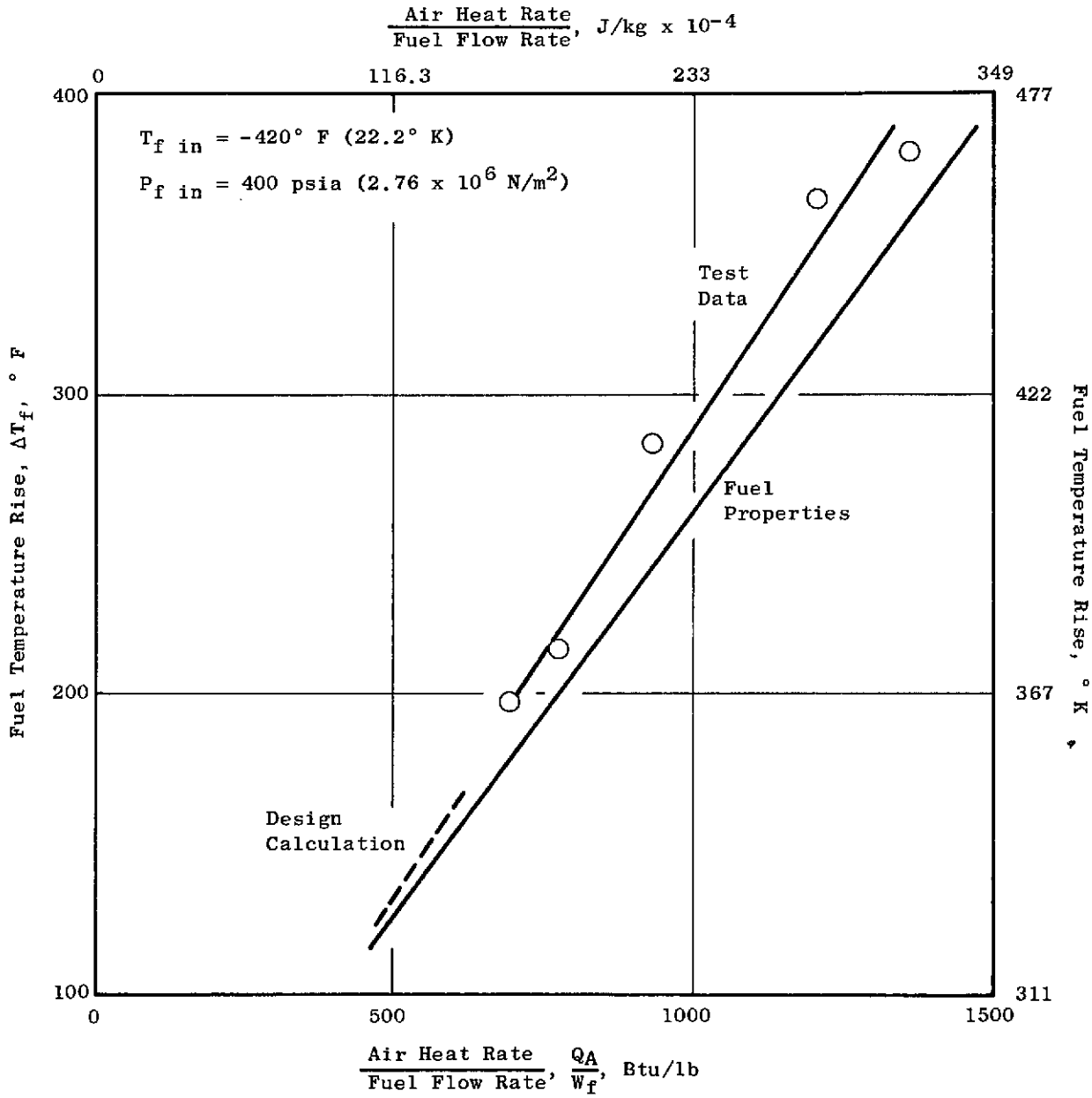


Figure 53. Air-to-Hydrogen Heat Exchanger Performance.

Table XVIII. Heat Exchanger B Icing Run $LH_2$ Fuel Altitude Idle Flow Condition.

| Fuel Side | | | | | | | | | | |
|---|---|---|---|---|---|---|---|---|---|---|
| Time Min. | $T_2$ Fuel In ° F | $T_2$ Fuel In (°K) | $T_6$* Fuel Out °F | $T_6$* Fuel Out (°K) | $T_7$* Mixed Fuel Out °F | $T_7$* Mixed Fuel Out (°K) | $W_8$ Fuel Flow pps | $W_8$ Fuel Flow (kg/sec) | $P_2$ Fuel Press psia | $P_2$ Fuel Press ($N/M^2 \times 10^{-6}$) |
| 0 | -417 | (23.9) | 159.6 | (344.0) | -206.6 | (141.0) | 0.030 | (0.0136) | 391.6 | (2.70) |
| 10 | -417 | (23.9) | 158.4 | (343.5) | -202.3 | (143.0) | 0.030 | (0.0136) | 393.9 | (2.71) |
| 20 | -416.7 | (24.0) | 157.2 | (343.0) | -203.7 | (142.5) | 0.030 | (0.0136) | 391.6 | (2.70) |
| 30 | -417.1 | (23.8) | 155.9 | (342.0) | -202.3 | (143.0) | 0.030 | (0.0136) | 392.8 | (2.705) |
| Air Side | | | | | | | | | | |
| Time Min. | $T_{13}$ Air In ° F | $T_{13}$ Air In (°K) | $T_{14}$ Air Out °F | $T_{14}$ Air Out (°K) | $W_A$ Air Flow pps | $W_A$ Air Flow (Kg/sec) | $P_{13}$ Air In psia | $P_{13}$ Air In ($N/M^2 \times 10^{-5}$) | | |
| 0 | 439.2 | (500) | 194.7 | (363) | 0.405 | (0.184) | 41.4 | (2.85) | | |
| 10 | 425.9 | (492) | 186.3 | (359) | 0.398 | (0.181) | 37.1 | (2,56) | | |
| 20 | 442.5 | (501) | 183,7 | (358) | 0.398 | (0.181) | 41.0 | (2.83) | | |
| 30 | 431.0 | (495) | 182.2 | (357) | 0.357 | (0.162) | 57.1 | (3.94) | | |

*Approximately 50% fuel bypass.

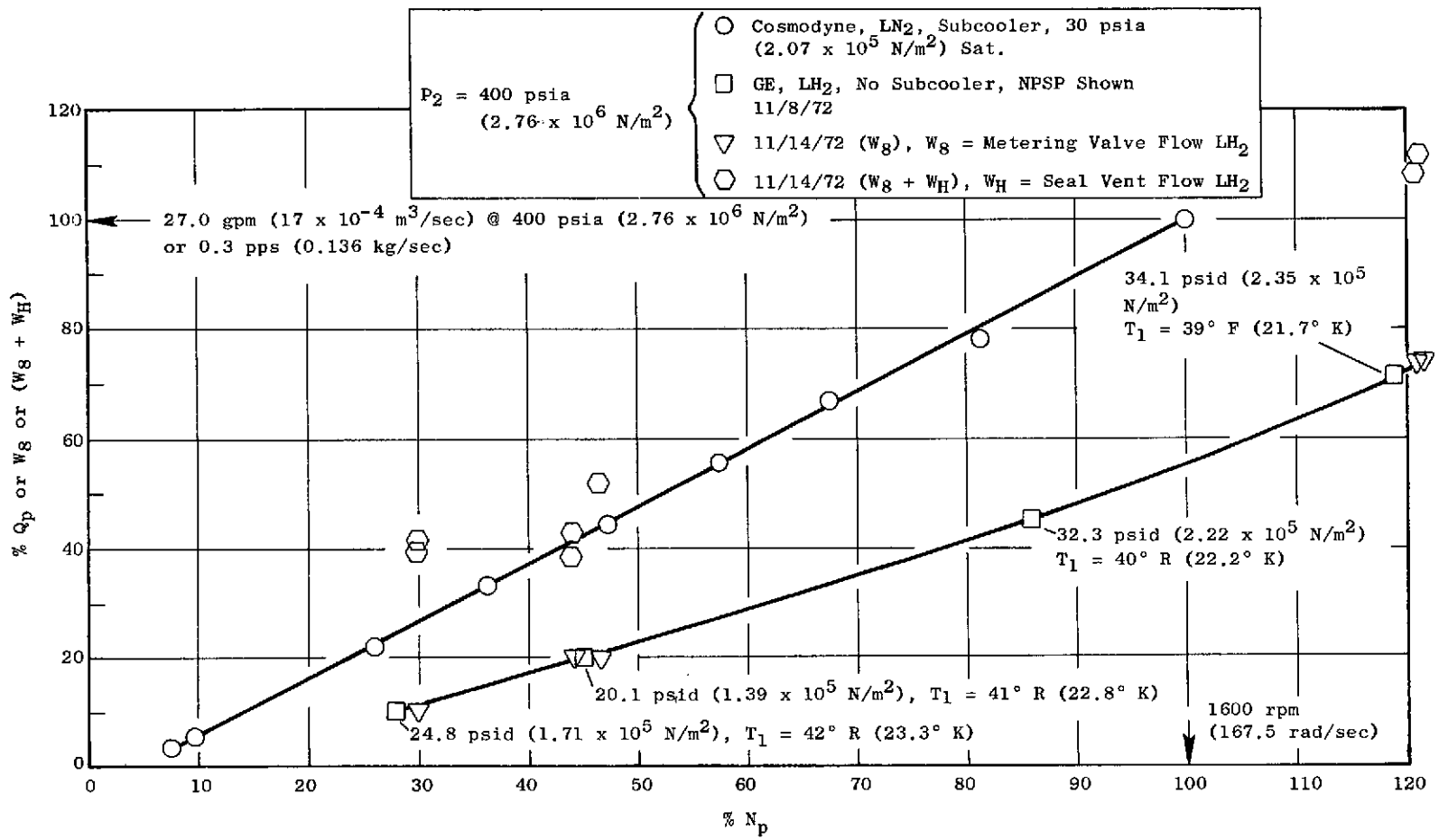


Figure 54. Hydrogen Fuel Pump Check-Out Data Compared to Original Liquid Nitrogen Calibration Data.

85% engine speed points. Several part-speed throttle-burst accelerations from idle speed to 85% engine speed were made successfully. The shortest acceleration time obtained between idle and 85% speed points was 13 seconds without schedule optimization. Figure 55 illustrates the time traces of significant parameters recorded.

Although the fuel pump piston seal vent cavity leakage again indicated substantial quantities on the order of 0.05 to 0.06 lb/sec. (0.0227 to 0.0272 Kg/sec.), the measurement was suspected to be erroneously high in view of the continued low pump delivery flow. Pump delivery measured both by the metered flow and a pump discharge venturi are compared in Figure 56. Further bench and disassembly investigation of the fuel pump was initiated.

A gaseous nitrogen pressure check of the fuel pump ball discharge valve assembly indicated that 200 psid ($1.38 \times 10^{-6}$ N/M$^2$) back pressure was required to close the No. 2 piston check valve at room temperature. The ball check valve assembly, which had not previously been removed, was disassembled. The No. 2 piston valve ball was found to be severely worn and out of round. Substantial quantities of wear particle deposition were seen on the mating valve seat and guide bore. A second ball also showed a dull finish and the beginnings of wear. The ball guide bore diameters were checked and were slightly under print.

Discussion of the observed ball wear with Cosmodyne revealed that two experimental balls made of 300 series stainless using a proprietary coating had been included in the assembly in place of the intended 440C balls. The two 300 series balls exhibited wear, while the three 440C balls showed no distress. It was concluded that the severely worn No. 2 ball had stuck in the open position at $LH_2$ temperatures, causing the effective pump delivery flow to be reduced 40% below the normal value delivered by five pistons. Cosmodyne provided a new discharge ball valve assembly containing five 440C balls with guide bore clearance increased slightly over the original design.

The limited exhaust gas emissions samples taken during the December engine run yielded $NO_x$ concentrations as plotted in Figure 57. The Envirometrics analyzer used did not recalibrate normally at the end of the run. Subsequently, a back-to-back reference run was made with a chemiluminescence analyzer and the Envirometrics analyzer sampling exhaust gases from a hydrogen-air torch igniter. The torch calibration yielded $NO_x$ concentrations for the Envirometrics analyzer which were approximately 30% lower than the values shown by the chemiluminescence analyzer.

An $LH_2$ test run of the system and J85 engine was attempted on February 8, 1973. The fuel pump contained a new discharge ball valve assembly.

Several occurrences of failure to obtain pump rotation after chilldown were experienced. Chilldown was finally achieved by continuous engine motoring and pump rotation. Starting fuel flows were set with subnormal system metering pressure, since the fuel pump delivery and speed were limited by available engine motoring speed and hydraulic flow. The pump conditions obtained yielded 7% rated fuel delivery at 20% rated pump speed and 125 psia ($0.862 \times 10^{-6}$ N/M$^2$) metering pressure. This delivery point aligns with pump flow vs speed calibra-

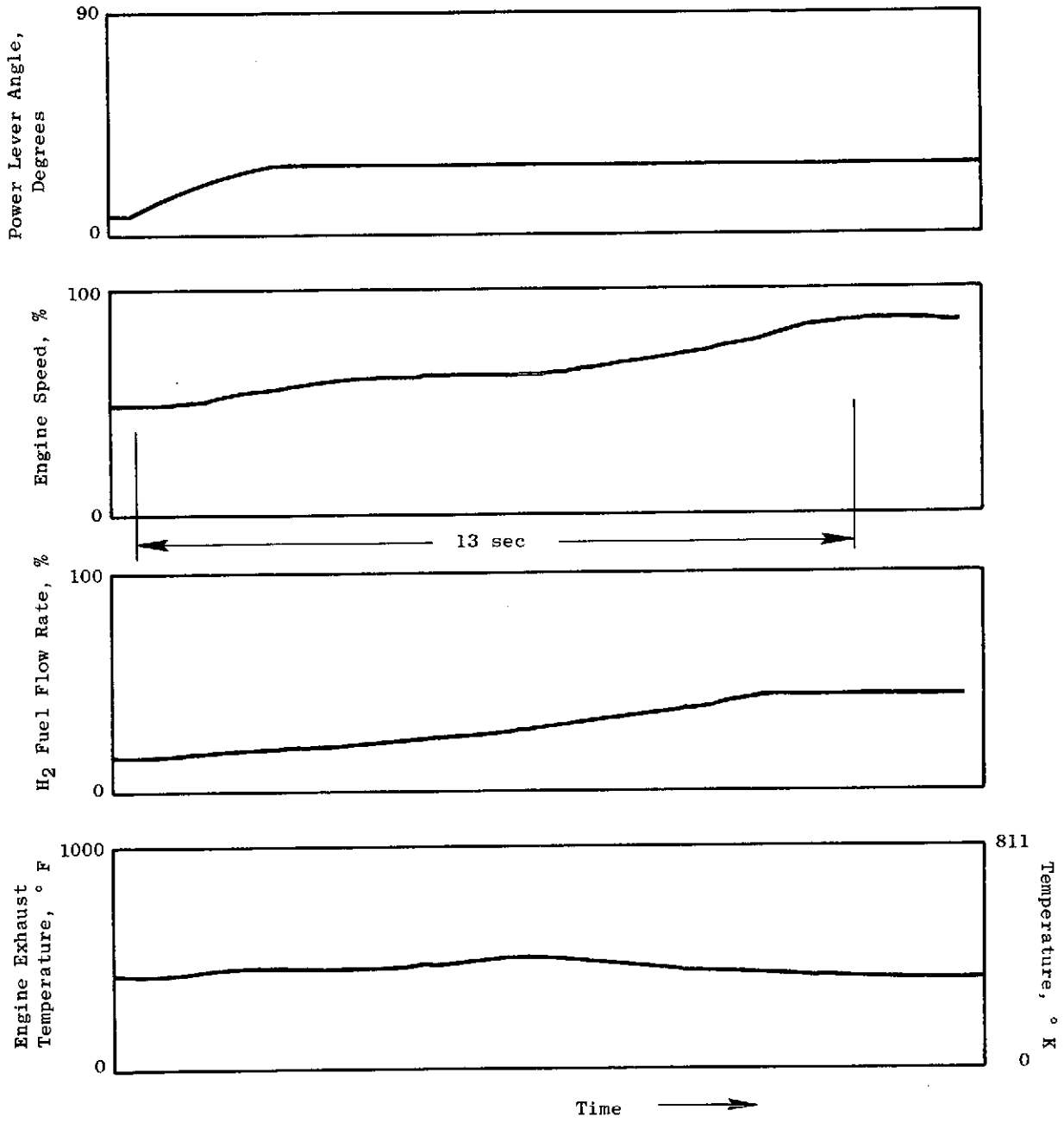


Figure 55. Engine Throttle Burst Time Traces for Hydrogen Fuel System.

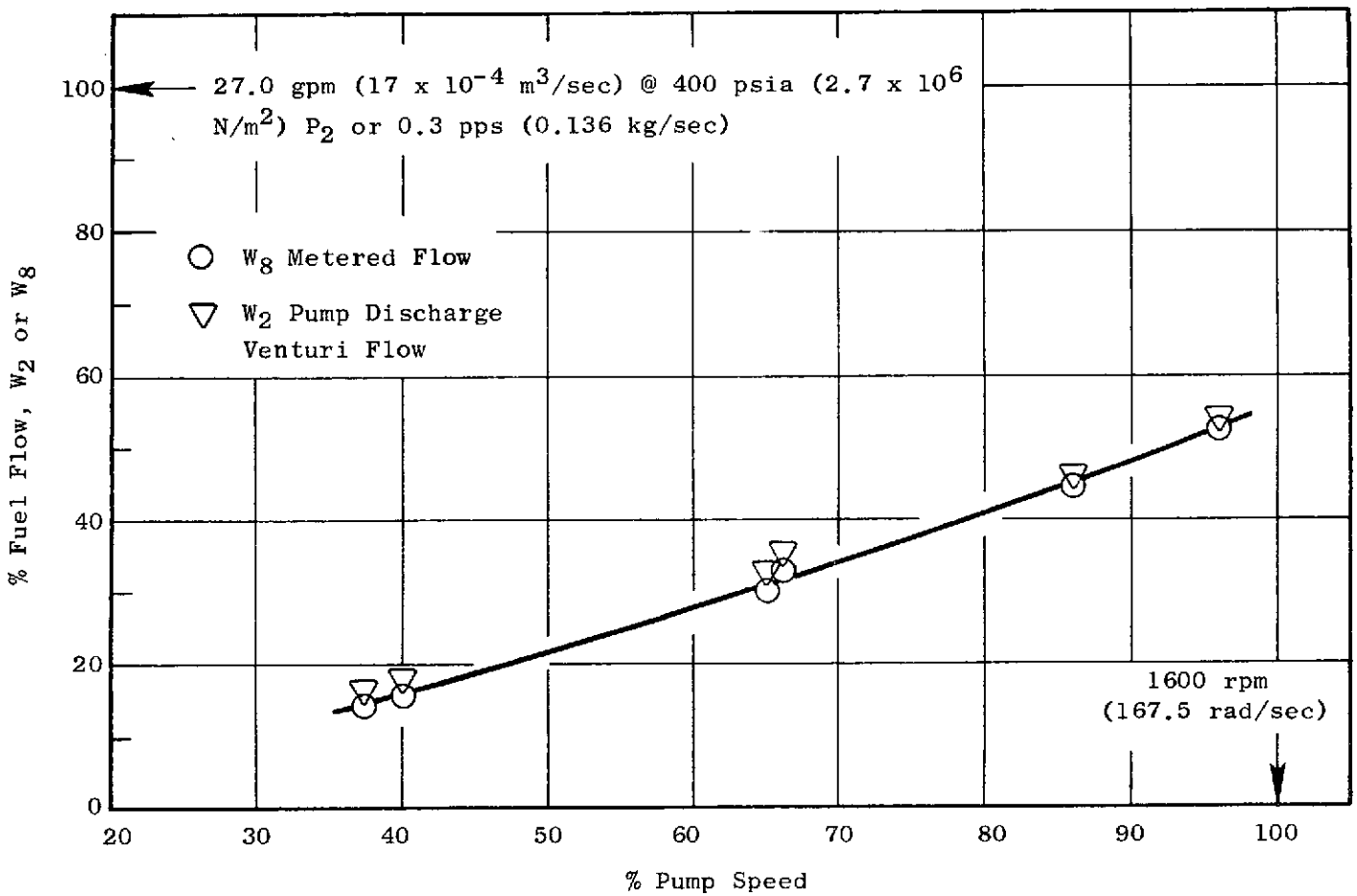


Figure 56. Hydrogen Fuel Pump Flow Correlation, Comparison of Metered Flow with Pump Discharge Venturi Flow.

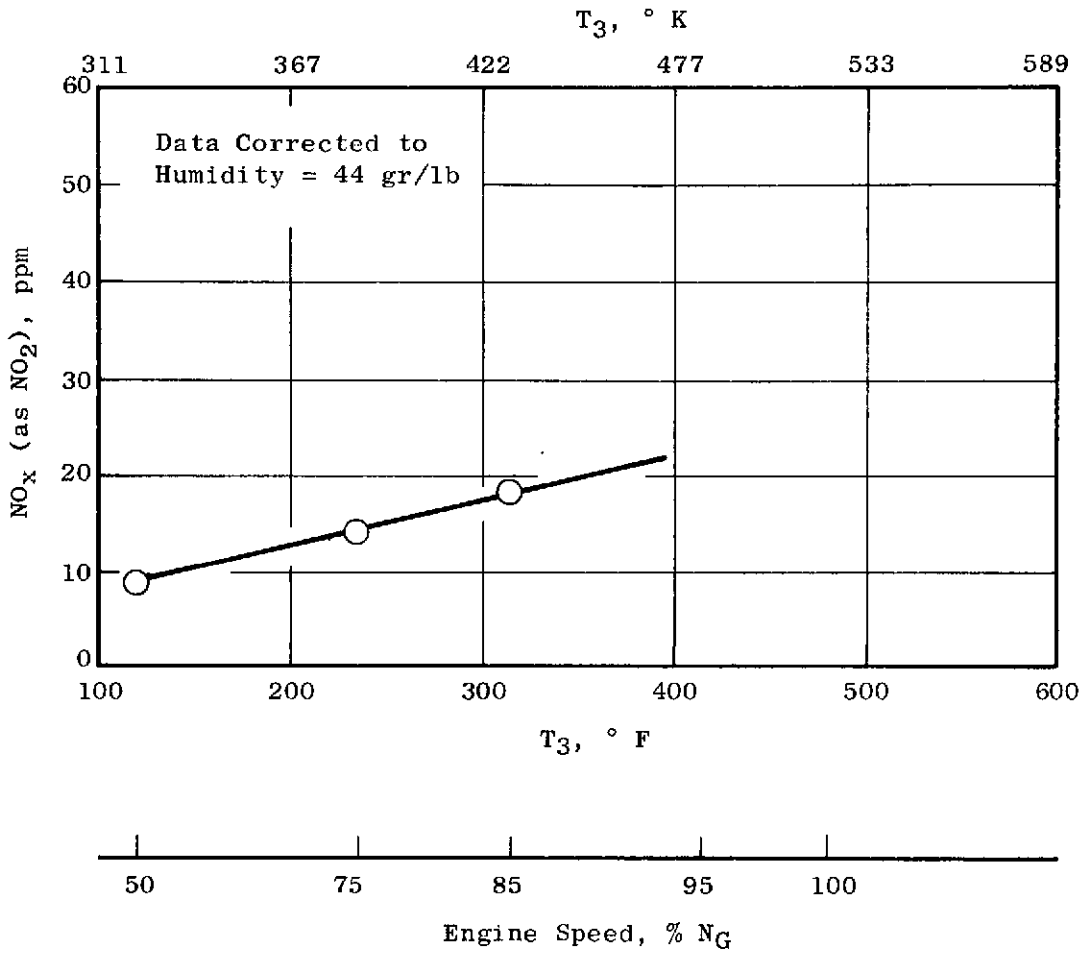


Figure 57. Hydrogen Fueled J85 Engine $NO_x$ Emissions Analysis.

tions obtained on previous $LH_2$ runs. When engine light-off was attempted, the system vent valve was found to be frozen in the open position, preventing diversion of fuel flow to the engine.

The run was aborted due to the frozen vent valve. Later investigation after warm-up revealed the presence of water in the valve body and discharge line. Steam condensate from the system vent stack had backed up into the valve during the lengthy down period preceding the run. A procedural precaution to leave the vent valve discharge disconnected until just before system purge was instituted.

Another $LH_2$ test run of the system and J85 engine was attempted on March 15, 1973. Action was taken to prevent accumulation of steam condensate into the system fuel vent valve which had frozen during the February test run, preventing engine ignition.

Chilldown of the system on $LH_2$ was begun with the fuel pump motor rotating and supplied from the system auxiliary hydraulic supply. As priming temperature was reached at the fuel pump inlet, discharge pressure buildup was initiated. The pump stopped rotation at this point, and could not be restarted with 3000 psig ($2.07 \times 10^7$ $N/M^2$) hydraulic supply. Again the engine run was aborted without obtaining data.

Subsequent experimentation by hand cranking the pump motor showed the motor initially frozen tight, but it was eventually worked free with abnormally high cranking torque. Rotation under hydraulic pressure was then restored, but the pump displayed unusual internal noises.

Disassembly of the fuel pump and motor was performed to investigate the sources of abnormal noise. Several failed parts were found in the hydraulic motor section:

1) Two return spacers which form one side of a spherical joint connecting the piston rod to the nutating plate connecting link were fractured. The spacers were located on No. 2 and No. 5 piston locations.

2) No. 5 spherical joint which connects the nutating plate to the rod connecting link was scored and pounded, exhibiting excess clearance.

3) The anti-rotation pin which retains the nutating plate was sheared.

4) Numerous nicks and scratches on other motor parts caused by debris were noted.

Since the failed return spacers normally carry no load and were located on the same two pistons for which damaged discharge ball valves had been discovered during a teardown in December 1972, it is believed that the failures were related to the earlier ball valve problems. Under conditions where sticking of

the discharge ball valves occurs, an abnormal compressive load can be applied to the return spacers because of the presence of $LH_2$ piston pressure remaining after piston hydraulic pressure is removed by the timing valve. These compressive loads on the spacers are believed to have initiated the spacer failures, permitting subsequent impact loading of the connecting links to the nutating plate and subsequent failure of the anti-rotation pin due to impacting tangential loads on the nutating plate.

The pump assembly was returned to Cosmodyne for assessment of repair and improvement action required.

Since the testing funds available to the program had been depleted by the various J85 engine test attempts, and since the $LH_2$ fuel pump required obviously significant repair and improvement effort, NASA directed that further test effort be terminated and the program closed out with the partially completed $LH_2$ engine test status existing as of April 1973.

## DISCUSSION OF RESULTS

The steady-state and transient data recorded during the J85 engine runs on both liquid natural gas and liquid hydrogen fuel demonstrate the basic workability of the fuel delivery system which was designed for the program. Although deficient fuel pump delivery limited the maximum engine speed attained with liquid hydrogen to 88% of rated, the stable part speed operation indicates that operation at 100% flows and engine speeds should pose no particular difficulty if pump delivery were increased. The system modeling results obtained from the analytical design phase of the program also confirm that the hydrogen configuration of the system behaves much like the methane configuration for both transient and steady-state operation to 100% engine speed.

The gaseous flow metering and computation circuits performed generally as expected with both fuels, although difficulty with failures of the resistance temperature detectors used for density correction was encountered. Correlation flow measurements using a pump discharge venturi section were made, but difficulty with inconsistency of the venturi differential pressure measurements plagued the flow and thermal calibration tests. Correlation data were taken during engine runs with both fuels, however. The venturi flow data ($W_2$) measured during the liquid natural gas engine run of August 16, 1972 (Figure 47) roughly confirms the $W_8$ metered flow computation. The metered flow data also correlate well with the Cosmodyne pump calibration performed on liquid nitrogen. The venturi data indicate more scatter and unrepeatability than the $W_8$ metered flow data. Venturi correlation measurements taken during the liquid hydrogen engine run of December 8, 1972 (Figure 56) match the $W_8$ metered flow computation within +3% of rated flow for the limited data taken. Evidently the gaseous metering computation was performing within the predicted flow measurement accuracy for this run. The $W_8$ metered flow measurements on liquid hydrogen were also consistent from one test run to another as indicated by Figures 54 and 56.

Performance of the air-to-fuel heat exchangers was generally satisfactory in that predicted heat transfer rates were met or exceeded at nearly all operating conditions, and no air-side icing occurred as judged by stability of the air exit temperatures during a 30 minute test period. The air-to-methane heat transfer data tabulated in Table XVII show quite close correlation with predicted parameter values at most operating conditions; the notable departures from predicted values are seen in the cruise and deceleration operating conditions where the air-side heat rates and temperature drops substantially exceed predictions. These performance results were undoubtedly influenced by the nonoperational oil-to-fuel heat exchanger which would normally be heating the fuel upstream of Heat Exchanger B. Fuel entrance temperatures to Heat Exchanger B were significantly lower than predicted at the cruise and deceleration conditions as a result of Heat Exchanger A being bypassed. Air-side pressure drops, which include flow distributor slots, were well within predicted values except at the climb point. Data for Heat Exchanger B in the hydrogen system is shown in Figure 53. With this exchanger, heat rates and fuel temperature changes exceed predictions at all points tested. Apparently the double-tube fuel-side arrangement used in the design was more conductive than expected. However, no evidence of air-side icing was noted.

The tendency of the oil-to-methane heat exchanger to freeze repeatedly at the higher values of fuel flow indicates that design assumptions made as to heat transfer properties of the fluids were significantly in error. The SF8150 type oil used was chosen for its advantageously low pour point at -120° F (189° K); however, only room temperature viscosity data were available and the viscosity data were extrapolated for higher and lower temperatures in keeping with the known data for other silicone-base oils. The viscosity assumption may have resulted in significant errors in calculating oil-side film conduction coefficients. These results suggest that any future design of a cryogenic-to-oil heat exchanger should be based on complete data for oil properties if freezing is to be avoided. Variations in the tube design arrangement such as the double-walled fuel tube used in the air-to-hydrogen heat exchanger might also be employed to maintain a non-freezing tube wall temperature.

Fuel pump delivery performance, while quite satisfactory when used with the liquid natural gas system, was disappointing when operated with liquid hydrogen. The delivery deficiency is believed to be associated with leakage losses at the pump discharge rather than with intake or filling conditions. As shown in Figure 54, the low delivery was obtained with net positive suction pressures ranging from 20 to 35 psid ($1.38 \times 10^5$ to $2.41 \times 10^5$ $N/M^2$). Variation of the suction pressures to levels ranging from 20 to 40 psid ($1.38 \times 10^5$ to $2.76 \times 10^5$ $N/M^2$) while operating at a steady-state flow condition did not effect any significant change of delivery. Also, the delivery characteristic for liquid hydrogen indicates a slightly increasing slope as a function of increasing pump speed while decreasing slope would be expected with increasing piston velocity if intake filling were limiting the delivery. Both piston seal ring leakage and discharge check valve hang-up or leakage are believed to contribute to the delivery losses, although separate attempts to improve these areas with parts replacement were unsuccessful. Redesign of the piston ring seal configuration and improvement of the discharge ball valve seating are believed to be required to improve the liquid hydrogen delivery performance.

Exhaust emissions data obtained when running the J85 engine on the two fuels are of limited value to compare the fuels because of the low engine power level at which hydrogen data were obtained and the questionable accuracy of the Envirometrics analyzer measurement of $NO_x$ concentrations taken with hydrogen fuel. If the hydrogen $NO_x$ measurement at 85% engine speed (Figure 57) is corrected upward by 30% based on the hydrogen torch calibration of the Envirometrics analyzer made after the run, the resulting concentration of $NO_x$ compares quite closely to the $NO_x$ concentration of 26 parts per million (Figure 49) obtained with liquid natural gas at 85% engine speed. The hydrogen emissions are, of course, free of the CO, $CO_2$, and unburned $CH_4$ constituents obtained with the liquid natural gas fuel.

## CONCLUSIONS

Use of liquid hydrogen or liquid natural gas as fuel for airbreathing propulsion engines offers the potential of using the fuel heat sink both for an engine air coolant, with implied cycle performance benefits, and as an aircraft system coolant. The use of this available heat sink requires gasification of the liquid fuel flow. Questions were raised as to whether a suitable nonfreezing thermal design of heat exchangers could be accomplished and whether a stable, responsive pumping and fuel control system incorporating the gasifier could be accomplished. The analysis, design, and test demonstration of such a system performed in this program supports the following conclusions:

1. A control system arrangement consisting of liquid fuel pumping, gasification of pump discharge flow at supercritical pressure, and gaseous metering which excludes the gasifier from the engine flow control loop can be made acceptably stable and responsive for operation of a turbojet engine using either liquid natural gas or liquid hydrogen fuel.

2. Air-to-fuel heat exchangers for either liquid natural gas or liquid hydrogen fuel which fully gasify the engine fuel flow without air-side freezing can be accomplished. A curved tube core shape is feasible and compatible for mounting within an engine structural shell.

3. Oil-to-fuel heat exchanger design using a single walled tube arrangement was not successful in avoiding oil freeze-up at all system fuel flow levels; further design development would be required to accomplish a nonfreezing oil heat exchanger for either liquid natural gas or liquid hydrogen fuel.

4. Variable speed displacement pumping of both liquid natural gas and liquid hydrogen to supercritical pressures is feasible, and pump delivery turndown ratios up to 20/1 can be provided. Further design development to assure adequate pump life and liquid hydrogen delivery performance are required.

5. No comprehensive conclusions regarding comparative exhaust gas emissions of liquid natural gas and liquid hydrogen fuels in a J85 engine can be made because of the limited power levels at which data were taken, and because of the questionable accuracy of the nitrous oxide concentrations measured with the Envirometrics analyzer during the liquid hydrogen run.

## APPENDIX A

## DEFINITION OF SYMBOLS FOR ENGINE MODEL

| Symbol | Definition | Units |
|---|---|---|
| Z | Compressor Stall Margin Parameter | none |
| $Q_c$ | Compressor Torque | ft-lb |
| $T_{3e}$ | Compressor Discharge Temperature | °R |
| $W_{3e}$ | Compressor Discharge Airflow | lb/sec |
| $N_g$ | Engine Rotor Speed | rpm |
| $P_{3e}$ | Compressor Discharge Pressure | psia |
| $P_{2e}$ | Compressor Inlet Pressure | psia |
| $\Delta H_c$ | Compressor Drive Power | Btu/sec |
| $W_{2e}$ | Compressor Inlet Airflow | lb/sec |
| $H_{2e}$ | Compressor Inlet Air Enthalpy | Btu/lb |
| $H_{3e}$ | Compressor Discharge Air Enthalpy | Btu/lb |
| J | Energy Conversion Factor | ft-lb/BTU |
| $T_{2e}$ | Compressor Inlet Air Temperature | °R |
| Cp | Specific Heat of Air at Constant Pressure | Btu/lb-°R |
| $W_{3.0e}$ | Compressor Discharge Airflow after Leakage | lb/sec |
| $W_{4e}$ | Turbine Inlet Airflow | lb/sec |
| $T_{4e}$ | Turbine Inlet Temperature | °R |
| $P_{4e}$ | Turbine Inlet Pressure | psia |
| $W_{3.1e}$ | Combustor Inlet Air Flow | lb/sec |
| $W_{Fe}$ | Engine Fuel Flow | lb/sec |
| Q | Fuel Heating Value | Btu/lb |
| $\eta_b$ | Combustion Efficiency | none |

| Symbol | Definition | Units |
|---|---|---|
| $N_b$ | Combustion Temperature Function | Btu/lb |
| $\beta_e$ | Combustor Emperical Function | none |
| $\alpha_e$ | Combustor Emperical Function | none |
| $\theta_{2e}$ | Compressor Inlet Temperature Correction Factor | none |
| $\delta_{2e}$ | Compressor Inlet Pressure Correction Factor | none |
| $\gamma$ | Specific Heat Ratio - Air | none |
| $M_{E3.1}$ | Combustor Inlet Mach Number | none |
| $W_{be}$ | Compressor Discharge Bleed Airflow | lb/sec |
| $T_{5e}$ | Turbine Discharge Temperature | °R |
| $Q_T$ | Turbine Torque | ft-lb |
| $P_{5e}$ | Turbine Discharge Pressure | psia |
| $\Delta H$ | Turbine Enthalpy Drop | Btu/lb |
| I | Rotor Inertia | slug-ft$^2$ |
| $W_{5e}$ | Turbine Discharge Airflow | lb/sec |
| $A_{8e}$ | Exhaust Nozzle Area | in$^2$ |
| $A_{E8e}$ | Exhaust Nozzle Effective Flow Area | in$^2$ |
| $P_{oe}$ | Exhaust Ambient Pressure | psia |
| $P_{8e}$ | Exhaust Nozzle Inlet Pressure | psia |

## APPENDIX A

## DEFINITION OF SYMBOLS FOR CONTROL SYSTEM

| Symbol | Definition | Units |
|---|---|---|
| $P_o$ | Subcooler Inlet Static Pressure | psia |
| $P_{TO}$ | Subcooler Inlet Vapor Pressure | psia |
| $P_{fi}$ or $P_1$ | Fuel Pump Inlet Static Pressure | psia |
| $P_{T1}$ | Fuel Pump Inlet Vapor Pressure | psia |
| $P_p$ or $P_{pump}$ or $P_2$ | Fuel Pump Disch. Static Pressure | psia |
| $T_2$ | Fuel Pump Disch. Temperature | °F |
| $P_3$ | HZ-A Fuel Inlet Static Pressure | psia |
| $P_4$ | HX-A Fuel Disch. Static Pressure | psia |
| $P_{fi}$ or $P_5$ | HX-B Fuel Inlet Static Pressure | psia |
| $P_{HE}$ or $P_{fo}$ or $P_6$ | HX-B Fuel Disch. Static Pressure | psia |
| $P_7$ | PRV Fuel Inlet Static Pressure | psia |
| $P_R$,$P_F$,$P_v$,$P_{Mv}$ or $P_8$ | VCV Fuel Inlet Static Pressure | psia |
| $P_{10}$ | SOV Engine Fuel Disch. Static Press. | psia |
| $W_p$ or $W_2$ | Fuel Pump Disch. Flow Rate | pps |
| $W_f$ or $W_8$ | VCV Fuel Flow Rate | pps |
| $T_4$ | HX-A Fuel Disch. Temperature | °F |
| $T_{fi}$ or $T_5$ | HX-B Fuel Inlet Temperature | °F |
| $T_{fo}$ or $T_6$ | HX-B Fuel Disch. Temperature | °F |
| $T_R$ or $T_7$ | PRV Fuel Inlet Temperature | °F |
| $T_v$ or $T_F$ or $T_8$ | VCV Fuel Inlet Temperature | °F |
| $T_{10}$ | SOV Engine Fuel Disch. Temperature | °F |
| $X_3$ | HX/A Fuel Bypass Valve Position | % |
| $X_5$ | HX/B Fuel Bypass Valve Position | % |

APPENDIX A - DEFINITION OF SYMBOLS FOR CONTROL SYSTEM (Continued)

| Symbol | Definition | Units |
|---|---|---|
| $P_{11}$ | Air Supply Static Pressure | psia |
| $P_{12}$ | Burner Inlet Static Pressure | psia |
| $P_{13}$ | HX-B Air Supply Static Pressure | psia |
| $P_{14}$ | HX-B Air Exhaust Static Pressure | psia |
| $\Delta P_{13-14}$ | HX-B Core Air Differential Pressure | psid |
| $T_{ai}$ or $T_{13}$ | HX-B Air Supply Temperature | °F |
| $T_a$ or $T_{14}$ | HX-B Air Exhaust Temperature | °F |
| $X_{14}$ | Air Flow Control Valve Position | % |
| $P_{15}$ | Hyd. Pump Inlet Pressure | psia |
| $P_{16}$ | Hyd. Pump Disch. Pressure | psia |
| $P_{17}$ | Hyd. Reservoir Pressure | psia |
| $T_{15}$ | Hyd. Pump Inlet Temperature | °F |
| $T_{16}$ | Hyd. Pump Disch. Temperature | °F |
| $T_{17}$ | Hyd. Return Temperature | °F |
| $N_p$ or $N_{pump}$ or $N_2$ | Fuel Pump Speed | rpm |
| $T_{5.1}$ | Engine Exhaust Gas Temperature | °F |
| $N_g$ | Engine Rotor Speed | rpm |
| $X_{Mv}$ or $X_8$ | VCV Position | in. |
| $A_8$ | Engine Exhaust Nozzle Area | % |
| $\alpha$ or PLA | Power Lever Angle | deg. |
| $P_{18}$ | HX-A Oil inlet Pressure | psig. |
| $P_{19}$ | HX-A Oil Disch. Pressure | psig. |
| $T_{18}$ | HX-A Oil Inlet Temperature | °F |
| $T_o$ or $T_{19}$ | HX-A Oil Disch. Temperature | °F |

| Symbol | Definition | Units |
|---|---|---|
| $W_{18}$ | HX-A Oil Flow Rate | pps |
| $\phi_i$ | Ideal Gas Flow Factor | $sec\text{-}°R^{1/2}/ft$ |
| $\phi$ | Real Gas Flow Factor | $sec\text{-}°R^{1/2}/ft$ |
| $W_{ai}$, WA or $W_{14}$ | Heat Exchanger Air Flow Rate | pps |
| $V_{wf}$ | Analog of $W_8$ or $W_f$ | volts |
| $V_{pp}$ | Analog of $P_2$ or $P_p$ | volts |
| $W_R$ | Pressure Regulator Fuel Flow | pps |
| $A_v$ or $A_{mv}$ or $A_{x8}$ | VCV Metering Throat Area | $in^2$ |
| $\dot{W}_8$ | VCV Fuel Flow Rate of Change | pps/sec |
| C* or Cg | Valve Flow Coefficient | -- |
| R | Gas Constant | $\frac{ft\text{-}lb}{lb\text{-}°R}$ |
| $H_c$ | Enthalpy at Metering Throat | Btu/lb |
| J | Energy Conversion Factor | ft-lb/Btu |
| $V_c$ | Critical Throat Velocity | ft/sec |
| $\rho_c$ | Critical Throat Density | $lbm/ft^3$ |
| $K_u$ | Unitary Conversion Constant | none |

## APPENDIX B

## REFERENCES


(1) Robert C. Johnson, "Real Gas Effects in Critical Flow Through Nozzles and Tabulated Thermodynamic Properties," NASA TN D-2565, January 1965.

(2) T.J. Petrozzi, P.H. Davison, et al, "Properties of Principal Cryogenics," Aerojet General Corporation Report No. 9050-111-65, November 1965.

(3) Robert C. Johnson, "Real Gas Effects in Flow Metering," NASA TMX-52965, May 1971.